THE USE OF ALGINATES AND POLYPHENOLS IN MEDICINAL IRON CHELATION FOR THE IMPROVEMENT OF COLONIC HEALTH.

Richard D. Horniblow

A thesis submitted to

University of Birmingham

For the degree of

DOCTOR OF PHILOSOPHY

Institute of Cancer & Genomic Sciences
Medical and Dental School
University of Birmingham
September 2015

UNIVERSITYOF BIRMINGHAM

University of Birmingham Research Archive

e-theses repository

Synopsis: Chelation of 'ferrotoxic' iron within the colon

Iron is central to the aetiology of gastrointestinal disease. Specifically, the toxic effects of excess, unabsorbed '*luminal*' iron ingested from the diet has been shown to be important in the development of inflammatory bowel disease and intestinal cancer. A platform for therapeutic intervention is likely to involve chelation of this luminal pool of iron. As such, a range of dietary iron chelators have been tested for their iron binding capacity.

Natural biopolymers extracted from seaweed (alginates) and a variety of natural polyphenolic compounds were stratified in terms of their iron binding potential. With respect to alginate, it was demonstrated that chemical composition had profound effects on iron chelation potential and competition from other metal cations. It was also identified that alginates bind iron and subsequently format the chelated iron into a nanoparticle; such activity is likely to modulate cellular iron concentrations. One alginate, Manucol LD, was unique in its iron binding, and decreased iron absorption *in vitro* and *in vivo* with results demonstrating the chelation of luminal iron.

The chemical composition that endows Manucol LD with this unique iron binding potential was probed and it was concluded that the specific monomeric composition of the alginate, alongside its polymer chain length are implicit in forming a 'protein-like' iron binding pocket. Disruption of the chemical nature of Manucol LD removed its iron binding ability. With respect to the polyphenols, only one of the tested compounds (quercetin) displayed iron chelation activity *in vitro* and was able to suppress cellular concentrations of reactive oxygen species acting as an antioxidant.

As such, it has been demonstrated that a unique alginate, Manucol LD, is an excellent candidate for sequestering luminal iron present in the gastrointestinal tract and *in vivo* shows promising anti-neoplastic activity. These results underpin the rationale in utilising these types of natural and safe bio-polymers for the prevention and treatment of gastrointestinal disease.

Acknowledgments

My supervisor Dr Chris Tselepis deserves the biggest thanks. He has not only given me the opportunity to undertake this exciting research in his lab but also to allow me to collaborate and work with many other experts in the field, think for myself as a scientist, to try out my ideas and has been a supportive friend when things just didn't go to plan. As busy as supervisors always are, he always found time for me. Thanks also to my supervisor Prof Zoe Pikramenou in chemistry and Prof Ian Norton in chemical engineering for their insightful scientific contributions.

Fellow labmates, both past and present cannot go without a mention. Research groups in chemistry (Nicola, Kim, Sam and Sully) and cancer (Elisabeth, Dan, Imogen, Matt, Pritesh, Victoria (and I guess I'll have to include KSHV Rob!)) have always been on hand to help in the lab, been there for a good chat over a cup of tea and to keep me company in the pub- the basis of a good scientific performance! A special thank you goes to Alison Savage, who has been especially supportive in many aspects of science and life; always on hand to offer her wisdom.

I have also had the opportunity to supervise many students over the period of my research which has been a great experience and many of them have become good friends rather than project students. A special thanks has to go to the best student I have had the pleasure to supervise, Melanie Schneider, who worked closely with me during some of the most exciting finds in my research.

Lastly, I would like to say a massive thank you to my family; my Mum, Dad, Laura and Joe who have always been there to support me in anything I do and to always offer guidance (even scientific help!) trying to give constructive advice to my common 'my experiment isn't working' problem. Your encouragement has been immeasurable, and you have all pushed me to achieve my goals. You believe in me more than I do myself, which has been inspiring, and I hope I can equally inspire you all in return. Thank you.

Contents

Chapter 2   Alginate iron binding: a chemical characterisation

Chapter 3 — Alginate iron chelation *in vitro* and *in vivo*

Chapter 4   Alginate chemical modification: an understanding of iron chelation bioactivity

Chapter 5   Polyphenolic iron complexation: a chemical and cellular study.

Chapter 6   Conclusions and future work   258

Appendices

List of Figures

List of Tables

List of Abbreviations

$[\eta]$	Intrinsic viscosity
°C	degrees Celsius
Å	Angstrom (1.0×10^{-10} metres)
AFH	Alginate Protsea AFH
AlgE	Alginate Epimerase
APC	Adenomatous polyposis coli
AUC	Analytical ultra-centrifugation
C	Colon (dissection)
C3G	Cyanidin-3-O-glucoside
cal	Calories
CD	Circular dichroism
C_n	Carbon number
D	Duodenum (dissection)
Da	Daltons
Dcytb	Duodenal cytochrome b
deg	degree
DFO	Desferrioxamine
DGA	D-guluronic acid
DH	Alginate Manucol DH
DMEM	Dulbecco's modified eagles medium
DMT1	Divalent metal transporter 1
DNA	Deoxyribonucleic acid
DW	Duodenal wash
ECL	Enhanced chemiluminescence
EDX	Energy-dispersive X-ray spectroscopy
EGF	Epidermal growth factor
EpLD	Epimerised Manucol LD
F	Fraction
FAP	Familial adenomatous polyposis
FCS	Foetal calf serum
Fe(II)	Ferrous iron
Fe(III)	Ferric iron
FeO-NPs	Iron oxide nanoparticles
FITC-LFR5/60	Fluorescent LFR5/60
FPN	Ferroportin
g	gram
GHB	Alginate Manugel GHB
GLUT	Glucose transporter
GSK	Glycogen synthase kinase
H	Enthalpy
HAADF	High-angle annular dark-field
HCP	Haem carrier protein
HEPH	Hephaestin
HFE	Hemochromatosis
HH	Hereditary hemochromatosis
HO-1	Haem oxygenase 1
HS	High spin
Hz	Hertz
I	Ileum dissection
IL-6	Interleukin 6

inh	inherent
IRE	Iron responsive element
IRP1/2	Iron regulatory protein
ITC	Isothermal titration microcalorimetry
J	Jejunum dissection
JW	Jejunal wash
k	Kilo (10^3)
K	Binding constant
KEL	Alginate Keltone
LD	Alginate Manucol LD
LS	Low spin
m	Milli (10^{-3})
m	Meter
M	Mega (10^6)
M	Molar
min	Minutes
MRI	Magnetic resonance imaging
mRNA	Messenger RNA
MW	Molecular weight
n	Nano (10^{-9})
N	Binding site number
NF-κB	Nuclear factor κB
NMR	Nuclear magnetic resonance
NTBI	Non-transferrin bound iron
OH	Hydroxyl
Pa	Pascal
PBS	Phosphate buffered saline
PCBP1	Poly(rC)-binding protein 1
ppm	Parts per million
red	Reduced
RF6650	Alginate Protanal RF6650
RNA	Ribonucleic acid
ROS	Reactive oxygen species
RPM	Rotations per minute
s	Svedberg
S	Stomach dissection
S	Entropy
sp	Specific
STEM	Scanning transmission electron microscopy
TEM	Transmission electron microscopy
Tf	Transferrin
TfR	Transferrin receptor
TGF-β	Transforming growth factor β
TNF	Tumour necrosis factor
UC	Ulcerative colitis
v/v	volume/volume
w/v	weight/volume
λ	Wavelength
μ	Micro (10^{-6})
τ	Tumbling time
η	Viscosity

Chapter 1

Iron, Cancer and Chelation.

1.1 Iron

Iron is central to health and wellbeing, whereas iron excess and accumulation is associated with detrimental effects. For this reason complex homeostatic mechanisms have evolved to keep iron concentrations within physiological ranges. Iron is classified as a micronutrient, despite playing a crucial role in the regulation of many cellular functions and as such the total amount of body iron is between $3 - 4$ g.[1, 2] When iron is used in biology, for instance within the active site of an enzyme, its presence and exposure within that protein structure is carefully regulated to ensure it is unable to partake in any toxic related processes. The apparent importance of iron becomes evident upon consideration of the numerous proteins reliant upon iron such as haemoglobin, myoglobin, cytochrome enzymes, ribonucleotide reductase and NADH dehydrogenase.[3, 4]

1.1.1 Cellular iron absorption

Dietary iron exists in two major forms; haem (or 'organic') iron and inorganic iron. Both forms of iron are absorbed by distinct mechanisms.[5] It is known that only 10-20 % of the

daily ingested intake of iron (around 10 – 15 mg) is absorbed, with haem iron being absorbed more efficiently than inorganic iron, yet inorganic iron is the most prevalent dietary form accounting for around 80 – 90 % of total daily intake.[5-7] Recommended daily allowances of iron are 10 and 15 mg day^{-1} for men and women respectively. Table 1.1 illustrates the iron content of some foods and the prevalent form of iron within.

Table 1.1: Iron concentrations and type from a variety of food sources.[8]

Dietary iron form	Food source	Iron amount per serving (mg)
Inorganic	Oatmeal (90 g)	11.0
Inorganic	Lentils (200 g)	6.6
Inorganic	Spinach (225 g)	3.2
Inorganic	White bread (1 slice)	0.9
Haem	Turkey (85 g)	2.0
Haem	Beef (85 g)	2.2
Haem	Tuna (85 g)	1.3
Haem	Pork (85 g)	0.7

Inorganic iron absorption takes places within the duodenum; the enterocytes of the proximal small intestine express many proteins involved in cellular iron transport; the more distal along the small intestine the more reduced the capacity for iron absorption becomes.[9] Inorganic iron from the diet can exist in two forms (ferric or ferrous iron). Many factors dictate the bioavailability of both forms. Ferric iron with its high charge readily forms salt complexes with anionic species present within the diet resulting in diminished absorption.[5] Another confounding factor on ferric-iron bioavailability is its solubility in less-acidic environments, specifically above pH 3. In contrast, ferrous iron does not complex as readily and is soluble at

higher pH levels.[5] As such, gastric acid promotes the reduction and solubilisation of dietary ferric iron.[5] The chronic use of proton pump inhibitors, *Helicobacter pylori* infection and inflammatory conditions decrease non-haem iron absorption.[10] Not only can the pH environment have an impact on iron bioavailability but chemicals within the diet can also have considerable influences. Two notable examples include ascorbic acid and tannins found in fruit juices and tea respectively; these can be classed as *dietary iron chelators*.[11, 12] Ascorbic acid can bind to iron increasing its solubility which in turn enhances its bioavailability whereas tannins bind iron to form insoluble complexes which decreases irons absorbability.[13] Phytic acid, which forms a considerable component of rice and grains also binds iron to limit its absorption likelihood and the effect is so prominent that it has been hypothesised that in countries where consumption of phytic-acid containing food is high, the increased prevalence of iron deficiency anaemia is due to this diet.[14-17]

The first phase of inorganic iron absorption, at the apical membrane of the enterocyte, a ferric reductase, namely Duodenal cytochrome B (Dcytb), reduces ferric iron to ferrous iron, before it is transported into the cell through divalent metal transporter-1 (DMT1).[18] DMT1 co-transports Fe(II) and hydrogen ions into the cell. Interestingly, although ascorbic acid binds to iron to increase its bioavailability it has been reported that Dcytb facilitates the reduction of ferric iron by electron transfer with intracellular ascorbate, and thus this maybe the mechanism by which vitamin C enhances iron absorption.[19] DMT1 protein in the proximal duodenum is expressed exclusively to the villi and is absent within the crypts.[20] Once inside the enterocyte, iron is either stored in an inert form for later use in ferritin (an iron storage protein) or it can be utilised immediately for the various cellular processes stated. Recently an iron-chaperone has been identified, poly-r(V)-binding protein 1 (PCBP1), which transports iron to ferritin and other iron proteins within the cell.[21] If homeostatic iron

demand is high, then the iron will be transported out of the enterocyte into systemic circulation. Exit from the enterocyte is orchestrated by ferroportin (FPN) and the ferroxidase hephaestin (HEPH) at the basolateral membrane.[22] Iron exits via FPN as ferrous iron, where it is oxidised to ferric iron before complexation to transferrin (Tf); it is within this transferrin carrier protein that iron is safely transported around the body in the serum (figure 1.1).[23, 24]
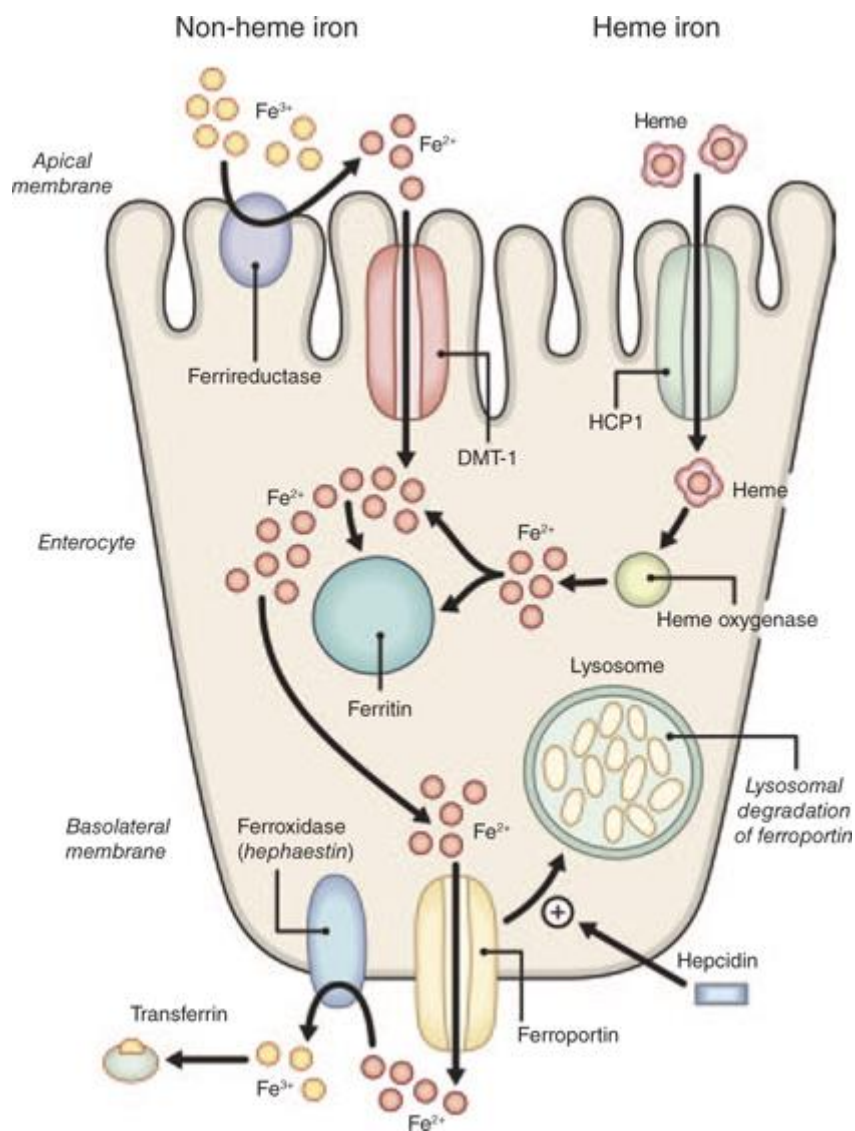
Figure 1.1: Intestinal absorption of iron.[25]

Organic iron is also absorbed at the brush border of the enterocyte but occurs via a different mechanism which to date is still not clearly defined. Haem iron is imported into the cell through haem carrier protein (HCP1), however this candidate for haem-transport is still debated as recent evidence suggests HCP1 is likely to be a folate transporter.[26] Once inside the enterocyte, haem is broken down into biliverdin releasing its coordinated iron by haem oxygenase-1 (HO-1).[27, 28]   The free ferrous iron is subsequently processed in an identical manner to inorganic iron absorption. More recently it has been described that absorption of iron may occur via an endocytic mechanism within the small bowel,[29, 30]   since it is unlikely that iron will reach the small bowel in its 'free' form due to the chemical conditions throughout gastro-intestinal transit. The more likely form is a precipitated mineralised form of iron oxo-hydroxo species, that have been found to be in the form of nanoparticles.[31, 32]

1.1.2   Regulation of cellular and systemic iron metabolism

Unlike most essential nutrients, no active mechanisms exist for iron excretion in humans, although small amounts are lost through skin cell exfoliation and the sloughing of gastro-intestinal cells.[33] At a cellular level, the usage and storage of iron is coordinated by iron-regulatory proteins 1 and 2 (IRP1 and IRP2). These proteins are directly sensitive to intracellular iron concentrations and are able to bind to the 5' or 3' iron responsive elements (IREs) on the untranslated regions of iron transport protein mRNA to either stabilise or destabilise the transcript.[34] During low intracellular iron concentrations, IRPs bind to the 3' IREs of iron uptake proteins and the 5' of iron storage protein mRNA to stabilise and inhibit its translation respectively. Conversely, in augmented cellular iron concentrations, IRPs are unable to bind to the IREs to limit the cells ability to acquire iron (figure 1.2).[35]
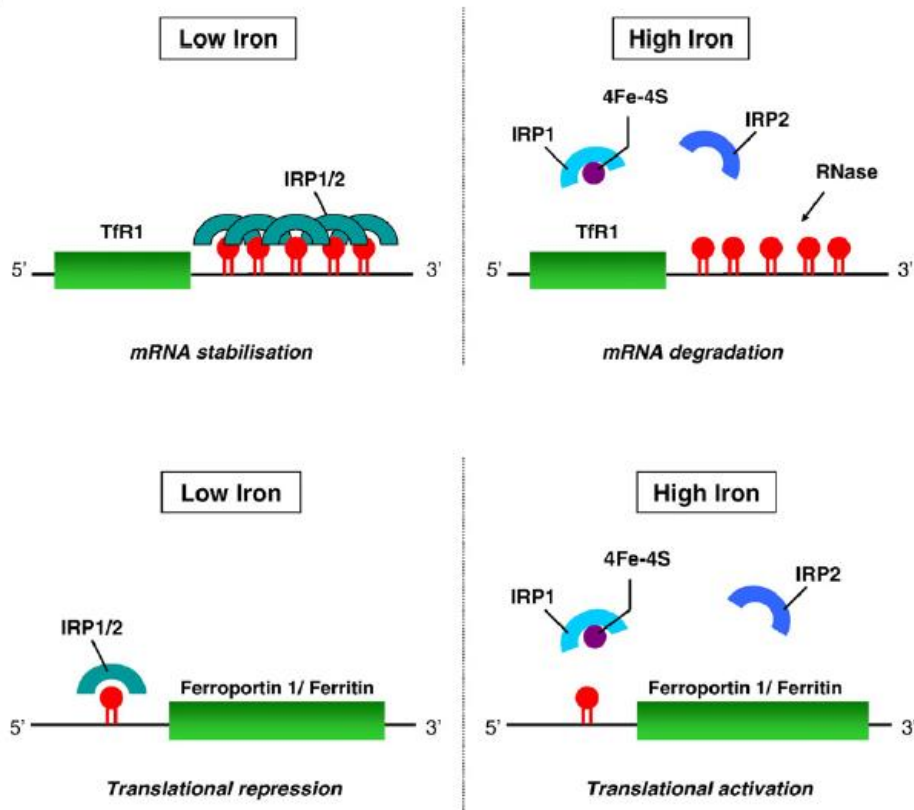
Figure 1.2: Iron-regulatory protein interaction in response to high and low intracellular iron levels.

Control of systemic iron levels is solely maintained by modulation of iron absorption. It has been found that Dyctb is upregulated in the duodenum when body iron stores are low.[36] Iron absorption is precisely orchestrated by circulating hepcidin (HEPC) which acts on the duodenum and also influences the release of iron from hepatocytes and macrophages that are involved in the recycling of iron from senescent erythrocytes.[37] HEPC binds to FPN1 which initiates its internalisation and lysosomal degradation. This process results in the inhibition of iron release to decrease serum iron levels.[38]

Hepcidin is a key hormone that is involved in the control of iron homeostasis in the body. Physiologically, hepcidin is controlled by iron stores, inflammation, hypoxia, and

erythropoiesis and its regulation and release from hepatocytes is coordinated by complex processes.[39] As well as the historical mediation of HEPC by hemojuvelin, TfR2 and HFE, other more recently identified pathways exist to regulate HEPC expression (i.e. bone morphogenetic protein and JAK2/STAT3 signalling).[40, 41] The pathophysiology of hereditary hemochromatosis as an iron metabolism disorder arises from mutations in the HFE protein such that the function of HEPC is lost.[40] The evolutionary use of HEPC is thought to be one of mediating host defence against siderophilic infections, since it has a potent ability to limit the accessibility of iron to infectious bacteria.[42]

1.1.3 Disorders of iron metabolism

Dysregulation of iron metabolism can lead to diseases of iron deficiency or diseases of iron overload. Iron deficiency anaemia arises when the dietary intake of iron does not meet the body's homeostatic demands.[2] This may be due to inadequate absorption (from poor bioavailability, high gastric pH environments, bowel resection or disease) or due to blood loss (for example due to gastritis, tumours and ulcers).[2] Another disease implicated in the dysregulation of metabolism is anaemia of chronic inflammation, whereby elevated basal levels of interleukin 6 (IL-6) stimulate HEPC expression which in turn 'locks up' iron within the macrophages and hinders iron export from the enterocytes.[43] Conversely, iron overload can be caused by Hereditary Haemochromatosis (HH) and by frequent blood transfusions.[2] Patients with HH absorb two to three times more dietary iron than a normal person, and as such once transferrin becomes saturated and is unable to sequester any more absorbed iron from enterocytes and as a consequence so called 'non-transferrin bound iron' (NTBI) is produced.[44] Excess iron is deposited in parenchymal cells of the liver, heart, pancreas,

pituitary gland and the parathyroid gland in these clinical cases.[2] Interestingly, HH patients carry a 20 to 200 fold increase in the risk of developing hepatocellular carcinoma and, as such transferrin saturation is a biochemical marker that can be correlated to cancer incidence.[45-47] The toxic nature of NTBI is the cause of disease in iron overload, since the usual mechanisms that regulate the toxic nature of 'free iron' are disrupted.[48]

1.1.4 Redox cycling of iron

The body prevents the possible toxic chemical activity of iron by storing and transporting it around the body in ferritin and transferrin alike. Ferritin is a complex protein, with a molecular weight of 450 kDa and being composed of 24 individual sub-unit proteins, which together form the protein coat that surrounds the core of iron. In total, ferritin can hold up to 4,500 atoms of iron in the form of hydrous ferric oxides (such as ferrihydrite).[49] Such arrangement minimises the production of potentially harmful redox products from 'free' iron. Similarly, transferrin binds iron but is a much smaller protein and has the capacity for only two iron atoms, yet the affinity of iron binding is strong.[50] Despite its smaller size, the four subunits of Tf interact to form a deep hydrophilic metal binding site, removing iron from exposure to the surrounding environment where it can have damaging effects.[51]

Iron thus represents a paradox for living organisms, by being essential for life with its labile, reactive nature but also having the potential to be toxic. Iron can be toxic through its ability to redox cycle, in such a way that it is able to catalyse the formation of reactive oxygen species (ROS). Physiological ROS include superoxide (O_2^-), hydroxyl radicals ($OH\cdot$), alkoxy radicals ($RO\cdot$) and hydroperoxyl radicals ($HO_2\cdot$).[52] Iron being a transition metal has many accessible atomic orbitals allowing it to accept and donate electrons of any spin state. As

such, in a reaction with molecular oxygen (that in its ground electronic state has two single electrons in two different orbitals) iron can interact in Fenton-type chemistry (figure 1.3).

$$I \quad Fe^{2+} + H_2O_2 \longrightarrow Fe^{3+} + OH^- + OH\cdot$$

$$II \quad Fe^{3+} + O_2\cdot^- \longrightarrow Fe^{2+} + O_2$$

$$III \quad O_2\cdot^- + H_2O_2 \xrightarrow{Fe} OH^- + OH\cdot$$
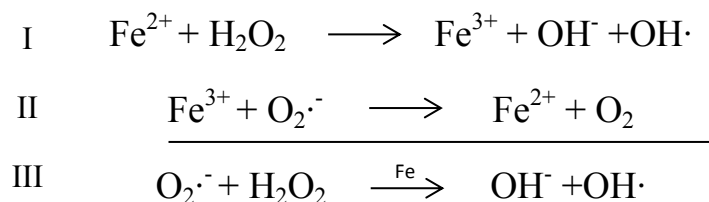
Figure 1.3: Fenton chemistry. (I) Fenton-type reaction of ferrous iron with hydrogen peroxide to form the hydroxyl radical. (II) Reduction of ferric iron by the superoxide anion. (III) Sum of reactions (I) and (II) to give the Haber-Weiss reaction, which is iron-catalysed formation of the hydroxyl radical.[53]

In order to prevent iron from participating in such a catalytic cycle, its redox potential needs to be controlled by iron chelation which alters the electronic configuration of iron and sterically hinders access to other compounds (such as H_2O_2) as only when a free and exchangeable coordination site on iron is accessible can such reactions take place.[53, 54]

Free radicals target DNA, RNA, proteins and lipids to elicit mutations or cause damage ultimately resulting in the impairment of cellular function which can lead to cell death.[55] The earliest study to document the action of free radicals in DNA damage was the observation that chromosomes become fragmented in the presence of hydrogen peroxide and a peroxidation activator, such as iron.[56] Such damaging effects of ROS can promote many aspects of tumour development and progression in cancer.[57]

1.2 Colorectal cancer incidence and prevalence

Over 40,000 people are diagnosed with colorectal cancer in the UK each year, making it the 4th most common cancer, behind breast, lung and prostate. It is the 2nd leading cause of cancer related death, with over 16, 000 deaths yearly.[58] More than 85 % of bowel cancers occur in cohort ages 60 and over; this reflects the life-span of the disease and its slow, progressive nature. Approximately 30 % of colorectal cancers arise from the rectum, 25 % in the caecum and ascending colon respectively and 20 % in the sigmoid colon.

1.2.1 Structure and function of the colon

Unlike the small intestine, which utilises endogenous enzymes to break down food into absorbable nutrients, the large intestine relies on billions of bacteria, namely the gut flora, to process the food in ways that enzymes secreted more proximally are unable to perform.[9] The large intestine consists of the caecum, appendix, colon and rectum with its main function in desiccation of remnant digesta, storage of faeces and as mentioned, breakdown of complex nutrients (for example carbohydrates).

At a histological level, the intestine is composed of an epithelial layer which contains rapidly proliferating cells that reside within the crypts of Lieberkühn, this proliferation is under orchestration of the Wnt signalling pathway. [59] The crypts harbour stem cells, which in time differentiate to transit-amplifying cells. Transit-amplifying cells spend approximately two days in the crypt, in which they divide 4–5 times before they terminally differentiate into the specialised intestinal epithelial cell types.[60-62] With respect to nutrient absorption, the mucosal surfaces of the large intestine consists of three layers; the first containing a single

layer of epithelial cells (the epithelium), the second which is the lamina propria which consists of subepithelial connective tissue and lymph nodes to the third layer which is the muscularis mucosae.[63] The mucosa of the large intestine folds to form crypts that invaginate deep into the submucosa (figure 1.4).[64]
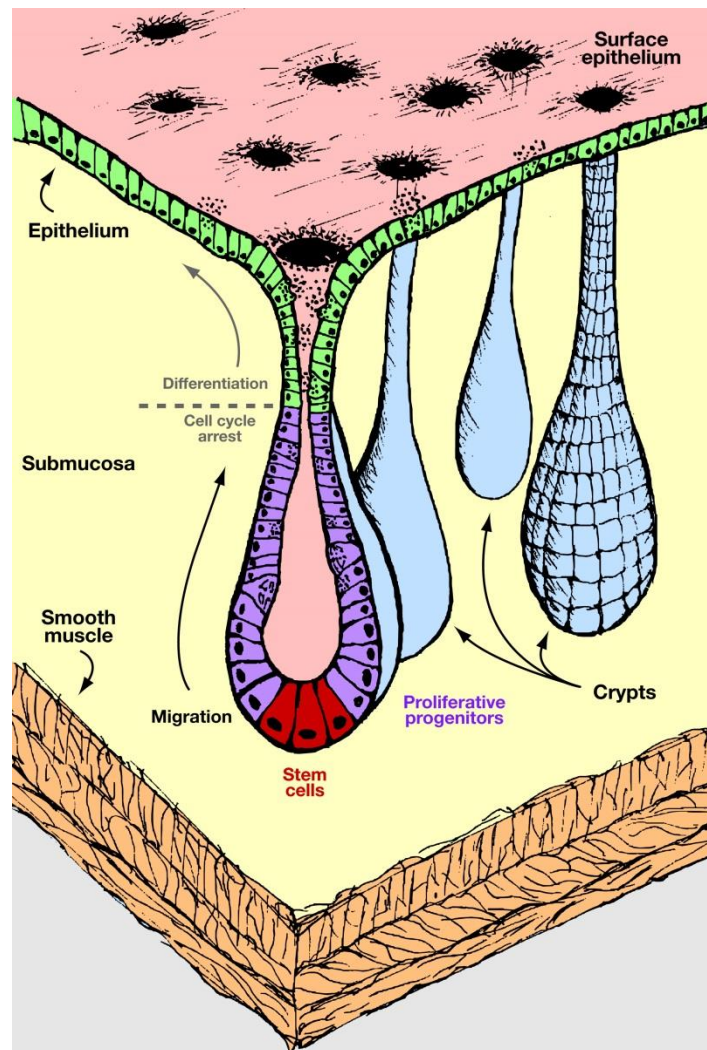
Figure 1.4: formation of crypt. Stem cells reside at the crypt bottom and progenitors are amplified by constant division along the bottom two thirds of the crypts. Cell cycle arrest and differentiation occur along the villus-crypt axis.[64]

Four differentiated cell types mediate the functions of the intestinal epithelium, yet the colonocyte which is responsible for absorption within the large intestine is the most abundant.

1.2.2 Colorectal cancer symptoms, diagnosis and treatment

Typically, colorectal cancer patients present with abdominal bloating, pain, blood present in the faeces, weight loss or iron deficiency (and as such tiredness) or in emergency situations with bowel obstruction.[65] The faecal occult blood screening test is now established within the UK to screen for patients who are asymptomatic but have possible colorectal cancer. In England alone, men and women aged between 60 and 74 are invited to partake, of which, 2 % of the cohort will be identified as abnormal. Of this 2 % cancer will be incident and 38 % will have confirmed polyps.[66]

Colorectal cancer is diagnosed through histological examination of a suspected tissue biopsy and following confirmation, the cancer is then staged using computed tomography (CT). The Tumour, Node and Metastasis (TNM) staging system is referenced to rank the progression of the identified cancer. A 'T' stage describes the size of the primary tumour, with T1 indicating localisation to the inner layer of the bowel, through to T4 whereby the tumour is invaded into adjacent organs. The 'N' stage describes presence of cancer within the lymph nodes, with N0 indicated no lymph node metastasis through to N2 where positive identification in several lymph nodes is found. The 'M' stages describe the presence of distant metastasis, with M0 and M1 signifying no metastasis and found metastasis respectively.[67]   Unsurprisingly, a stage I cancer with TNM rating T1 N0 has a 91 % 5-year survival rate whereas a stage III T4N2 has a 27 % 5-year survival rate.[68]

The tumour stage dictates the extent of treatment required. Low staged, localised tumours are commonly removed, without the need for chemotherapy or sectional removal of the colon. Partial colectomy is the standard treatment, with the need for adjuvant chemotherapy if there

is an associated high risk of reoccurrence.[69] It is hoped that screening programmes will identify pre-cancerous lesions (benign polyps) within the colon before malignancy is evident.

1.2.3 Colorectal cancer development; a genetic basis

It is well understood how colorectal cancer results from genetic alterations, tumour-suppressor inactivation and alterations in cellular molecular pathways.[70] Changes in the Wnt signalling pathway are regarded as the initiating event in colorectal cancer, which is unsurprising since Wnt controls cellular proliferation within the intestinal crypts.[71, 72] Other molecular pathways which are abrogated in colorectal cancer include p53 and TGF-β.[73, 74] These are typical pathological changes that occur in many sporadic colorectal carcinomas, with over 85 % showing loss of APC function (figure 1.5).[75, 76]
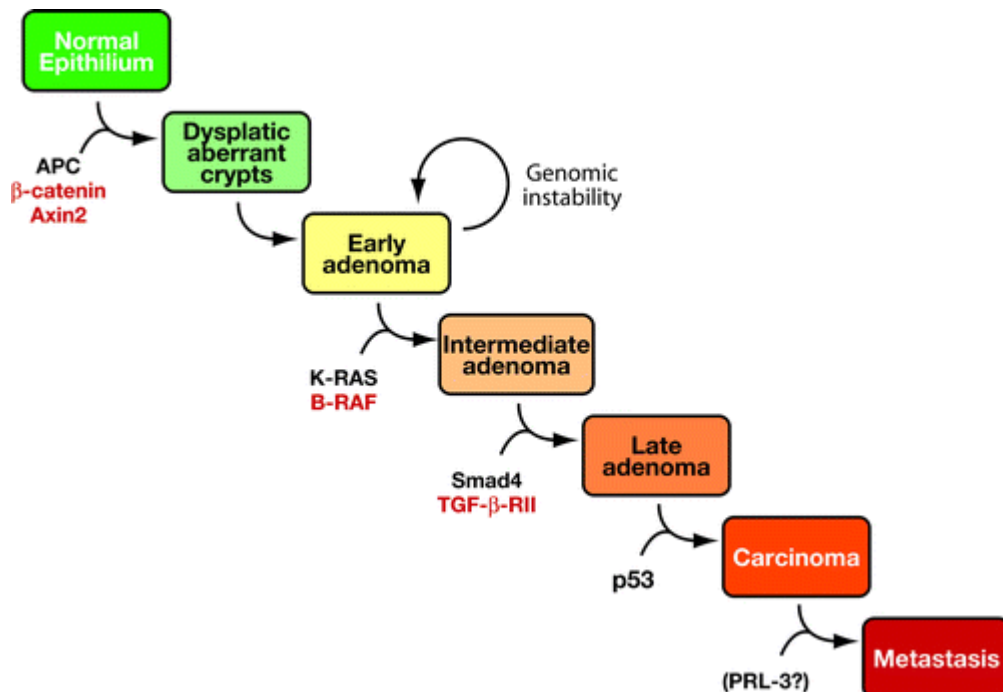
Figure 1.5: Correlation between CRC progression and the accumulation of genetic alterations.[64, 77]

Homozygous deletion of *APC*, the initial driver in colorectal cancer formation, leads to polyp growth through activation of the Wnt signalling pathway. Normal functioning APC serves to dampen Wnt signalling through its formation of a destruction complex, coupled with glycogen synthase 3β (GSK3β) and axin which phosphorylates β-catenin, targeting it for ubiquitination and subsequent degradation.[71] As such, colon cancer cells with loss of *APC* contain high levels of β-catenin, which is able to translocate to the nucleus where it can bind to transcription factors activing oncogenes such as c-myc and cyclin D1 (figure 1.6).[78]
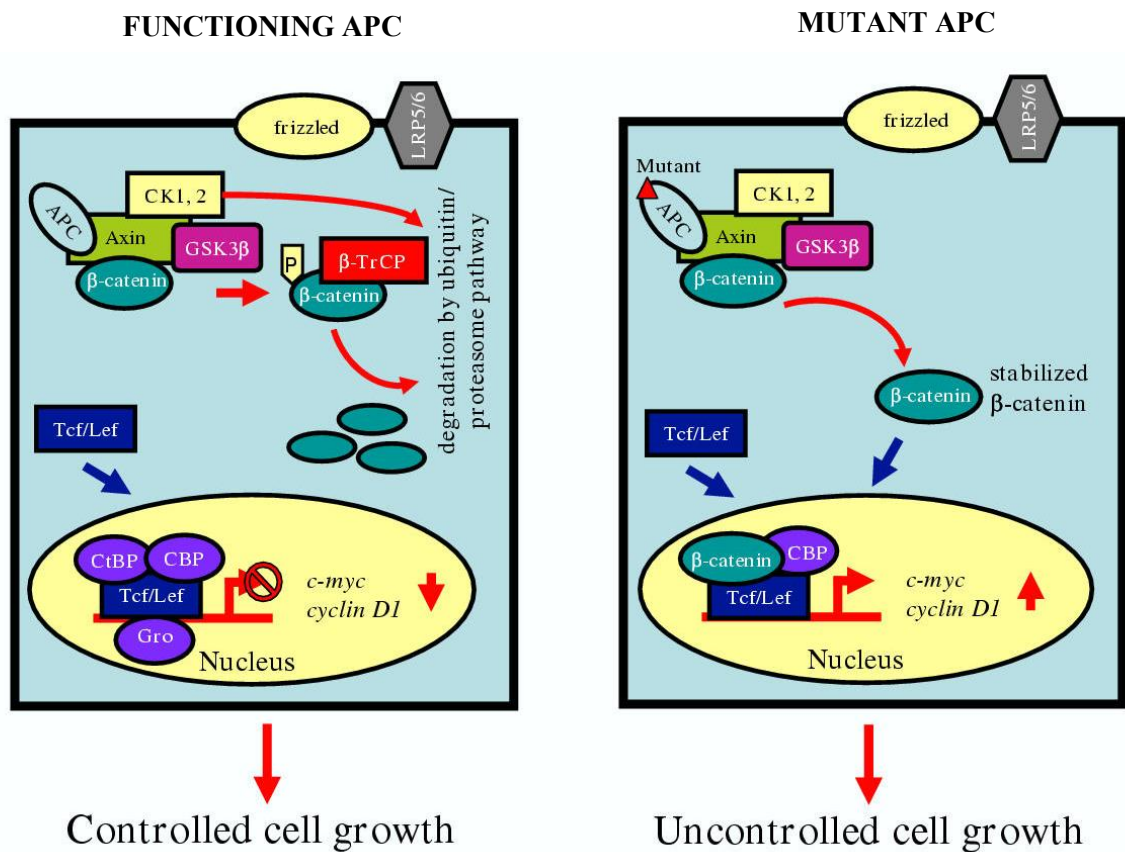
Figure 1.6: Cellular functions of APC in Wnt signalling.[78]

The importance of Wnt is further exemplified by the inherited condition of familial adenomatous polyposis (FAP), which is one of many risk factors for the development of colorectal cancer.

1.2.4   Risk factors associated with colorectal cancer

Most cases of colorectal cancer arise sporadically.[79]   Despite this, two hereditary genetic conditions, namely, familial adenomatous polyposis (FAP) and hereditary non polyposis colorectal (HNPCC or Lynch syndrome) account for around 5 % of bowel cancers.[80, 81] FAP originates with germ line mutations in *APC* and with subsequent loss of a second copy of APC within intestinal cells leads to many small, polyps or adenomas to develop within the large bowel.[76]   Most bowel cancers stem from adenomas and it has been estimated that a 1 cm^2 polyp has a 1 in 6 chance of becoming neoplastic within 5 years of initial growth.[80] Risk of colorectal cancer development is almost certain if mutations in other tumour suppressors and oncogenes arises.[82]

Inflammatory bowel disease; Ulcerative Colitis (UC) and Crohn's disease both augment the risk of colorectal cancer development.[83-86]   The majority of gastro-intestinal disease originates from an inflammatory state, and the toxic effects of iron are able to aggravate this inflammatory phenotype.[87]   As such, iron has been implicated in Crohn's disease, inflammatory bowel disease and ulcerative colitis.[88-91]   It has been suggested that iron present within the lumen on the colon is able to augment the inflammatory environment through its ROS generating potential.[92, 93]   Paradoxically, sufferers of gastrointestinal disease are commonly supplemented with iron to combat anaemia which is likely to be a

consequence of blood loss or anaemia of chronic disease. Other likely risk factors for colorectal cancer include smoking, alcohol consumption, physical inactivity and obesity.[58]

Diet and lifestyle are without doubt the main contributing factor in risk to developing colorectal cancer, with between 30-40 % of cancer cases worldwide being preventable by a change in diet.[94, 95] High amounts of fat, protein and low fibre diets have been correlated with an increased risk of developing colorectal cancer, alongside diets that contain high proportions of red and processed meat.[96] Iron is highly concentrated in red meat, and although there are other possible mechanisms in which red meat can cause colorectal cancer, high consumption of iron has been implicated.[93]

1.2.4.1 Iron and cancer association; human studies

It has been observed that the incidence of colorectal cancer is greater in those continents where high amounts of red and processed meats are consumed, compared to continents whose diet is primarily vegetable and fish based (figure 1.7).[97]
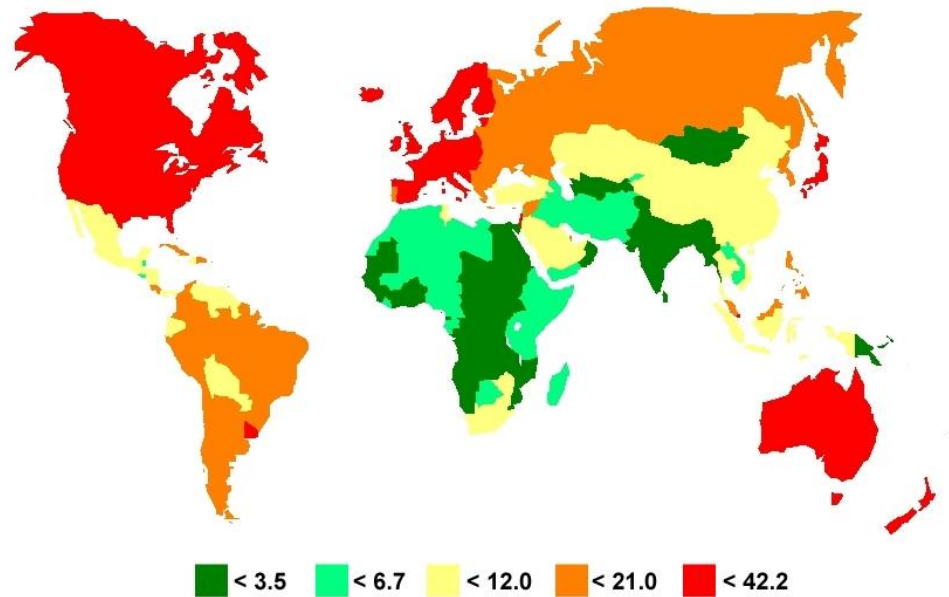
Figure 1.7: Map of global incidence (per 100,000) distribution of colorectal cancer.

Increased prevalence of colorectal cancer is evident in western continents where red and processed meat consumption is high, as such, considered that since these foods contain high amounts of iron that dietary iron intake has been may be a risk factor in colorectal cancer development.[46, 98, 99] A meta-analysis of 33 epidemiological studies showed that 75 % of studies supported an association between excess iron and colorectal cancer incidence, however clarification between the difference of iron 'exposure' and body iron levels needs to be better defined.[100]   In a more recent meta-analysis of red-meat and processed meat consumption correlation with colorectal cancer incidence, the same relationship was found and results suggest that the risk of colorectal cancer development increases linearly up to approximately 140 g/day of intake.[101] With respect to body iron stores, and transferrin saturation, Mainous *et al*. demonstrated that daily intake of dietary iron exceeding more than 18 mg is associated with an increased risk of cancer.[46]

Likewise, Hereditary Haemochromatosis (HH), a highly prevalent genetic disease in western populations, is a condition characterised by iron overload and high cellular loading of iron within the liver, heart and endocrine organs due to mutations in the haemochromatosis (HFE) gene.[102, 103] As such, this condition presents itself as an excellent case for an association study, and indeed, it has been found that there is a positive correlation between heterozygosity of HFE and the risk of colorectal cancer.[102, 104]

1.2.4.2   Iron and cancer association; cell studies

The crucial role of iron in cellular proliferation, growth and cell cycle progression makes it somewhat unsurprising that iron has been implicated in the development of cancer.[105, 106] Neoplastic cells therefore have a higher demand for iron.[107] It has been observed that cancer cells do indeed have increased intracellular iron concentrations and increased expression of iron acquisition proteins, namely TfR1 and DMT1 have been reported.[108, 109]. Increased iron acquisition, along the adenoma-carcinoma progression pathway has also been established.[110]   As such, iron can not only drive cancer growth, but also, as discussed, its redox ability maybe such that it can also act as a mutagenic initiator.[111] The ability for 'free' iron to redox cycle and catalyse ROS formation has been demonstrated as a potential carcinogenic initiator in cancer development. [112]

Loss of functioning APC is implicated in the neoplastic advancement from adenoma to carcinoma.[64] It has been found that iron can amplify the effects of APC loss in enterocytes, exacerbating the cancer phenotype.[113] Likewise, the target gene of Wnt is the proto-oncogene c-myc, which is able to regulate TfR1, enabling the cancer cell to acquire more

systemically circulating iron.[114] It has been demonstrated that iron chelation can serve as an effective mechanism to inhibit Wnt signalling, which may present a possible chemotherapeutic mechanism in colorectal cancer treatment.[115] Evidence suggesting irons ability to suppress expression of the cell adhesion protein E-cadherin further suggests that a dysregulation of iron metabolism is intimately linked to tumorigenesis.[113]

1.2.4.3 Animal evidence; a role for luminal iron

The earliest study performed to demonstrate the carcinogenic potential of iron *in vivo* demonstrated that 70 % of rats injected subcutaneously with iron (dextran) formed tumorous lesions at the site of administration.[116] Many *in vivo* studies have followed with paralleled findings that there is a synergy between iron and carcinogenic initiators (chemical or genetic) driving tumorigenesis.[117-122]

It has recently been demonstrated that it is specifically an excess of iron residing within the colonic lumen that is driving colorectal cancer.[120] This is best exemplified by a study conducted using APC min/+ mice, a model of human intestinal cancer. In this study, when APCmin/+ mice were fed an iron deficient diet tumour burden was dramatically reduced compared to their control cohort who received a standard iron-containing diet. However, the reduced tumour burden could be due to i) systemic iron deficiency or ii) the loss of so-called 'luminal iron' (excess iron present within the large bowel). To delineate which pool of iron was associated with the decrease in tumour burden the same group of mice that were fed an iron deficient diet were maintained systemically iron replete, by intravenous injection of iron dextran. Tumour burden was again significantly lower in this group compared to those fed an standard iron diet (figure 1.8).[120]
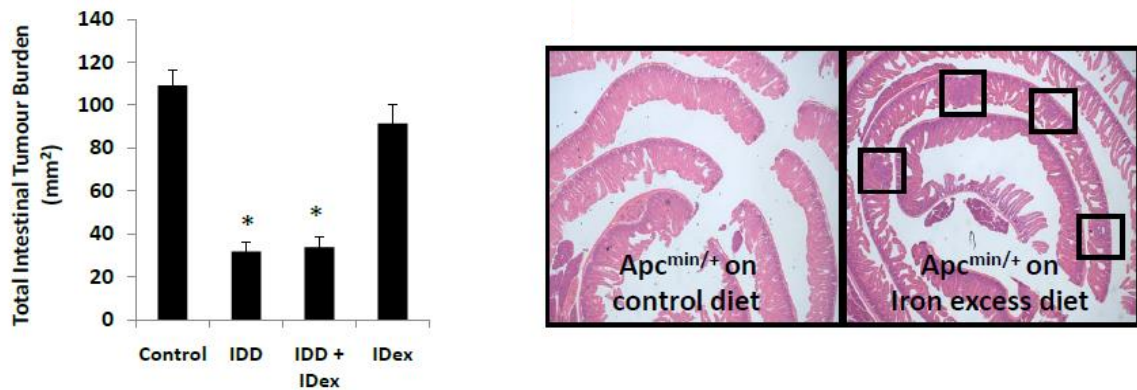
Figure 1.8: Tumour burden for APC min/+ mice fed a control diet, iron deficient diet (IDD), iron deficient diet with intravenous iron-dextran supplementation and iron dextran (IDex) alone with associated histological gut cross sections highlighting tumour presence (boxes).[120]

Thus these experiments were able to delineate the pool of iron that is responsible for colorectal cancer development, whereby it is excess iron within the *lumen* of the gastrointestinal tract that is driving tumorigenesis and not systemic iron. In this setting iron can indeed be coined 'ferrotoxic' and is driving cancer. A possible platform for therapeutic intervention could be around iron chelation, such that the toxic effects of iron are quenched by a chelating agent; the removal of iron would decrease colorectal cancer risk (figure 1.9).
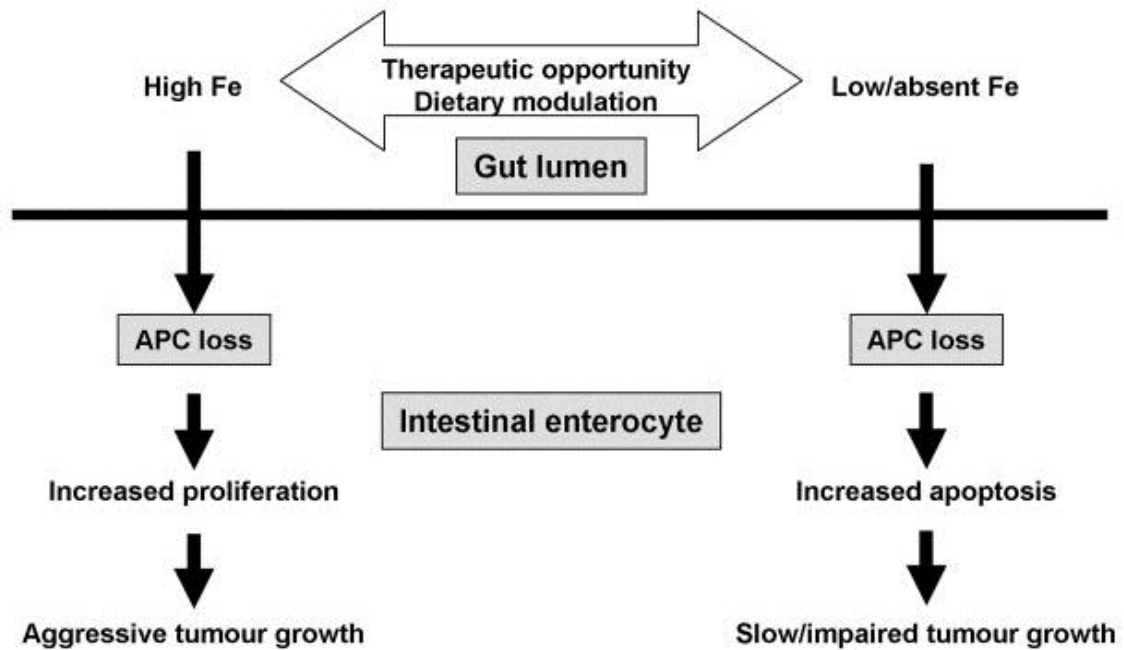
Figure 1.9: Representation of the therapeutic opportunity offered by dietary iron modulation.[120]

In support of this, it has been demonstrated that regular blood donation is associated with decreased incidence of colorectal cancer development; this may be related to regular depletion of systemic iron concentrations.[123-126] Although, this data suggests that systemic iron is still an important factor, in disagreement to Radulescu *et al*.[120] With respect to removal of the luminal pool of iron, results from EPIC found that dietary fibre intake from the consumption of fruit and vegetables is inversely related to bowel cancer.[127] This can be rationalised by considering the increased transit time of stools and dilution of digesta from fibre intake; perhaps impacting on the concentration and ability of iron to redox-react within the gastro-intestinal tract.[128] The literature correlating intake of dietary fibre to digestive health is a controversial one. A multicentered epidemiological study with over 1000 participants concluded that doubling total fibre intake from foods could reduce the risk of colorectal cancer by 40 %'.[129, 130] The first report linking high dietary fibre intake with

decreased colorectal cancer incidence was proposed by Burkitt, who observed trends in eating habits high-fibre low-fat diets vs. a low-fibre high fat diets; the latter correlated with elevated death rates due to colon cancer.[131, 132] The underlying mechanisms for this finding is unclear, yet it is likely that fibres decrease transit time, dilute the colonic contents and stimulate the microbiome fermentation process, all of which reduced the contact between the intestinal contents and the mucosa, reducing the likelihood of iron participating in toxic reactions.[129, 133, 134] However, caution must be taken as studies have concluded no effect of fibre intake and risk of colorectal cancer.[135-138]

1.2.5   Iron presence within the colon

Normally, between 0.7 – 22.9 % of iron ingested from the diet is absorbed nutritionally and as such the remaining iron resides within the lumen on the colon.[139] The characterisation of the form of iron present within the large bowel would demonstrate the possible mechanism by which iron is ferrotoxic. It can be envisaged that any iron present within the colon at this point of the digestive process would be bound within the digesta. However, since the chemical environment of the alimentary tract is translationally in change (acidic pH within the stomach to a more basic pH within the small intestine) the form of the iron needs to be understood. Some studies have been performed to decipher the iron species present within the gastro intestinal tract.[29, 31, 140, 141] Both ferric and ferrous iron have been demonstrated to reach the intestinal epithelial surface.[142, 143] It has already been discussed that iron solubility will be high within the presence of the acidic stomach. Ferric iron, however, is remarkably insoluble at duodenal pH, immediately precipitating as ferric poly oxo-hydroxide (rust).[29, 144] To slow the rate of iron hydrolysis and as such allow iron to remain soluble

in this region of the alimentary tract, it is proposed that a range of endogenous, low molecular weight ligands could chelate iron inhibiting this precipitation.[31] Gastrointestinal mucins have been identified as these potential iron-solubilisers, which, with initial hydrolysis reactions still occurring, the mucin hinders the rate of condensation reactions within the lumen to inhibit nanoparticle formation.[141, 145, 146] Despite this, these iron-hydroxide-mucin complexes are as bioavailable as ferrous iron in the duodenum of rats.[141] Since chemical pH environments are at the extremes between the stomach and the duodenum, it could be envisaged that these iron-composites are present throughout the rest of the alimentary tract, however this is not known. There is the possibility that within the large intestine, iron maybe 'free', bound to digesta or even particulate; this area of gastrointestinal iron speciation requires further study. Altogether, if indeed free iron is present in the colon, which is the redox-active form of iron, an iron-chelation therapy is still required.

1.3   Iron chelation

Chelation, derived from the Greek for 'crab's claw', is so termed based on the resemblance that complexing interactions of coordinating molecules 'wrap around' a host 'clasping' it, akin to a claw of a crab.[147] By definition, chelation is the process of coordination of a single atom, molecule or ion by more than one donor atom on a coordinating species. This process of coordination is energetically driven by a supramolecular interaction, where coulombic, ion-dipole and dipole-dipole electrostatic contacts stabilise the interaction.[147] Denticity relates to the number of donor atoms present on the ligand that chemically interact with the guest. Bidentate, tridentate and polydentate refer to two, three and multiple donor

atoms on the ligand respectively. With respect to iron, bidentate, tridentate and polydentate interactions are available (figure 1.10).
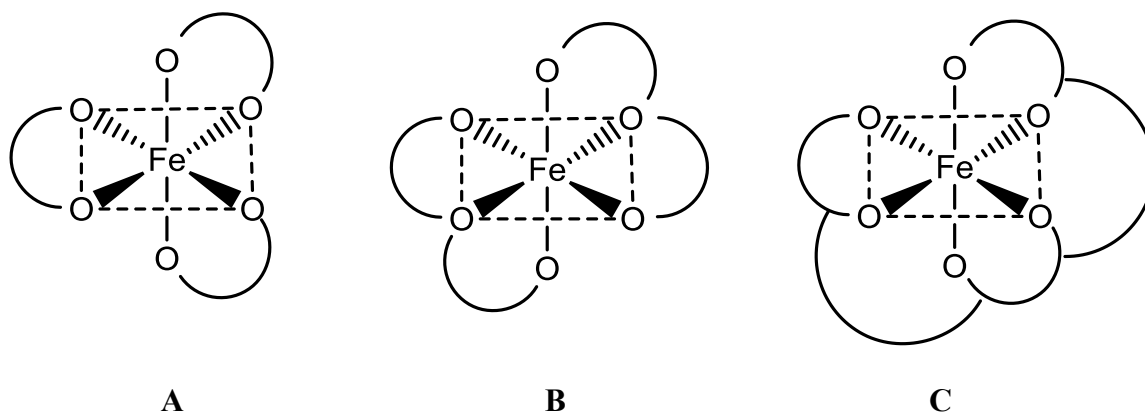
Figure 1.10: Iron chelation and denticity; (A) bidentate ligands coordinate iron in a 3:1 complex, (B) tridentate ligands coordinate iron in a 2:1 complex and (C) hexadentate ligands coordinate iron in a 1:1 complex.[148]

There are numerous factors that govern the type of chelation interaction between host and guest including the polarizability of both species, the chemical geometry imposed by the guest and the preferred donor atom type. With respect to iron, the most important consideration is that of polarizability where Pearson's concept of Hard and Soft Acids and Bases (HSAB) can be used.

In brief, hard metal ions will favourably interact with hard donor atoms, whereas soft metal ions (such as mercury) will interact with soft donor atoms.[149] Hard and soft refer to the polarizability of the species, with hard ions being highly charged, small and non-polarisable whereas soft ions are large, of low charge and readily polarisable.[147] In Pearson's seminal paper on HASB concept, ferric iron is referred to as a hard acid, where ferrous iron (being of less charge) is so-called 'borderline'.

Equally important is the geometric requirements imposed by the metal under consideration. The favoured coordination geometry is defined by the relative energy levels of the d-orbitals of the metal ion since chelation involves the donation of electrons to the metal ion, electron orbitals need to be available for this process to proceed. With a focus on iron, it has been discussed that the two common oxidation states are Fe(III) and Fe(II), which can be regarded as d^6 and d^5 metal centres respectively (d^n where n = total number of d-electrons – charge). When these d-orbitals interact with chelating ligands in an octahedral arrangement, the d-orbitals become non-degenerate (the orbitals energies split to form the lowest energy/most stable confirmation); it is this reason why iron imposes an octahedral arrangement of donor atoms. As such, if the chelating species is pre-organised to adopt this geometry upon interaction, the strength of coordination will be enhanced.

1.3.1 Established clinical iron chelators

The earliest use of a clinical chelating ligand was to remove toxic arsenic from arsenic-containing syphilis therapies, and since its establishment in 1956, D-penicillamine (DPEN) has been utilised as a copper chelator for the treatment of copper overload in Wilson's disease.[150] Ethylenediaminetetraacetic acid (EDTA) is an approved chelator for lead overload disorders (figure 1.11).
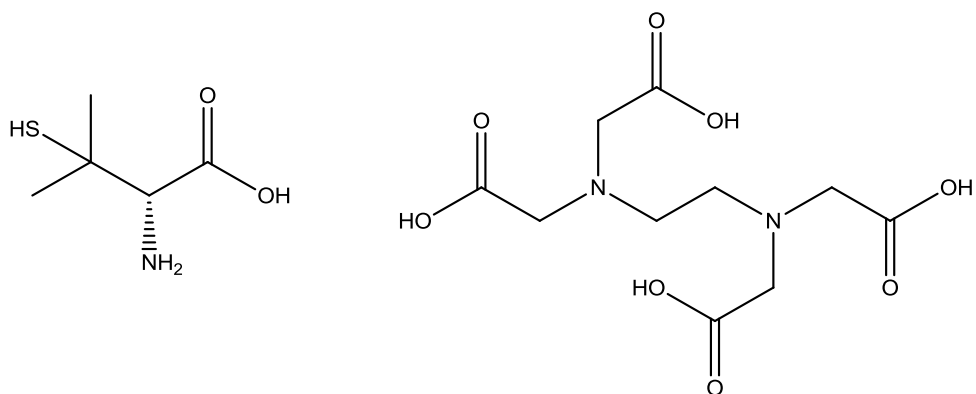
Figure 1.11: Chemical structures of DPEN and EDTA.

The first treatment for iron overload was introduced in the early 1970s, and today, desferrioxamine (DFO) is still used as a clinical agent.[151] Deferiprone and deferasirox have been developed to supersede DFO in relation to their pharmacokinetic formulation characteristics. Iron-overload, due to iron poisoning, transfusional overload, haemochromatosis or β-thalassemia is treated using a 'systemic' iron chelator, where the bioavailability of the iron-chelator administered dictates its effectiveness at depleting systemic iron levels. Deferiprone, a bidentate hydroxypyridone iron chelator, complexes with iron in a 3:1 ligand:iron ratio (figure 1.12). In light of the chelation principles discussed, deferiprone contained hard and soft donor atoms and the chelate angle allows for the octahedral geometry imparted by ionic iron.
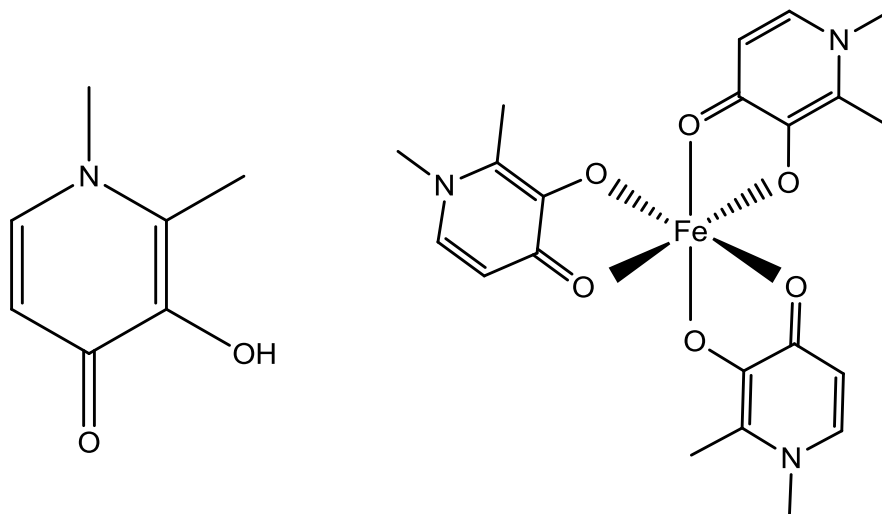
Figure 1.12: Deferiprone and a 3:1 complex with ferric iron.

Desferrioxamine, a multidentate iron chelator, is seldom used in clinical practice due to its intravenous formulation which is administered over a period of 8 to 12 hours daily (figure 1.13).[152]
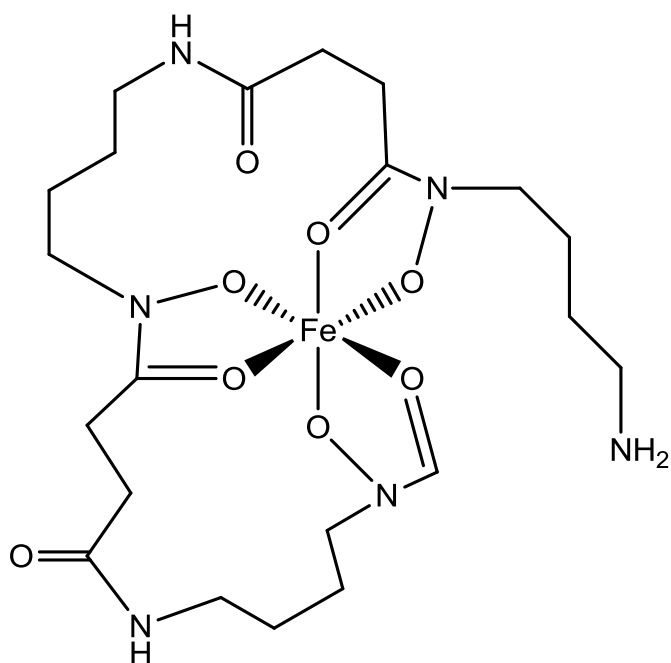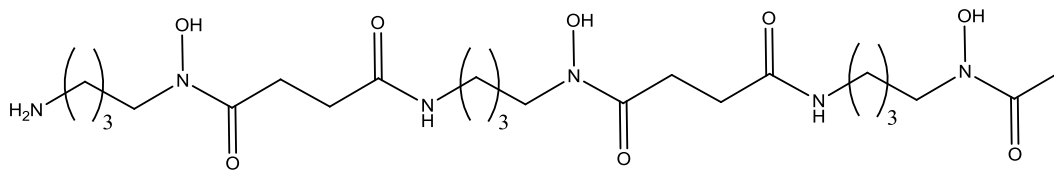
Figure 1.13: Desferrioxamine and a 1:1 complex with ferric iron.

The gold-standard for systemic iron chelation is deferasirox (EXJADE®), which is a tridentate ligand formation a 2:1 ligand:iron complex and perfect octahedral geometry surrounding the iron ion (figure 1.14).[153]
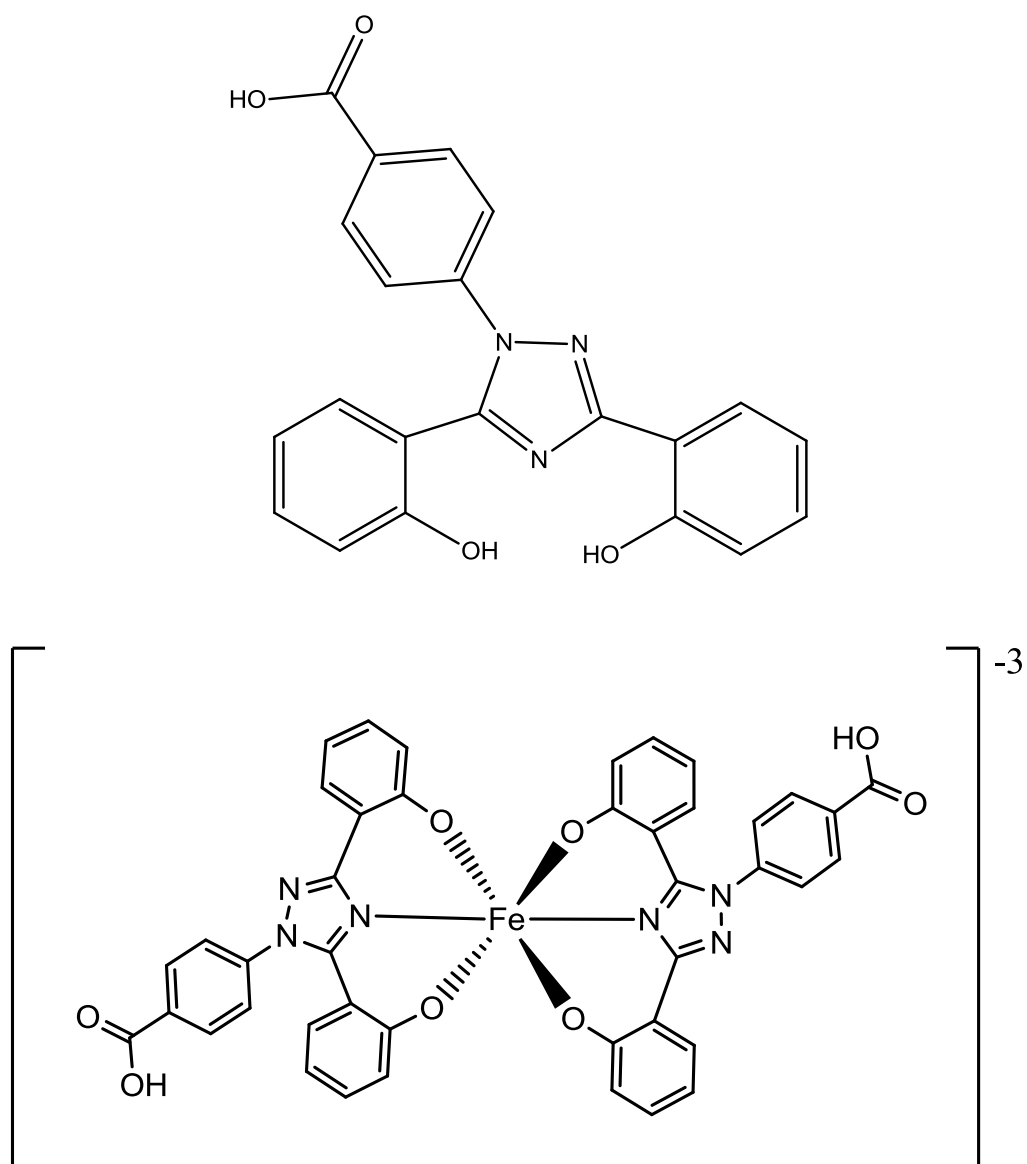
Figure 1.14: Deferasirox and a 2:1 complex with ferric iron.

Many iron chelators contain common chemical moieties used for iron binding such as catechol, hydroxamates, hydroxypyridinones and aminocarboxylates (figure 1.15).
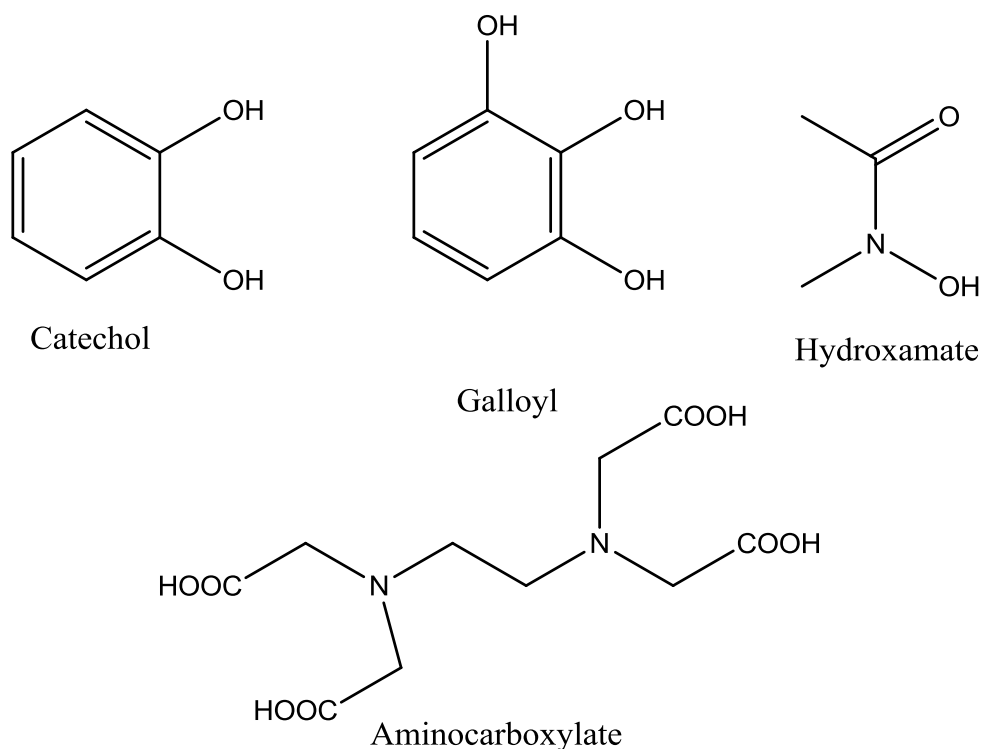
Figure 1.15: Common iron binding moieties.[154]

Given the association between the homeostatic changes in iron metabolism in cancer, there is a now significant research effort to investigate and develop iron-chelating drugs as anti-neoplastic agents.[109, 155-158]

1.3.2 Experimental iron chelators and anti-cancer activity

Only recently has iron chelation as a novel medicinal route to cancer treatment been considered. Just as the archetypal anti-neoplastic drug methotrexate starves the cell of essential tetrahydrofolate for DNA synthesis, an iron chelator can starve the cell of iron, which is required for many vital cellular activities.[159] However, other mechanisms have been proposed for anti-neoplastic iron chelators including the induction of apoptosis, cell

cycle modulation effects and the ability to enhance iron redox cycling to produce toxic levels of ROS.[155] Clinical iron chelators have been explored for their use as antineoplastic agents.[155] As early as 1988, DFO was found to have anti-tumour effects on human neuroblastoma cells.[160] Similarly, deferiprone has demonstrated promising anti-proliferative effects in a variety of cancer cells lines.[161, 162] Most notably are the anti-neoplastic activities of deferasirox.[163-165]

Of interest the thiosemicarbazone iron chelator (experimentally known as Dp44MT) has demonstrated effective anti-neoplastic activity.[166, 167] The mechanism of action remains to be fully elucidated, yet it has been demonstrated to invoke cell-cycle arrest and apoptosis and through redox-cycling processes.[168, 169]

Despite iron chelators representing a novel route to target sites of tumorigenesis there are two inherent limitations of their use, specifically their likelihood to abrogate anaemia in already anaemic cancer patients and their associated side effects.[155, 156, 170-172] To circumvent any systemic-iron depletion and to diminish the likelihood of side effects, there are an abundance of naturally occurring '*dietary iron chelators*' that may have *in vivo* iron binding potential that could chelate the 'luminal' iron pool present within the gastro-intestinal tract.

1.3.3 Metal binding fibres as dietary iron chelators; alginates and polyphenols

The human diet consists of a significant proportion of dietary fibres, and it is estimated that on average a typical western diet contains 17.2 g of fibre, with a total of 12.3 mmol uronic acid residues (metal binding sites) per day.[173] It is however difficult to estimate how much of this fibre is responsible for cation binding *in vivo* since other components of the diet and the digestive process (such as pH changes, ionic strength and colonic bacteria) would interfere

with metal binding; for this reason extrapolation of reports of metal binding by fibres *ex vivo* into the human setting need to be carefully justified.[173]   Despite this, there are many accounts of fibres altering metal bioavailability through chelation. [173-182] Not only have fibres been documented to bind metals during digestive transit, but they have also been implicated in the binding of cholesterol, lipids and bile acids.[175, 183] For this reason they have been labelled as 'functional foods' whereby the food plays a greater role than merely providing nutrition, despite originally being thought as an inert substance.[182]

1.4   Alginates

Alginates, are natural polysaccharides found in the cell walls of brown seaweeds.[184] 'Algin' or now known as soluble sodium alginate, was first documented and patented by an English chemist in the late 19th century, which details how alginate can be extracted by soaking seaweed in water or dilute acid, which, following alkali treatment yielded sodium alginate.[185]   Alginates sourced from algae are formed of unbranched (1-4) linked β-D-mannuronic acid (M) and α-L-guluronic acid (G), its C5 epimer (figure 1.16).
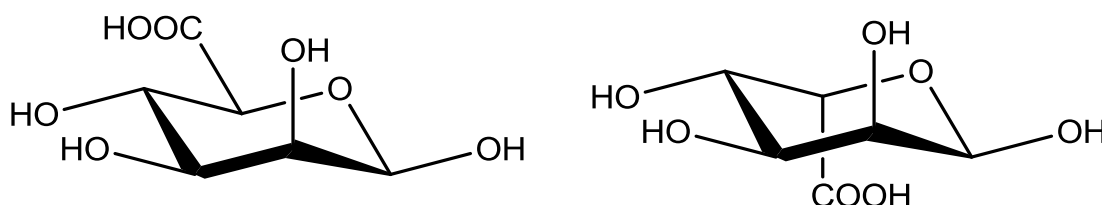
Figure 1.16: Chemical compositions of G and M alginate monomeric units.

The arrangement of G and M residues along the polymeric back-bone sequence is not random but ordered, occurring in alternating GM sequences being heteropolymeric in nature, or

conversely homopolymeric, with extensive M or G block sequences.[186]   The structural

packing of these sequences and the restricted confirmations at the anomeric position of the

ring (the β and α links) has a direct influence on the overall shape of the polymers. Extended

M regions are regarded as 'ribbon-like' whereas extended G regions are 'buckled' (figure

1.17).[187]
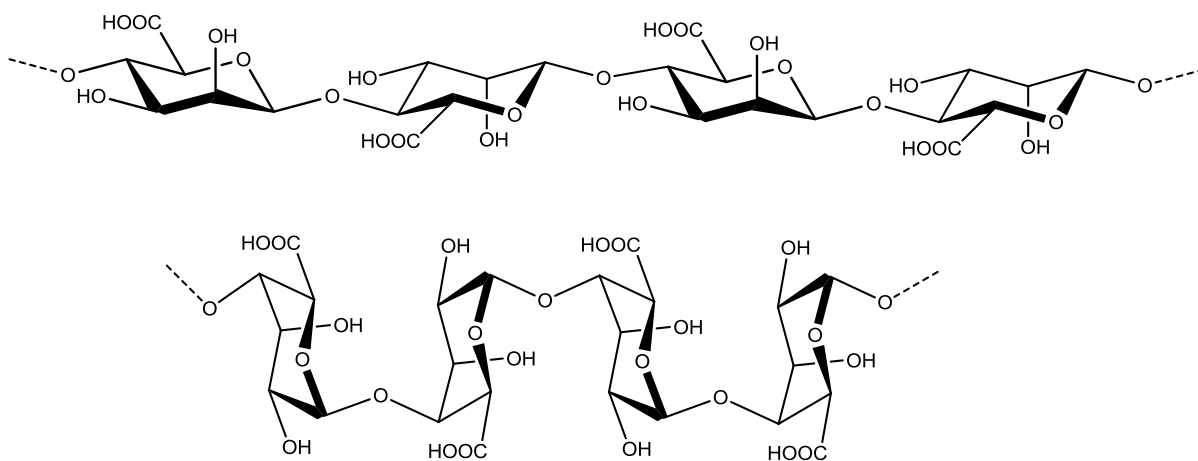
Figure 1.17: Extended M regions of alginate forming so called 'ribbons' and 'buckled' chains
of G sections.[186]

The physical properties of alginate can differ depending on their average molecular weight

and GM sequence throughout the polymer; these structural differences give rise to a plethora

of possible structural compositions that alginates can have.

1.4.1   Alginate variation and chemical properties

Alginate occurs naturally in seaweed in the forms of calcium, magnesium and sodium alginate

salts. The processes in alginate purification from seaweed involves multiple steps of washing

and grinding to extract the raw product from the cell wall. The process of purification can be

varied, thus allowing for the extraction of different alginate fractions which will have

different chemical compositions; one individual source processed in this way can produce a variety of alginate types in terms of their chemical structure.[188] Compositional differences are found between 'alginophytes' that are harvested from different locations.[189] Alginates have no regular repeating unit or sequence arrangement nor can the sequence arrangement be described by Bernoullian statistics; simply, inferring alginate sequence from its monomeric composition is not possible.[190] The use of high resolution ^{1}H and ^{13}C NMR spectroscopy does allow determination of monad composition, F_M and F_G, diad frequencies, F_{GG}, F_{MG}, F_{GM} and F_{MM} and the triad frequencies.[187, 191, 192] Table 1.2 describes the source and sequence parameters of some algal alginates.[185]

Table 1.2: A variety of alginophytes with their respective monad and diad compositions.

Source	F_G	F_M	F_{GG}	F_{MM}	$F_{GM,MG}$
Laminaria japonica	0.35	0.65	0.18	0.48	0.17
L. digitata	0.41	0.59	0.25	0.43	0.16
L. hyperborean (leaf)	0.55	0.45	0.38	0.28	0.17
L. hyperborean (stripe)	0.68	0.32	0.56	0.20	0.12
Macrocystis pyrifera	0.39	0.61	0.16	0.38	0.23
Durvillaea antarctica	0.29	0.71	0.15	0.57	0.14
Ascophyllum nodosum (fruiting body)	0.10	0.90	0.04	0.84	0.06

Alginates with more extreme guluronic acid and mannuronic acid compositions can be isolated from bacteria, namely Pseudomonas and Azotobacter as these organisms express alginate M→G conversion enzymes.[193]

1.4.2 Alginate modification

There are two accessible modifications to the inherent alginate biopolymer; conversion of the monomer stereochemistry (epimerisation) and shortening of chain length (degradation). *De novo* alginates are synthesised as poly-mannuronic acid by the polymerisation of GDP-mannuronic acid, which is then subsequently enzymatically epimerised to the required G:M compositions. Many alginate producing organisms encode more than one mannuronan C-5 epimerase as each epimerase has its unique activity in introducing a specific sequence pattern to the alginate backbone.[194] Alginate epimerases (AlgE) are able to introduce distinct G-sequences in patterns that confer the properties required in a specific alginate tissue. *Azotobacter vinelandii* secrete seven calcium ion dependent epimerases (AlgE1-AlgE7), each having its own unique G-sequence introduction.[194] AlgE1 creates MGMG stretches whereas AlgE6 creates GGG blocks; the other epimerases have mixed activity with some associated lysis activity (figure 1.18).[194-198]
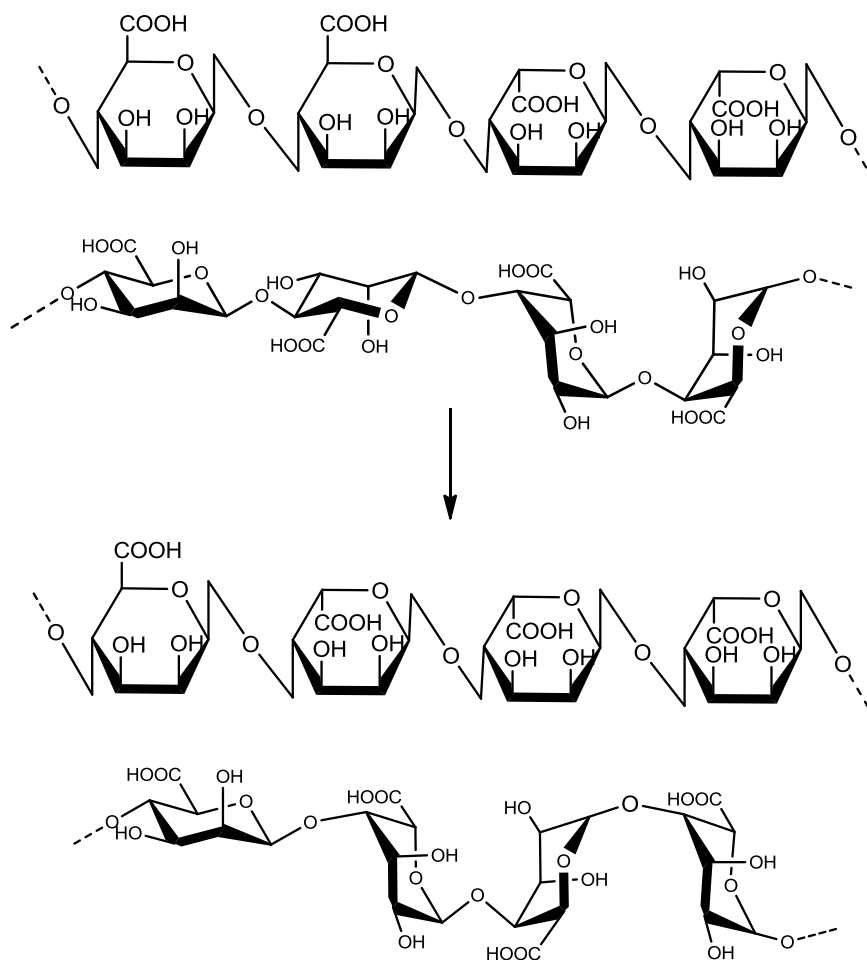
Figure 1.18: Epimerisation of alginate. Top MMGG stretch is converted to a MGGG stretch.

The abundance of glycosidic linkages present in alginate make them a susceptible target to chemical breakage and as such there has been many reported methods to shorten alginate chain length including gamma-radiation,[199] ultra-violet photolysis,[200] lysis enzymes,[201-203] and heat, acid and alkali mediated hydrolysis.[204-206] Heating alginates at moderate temperatures without exceeding 100 °C results in alginate depolymerisation whereas heating to higher temperatures, in excess of 250 °C, alginate breakdown at the monomer level occurs.[207] Depolymerisation of alginates and polysaccharides in general occurs via cleavage of the glyosidic bonds that link the monomeric units in the polymer chain.

Recent investigation have found that the rate of polymerisation of alginates increased with increasing temperatures, with no dependency on rate with respect to G:M composition.[208] In neutral conditions, either an acid catalysed or alkaline mediated hydrolysis may prevail, depending on the function of water, acting as catalytic protons or hydroxide ions respectively (figure 1.19).
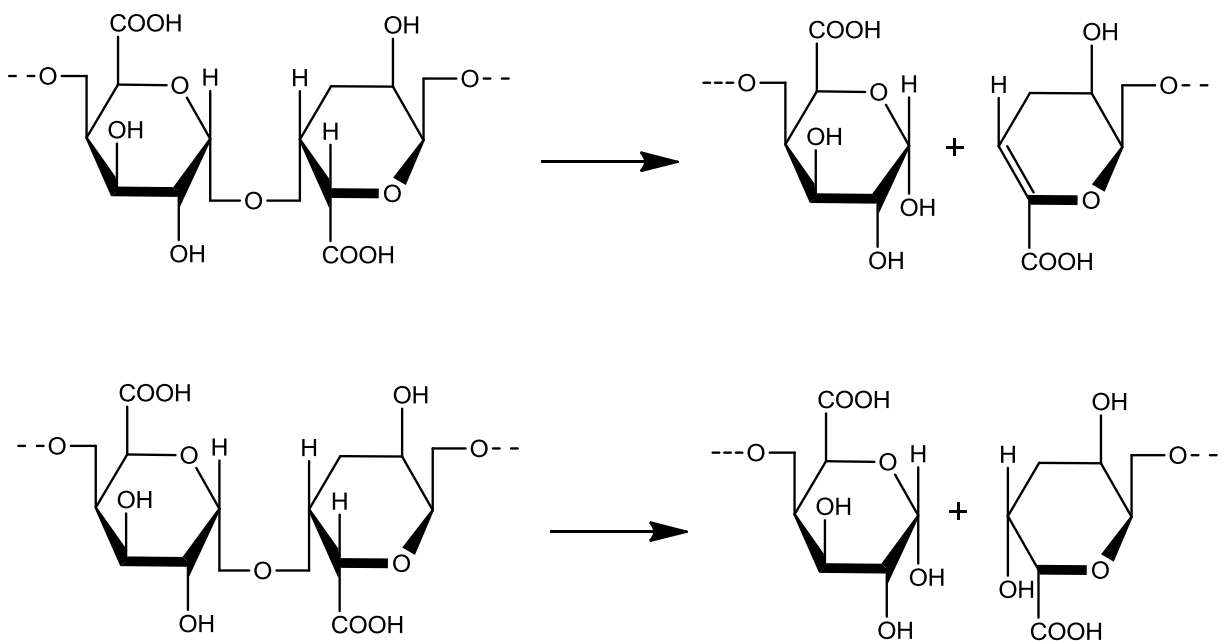
Figure 1.19: Acid-catalysed alginate hydrolysis and alkali mediate beta-elimination reactions to shorten alginate chain length.

.

Viscosity decreases at a hyperbola by time, which is unsurprising since the break of a glycosidic bond within an long alginate polymer chain will have profound effects on viscosity in comparison to a degrade product at longer time points of reaction.[209]

As highlighted, the variation of alginate chemical composition is extensive. Importantly, a plethora of alginate compounds will have to be examined for their iron chelation ability, since chemical structure of alginates impacts iron metal binding ability.

1.4.3   Alginate iron binding

Iron binding by alginate within the gastrointestinal tract was first reported by Berner and Hood (1983) where it is stated "the potential significance of iron binding by polysaccharide gums is twofold. First, a question about iron bioavailability can be raised since these gums generally are not digested in the small intestine where most iron is absorbed. Secondly, the binding of a potent catalyst of lipid autoxidation, such as iron, could be beneficial in food systems subject to oxidative deterioration". [210, 211] In this seminal paper alginates were demonstrated to bind iron as a function of the iron-chelate source (i.e. iron-NTA, iron-EDTA or ferrous sulphate) where alginate-iron chelation did not take with EDTA presence due to effective competition, but binding did occur with NTA. It was established that binding by alginate was not strictly an ionic phenomenon since iron binding decreased with increasing pH levels. Higher pH environments would increase the ionisation of the carboxylic acid residues present on the uronic acid monomers increasing their susceptibility to metal-binding, yet this was not observed. This could also be rationalised by the fact that iron hydroxides (rust), which are insoluble, may have been formed at these higher pH levels, or since alginates gel in more acidic conditions, iron entrapment occurred and as a consequence an observed 'enhanced' iron affinity at these pH's documented. It was also found that calcium severely impacted the iron binding potential of sodium alginate. Subsequent reports demonstrating the iron chelating abilities of alginate in cell culture conditions and *in vivo* are limited.[212,

213] Wöbling *et al.* demonstrated that a dose of sodium alginate fed to mice inhibited the absorption of iron by ca. 20 %.[212] However, it was found that in the ileostomy contents of subjects fed 7.5 g sodium alginate, no significant differences in iron concentration was detected.[213] Two more recent studies have emerged, again with conflicting conclusions. Firstly, in a Caco-2 model of intestinal absorption an enhancing effect of alginate on iron absorption was observed, augmenting ferritin expression by 10-fold; this was also found to be alginate dose dependent.[214] Ferritin is an iron storage protein whose expression is upregulated upon elevated intracellular iron levels. For this reason, ferritin can be used as a surrogate biomarker for intracellular iron concentrations. This finding, contradicted a subsequent report from the same research group detailing decreased iron absorption in individuals administered with alginate in a randomised, single blinded, cross-over human trial.[215] It is noteworthy that the alginates used in each of the studies were chemically different, and this may reflect the structure-activity relationships found between different alginates.

Despite little advancement in physiological alginate-iron interactions, one area of research where alginates and iron are used extensively is in the formation of iron oxide nanoparticles (**FeO-NPs**). Alginates, and biopolymers as a whole are routinely used in the fabrication **FeO-NPs**. Generally a three-step method is employed to synthesise **FeO-NPS**; i) alginate-iron gelation, ii) pH adjustment to form the ferrous hydroxide and iii) subsequent oxidation of the ferrous centre.[216-219] High pH conditions are utilised to force the iron towards the formation of its hydroxide analogue. Despite the growth of interest in this field and the range of biopolymers that are now utilised for this synthesis protocol (for example carrageenans, chitosan and cellulose), the mechanism of nanoparticle formation is still not fully understood; two possible modes of construction have been proposed. The 'site-binding model' describes

the binding of iron ions to the binding site moieties on the polymeric backbone whereas the 'colloidal model' suggests that the iron forms iron-oxyhydroxide precipitates which decorate the polymer (figure 1.20). As inferred within the study, a combination of the two hypothetical models would be more likely on chemical grounds as it is improbable that these two extremes act independently.[220] **FeO-NPS** have found roles in biomedicine for several applications such as i) contrast agents for MRI, ii) drug delivery and iii) magnetic induction hyperthermia.[221]
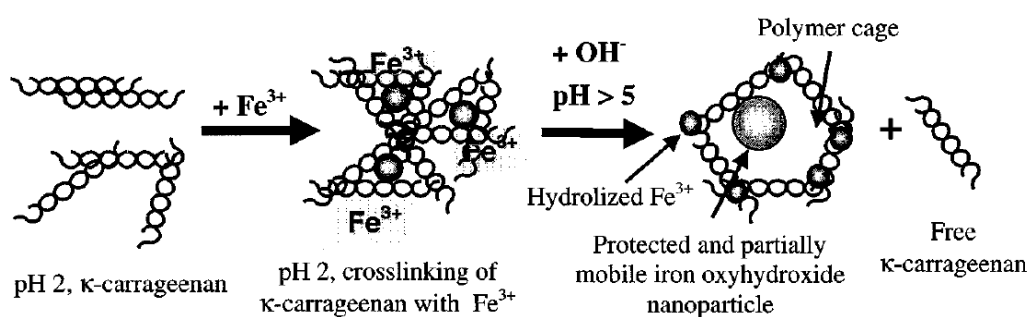
Figure 1.20: Proposed mixed mechanisms of bio-polymer iron binding involving initial metal binding, subsequent nucleation, followed by nanoparticle formation.[222]

The inherent chelating ability of alginates for binding iron, despite the widespread use of alginate-templated **FeO-NP** production, has not been assessed. Limited chemical characterisation of the alginate-iron interaction is reported, with only one publication detailing the iron(III) alginate interaction and calculating a binding constant of $K = 5.04 \times 10^4$ M^{-1}.[223]

In vivo experiments have examined the effect of alginate iron-chelation within the gastrointestinal tract. Harmuth-Hoene and Schelenz fed 10 % polysaccharide enriched diets (including carrageenan and sodium alginate with a specific alginate G:M composition of 13:87) to rats housed in metabolic cages whereby faecal samples could be collected

throughout the duration of the experiment. It was found that sodium alginate significantly decreased both calcium and iron absorption compared to control groups.[224] This indicated that alginate is indeed binding iron at some point along the gastro-intestinal tract and hindering iron absorption across the small intestine; alginate also had an impact on calcium absorption. It was also shown in both normal and iron-deficient rats that a dose of ^{59}Fe could be subject to decreased bioavailability across the jejunum epithelium by half with co-administration of 8-30 mg sodium alginate. Human studies have shown that a dose of oral pectin attenuated iron absorption compared to matched controls. [225] Even though pectin is a different biopolymer to alginate chemically, it is considered as a non-absorbable fibre providing some confidence in the 'luminal' mode of action sought after by sodium alginate.[226] There have been a number of *in vitro* and *in vivo* experiments describing the effects of fibre-like, non-alginate, dietary materials on mineral absorption with some fibres increasing and some decreasing metal solubility and thus having varied effects on overall bioavailability.[173, 227-229]

1.4.4 Alginate bioavailability

Alginate absorbability at the cellular level has not been widely studied, likely due to the fact that alginate is chemically a fibre, based on its polymeric chemical nature and as such is assumed to be inert and non-absorbable.[230] For this reason, alginate is commonly considered a fibre, and indeed studies have shown that alginates are non-absorbable and non-fermentable during gastrointestinal transit.[212, 213, 231, 232]

Most algal polysaccharides are resistant to degradation by human endogenous digestive enzymes.[233] A study undertaken in ileostomy patients had found that 95 % of uronic acids derived from alginates could be accounted for in the ileostomy contents; this does not however account for the fermentation of alginate and its polymeric degradation.[213] Alginate polymeric hydrolysis would not affect uronic acid moieties and as a consequence, uronic acid detection cannot be used as an indication for fermentation processes, it can be used as a readout for alginate presence. Fermentation of alginate to smaller oligosaccharides has been documented; [231] however the microbiota able to ferment alginate required conditioning over time by repeated alginate exposure. There is evidence to suggest that alginates may be degraded via fermentation by human faecal bacteria.[234] These have been identified as anaerobic bacteria from the human colon including Bacteroides and Bifidobacterium.[235] Contradictory to this, the inert nature of alginate within the gastrointestinal tract has been utilised for a treatment in weight management, whereby the very property of limited bioavailability of an indigestible formulation is key to its physiological, 'fat-binding' action.[183, 236] Sodium alginate has been shown to cause significant bio-adhesion with the mucosal membrane, suggesting that the polymeric-nature of the alginate, the must be intact throughout gastrointestinal transit to allow adhesion to the epithelial mucosal layer.[237] This, however, does not necessarily indicate the alginate is chemically intact in its ingested form.

One extensive use of alginates is in drug delivery to control and or sustain the release of therapeutic agents; this again is owed to their non-absorbable nature. Of note, it has been reported that the diffusion rate of release of the entrapped drug can be controlled by the chemical compositions of the alginate, its M:G ratio and its molecular weight.[238] Alginate

forms the main ingredient of the common anti-reflux preparation Gaviscon® whereby its resistant nature to the stomach environment forms so-called rafts inhibiting reflux.[239] The mechanism of action is reliant on the stomach acid and the calcium component of the formulation, since a rigid raft is formed upon the strong interaction of alginate with calcium.

1.4.5   Alginate-alkali metal binding

The calcium binding of alginates has been extensively studied owed to their use in food products as thickeners and gelling agents. It is widely accepted that calcium binds to G-units preferentially as regions of poly-guluronic acid support a further favourable supramolecular interaction; cations of the *perfect* ionic radii will fit into so-called 'egg-box' junctions formed by the lateral interaction of alginate poly-guluronic acid strands.[240] These junction zones chelate calcium ions, which have the right ionic radii to fit into the pre-formed 'pockets' (figure 1.21).[184]
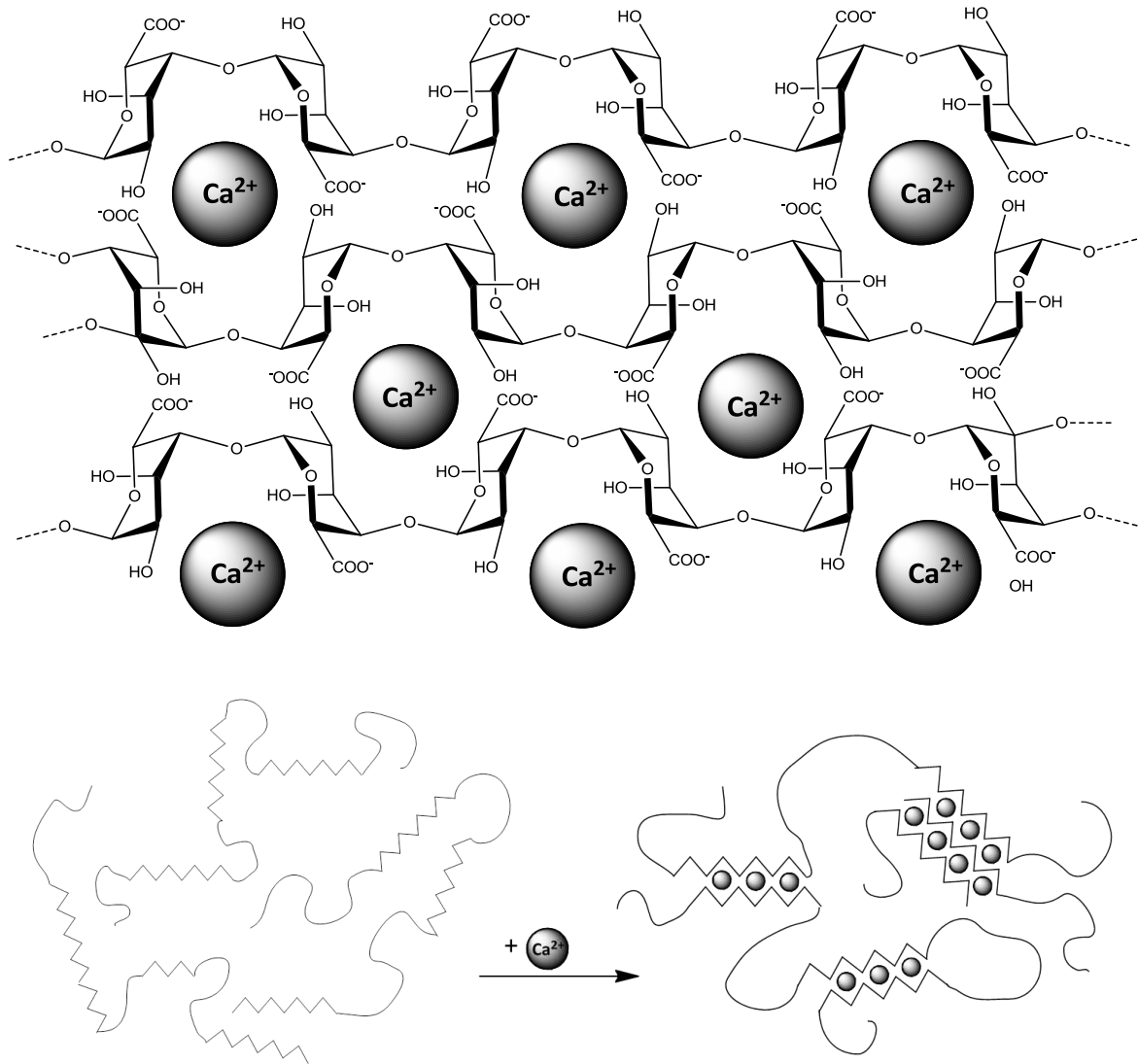
Figure 1.21: Calcium interactions with alginate and formation of 'egg-box' architecture.[184]

It is for this reason that alginates with higher G compositions are mostly found in food products since the gels formed by these alginates will be stronger and more viscous. The changes in alginate structure associated with calcium interaction were monitored by circular dichroism spectroscopy.[241-244] Circular Dichroism (CD) spectroscopy is a spectroscopic technique that uses polarised light, enabling the chirality of compounds to be probed.

Alginate with its many chiral carbons within the uronic acid units as well as its inherent chirality formed by its secondary structure in solution makes it highly applicable in the use of this spectroscopy. It was found that there is a strong auto-cooperative effect observed when calcium ions bind to G-units in which all the functional groups present (hydroxyls and carboxylates) participate in the chelation of calcium. In the same study, it was demonstrated that the transition metals copper, cobalt and manganese only interact with the carboxylate groups, and the hydroxyl groups do not participate in the binding to metal ions for both the G-units and M-units equally.[245]

These results raise the question of the relationship between ionic radii and the strength of alginate chelation, and whether ionic radii of iron could be used as a predictive tool to provide insight as to whether it would bind to alginate in the well-defined 'egg-box' structure (table 1.3).

Table 1.3: Listed values of ionic radii for group two metal ions, first row transition metals and group three metal ions. LS and HS donate the electron arrangement in the *d*-orbitals, high spin and low spin respectively.[147]

	Element	Ionic radius/ pm	Charge on ion	
Group 2	Be	27	2+	
	Mg	72	2+	
	Ca	**100**	**2+**	
	Sr	126	2+	
	Ba	142	2+	
First row *d*-block	Cr	73	2+	LS
		80	2+	HS
		62	3+	
	Mn	67	2+	LS
		83	2+	HS
		58	3+	LS
		65	3+	HS
		39	4+	
		53	4+	
	Fe	**61**	**2+**	LS
		78	**2+**	HS
		55	**3+**	LS
		65	**3+**	HS
	Co	65	2+	LS
		75	2+	HS
		55	3+	LS
		61	3+	HS
Group 13	B	88	3+	
	Al	130	3+	
	Ga	122	3+	
	Ln	150	3+	
	Tl	155	1+	

It is found that the binding affinity of group II metal ions for alginate follows the series $Ba^{2+} > Sr^{2+} > Ca^{2+} \gg Mg^{2+} > Be^{2+}$ indicating that the larger the ionic radii, the greater the energetic gain when complexation occurs in this way.[246-248] This does however depend on the

composition of the alginate under investigation and the mode of interaction (i.e. if the metal ion allows for alginate cross-linking as with calcium). Taking into account these approximations, it could be argued that iron will not conform to the egg-box model of binding since all energetic states of the ferrous and ferric forms are much smaller than that of calcium. As discussed earlier, it has been shown that cobalt and manganese only interact with the carboxylate units; having similar ionic radii and charge densities as iron it can be predicted iron will interact with alginate in a very different way to calcium.[245]

The binding constant (K) for calcium binding to alginate was calculated to be 10.7×10^3 and 10.6×10^3 M^{-1} for 64 and 46 % G-unit composition alginates respectively.[249] This is unsurprising since K relates to the affinity for binding within the binding site (the egg-box) which would be analogous for both samples. The enthalpy of interaction between the two samples which refers to the strength of binding was different, calculated to be -15.0 and -11.6 kJ mol^{-1} respectively.[249] This suggests that the higher the G-composition of the alginate, the stronger the strength of interaction with calcium.

1.5 Polyphenols

Specificity towards iron would be an ideal property of a medicinal iron chelator, and interactions with other metal cations may prove problematic (as with alginates); polyphenolic compounds are a range of compounds that have a high specificity towards iron ions. Polyphenol compounds are found in fruits and vegetables and form a significant constitute of our everyday diets.[250] Polyphenol-containing compounds represent a huge 'chemical catalogue' of natural compounds. They all share similar chemical moieties containing either catechol or galloyl units, which were described in section 1.3.2 to be the unit of choice when

designing chemical iron chelators. Polyphenols of fruit and vegetable origin share a similar

chemical base unit, namely, the 'flavin'. This three-membered ring system can be decorated

in many chemical poly-hydroxyl phenol compounds which are then loosely termed

flavonoids. Specifically, fla**van**oids are non-ketone containing in contrast to the ketone

containing fla**von**oid. Flavan-3-ol is the simplest flavonoid which is also known as flavanol

and is chemically similar to the common polyphenol (+/-)-catechin (figure 1.22).
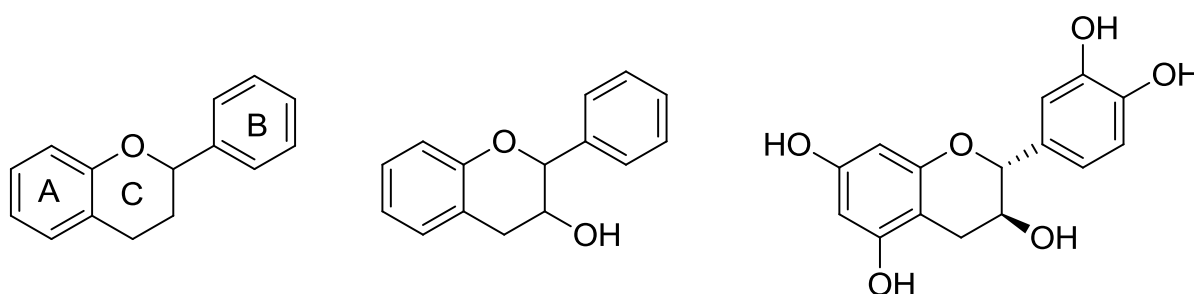
Figure 1.22: Chemical structures of flavin, flavan-3-ol and polyphenol (+)-catechin.

Quercetin, the ketone-containing analogue of catechin is highly concentrated in onions.[251]

Being of natural sources the glycosylation of these compounds is a common chemical

modification; rutin is chemically identical to quercetin yet is glycosylated (figure 1.23).
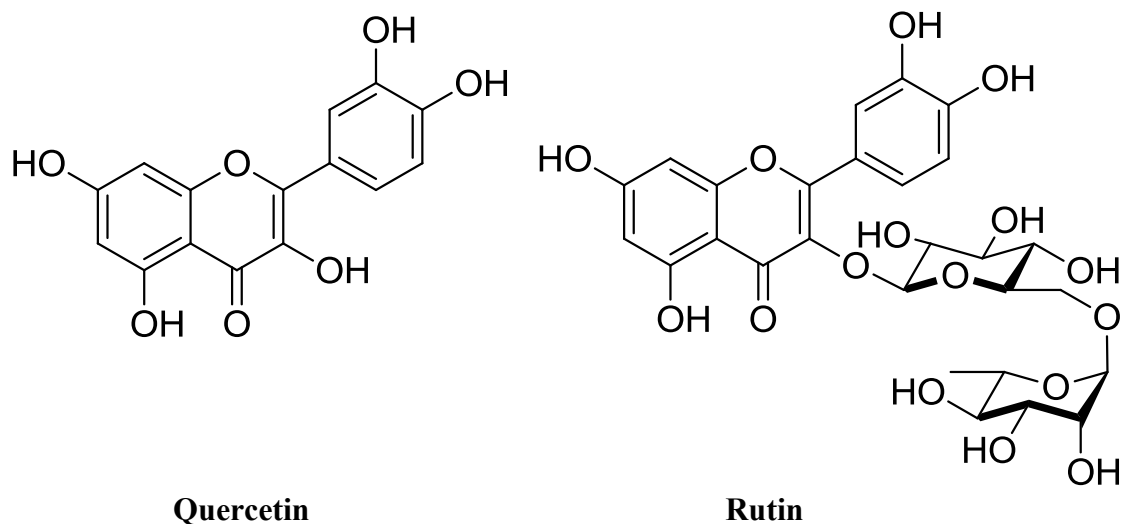
Quercetin   **Rutin**

Figure 1.23: Chemical structures of quercetin and rutin.

Rutin (quercetin-3-rutinoside) is highly concentrated in asparagus, citrus fruit rinds and many berries.[252] As it contains catechol units and also a 1,3,-hydroxy ketone moiety there are two possible iron binding sites.

Anthocyanins are related to flavanols, but are ionic forms. Anthocya**nid**ins are the aglycone forms of anthocy**an**ins. Cyanidin-3-O-glucoside is an anthocyanin with chemical similarity to the polyphenol compounds discussed (figure 1.24). Anthocyanins such as cyanidin-3-O-glucoside are mainly found in dark fruit berries such as blackcurrant, blackberry, strawberries and blueberries.[252, 253]
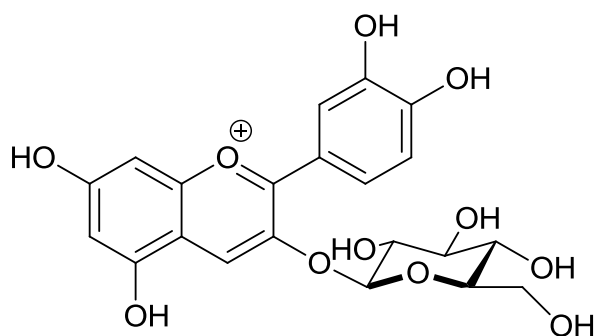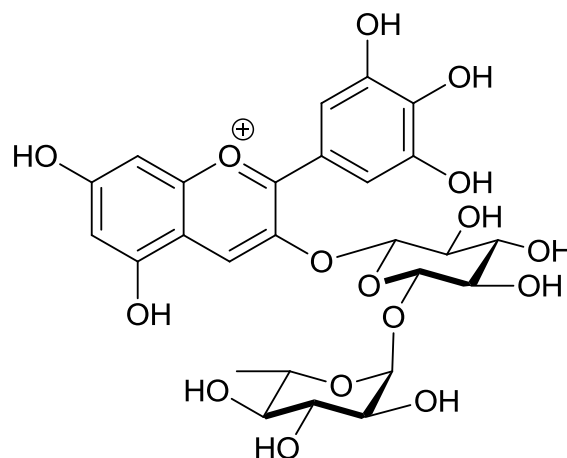
Cyanidin-3-O-glucoside   **Delphinidin-3-O-rutinoside**

Figure 1.24: Chemical structure of cyanidin-3-O-glucoside and delphinidin-3-O-rutinoside.

In relation to addressing polyphenolic iron-binding characteristics, a simplistic view of how polyphenols complex with iron would be to examine the individual iron binding moieties on the polyphenols alone and extrapolate the findings across the different polyphenolic compounds that withhold that moiety within the basic flavonoid structure. A similar study was performed by Khokhar *et al*. and specific functional groups were identified as necessary for iron binding (figure 1.25).[254]

1) Ortho-dihydroxyl groups;

2) 5-OH and or 3-OH in conjunction with a C4 keto group; and

3) A large number of OH groups.
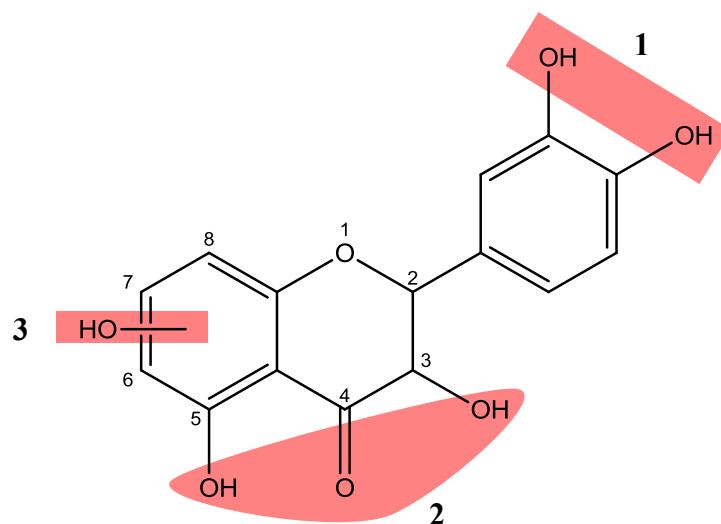
Figure 1.25: Chemical requirements (highlighted in red) of a flavonoid to demonstrate iron binding properties.

These findings allow for an initial screen of the potential polyphenolic compounds to be tested. With this, and in the focus of this thesis, four polyphenolic compounds were selected, namely, quercetin, rutin, catechin and cyanidin-3-glucoside (figure 1.26). This compound selection provides a range of functionality homology to assess the potential differences in iron binding with respect to structure.
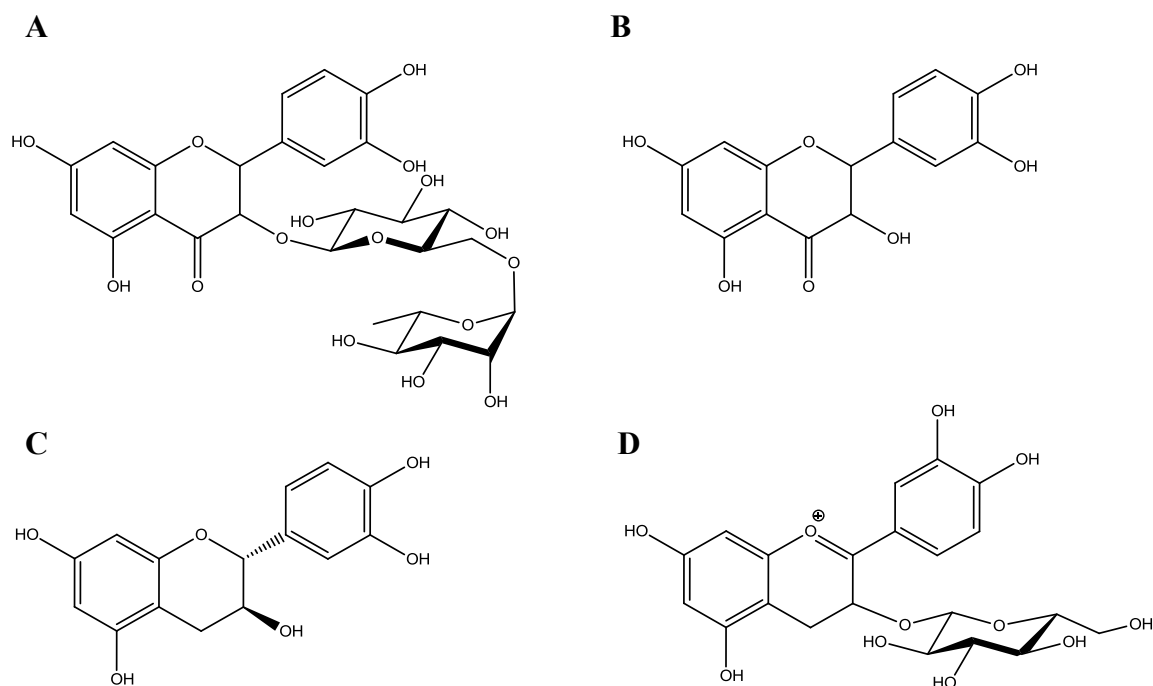
Figure 1.26: Chemical structures of (A) rutin, (B) quercetin, (C) catechin and (D) cyanidin-3-O-glucoside.

1.5.1 Quercetin iron binding

Quercetin is markedly the most studied polyphenol with respect to its iron binding properties and bioavailability, undoubtedly owed to the fact that consumption of quercetin exceeds that of any other polyphenol (estimated between 6 – 18 mg per day).[255-259]   Quercetin has three potential binding sites and among the different stoichiometries accessible, namely the 1:1, 1:2, 2:2 and 2:3 metal: quercetin complexes; the 1:2 complex is the most energetically stable and as such is preferred despite not fulfilling the desired hexa-coordinate coordination sphere of iron ions (section 1.3).[260-262] Using electrospray ionisation mass spectroscopy, the preferred complexation site for iron is that where by the hydroxyl at C3 or C5 acts as donor sites with the adjacent 4-carbonyl (figure 1.27).[263]   This correlates with the potentiometric data that suggests with most acidic proton of quercetin is indeed the hydroxyl group at position C3 with a pKa calculated to be 6.7).[264]
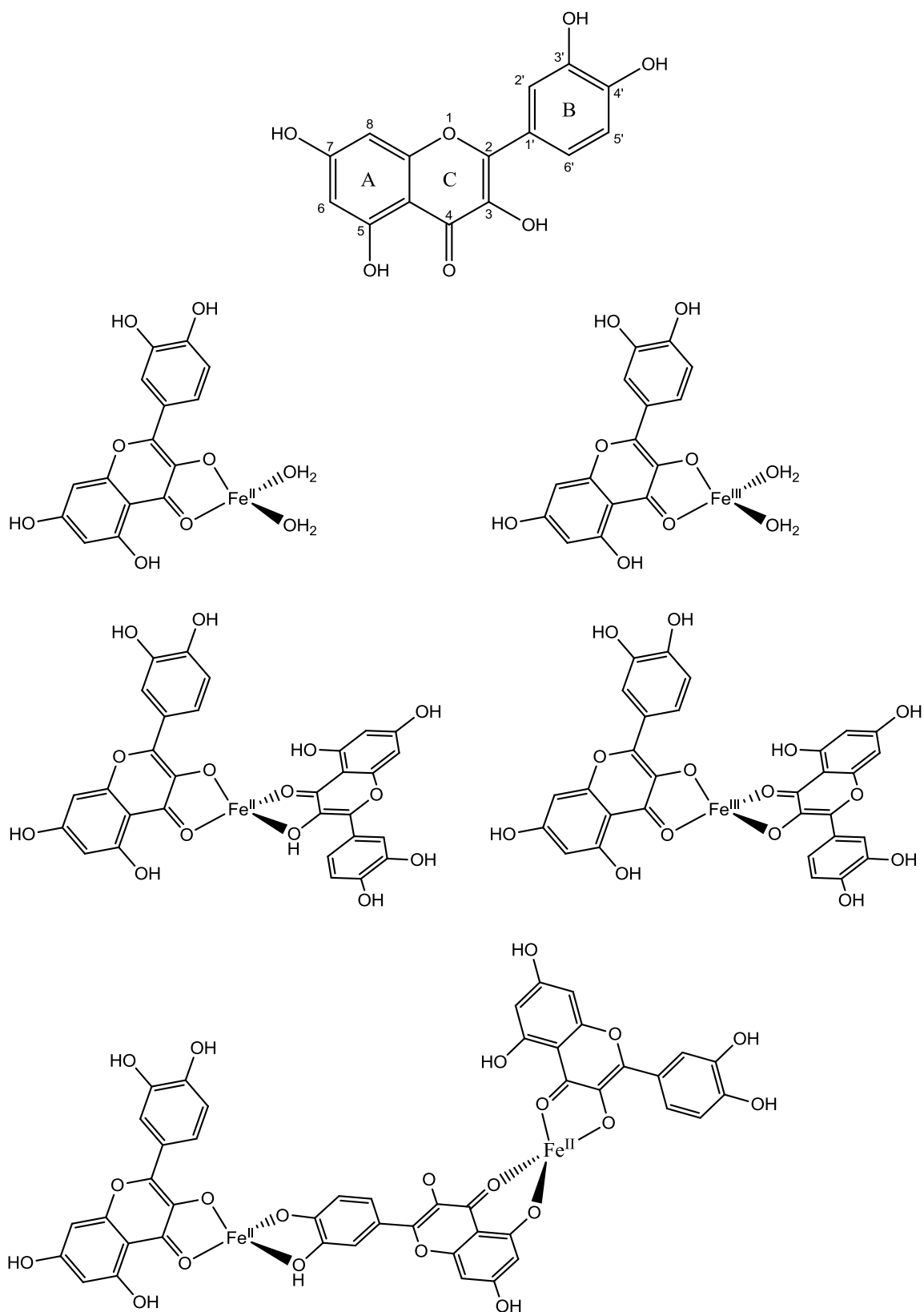
Figure 1.27: Chemical structure of quercetin (3, 3', 3', 5, 5-pentahydroyflavone) and its complexes with ferrous and ferric iron.

Iron binding constants have been estimated for the mono- and di- iron complexes in physiological pH environments, and calculated to be between $K = 10^6 - 10^7 \, M^{-1}$.[265]

The well documented pro-radical generation nature of iron, in hand with the iron binding ability of quercetin means that there have been several reports of iron chelation *in vitro* and *in vivo*.[257, 266-272] Quercetin in many studies has been found to be a potent inhibitor of intestinal iron absorption, which if mediated through iron chelation within the lumen would make quercetin an ideal small-molecule chelator for luminal iron chelation. It was shown using microsomes from rat liver that quercetin prevented iron-induced lipid peroxidation, concluding on a radical blocking mechanism via iron chelation.[273] Many anti-oxidant actions of quercetin have been reported.[267, 268] Quercetin has also been identified as a shuttle for labile iron, whereby quercetin binds labile plasma iron and transfers it into transferrin; it was also observed that quercetin decreased intracellular iron pools with the resultant iron-quercetin complexes able to cross the cell membrane to allow cellular export.[269] Further to this, it was identified that quercetin-iron complexes can be transported via glucose transporters (GLUTs), whereby complexes were exported via GLUT1 to decrease cellular iron levels.[266, 274] Despite this wide range of reports demonstrating quercetin's anti-oxidant effect via an iron-chelation mediated process *in vitro*, there have been recent reports of a direct action of quercetin on molecular targets to control intracellular iron metabolism.[257] It was found that quercetin decreased intestinal ferroportin expression in rat duodenal cells with an associated down regulation of DMT1, yet the mechanism of this process was unclear.[257] Through the use of methylated quercetin analogues the chelation of iron by quercetin was highly reliant on the 3-hydroxy group, which maybe translatable in understanding the iron binding properties of other polyphenolic compounds.[275]

1.5.2 Quercetin bioavailability

In general quercetin bioavailability is poor, yet reports in the literature are highly inconclusive.[276] In a study undertaken with ileostomy patients who were orally administered quercetin in different formulations, it was found that quercetin aglycone absorption was 24 % lower compared to the glycoside which enhanced its absorbability.[250] In rats fed diets with supplemented quercetin, absorption was incident within the small intestine however plasma levels were low.[277] It is argued that the complex metabolic pathways of quercetin warrants a need to take into consideration its metabolites to get a fuller understanding of its degradation. One recent study, which employed the use of a radioactive labelled analogue of quercetin confirmed a bioavailability of 44.8 %.[278] This is conclusive evidence of the definite disposition of quercetin, since the absorbability of its metabolites (only if radiolabelled themselves) are considered in the whole calculation of absorbability. With an inconclusive yet largely low bioavailability, efforts are being made to formulate quercetin in a way to render its cellular absorbability much higher.[279, 280]

Notwithstanding the conflicting evidence on quercetin bioavailability, bacterial-metabolism studies have been performed which have confirmed degradation by intestinal microbiota.[281-283] Whether this degradation produces iron-chelating fermentation bi-products that are themselves non-bioavailable, is unknown. Quercetin is metabolised by *Bacteroides*, *Clostridium* and *Eubacterium* via ring cleavage reactions and dihydroxylation, to yield a range of phenolic acids (figure 1.28).[284, 285] It is evident upon consideration of the chemical structures of the degradation products that they would also possess iron-binding activities.
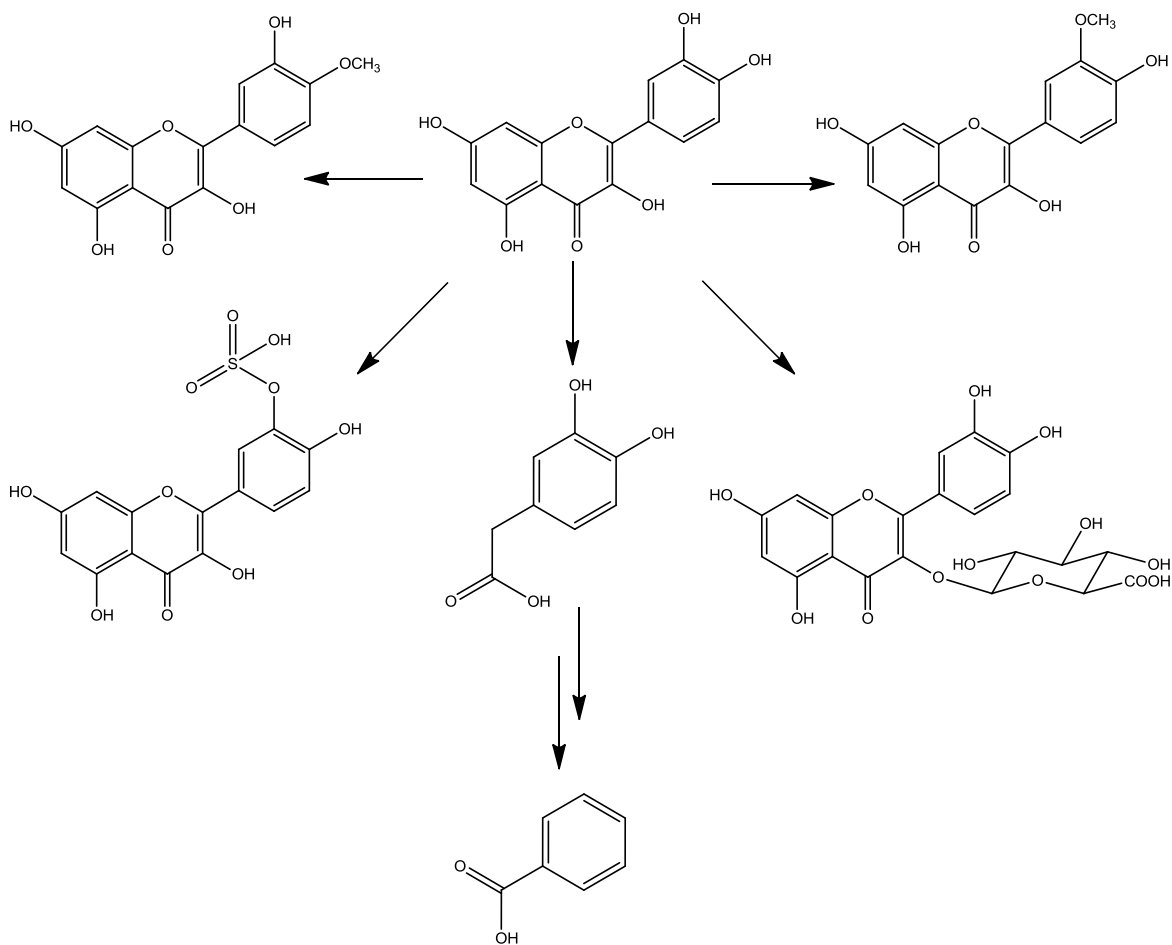
Figure 1.28: Chemical modification of quercetin by colonic microbiota.[278]

1.5.3 Quercetin efficacy against colorectal cancer

Both *in vitro* and human studies largely support an anti-cancer function of quercetin, though it is unknown as to whether the anti-cancer action of quercetin is directed through its iron chelation properties.[286]

In one human study with a cohort of nearly 10, 000 participants, an inverse relationship between dietary intake of quercetin (ca. 4 mg each day) and colorectal cancer incidence was observed.[287]   Furthermore, flavonoid intake has been shown to decrease the risk of

advanced adenoma reoccurrence in patients with a previous history of colorectal adenoma.[288]

In vivo and *in vitro* studies also demonstrate an inverse relationship between quercetin and carcinogenesis. A study performed in rats with colorectal cancer, induced using azoxymethane found that a 10 g kg^{-1} quercetin supplemented diet, dose dependently decreased the tumour incidence, multiplicity and size compared to the control cohort.[289] This protective effect was explained through a decreased cell proliferation and apoptosis induction activities, which has been reported previously reducing crypt cell proliferation by 50 % in the small intestine of healthy rats.[290-292] These effects and mechanisms have also been supported by studies *in vitro*.[293, 294] Of most interest is work carried out by Murphy *et al.,* who, using ApcMin/+ mice reported that administration of a 0.2 % quercetin diet decreased total intestinal polyp formation by 67 % compared to the placebo cohort.[295] This effect was attributed to quercetins ability to reduce the inflammatory response of macrophages, which contributes to the carcinogenic phenotype of the cell.[296] Most recently it has been shown that quercetin can reduce circulating IL-6 plasma levels in the ApcMin/+ mouse.[297]

1.5.4 Rutin iron binding

Rutin (quercetin-3-O-rutinoside) can be considered the glycone of quercetin (figure 1.29).
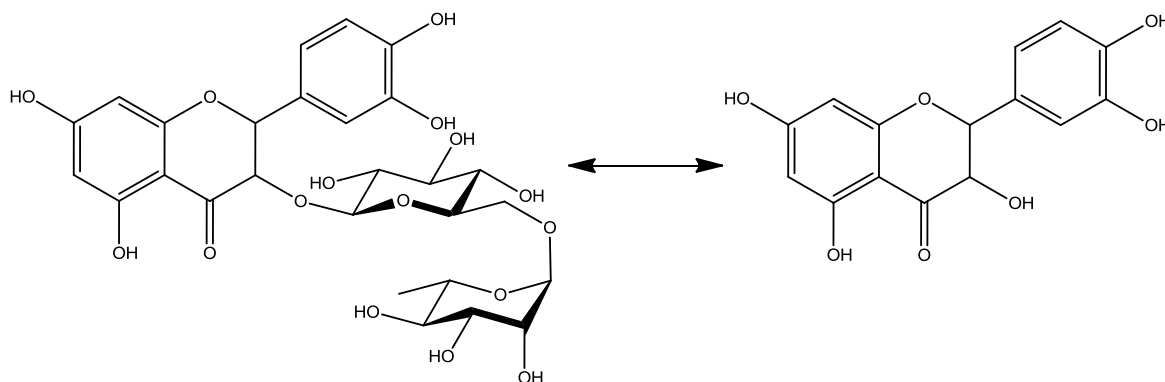
Figure 1.29: Chemical similarity of rutin and quercetin.

Its chemical interaction with iron has been seldom studied, yet several reports have documented important complexation results.[265, 298-300] The most favourable complex of iron with rutin is the 1:2 metal: rutin complex, with the full octahedral coordination sphere completed by two coordinating water molecules.[298] In comparison to quercetin, which has three iron binding sites, rutin nominally has two due to the third being blocked by the sugar moiety (figure 1.30).
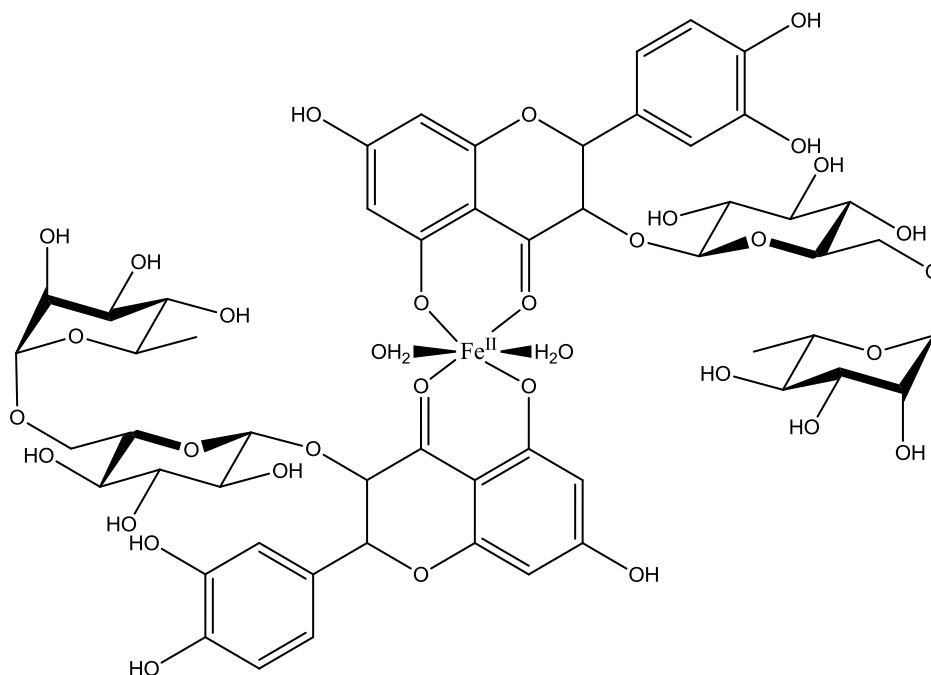
Figure 1.30: Chemical structure of the di-rutin iron complex.

The di-rutin iron complex has been shown to have iron binding constants of $4 \times 10^{11} - 1 \times 10^{12}$ M^{-2}.[265, 300] Spectroscopic studies have demonstrated the inert properties of the ferrous-rutin complex at physiological relevant pH yet there is evidence to suggest that rutin is chemically labile with respect to ferric iron interaction, whereby a direct oxidation reaction is observed upon interaction.[299]

1.5.5 Rutin bioavailability

Degradation of rutin to quercetin has been documented within the large intestine and as such, *in vivo* activity of rutin has been reported to be mainly attributed to its metabolite quercetin.[297] Rutin is poorly absorbed in the intestine; only in the large bowel does hydrolysis by gut microbiota take place.[301] A human study involving the oral administration of 200 mg rutin revealed no rutin presence within the plasma or urine.[302] It

59

is argued that the lower absorption profile of rutin in comparison to quercetin is due to its glycosylation status which hinders its bioavailability.[277, 303]

1.5.6   Rutin efficacy against colorectal cancer

Upon review of the literature supporting the anti-cancer action of rutin, it is evident that its effects are largely dose dependent. In mice with colonic neoplasia induced with azoxymethanol, the cohort fed a 4 % rutin containing diet demonstrated the fewest number of colonic dysplasias whereas lower concentrations displayed no discernible effects.[304] In a later study, no effect was observed in the ApcMin/+ mouse fed a 2 % rutin containing diet.[305] Again, lower rutin diet concentrations had no chemopreventive effect in azoxymethane induced foci in the rat colon, compared to a higher concentration which did decrease foci statistically by 78 % compared to control.   Similar studies have also been documented.[292, 306, 307] With respect to a mechanistic understanding of these protective effects, inductions of apoptosis and cell cycle arrest have been implicated.

1.5.7   Cyanidin-3-O-glucoside iron binding

The only documented evidence of Cyanidin-3-O-glucoside iron binding is in a study monitoring changes in peach-skin colour by the formation of iron-pigment complexes such as iron-Cyanidin-3-O-glucoside.[308] No other studies have reported evidence of iron binding.

1.5.8 Cyanidin-3-O-glucoside bioavailability

The fact that anthocyanin consumption is greatest out of all the flavanols ($180 – 215$ mg day^{-1} cf. 23 mg day^{-1} for quercetin), the bioavailability and metabolism profile of cyanidin-3-O-glucoside has been extensively studied and, in comparison to other polyphenols discussed here, the evidence is more consistent.[309] Studies undertaken in animals and man suggest that cyanidin-3-O-glucoside is absorbable.[310-315] Formulations containing cyanidin-3-O-glucoside were detected in the blood stream of rats and man in their intact glycosylated forms.[311] Further experimentation using nasal intubations directly into the jejunum in humans demonstrated that the main site of absorption is the small intestine,[313] this was confirmed in rats with 22 % of the administration absorbed in the jejunum and ileum.[314] No absorption has been documented to take place within the colon.[316] Understanding the integrity of polyphenols reaching the large intestine and colon intact have been performed and it was found that 28 % of administrated cyanidin-3-O-glucoside reached the large intestine in ileostomy patients.[317] In a complementing study, 44 % of administered cyanidin-3-O-glucoside in humans were recovered in the faeces, albeit, metabolites of the anthocyanin; this suggests that most cyanidin-3-O-glucoside entering the large intestine is excreted in the faeces (figure 1.31).[318]
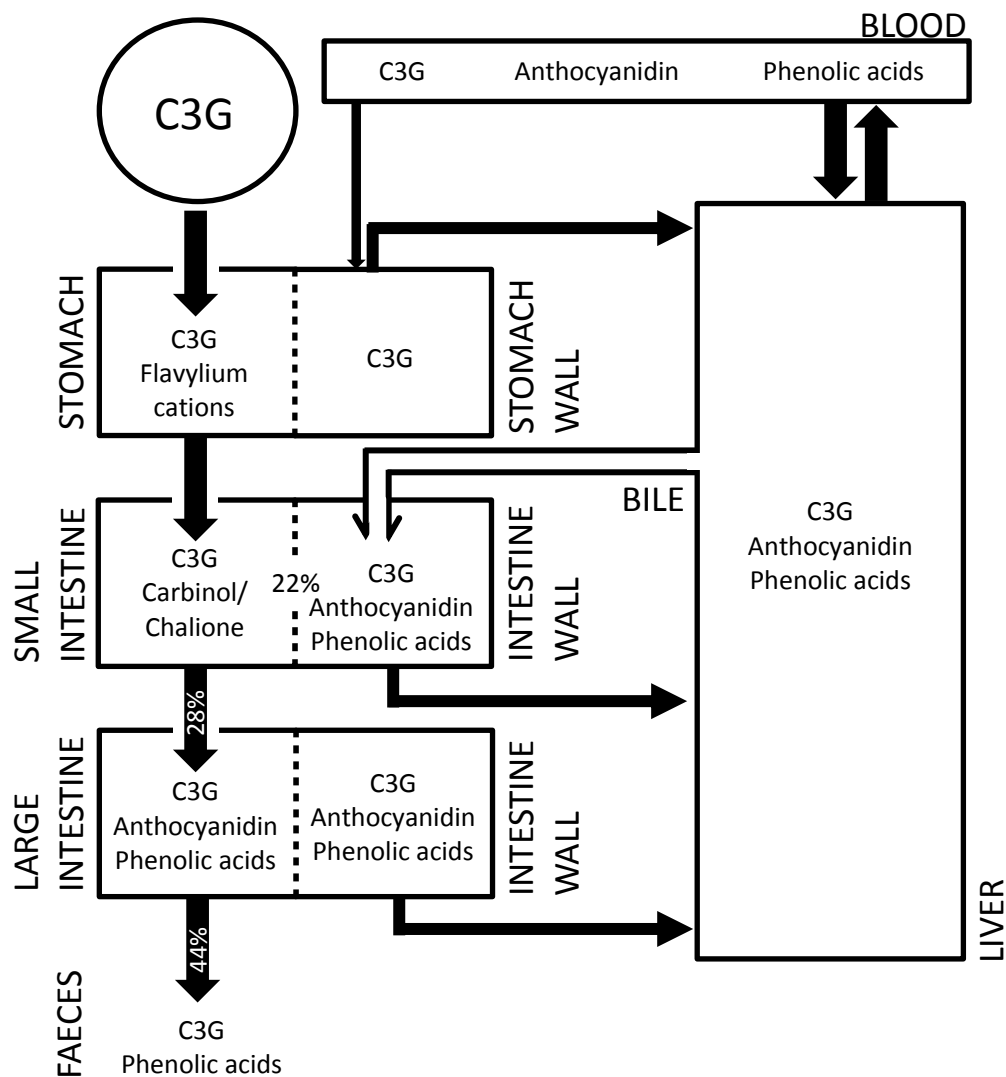
Figure 1.31: Distribution and absorption profile of Cyanidin-3-O-glucoside (C3G).[316]

Degradation of cyanidin-3-O-glucoside by the intestinal microbiota is also well understood. A total of 35 metabolites were identified in humans administered a radio-labelled cyanidin-3-O-glucoside, of which 28 were found in the faeces.[319] The microbiota in the large intestine responsible for anthocyanin decomposition have been identified.[320, 321]

Despite the unequivocal data demonstrating cyanidin-3-O-glucoside absorbability by intestinal enterocytes, it is not 100 % bioavailable with some intact cyanidin-3-O-glucoside remaining for activity within the colon which maybe of importance.

1.5.9 Cyanidin-3-O-glucoside efficacy against colorectal cancer

There is a plethora of *in vitro* data which demonstrates different anti-cancer actions of cyanidin-3-O-glucoside albeit none rationalised by cellular iron metabolism alterations.[322-326] Mechanistic understanding of the results revealed possible cell-cycle arrest, inhibition of TNF-induced activation of cyclooxygenase and suppression of TNF-induced NK-κB-dependent reporter gene transcription.[327] There are no *in vivo* reports on the activity of cyanidin-3-O-glucoside in colorectal carcinoma.

1.5.10 Catechin iron binding

Despite catechin being a chemically simple compound there is considerably less data describing its iron binding ability.[328] Unlike cyanidin-3-O-glucoside, this may be attributed to its poor iron-chelation ability since it only conforms to one of the three original requisites for iron binding, namely, ortho-positioned hydroxyl groups.[254] In spite of this, a recent report documented the iron-binding of catechin *in vitro* to increase intracellular iron concentrations in the caco-2 model of intestinal absorption. There are two possible mechanisms by which catechin maybe increasing cellular iron. Firstly, the presence of catechin might be increasing the solubility of iron within the cellular environment, promoting its uptake at membrane-bound transport sites.[328] Secondly, as discussed for rutin,

oxidation by catechin may be occurring such that any ferric iron present will be reduced to ferrous iron rendering it more bioavailable to the cell.[329]

1.5.11 Catechin bioavailability

Catechin has poor stability and poor oral bioavailability due to its high hydrophilicity which imparts low lipid solubility and hence limited penetration through the cell membrane.[330-332] Interestingly there are significant bioavailability differences between (+)-catechin and (-)-catechin despite only being enantiomers.[333] In human ileostomy studies a 350 mL polyphenol rich drink that contained ca. 127 µM catechin was administered and following a 24 hour time period, ileal fluid and urine was analysed for catechin presence.[334] It was concluded that catechin was non-bioavailable since > 100 % was recovered in the ileal fluid, and only 20 % detected within the urine of the treatment cohort. There are many reports that suggest catechin is mainly non-bioavailable with slow plasma concentrations detected in humans post consumption.[251, 335, 336]

1.5.12 Catechin efficacy against colorectal cancer

Several *in vitro* reports have confirmed the antiproliferative effects of catechin, although these effects have been minimal.[337, 338] These unconvincing results have been mirrored in epidemiological studies, with mixed conclusions correlating catechin intake and colorectal cancer incidence.[339, 340]

1.6   Summary and conclusions

The evidence discussed eludes to the carcinogenic nature of excess, unabsorbed, 'free', luminal iron present in the colon.[93, 120] The exact form of iron within the colon is yet to be elucidated, however it is known that 'free' iron is the redox cycling form.[54] Exactly how iron is driving tumorigenesis in this setting is unknown, yet possible mechanisms have been proposed including the activation of Wnt and the generation of ROS.[113, 341] It has been demonstrated how systemic iron chelators are widely used within a clinical setting and some evidence suggests anti-neoplastic activity of these plasma-circulating iron chelators.[115, 155, 168] Iron chelators targeted at sequestering 'luminal' iron have not been developed to date, yet a range of dietary iron chelating compounds have demonstrated iron binding activity although not in the setting of the colorectal cancer.[212] If such a dietary iron chelator was to be used as a therapy in this setting, the design of an iron chelator would need to fulfil the following criteria:

i)   To be non-absorbable within the gastrointestinal tract.

ii)   To be non-fermentable by the colonic microbiota.

iii)   To bind iron with a high affinity, with selectivity, removing it from the colon.

iv)   Preferable iron binding in the colon.

v)   To be a natural, and safe for human consumption.

The range of dietary iron chelators discussed all fulfil these criteria.

1.6.1 Research hypothesis and aims

The hypothesis formed upon consideration of the literature is such:

Excess luminal iron present within the colon is having a detrimental effect on gastrointestinal health, especially in relation to colorectal cancer. The development of a luminal iron chelator that will chelate and sequester excess 'free iron' present in the colon, will as such be a therapeutic platform to improve gastrointestinal health

Such a task will require the fundamental effects on iron metabolism by iron chelators to be assessed as it has been discussed how iron chelation within the gastrointestinal tract can render iron more or less bioavailable. This study will focus on the chelation of 'free' iron, despite the fact that it is unknown what form of iron is within the colon. With respect to the pathological progression of colorectal cancer, evidence suggests that earlier detection of benign polyps allows for improved clinical outcomes. Iron has been demonstrated to drive these initial events in carcinogenesis and as such, it could be envisaged that a luminal iron chelator could be given as either a chemopreventive measure to high-risk patients, or as an intermediary intervention for those identified with polyps or adenomas.

The aims of the research presented in this thesis are:

1) To assess the iron chelation ability of a range of alginate and polyphenol compounds and identify, through iron-binding stratification experiments, the best iron chelators with therapeutic potential.

2) To examine the effects of alginates and polyphenols on iron metabolism *in vitro* and *in vivo* and to determine their physiological actions.

3) To understand how iron chelation bioactivity is related to the chemical composition of the alginates and polyphenols.

A chelator which can bind iron within the colon will be novel, not only for the treatment and prevention of colorectal cancer but also for use in other gastrointestinal diseases that are exacerbated by the toxic effects of iron.

1.7 References

1. Kohgo, Y., et al., *Body iron metabolism and pathophysiology of iron overload.* International Journal of Hematology, 2008. **88**(1): p. 7-15.
2. Andrews, N.C., *Disorders of Iron Metabolism.* New England Journal of Medicine, 1999. **341**(26): p. 1986-1995.
3. Solomon, E.I., A. Decker, and N. Lehnert, *Non-heme iron enzymes: contrasts to heme catalysis.* Proceedings of the National Academy of Sciences, 2003. **100**(7): p. 3589-3594.
4. Mims, M.P. and J.T. Prchal, *Divalent metal transporter 1.* Hematology, 2005. **10**(4): p. 339-45.
5. Boron, W.F. and E.L. Boulpaep, *Medical Physiology, 2e Updated Edition: with STUDENT CONSULT Online Access.* 2012: Elsevier Health Sciences.
6. Fleming, R.E. and B.R. Bacon, *Orchestration of Iron Homeostasis.* New England Journal of Medicine, 2005. **352**(17): p. 1741-1744.
7. Seril, D.N., et al., *Systemic iron supplementation replenishes iron stores without enhancing colon carcinogenesis in murine models of ulcerative colitis: Comparison with iron-enriched diet.* Digestive Diseases and Sciences, 2005. **50**(4): p. 696-707.
8. USDA, *National Nutrient Database for Standard Reference*, T.N.A. Library, Editor. 2013.
9. Smith, M.E. and D.G. Morton, *The Digestive System: Systems of the Body Series*. 2011: Elsevier Health Sciences.
10. Collins, J.F. and G.J. Anderson, *Chapter 71 - Molecular Mechanisms of Intestinal Iron Transport*, in *Physiology of the Gastrointestinal Tract (Fifth Edition)*, L.R.J.K.G.D.K.L.M.M.S.D. Wood, Editor. 2012, Academic Press: Boston. p. 1921-1947.
11. Cook, J.D. and M.B. Reddy, *Effect of ascorbic acid intake on nonheme-iron absorption from a complete diet.* The American journal of clinical nutrition, 2001. **73**(1): p. 93-98.
12. Graham, H.N., *Green tea composition, consumption, and polyphenol chemistry.* Preventive medicine, 1992. **21**(3): p. 334-350.
13. Jin, F., et al., *Effects of ascorbic acid, phytic acid and tannic acid on iron bioavailability from reconstituted ferritin measured by an in vitro digestion-Caco-2 cell model.* Br J Nutr, 2009. **101**(7): p. 972-81.
14. Schlemmer, U., et al., *Phytate in foods and significance for humans: food sources, intake, processing, bioavailability, protective role and analysis.* Mol Nutr Food Res, 2009. **53 Suppl 2**: p. S330-75.
15. Lucca, P., R. Hurrell, and I. Potrykus, *Fighting iron deficiency anemia with iron-rich rice.* Journal of the American College of Nutrition, 2002. **21**(3): p. 184S-190S.
16. Zhou, J.R. and J.W. Erdman, *PHYTIC ACID IN HEALTH AND DISEASE.* Critical Reviews in Food Science and Nutrition, 1995. **35**(6): p. 495-508.
17. Samuel, T.M., et al., *Correlates of anaemia in pregnant urban South Indian women: a possible role of dietary intake of nutrients that inhibit iron absorption.* Public Health Nutrition, 2013. **16**(2): p. 316-324.

18. Gunshin, H., et al., *Cloning and characterization of a mammalian proton-coupled metal-ion transporter.* Nature, 1997. **388**(6641): p. 482-8.

19. Luo, X., et al., *Modulation of Dcytb (Cybrd 1) expression and function by iron, dehydroascorbate and Hif-2alpha in cultured cells.* Biochim Biophys Acta, 2014. **1840**(1): p. 106-12.

20. Canonne-Hergaux, F., et al., *Cellular and subcellular localization of the Nramp2 iron transporter in the intestinal brush border and regulation by dietary iron.* Blood, 1999. **93**(12): p. 4406-4417.

21. Leidgens, S., et al., *Each member of the poly-r(C)-binding protein 1 (PCBP) family exhibits iron chaperone activity toward ferritin.* J Biol Chem, 2013. **288**(24): p. 17791-802.

22. Morgan, E.H. and P.S. Oates, *Mechanisms and regulation of intestinal iron absorption.* Blood Cells Molecules and Diseases, 2002. **29**(3): p. 384-399.

23. Vulpe, C.D., et al., *Hephaestin, a ceruloplasmin homologue implicated in intestinal iron transport, is defective in the sla mouse.* Nat Genet, 1999. **21**(2): p. 195-9.

24. McKie, A.T., et al., *A novel duodenal iron-regulated transporter, IREG1, implicated in the basolateral transfer of iron to the circulation.* Mol Cell, 2000. **5**(2): p. 299-309.

25. Rizvi, S. and R.E. Schoen, *Supplementation With Oral vs. Intravenous Iron for Anemia With IBD or Gastrointestinal Bleeding: Is Oral Iron Getting a Bad Rap[quest].* Am J Gastroenterol, 2011. **106**(11): p. 1872-1879.

26. Le Blanc, S., M.D. Garrick, and M. Arredondo, *Heme carrier protein 1 transports heme and is involved in heme-Fe metabolism.* Am J Physiol Cell Physiol, 2012. **302**(12): p. C1780-5.

27. Qiu, A., et al., *Identification of an intestinal folate transporter and the molecular basis for hereditary folate malabsorption.* Cell, 2006. **127**(5): p. 917-28.

28. Shayeghi, M., et al., *Identification of an intestinal heme transporter.* Cell, 2005. **122**(5): p. 789-801.

29. Pereira, D.I.A., et al., *Caco-2 Cell Acquisition of Dietary Iron(III) Invokes a Nanoparticulate Endocytic Pathway.* PLoS ONE, 2013. **8**(11): p. e0119747.

30. Latunde-Dada, G.O., et al., *A Nanoparticulate Ferritin-Core Mimetic Is Well Taken Up by HuTu 80 Duodenal Cells and Its Absorption in Mice Is Regulated by Body Iron.* Journal of Nutrition, 2014. **144**(12): p. 1896-1902.

31. Powell, J.J., et al., *Dietary minerals in the gastrointestinal tract: hydroxypolymerisation of aluminium is regulated by luminal mucins.* Journal of inorganic biochemistry, 1999. **75**(3): p. 167-180.

32. Aslam, M., et al., *THE ABSORPTION OF NANOPARTICULATE IRON HYDROXIDE IS FERROPORTIN-MEDIATED.* American Journal of Hematology, 2013. **88**(5): p. E191-E191.

33. De Domenico, I., D.M. Ward, and J. Kaplan, *Regulation of iron acquisition and storage: consequences for iron-linked disorders.* Nature Reviews Molecular Cell Biology, 2008. **9**(1): p. 72-81.

34. Galy, B., et al., *Iron regulatory proteins are essential for intestinal function and control key iron absorption molecules in the duodenum.* Cell Metab, 2008. **7**(1): p. 79-85.

35. Hentze, M.W., M.U. Muckenthaler, and N.C. Andrews, *Balancing acts: molecular control of mammalian iron metabolism.* Cell, 2004. **117**(3): p. 285-97.

36. Latunde-Dada, G.O., et al., *Molecular and functional roles of duodenal cytochrome B (Dcytb) in iron metabolism.* Blood Cells Mol Dis, 2002. **29**(3): p. 356-60.

37. Gulec, S., G.J. Anderson, and J.F. Collins, *Mechanistic and regulatory aspects of intestinal iron absorption.* Vol. 307. 2014. G397-G409.

38. Nemeth, E., et al., *Hepcidin regulates cellular iron efflux by binding to ferroportin and inducing its internalization.* Science, 2004. **306**(5704): p. 2090-3.

39. Zhao, N., A.S. Zhang, and C.A. Enns, *Iron regulation by hepcidin.* J Clin Invest, 2013. **123**(6): p. 2337-43.

40. Babitt, J.L. and H.Y. Lin, *The molecular pathogenesis of hereditary hemochromatosis.* Semin Liver Dis, 2011. **31**(3): p. 280-92.

41. Ganz, T., *Hepcidin and iron regulation, 10 years later.* Blood, 2011. **117**(17): p. 4425-33.

42.   Michels, K., et al., *Hepcidin and Host Defense against Infectious Diseases.* PLoS Pathog, 2015. **11**(8): p. e1004998.

43.   Weiss, G. and L.T. Goodnough, *Anemia of Chronic Disease.* New England Journal of Medicine, 2005. **352**(10): p. 1011-1023.

44.   de Valk, B., et al., *Non-transferrin-bound iron is present in serum of hereditary haemochromatosis heterozygotes.* Eur J Clin Invest, 2000. **30**(3): p. 248-51.

45.   Niederau, C., et al., *Long-term survival in patients with hereditary hemochromatosis.* Gastroenterology, 1996. **110**(4): p. 1107-1119.

46.   Mainous, A.G., J.M. Gill, and C.J. Everett, *Transferrin Saturation, Dietary Iron Intake, and Risk of Cancer.* Annals of Family Medicine, 2005. **3**(2): p. 131-137.

47.   Stevens, R.G., et al., *Body iron stores and the risk of cancer.* N Engl J Med, 1988. **319**(16): p. 1047-52.

48.   Fleming, R.E. and P. Ponka, *Iron overload in human disease.* New England Journal of Medicine, 2012. **366**(4): p. 348-359.

49.   Chasteen, N.D. and P.M. Harrison, *Mineralization in ferritin: an efficient means of iron storage.* J Struct Biol, 1999. **126**(3): p. 182-94.

50.   Parkkinen, J., et al., *Function and Therapeutic Development of Apotransferrin.* Vox Sanguinis, 2002. **83**: p. 321-326.

51.   Gomme, P.T., K.B. McCann, and J. Bertolini, *Transferrin: structure, function and potential therapeutic actions.* Drug Discov Today, 2005. **10**(4): p. 267-73.

52.   Chevion, M., E. Berenshtein, and B.-Z. Zhu, *The Role of Transition Metal Ions in Free Radical-Mediated Damage*, in *Reactive Oxygen Species in Biological Systems*. 2002, Springer US. p. 103-131.

53.   Crisponi, G. and M. Remelli, *Iron chelating agents for the treatment of iron overload.* Coordination Chemistry Reviews, 2008. **252**(10): p. 1225-1240.

54.   Graf, E., et al., *Iron-catalyzed hydroxyl radical formation. Stringent requirement for free iron coordination site.* J Biol Chem, 1984. **259**(6): p. 3620-4.

55.   Sun, Y., *FREE-RADICALS, ANTIOXIDANT ENZYMES, AND CARCINOGENESIS.* Free Radical Biology and Medicine, 1990. **8**(6): p. 583-599.

56.   Phillips, L.L., *Effect of Free Radicals on Chromosomes of Barley.* Science, 1956. **124**(3227): p. 889-90.

57.   Liou, G.-Y. and P. Storz, *Reactive oxygen species in cancer.* Free radical research, 2010. **44**(5): p. 10.3109/10715761003667554.

58.   CRUK. *Bowel cancer statistics*. 2011 [cited 2015; Available from: http://www.cancerresearchuk.org/health-professional/cancer-statistics/statistics-by-cancer-type/bowel-cancer.

59.   Jaladanki, R.N. and J.-Y. Wang. *Regulation of gastrointestinal mucosal growth*. in *Colloquium Series on Integrated Systems Physiology: From Molecule to Function*. 2011. Morgan & Claypool Life Sciences.

60.   van der Flier, L.G. and H. Clevers, *Stem cells, self-renewal, and differentiation in the intestinal epithelium.* Annu Rev Physiol, 2009. **71**: p. 241-60.

61.   Heath, J.P., *Epithelial cell migration in the intestine.* Cell Biol Int, 1996. **20**(2): p. 139-46.

62.   Marshman, E., C. Booth, and C.S. Potten, *The intestinal epithelial stem cell.* Bioessays, 2002. **24**(1): p. 91-8.

63.   Johnson, L.R., *Regulation of gastrointestinal mucosal growth.* Physiol Rev, 1988. **68**(2): p. 456-502.

64.   Sancho, E., E. Batlle, and H. Clevers, *Signaling pathways in intestinal development and cancer.* Annu Rev Cell Dev Biol, 2004. **20**: p. 695-723.

65.   Underwood, J.C. and S.S. Cross, *General and systematic pathology*. 2009: Elsevier Health Sciences.

66.   CRUK. *About bowel cancer screening*. 2015 [cited 2015; Available from: http://www.cancerresearchuk.org/about-cancer/type/bowel-cancer/about/screening/about-bowel-cancer-screening.

67.   Sobin, L.H., et al., *Introduction*, in *TNM Online*. 2003, John Wiley & Sons, Inc.

68.   Gunderson, L.L., et al., *Revised TN categorization for colon cancer based on national survival outcomes data.* J Clin Oncol, 2010. **28**(2): p. 264-71.

69.   NICE. *Colorectal cancer: The diagnosis and management of colorectal cancer*. 2011   [cited 2015; Available from: http://www.nice.org.uk/guidance/cg131.

70.   Markowitz, S.D. and M.M. Bertagnolli, *Molecular origins of cancer: Molecular basis of colorectal cancer.* N Engl J Med, 2009. **361**(25): p. 2449-60.

71.   Bienz, M. and H. Clevers, *Linking Colorectal Cancer to Wnt Signaling.* Cell, 2000. **103**(2): p. 311-320.

72.   Goss, K.H. and J. Groden, *Biology of the adenomatous polyposis coli tumor suppressor.* Journal of Clinical Oncology, 2000. **18**(9): p. 1967-1979.

73.   Grady, W.M., et al., *Mutation of the type II transforming growth factor-beta receptor is coincident with the transformation of human colon adenomas to malignant carcinomas.* Cancer Research, 1998. **58**(14): p. 3101-3104.

74.   Baker, S.J., et al., *P53 GENE-MUTATIONS OCCUR IN COMBINATION WITH 17P ALLELIC DELETIONS AS LATE EVENTS IN COLORECTAL TUMORIGENESIS.* Cancer Research, 1990. **50**(23): p. 7717-7722.

75.   Morin, P.J., B. Vogelstein, and K.W. Kinzler, *Apoptosis and APC in colorectal tumorigenesis.* Proceedings of the National Academy of Sciences, 1996. **93**(15): p. 7950-7954.

76.   Kinzler, K.W. and B. Vogelstein, *Lessons from Hereditary Colorectal Cancer.* Cell, 1996. **87**(2): p. 159-170.

77.   Fearon, E.R. and B. Vogelstein, *A genetic model for colorectal tumorigenesis.* Cell, 1990. **61**(5): p. 759-767.

78.   Narayan, S. and D. Roy, *Role of APC and DNA mismatch repair genes in the development of colorectal cancers.* Mol Cancer, 2003. **2**: p. 41.

79.   Cunningham, D., et al., *Colorectal cancer.* Lancet, 2010. **375**(9719): p. 1030-47.

80.   Summers, R.M., *Polyp Size Measurement at CT Colonography: What Do We Know and What Do We Need to Know?* Radiology, 2010. **255**(3): p. 707-720.

81.   Bonadona, V., et al., *CAncer risks associated with germline mutations in mlh1, msh2, and msh6 genes in lynch syndrome.* JAMA, 2011. **305**(22): p. 2304-2310.

82.   Nishisho, I., et al., *Mutations of chromosome 5q21 genes in FAP and colorectal cancer patients.* Science, 1991. **253**(5020): p. 665-669.

83.   NACC. *Bowel Cancer and IBD*. 2013   [cited 2015; Available from: http://www.crohnsandcolitis.org.uk/Resources/CrohnsAndColitisUK/Documents/Publications/Info-Sheets/Bowel%20Cancer%20and%20IBD.pdf.

84.   Freeman, H.J., *Colorectal cancer risk in Crohn's disease.* World Journal of Gastroenterology : WJG, 2008. **14**(12): p. 1810-1811.

85.   Weedon, D.D., et al., *Crohn's disease and cancer.* New England Journal of Medicine, 1973. **289**(21): p. 1099-1103.

86.   Gyde, S., et al., *Malignancy in Crohn's disease.* Gut, 1980. **21**(12): p. 1024-1029.

87.   Gasche, C., et al., *Iron, anaemia, and inflammatory bowel diseases.* Gut, 2004. **53**(8): p. 1190-1197.

88.   Werner, T., et al., *Depletion of luminal iron alters the gut microbiota and prevents Crohn's disease-like ileitis.* Gut, 2011. **60**(3): p. 325-333.

89.   LihBrody, L., et al., *Increased oxidative stress and decreased antioxidant defenses in mucosa of inflammatory bowel disease.* Digestive Diseases and Sciences, 1996. **41**(10): p. 2078-2086.

90.   Coplin, M., et al., *Tolerability of iron: a comparison of bis-glycino iron II and ferrous sulfate.* Clin Ther, 1991. **13**(5): p. 606-12.

91.   Millar, Rampton, and Blake, *Effects of iron and iron chelation in vitro on mucosal oxidant activity in ulcerative colitis.* Alimentary Pharmacology & Therapeutics, 2000. **14**(9): p. 1163-1168.

92.   Nelson, R.L., et al., *Body iron stores and risk of colonic neoplasia.* J Natl Cancer Inst, 1994. **86**(6): p. 455-60.

93.   Nelson, R.L., *Dietary iron and colorectal cancer risk.* Free Radical Biology and Medicine, 1992. **12**(2): p. 161-168.

94.   Anand, P., et al., *Cancer is a Preventable Disease that Requires Major Lifestyle Changes.* Pharmaceutical Research, 2008. **25**(9): p. 2097-2116.

95.   Chan, A.T. and E.L. Giovannucci, *Primary Prevention of Colorectal Cancer.* Gastroenterology, 2010. **138**(6): p. 2029-2043.e10.

96.   Block, G., B. Patterson, and A. Subar, *FRUIT, VEGETABLES, AND CANCER PREVENTION - A REVIEW OF THE EPIDEMIOLOGIC EVIDENCE.* Nutrition and Cancer-an International Journal, 1992. **18**(1): p. 1-29.

97.   Ferlay, J., et al., *Estimates of worldwide burden of cancer in 2008: GLOBOCAN 2008.* International journal of cancer, 2010. **127**(12): p. 2893-2917.

98.   Lee, D.-H., et al., *Heme Iron, Zinc, Alcohol Consumption, and Colon Cancer: Iowa Women's Health Study.* Journal of the National Cancer Institute, 2004. **96**(5): p. 403-407.

99.   Larsson, S.C., et al., *Re: Heme Iron, Zinc, Alcohol Consumption, and Risk of Colon Cancer.* Journal of the National Cancer Institute, 2005. **97**(3): p. 232-233.

100.   Nelson, R.L., *Iron and colorectal cancer risk: human studies.* Nutrition reviews, 2001. **59**(5): p. 140-148.

101.   Chan, D.S.M., et al., *Red and Processed Meat and Colorectal Cancer Incidence: Meta-Analysis of Prospective Studies.* PLoS ONE, 2011. **6**(6): p. e20456.

102.   Nelson, R.L., et al., *Risk of neoplastic and other diseases among people with heterozygosity for hereditary hemochromatosis.* Cancer, 1995. **76**(5): p. 875-9.

103.   Shaheen, N.J., et al., *Association between hemochromatosis (HFE) gene mutation carrier status and the risk of colon cancer.* J Natl Cancer Inst, 2003. **95**(2): p. 154-9.

104.   Osborne, N.J., et al., *HFE C282Y homozygotes are at increased risk of breast and colorectal cancer.* Hepatology, 2010. **51**(4): p. 1311-8.

105.   Huang, X., *Iron overload and its association with cancer risk in humans: evidence for iron as a carcinogenic metal.* Mutat Res, 2003. **533**(1-2): p. 153-71.

106.   Kwok, J.C. and D.R. Richardson, *The iron metabolism of neoplastic cells: alterations that facilitate proliferation?* Crit Rev Oncol Hematol, 2002. **42**(1): p. 65-78.

107.   Andrews, N.C., *Forging a field: the golden age of iron biology.* Blood, 2008. **112**(2): p. 219-30.

108.   Boult, J., et al., *Overexpression of cellular iron import proteins is associated with malignant progression of esophageal adenocarcinoma.* Clin Cancer Res, 2008. **14**(2): p. 379-87.

109.   Brookes, M.J., et al., *Modulation of iron transport proteins in human colorectal carcinogenesis.* Gut, 2006. **55**(10): p. 1449-1460.

110.   Han, H.S., et al., *Presence of Iron in Colorectal Adenomas and Adenocarcinomas.* Gut and Liver, 2008. **2**(1): p. 19-22.

111.   Torti, S.V. and F.M. Torti, *Iron and cancer: more ore to be mined.* Nat Rev Cancer, 2013. **13**(5): p. 342-55.

112.   Bystrom, L.M., M.L. Guzman, and S. Rivella, *Iron and Reactive Oxygen Species: Friends or Foes of Cancer Cells?* Antioxidants & Redox Signaling, 2014. **20**(12): p. 1917-1924.

113.   Brookes, M.J., et al., *A role for iron in Wnt signalling.* Oncogene, 2008. **27**(7): p. 966-975.

114.   Wu, K.J., A. Polack, and R. Dalla-Favera, *Coordinated regulation of iron-controlling genes, H-ferritin and IRP2, by c-MYC.* Science, 1999. **283**(5402): p. 676-9.

115.   Song, S., et al., *Wnt inhibitor screen reveals iron dependence of beta-catenin signaling in cancers.* Cancer Res, 2011. **71**(24): p. 7628-39.

116.   Richmond, H.G., *Induction of Sarcoma in the Rat by Iron—Dextran Complex.* British Medical Journal, 1959. **1**(5127): p. 947-940.3.

117.   Smith, A.G., et al., *Carcinogenicity of iron in conjunction with a chlorinated environmental chemical, hexachlorobenzene, in C57BL/10ScSn mice.* Int J Cancer, 1989. **43**(3): p. 492-6.

118.   Siegers, C.P., et al., *Influence of dietary iron overload on cell proliferation and intestinal tumorigenesis in mice.* Cancer Lett, 1992. **65**(3): p. 245-9.

119. Kim, J.H., et al., *Effects of selenium on colon carcinogenesis induced by azoxymethane and dextran sodium sulfate in mouse model with high-iron diet.* Lab Anim Res, 2011. **27**(1): p. 9-18.

120. Radulescu, S., et al., *Luminal Iron Levels Govern Intestinal Tumorigenesis after Apc Loss In Vivo.* Cell Reports, 2012. **2**(2): p. 270-282.

121. Hann, H.W., M.W. Stahlhut, and B.S. Blumberg, *Iron nutrition and tumor growth: decreased tumor growth in iron-deficient mice.* Cancer Res, 1988. **48**(15): p. 4168-70.

122. Siegers, C.P., et al., *Dietary iron enhances the tumor rate in dimethylhydrazine-induced colon carcinogenesis in mice.* Cancer Lett, 1988. **41**(3): p. 251-6.

123. MERK, K., et al., *The incidence of cancer among blood donors.* International journal of epidemiology, 1990. **19**(3): p. 505-509.

124. Kato, I., et al., *Iron intake, body iron stores and colorectal cancer risk in women: a nested case‐control study.* International journal of cancer, 1999. **80**(5): p. 693-698.

125. Edgren, G., et al., *Donation frequency, iron loss, and risk of cancer among blood donors.* J Natl Cancer Inst, 2008. **100**(8): p. 572-9.

126. Zacharski, L.R., et al., *Decreased cancer risk after iron reduction in patients with peripheral arterial disease: results from a randomized trial.* J Natl Cancer Inst, 2008. **100**(14): p. 996-1002.

127. Riboli, E., *The European prospective investigation into cancer and nutrition (EPIC): plans and progress.* The Journal of nutrition, 2001. **131**(1): p. 170S-175S.

128. Graf, E. and J.W. Eaton, *Suppression of colonic cancer by dietary phytic acid.* Nutr Cancer, 1993. **19**(1): p. 11-9.

129. Bingham, S.A., et al., *Dietary fibre in food and protection against colorectal cancer in the European Prospective Investigation into Cancer and Nutrition (EPIC): an observational study.* Lancet, 2003. **361**(9368): p. 1496-1501.

130. Terry, P., et al., *Fruit, Vegetables, Dietary Fiber, and Risk of Colorectal Cancer.* Journal of the National Cancer Institute, 2001. **93**(7): p. 525-533.

131. Burkitt, D.P., *Epidemiology of cancer of the colon and rectum.* Cancer, 1971. **28**(1): p. 3-13.

132. Burkitt, D., *RELATED DISEASE—RELATED CAUSE?* The Lancet, 1969. **294**(7632): p. 1229-1231.

133. Key, T.J., et al., *Mortality in vegetarians and non-vegetarians: a collaborative analysis of 8300 deaths among 76,000 men and women in five prospective studies.* Public Health Nutr, 1998. **1**(1): p. 33-41.

134. Harris, P.J. and L.R. Ferguson, *Dietary fibre: its composition and role in protection against colorectal cancer.* Mutation Research/Fundamental and Molecular Mechanisms of Mutagenesis, 1993. **290**(1): p. 97-110.

135. Fuchs, C.S., et al., *Dietary Fiber and the Risk of Colorectal Cancer and Adenoma in Women.* New England Journal of Medicine, 1999. **340**(3): p. 169-176.

136. Schatzkin, A., et al., *Lack of effect of a low-fat, high-fiber diet on the recurrence of colorectal adenomas. Polyp Prevention Trial Study Group.* N Engl J Med, 2000. **342**(16): p. 1149-55.

137. McKeown-Eyssen, G.E., et al., *A randomized trial of a low fat high fibre diet in the recurrence of colorectal polyps.* Journal of Clinical Epidemiology, 1994. **47**(5): p. 525-536.

138. Bonithon-Kopp, C., et al., *Calcium and fibre supplementation in prevention of colorectal adenoma recurrence: a randomised intervention trial.* The Lancet, 2000. **356**(9238): p. 1300-1306.

139. Collings, R., et al., *The absorption of iron from whole diets: a systematic review.* The American journal of clinical nutrition, 2013: p. 65-81.

140. Powell, J.J., et al., *A nano-disperse ferritin-core mimetic that efficiently corrects anemia without luminal iron redox activity.* Nanomedicine-Nanotechnology Biology and Medicine, 2014. **10**(7): p. 1529-1538.

141. Rudzki, Z., R. Baker, and D. Deller, *The iron-binding glycoprotein of human gastric juice. II. Nature of the interaction of the glycoprotein with iron.* Digestion, 1973. **8**(1): p. 53-67.

142. Simpson, R.J. and T.J. Peters, *Forms of soluble iron in mouse stomach and duodenal lumen: significance for mucosal uptake.* Br J Nutr, 1990. **63**(1): p. 79-89.

143. Latunde-Dada, G.O. and R.J. Neale, *Review: Availability of iron from foods.* International Journal of Food Science & Technology, 1986. **21**(3): p. 255-268.

144. Flynn, C.M., *Hydrolysis of inorganic iron(III) salts.* Chemical Reviews, 1984. **84**(1): p. 31-41.

145. Conrad, M.E., J.N. Umbreit, and E.G. Moore, *A role for mucin in the absorption of inorganic iron and other metal cations.* Gastroenterology, 1991. **100**(1): p. 129-136.

146. Berner, L.A., D.D. Miller, and D. Van Campen, *Absorption of iron from ferric hydroxide polymers introduced into ligated rat duodenal segments.* The Journal of nutrition, 1986. **116**(2): p. 259-264.

147. Housecroft, C.E. and A.G. Sharpe, *Inorganic Chemistry.* 2nd ed. 2005: Pearson Education.

148. Liu, Z.D. and R.C. Hider, *Design of clinically useful iron(III)-selective chelators.* Med Res Rev, 2002. **22**(1): p. 26-64.

149. Pearson, R.G., *Hard and Soft Acids and Bases.* Journal of the American Chemical Society, 1963. **85**(22): p. 3533-3539.

150. Vilensky, J.A. and K. Redman, *British anti-Lewisite (dimercaprol): an amazing history.* Ann Emerg Med, 2003. **41**(3): p. 378-83.

151. Scott, L.E. and C. Orvig, *Medicinal inorganic chemistry approaches to passivation and removal of aberrant metal ions in disease.* Chem Rev, 2009. **109**(10): p. 4885-910.

152. Pippard, M.J., S.T. Callender, and D.J. Weatherall, *Intensive iron-chelation therapy with desferrioxamine in iron-loading anaemias.* Clin Sci Mol Med, 1978. **54**(1): p. 99-106.

153. Poggiali, E., et al., *An update on iron chelation therapy.* Blood Transfusion, 2012. **10**(4): p. 411-422.

154. Zhou, T., et al., *Design of clinically useful macromolecular iron chelators.* J Pharm Pharmacol, 2011. **63**(7): p. 893-903.

155. Bedford, M.R., et al., *Iron Chelation in the Treatment of Cancer: A New Role for Deferasirox?* Journal of Clinical Pharmacology, 2013. **53**(9): p. 885-891.

156. Merlot, A.M., D.S. Kalinowski, and D.R. Richardson, *Novel chelators for cancer treatment: where are we now?* Antioxid Redox Signal, 2013. **18**(8): p. 973-1006.

157. Buss, J.L., F.M. Torti, and S.V. Torti, *The role of iron chelation in cancer therapy.* Current Medicinal Chemistry, 2003. **10**(12): p. 1021-1034.

158. Yu, Y., et al., *Iron chelators for the treatment of cancer.* Curr Med Chem, 2012. **19**(17): p. 2689-702.

159. Rajagopalan, P.T.R., et al., *Interaction of dihydrofolate reductase with methotrexate: Ensemble and single-molecule kinetics.* Proceedings of the National Academy of Sciences of the United States of America, 2002. **99**(21): p. 13481-13486.

160. Becton, D.L. and P. Bryles, *Deferoxamine inhibition of human neuroblastoma viability and proliferation.* Cancer Res, 1988. **48**(24 Pt 1): p. 7189-92.

161. Simonart, T., et al., *Antiproliferative and apoptotic effects of iron chelators on human cervical carcinoma cells.* Gynecol Oncol, 2002. **85**(1): p. 95-102.

162. Yasumoto, E., et al., *Cytotoxic activity of deferiprone, maltol and related hydroxyketones against human tumor cell lines.* Anticancer Res, 2004. **24**(2b): p. 755-62.

163. Ford, S.J., et al., *Deferasirox (ICL670A) effectively inhibits oesophageal cancer growth in vitro and in vivo.* Br J Pharmacol, 2013. **168**(6): p. 1316-28.

164. Lui, G.Y., et al., *The iron chelator, deferasirox, as a novel strategy for cancer treatment: oral activity against human lung tumor xenografts and molecular mechanism of action.* Mol Pharmacol, 2013. **83**(1): p. 179-90.

165. Fukushima, T., et al., *Iron chelation therapy with deferasirox induced complete remission in a patient with chemotherapy-resistant acute monocytic leukemia.* Anticancer Res, 2011. **31**(5): p. 1741-4.

166. Yuan, J., D.B. Lovejoy, and D.R. Richardson, *Novel di-2-pyridyl-derived iron chelators with marked and selective antitumor activity: in vitro and in vivo assessment.* Blood, 2004. **104**(5): p. 1450-1458.

167. Chen, Z., et al., *The Iron Chelators Dp44mT and DFO Inhibit TGF-beta-induced Epithelial-Mesenchymal Transition via Up-Regulation of N-Myc Downstream-regulated Gene 1 (NDRG1).* Journal of Biological Chemistry, 2012. **287**(21): p. 17016-17028.

168. Richardson, D.R., *Molecular mechanisms of iron uptake by cells and the use of iron chelators for the treatment of cancer.* Curr Med Chem, 2005. **12**(23): p. 2711-29.

169. Richardson, D.R., et al., *Dipyridyl thiosemicarbazone chelators with potent and selective antitumor activity form iron complexes with redox activity.* J Med Chem, 2006. **49**(22): p. 6510-21.

170. Ludwig, H. and E. Fritz, *Anemia in cancer patients.* Seminars in oncology, 1998. **25**(3 Suppl 7): p. 2-6.

171. Ceci, A., et al., *The safety and effectiveness of deferiprone in a large-scale, 3-year study in Italian patients.* Br J Haematol, 2002. **118**(1): p. 330-6.

172. Gattermann, N., et al., *Deferasirox treatment of iron-overloaded chelation-naïve and prechelated patients with myelodysplastic syndromes in medical practice: results from the observational studies eXtend and eXjange.* European Journal of Haematology, 2012. **88**(3): p. 260-268.

173. Debon, S.J.J. and R.F. Tester, *In vitro binding of calcium, iron and zinc by non-starch polysaccharides.* Food Chemistry, 2001. **73**(4): p. 401-410.

174. Pabon de Rozo, M., D. VanCampen, and D.D. Miller, *Effects of some carbohydrates on iron absorption.* Archivos latinoamericanos de nutricion, 1986. **36**(4): p. 688-700.

175. Zhang, N., C. Huang, and S. Ou, *In vitro binding capacities of three dietary fibers and their mixture for four toxic elements, cholesterol, and bile acid.* Journal of Hazardous Materials, 2011. **186**(1): p. 236-239.

176. Serguschenko, I., E. Kolenchenko, and M. Khotimchenko, *Low esterified pectin accelerates removal of lead ions in rats.* Nutrition Research, 2007. **27**(10): p. 633-639.

177. Schlemmer, U., *STUDIES OF THE BINDING OF COPPER, ZINC AND CALCIUM TO PECTIN, ALGINATE, CARRAGEENAN AND GUM GUAR IN HCO3--CO2 BUFFER.* Food Chemistry, 1989. **32**(3): p. 223-234.

178. Nawirska, A., *Binding of heavy metals to pomace fibers.* Food Chemistry, 2005. **90**(3): p. 395-400.

179. Kunkel, M.E., A. Seo, and T.A. Minten, *Magnesium binding by gum arabic, locust bean gum, and arabinogalactan.* Food Chemistry, 1997. **59**(1): p. 87-93.

180. Ismailbeigi, F., B. Faraji, and J.G. Reinhold, *BINDING OF ZINC AND IRON TO WHEAT BREAD, WHEAT BRAN, AND THEIR COMPONENTS.* American Journal of Clinical Nutrition, 1977. **30**(10): p. 1721-1725.

181. Hu, G.H., et al., *Binding of four heavy metals to hemicelluloses from rice bran.* Food Research International, 2010. **43**(1): p. 203-206.

182. Camire, A.L. and F.M. Clydesdale, *EFFECT OF PH AND HEAT-TREATMENT ON THE BINDING OF CALCIUM, MAGNESIUM, ZINC, AND IRON TO WHEAT BRAN AND FRACTIONS OF DIETARY FIBER.* Journal of Food Science, 1981. **46**(2): p. 548-551.

183. Paxman, J.R., et al., *Alginate reduces the increased uptake of cholesterol and glucose in overweight male subjects: a pilot study.* Nutrition Research, 2008. **28**(8): p. 501-505.

184. Gacesa, P., *Alginates.* Carbohydrate Polymers, 1988. **8**(3): p. 161-182.

185. Draget, K.I., O. Smidsrød, and G. Skjåk-Bræk, *Alginates from Algae*, in *Biopolymers Online*. 2005, Wiley-VCH Verlag GmbH & Co. KGaA.

186. Haug, A., B. Larsen, and O. Smidsrod, *Studies on the sequence of uronic acid residues in alginic acid.* Acta Chem Scand, 1967. **21**: p. 691-704.

187. Grasdalen, H., *HIGH-FIELD, H-1-NMR SPECTROSCOPY OF ALGINATE - SEQUENTIAL STRUCTURE AND LINKAGE CONFORMATIONS.* Carbohydrate Research, 1983. **118**(JUL): p. 255-260.

188. McHugh, D.J. *Production, properties and uses of alginates.* 2006 [cited 2015; Available from: http://www.fao.org/docrep/x5822e/x5822e04.htm.

189.   Inger-Lill, A., et al., *Some Biological Functions of Matrix Components in Benthic Algae in Relation to Their Chemistry and the Composition of Seawater*, in *Cellulose Chemistry and Technology*. 1977, AMERICAN CHEMICAL SOCIETY. p. 361-381.

190.   Larsen, B., et al., *Calculation of nearest-neighbour frequencies in fragments of alginate from yields of free monomers after partial hydrolysis.* Acta Chemica Scandinavica, 1970. **24**(2): p. 726-731.

191.   Grasdalen, H., B. Larsen, and O. Smidsrød, *13C-N.m.r. studies of alginate.* Carbohydrate Research, 1977. **56**(2): p. C11-C15.

192.   Grasdalen, H., B. Larsen, and O. Smidsrød, *A p.m.r. study of the composition and sequence of uronate residues in alginates.* Carbohydrate Research, 1979. **68**(1): p. 23-31.

193.   Remminghorst, U. and B.A. Rehm, *Bacterial alginates: from biosynthesis to applications.* Biotechnology Letters, 2006. **28**(21): p. 1701-1712.

194.   Ertesvag, H., *Alginate-modifying enzymes: biological roles and biotechnological uses.* Front Microbiol, 2015. **6**: p. 523.

195.   Holtan, S., P. Bruheim, and G. Skjåk-Bræk, *Mode of action and subsite studies of the guluronan block-forming mannuronan C-5 epimerases AlgE1 and AlgE6.* Biochemical Journal, 2006. **395**(Pt 2): p. 319-329.

196.   Ertesvåg, H. and G. Skjåk-Bræk, *Modification of Alginate Using Mannuronan C-5-Epimerases*, in *Carbohydrate Biotechnology Protocols*, C. Bucke, Editor. 1999, Humana Press. p. 71-78.

197.   Ertesvag, H., et al., *Mannuronan C-5-epimerases and their application for in vitro and in vivo design of new alginates useful in biotechnology.* Metab Eng, 1999. **1**(3): p. 262-9.

198.   Skjåk-Bræk, G., O. Smidsrød, and B. Larsen, *Tailoring of alginates by enzymatic modification in vitro.* International Journal of Biological Macromolecules, 1986. **8**(6): p. 330-336.

199.   El-Mohdy, H.L.A., *Radiation-induced degradation of sodium alginate and its plant growth promotion effect.* Arabian Journal of Chemistry.

200.   Wasikiewicz, J.M., et al., *Degradation of chitosan and sodium alginate by gamma radiation, sonochemical and ultraviolet methods.* Radiation Physics and Chemistry, 2005. **73**(5): p. 287-295.

201.   Gacesa, P., *Alginate-modifying enzymes: A proposed unified mechanism of action for the lyases and epimerases.* FEBS Letters, 1987. **212**(2): p. 199-202.

202.   Wong, T.Y., L.A. Preston, and N.L. Schiller, *ALGINATE LYASE: review of major sources and enzyme characteristics, structure-function analysis, biological roles, and applications.* Annu Rev Microbiol, 2000. **54**: p. 289-340.

203.   Kim, H., C.-G. Lee, and E. Lee, *Alginate lyase: Structure, property, and application.* Biotechnology and Bioprocess Engineering, 2011. **16**(5): p. 843-851.

204.   Haug, A., B. Larsen, and O. Smidsrod, *A study of the constitution of alginic acid by partial acid hydrolysis.* Acta Chem Scand, 1966. **20**(1): p. 183-90.

205.   Smidsrod, O., A. Haug, and B. Larsen, *The influence of pH on the rate of hydrolysis of acidic polysaccharides.* Acta Chem Scand, 1966. **20**(4): p. 1026-34.

206.   HAUG, A., B. LARSEN, and O. SMIDSRQ'D, *Alkaline degradation of alginate.* Acta Chemica Scandinavica, 1967. **21**(10): p. 2859-2870.

207.   Oates, C.G. and D.A. Ledward, *Studies on the effect of heat on alginates.* Food Hydrocolloids, 1990. **4**(3): p. 215-220.

208.   Holme, H.K., et al., *Thermal depolymerization of alginate in the solid state.* Carbohydrate Polymers, 2003. **54**(4): p. 431-438.

209.   Holme, H.K., et al., *Thermal depolymerization of chitosan chloride.* Carbohydrate Polymers, 2001. **46**(3): p. 287-294.

210.   Berner, L.A. and L.F. Hood, *Iron Binding by Sodium Alginate.* Journal of Food Science, 1983. **48**(3): p. 755-758.

211.   Fernandez, R. and S.F. Phillips, *Components of fiber bind iron in vitro.* The American Journal of Clinical Nutrition, 1982. **35**(1): p. 100-6.

212. Wölbling, R.H., G. Becker, and W. Forth, *Inhibition of the Intestinal Absorption of Iron by Sodium Alginate and Guar Gum in Rats.* Digestion, 1980. **20**(6): p. 403-409.

213. Sandberg, A.S., et al., *Alginate, small-bowel sterol excretion, and absorption of nutrients in ileostomy subjects.* American Journal of Clinical Nutrition, 1994. **60**(5): p. 751-756.

214. Wawer, A.A., et al., *Evidence for an Enhancing Effect of Alginate on Iron Availability in Caco-2 Cells.* Journal of Agricultural and Food Chemistry, 2012. **60**(45): p. 11318-11322.

215. Wawer, A.A., et al., *Alginate inhibits iron absorption from ferrous gluconate in a randomized controlled trial and reduces iron uptake into caco-2 cells.* PloS one, 2014. **9**(11): p. e112144.

216. Kroll, E., F.M. Winnik, and R.F. Ziolo, *In situ preparation of nanocrystalline gamma-Fe2O3 in iron(II) cross-linked alginate gels.* Chemistry of Materials, 1996. **8**(8): p. 1594-&.

217. Llanes, F., D.H. Ryan, and R.H. Marchessault, *Magnetic nanostructured composites using alginates of different M/G ratios as polymeric matrix.* International Journal of Biological Macromolecules, 2000. **27**(1): p. 35-40.

218. Shen, F., et al., *Properties of a novel magnetized alginate for magnetic resonance imaging.* Biotechnology and Bioengineering, 2003. **83**(3): p. 282-292.

219. Ma, H.L., et al., *Preparation and characterization of superparamagnetic iron oxide nanoparticles stabilized by alginate.* International Journal of Pharmaceutics, 2007. **333**(1-2): p. 177-186.

220. Jones, F., H. Cölfen, and M. Antonietti, *Iron oxyhydroxide colloids stabilized with polysaccharides.* Colloid and Polymer Science, 2000. **278**(6): p. 491-501.

221. Gupta, A.K. and M. Gupta, *Synthesis and surface engineering of iron oxide nanoparticles for biomedical applications.* Biomaterials, 2005. **26**(18): p. 3995-4021.

222. Jones, F., H. Cölfen, and M. Antonietti, *Interaction of κ-Carrageenan with Nickel, Cobalt, and Iron Hydroxides.* Biomacromolecules, 2000. **1**(4): p. 556-563.

223. Sreeram, K.J., H. Yamini Shrivastava, and B.U. Nair, *Studies on the nature of interaction of iron(III) with alginates.* Biochimica et Biophysica Acta (BBA) - General Subjects, 2004. **1670**(2): p. 121-125.

224. Harmuth-Hoene, A.-E. and R. Schelenz, *Effect of Dietary Fiber on Mineral Absorption in Growing Rats.* The Journal of Nutrition, 1980. **110**(9): p. 1774-1784.

225. Monnier, L., et al., *Evidence and mechanism for pectin-reduced intestinal inorganic iron absorption in idiopathic hemochromatosis.* The American Journal of Clinical Nutrition, 1980. **33**(6): p. 1225-32.

226. Greger, J.L., *Nondigestible Carbohydrates and Mineral Bioavailability.* The Journal of Nutrition, 1999. **129**(7): p. 1434S-1435s.

227. Torre, M., A.R. Rodriguez, and F. Saura-Calixto, *Interactions of Fe(II), Ca(II) and Fe(III) with high dietary fibre materials: A physicochemical approach.* Food Chemistry, 1995. **54**(1): p. 23-31.

228. Kim, M. and M.T. Atallah, *INTESTINAL SOLUBILITY AND ABSORPTION OF FERROUS IRON IN GROWING RATS ARE AFFECTED BY DIFFERENT DIETARY PECTINS.* Journal of Nutrition, 1993. **123**(1): p. 117-124.

229. Gibson, R.S., *CONTENT AND BIOAVAILABILITY OF TRACE-ELEMENTS IN VEGETARIAN DIETS.* American Journal of Clinical Nutrition, 1994. **59**(5): p. 1223S-1232S.

230. Thebaudin, J.Y., et al., *Dietary fibres: Nutritional and technological interest.* Trends in Food Science & Technology, 1997. **8**(2): p. 41-48.

231. Jonathan, M., et al., *In vivo degradation of alginate in the presence and in the absence of resistant starch.* Food Chemistry, 2015. **172**(0): p. 117-120.

232. Jonathan, M.C., et al., *Separation and Identification of Individual Alginate Oligosaccharides in the Feces of Alginate-Fed Pigs.* Journal of Agricultural and Food Chemistry, 2013. **61**(3): p. 553-560.

233. Trowell, H., et al., *DIETARY FIBRE REDEFINED.* The Lancet, 1976. **307**(7966): p. 967.

234. Michel, C., et al., *In vitro fermentation by human faecal bacteria of total and purified dietary fibres from brown seaweeds.* British Journal of Nutrition, 1996. **75**(2): p. 263-280.

235. Salyers, A.A., J.K. Palmer, and T.D. Wilkins, *Degradation of polysaccharides by intestinal bacterial enzymes.* Am J Clin Nutr, 1978. **31**(10 Suppl): p. S128-s130.

236. Dettmar, P.W., V. Strugala, and J. Craig Richardson, *The key role alginates play in health.* Food Hydrocolloids, 2011. **25**(2): p. 263-266.

237. Miyazaki, S., et al., *DRUG-RELEASE FROM ORAL MUCOSAL ADHESIVE TABLETS OF CHITOSAN AND SODIUM ALGINATE.* International Journal of Pharmaceutics, 1995. **118**(2): p. 257-263.

238. Tønnesen, H.H. and J. Karlsen, *Alginate in Drug Delivery Systems.* Drug Development and Industrial Pharmacy, 2002. **28**(6): p. 621-630.

239. Mandel, K., et al., *Review article: alginate-raft formulations in the treatment of heartburn and acid reflux.* Alimentary pharmacology & therapeutics, 2000. **14**(6): p. 669-690.

240. Grant, G.T., et al., *Biological interactions between polysaccharides and divalent cations: the egg-box model.* FEBS letters, 1973. **32**(1): p. 195-198.

241. Morris, E.R., et al., *Conformations and interactions of pectins: I. Polymorphism between gel and solid states of calcium polygalacturonate.* Journal of Molecular Biology, 1982. **155**(4): p. 507-516.

242. Morris, E.R., D.A. Rees, and D. Thom, *CHARACTERIZATION OF ALGINATE COMPOSITION AND BLOCK-STRUCTURE BY CIRCULAR-DICHROISM.* Carbohydrate Research, 1980. **81**(2): p. 305-314.

243. Morris, E.R., D.A. Rees, and D. Thom, *CHARACTERIZATION OF POLYSACCHARIDE STRUCTURE AND INTERACTIONS BY CIRCULAR-DICHROISM - ORDER-DISORDER TRANSITION IN CALCIUM ALGINATE SYSTEM.* Journal of the Chemical Society-Chemical Communications, 1973(7): p. 245-246.

244. Thom, D., et al., *CHARACTERIZATION OF CATION BINDING AND GELATION OF POLYURONATES BY CIRCULAR-DICHROISM.* Carbohydrate Research, 1982. **100**(MAR): p. 29-42.

245. Wang, Z.-Y., et al., *Sol–gel transition of alginate solution by the addition of various divalent cations: 13C-nmr spectroscopic study.* Biopolymers, 1993. **33**(4): p. 703-711.

246. Seely, G.R. and R.L. Hart, *The Binding of Alkaline Earth Metal Ions to Alginate.* Macromolecules, 1974. **7**(5): p. 706-710.

247. Haug, A., *The Affinity of Some Divalent Metals for Different Types of Alginates.* Acta Chemica Scandinavica 1947 - 1999, 1961. **15**: p. 1794-1795.

248. Smidsrød, O. and A. Haug, *The Effect of Divalent Metals on the Properties of Alginate Solutions. I. Calcium Ions.* Acta Chemica Scandinavica 1947 - 1999, 1965. **19**: p. 143-152.

249. Fang, Y., et al., *Multiple Steps and Critical Behaviors of the Binding of Calcium to Alginate.* The Journal of Physical Chemistry B, 2007. **111**(10): p. 2456-2462.

250. Ross, J.A. and C.M. Kasum, *Dietary flavonoids: bioavailability, metabolic effects, and safety.* Annu Rev Nutr, 2002. **22**: p. 19-34.

251. Williamson, G. and C. Manach, *Bioavailability and bioefficacy of polyphenols in humans. II. Review of 93 intervention studies.* The American Journal of Clinical Nutrition, 2005. **81**(1): p. 243S-255S.

252. Rothwell, J.A., et al., *Phenol-Explorer 3.0: a major update of the Phenol-Explorer database to incorporate data on the effects of food processing on polyphenol content.* Database (Oxford), 2013. **2013**: p. bat070.

253. Kaack, K. and T. Austed, *Interaction of vitamin C and flavonoids in elderberry (Sambucus nigra L.) during juice processing.* Plant Foods Hum Nutr, 1998. **52**(3): p. 187-98.

254. Khokhar, S. and R.K. Owusu Apenten, *Iron binding characteristics of phenolic compounds: some tentative structure–activity relations.* Food Chemistry, 2003. **81**(1): p. 133-140.

255. Sampson, L., et al., *Flavonol and flavone intakes in US health professionals.* J Am Diet Assoc, 2002. **102**(10): p. 1414-20.

256. Hertog, M.G.L., et al., *Intake of potentially anticarcinogenic flavonoids and their determinants in adults in the Netherlands.* Nutrition and Cancer, 1993. **20**(1): p. 21-29.

257. Lesjak, M., et al., *Quercetin Inhibits Intestinal Iron Absorption and Ferroportin Transporter Expression In Vivo and In Vitro*. PLoS ONE, 2014. **9**(7): p. e102900.

258. Kroon, P.A., et al., *How should we assess the effects of exposure to dietary polyphenols in vitro?* Am J Clin Nutr, 2004. **80**(1): p. 15-21.

259. Olthof, M.R., et al., *Bioavailabilities of quercetin-3-glucoside and quercetin-4'-glucoside do not differ in humans*. J Nutr, 2000. **130**(5): p. 1200-3.

260. Leopoldini, M., et al., *Iron Chelation by the Powerful Antioxidant Flavonoid Quercetin*. Journal of Agricultural and Food Chemistry, 2006. **54**(17): p. 6343-6351.

261. Tereza Fernandez, M., et al., *Iron and copper complexation by angiotensin-converting enzyme inhibitors. A study by ultraviolet spectroscopy and electrospray mass spectrometry*. Journal of Inorganic Biochemistry, 1998. **71**(1–2): p. 93-98.

262. Ren, J., et al., *Complexation of flavonoids with iron: Structure and optical signatures*. Journal of Physical Chemistry B, 2008. **112**(6): p. 1845-1850.

263. Satterfield, M. and J.S. Brodbelt, *Enhanced Detection of Flavonoids by Metal Complexation and Electrospray Ionization Mass Spectrometry*. Analytical Chemistry, 2000. **72**(24): p. 5898-5906.

264. Ryan, P. and M.J. Hynes, *The kinetics and mechanisms of the reactions of iron(III) with quercetin and morin*. Journal of Inorganic Biochemistry, 2008. **102**(1): p. 127-136.

265. Guo, M., et al., *Iron-binding properties of plant phenolics and cranberry's bio-effects*. Dalton transactions (Cambridge, England : 2003), 2007(43): p. 4951-4961.

266. Vlachodimitropoulou, E., P.A. Sharp, and R.J. Naftalin, *Quercetin–iron chelates are transported via glucose transporters*. Free Radical Biology and Medicine, 2011. **50**(8): p. 934-944.

267. Morel, I., et al., *[43] Role of flavonoids and iron chelation in antioxidant action*, in *Methods in Enzymology*, P. Lester, Editor. 1994, Academic Press. p. 437-443.

268. Li, Y., et al., *Quercetin protects rat hepatocytes from oxidative damage induced by ethanol and iron by maintaining intercellular liable iron pool*. Hum Exp Toxicol, 2014. **33**(5): p. 534-41.

269. Baccan, M.M., et al., *Quercetin as a shuttle for labile iron*. Journal of Inorganic Biochemistry, 2012. **107**(1): p. 34-39.

270. Mladěnka, P., et al., *In vitro analysis of iron chelating activity of flavonoids*. Journal of Inorganic Biochemistry, 2011. **105**(5): p. 693-701.

271. Cook, J.D., M.B. Reddy, and R.F. Hurrell, *The effect of red and white wines on nonheme-iron absorption in humans*. Am J Clin Nutr, 1995. **61**(4): p. 800-4.

272. Kim, E.Y., et al., *Bioactive dietary polyphenolic compounds reduce nonheme iron transport across human intestinal cell monolayers*. J Nutr, 2008. **138**(9): p. 1647-51.

273. Yoshino, M. and K. Murakami, *Interaction of Iron with Polyphenolic Compounds: Application to Antioxidant Characterization*. Analytical Biochemistry, 1998. **257**(1): p. 40-44.

274. Cunningham, P., I. Afzal-Ahmed, and R.J. Naftalin, *Docking studies show that D-glucose and quercetin slide through the transporter GLUT1*. J Biol Chem, 2006. **281**(9): p. 5797-803.

275. Ioku, K., et al., *Antioxidative activity of quercetin and quercetin monoglucosides in solution and phospholipid bilayers*. Biochim Biophys Acta, 1995. **1234**(1): p. 99-104.

276. Manach, C., et al., *Bioavailability and bioefficacy of polyphenols in humans. I. Review of 97 bioavailability studies*. Am J Clin Nutr, 2005. **81**(1 Suppl): p. 230s-242s.

277. Manach, C., et al., *Bioavailability of rutin and quercetin in rats*. FEBS Letters, 1997. **409**(1): p. 12-16.

278. Guo, Y. and R.S. Bruno, *Endogenous and exogenous mediators of quercetin bioavailability*. The Journal of Nutritional Biochemistry, 2015. **26**(3): p. 201-210.

279. Xu, G., et al., *Enhancing the anti-colon cancer activity of quercetin by self-assembled micelles*. Int J Nanomedicine, 2015. **10**: p. 2051-63.

280. Sun, M., et al., *Enhanced oral bioavailability of quercetin by nanostructured lipid carriers (1044.24)*. The FASEB Journal, 2014. **28**(1 Supplement).

281. Winter, J., et al., *C-ring cleavage of flavonoids by human intestinal bacteria.* Applied and Environmental Microbiology, 1989. **55**(5): p. 1203-1208.

282. Schneider, H., et al., *Anaerobic transformation of quercetin-3-glucoside by bacteria from the human intestinal tract.* Arch Microbiol, 1999. **171**(2): p. 81-91.

283. Zhang, Z., et al., *Isolation and Identification of Quercetin Degrading Bacteria from Human Fecal Microbes.* PLoS ONE, 2014. **9**(3): p. e90531.

284. Kawabata, K., R. Mukai, and A. Ishisaka, *Quercetin and related polyphenols: new insights and implications for their bioactivity and bioavailability.* Food & Function, 2015. **6**(5): p. 1399-1417.

285. Serra, A., et al., *Metabolic pathways of the colonic metabolism of flavonoids (flavonols, flavones and flavanones) and phenolic acids.* Food Chemistry, 2012. **130**(2): p. 383-393.

286. RiceEvans, C.A., J. Miller, and G. Paganga, *Antioxidant properties of phenolic compounds.* Trends in Plant Science, 1997. **2**(4): p. 152-159.

287. Knekt, P., et al., *Dietary Flavonoids and the Risk of Lung Cancer and Other Malignant Neoplasms.* American Journal of Epidemiology, 1997. **146**(3): p. 223-230.

288. Bobe, G., et al., *Dietary Flavonoids and Colorectal Adenoma Recurrence in the Polyp Prevention Trial.* Cancer epidemiology, biomarkers & prevention : a publication of the American Association for Cancer Research, cosponsored by the American Society of Preventive Oncology, 2008. **17**(6): p. 1344-1353.

289. Dihal, A.A., et al., *Quercetin, but Not Its Glycosidated Conjugate Rutin, Inhibits Azoxymethane-Induced Colorectal Carcinogenesis in F344 Rats.* The Journal of Nutrition, 2006. **136**(11): p. 2862-2867.

290. Gee, J.M., H. Hara, and I.T. Johnson, *Suppression of Intestinal Crypt Cell Proliferation and Aberrant Crypt Foci by Dietary Quercetin in Rats.* Nutrition and Cancer, 2002. **43**(2): p. 193-201.

291. Warren, C.A., et al., *Quercetin may suppress rat aberrant crypt foci formation by suppressing inflammatory mediators that influence proliferation and apoptosis.* J Nutr, 2009. **139**(1): p. 101-5.

292. Volate, S.R., et al., *Modulation of aberrant crypt foci and apoptosis by dietary herbal supplements (quercetin, curcumin, silymarin, ginseng and rutin).* Carcinogenesis, 2005. **26**(8): p. 1450-6.

293. Dihal, A.A., et al., *Modulatory effects of quercetin on proliferation and differentiation of the human colorectal cell line Caco-2.* Cancer Letters, 2006. **238**(2): p. 248-259.

294. Wang, P., et al., *Effects of quercetin on the apoptosis of the human gastric carcinoma cells.* Toxicology in Vitro, 2012. **26**(2): p. 221-228.

295. Murphy, E.A., et al., *Quercetin's effects on intestinal polyp multiplicity and macrophage number in the Apc(Min/+) mouse.* Nutr Cancer, 2011. **63**(3): p. 421-6.

296. De Stefano, D., et al., *Lycopene, quercetin and tyrosol prevent macrophage activation induced by gliadin and IFN-gamma.* Eur J Pharmacol, 2007. **566**(1-3): p. 192-9.

297. Velazquez, K.T., et al., *Quercetin Supplementation Attenuates the Progression of Cancer Cachexia in Apc(Min/+) Mice.* Journal of Nutrition, 2014. **144**(6): p. 868-875.

298. Selvaraj, S., et al., *Synthesis, characterization and DNA binding properties of rutin-iron complex.* RSC Advances, 2012. **2**(7): p. 2797-2802.

299. Nowak, D., A. Kuźniar, and M. Kopacz, *Solid complexes of iron(II) and iron(III) with rutin.* Structural Chemistry, 2010. **21**(2): p. 323-330.

300. Bai, Y., et al., *Characterization of the rutin-metal complex by electrospray ionization tandem mass spectrometry.* Anal Sci, 2004. **20**(8): p. 1147-51.

301. Koval'skii, I.V., et al., *Mechanisms of Rutin Pharmacological Action (Review).* Pharmaceutical Chemistry Journal, 2014. **48**(2): p. 73-76.

302. Graefe, E.U., et al., *Pharmacokinetics and bioavailability of quercetin glycosides in humans.* J Clin Pharmacol, 2001. **41**(5): p. 492-9.

303. Crespy, V., et al., *Quercetin, but not its glycosides, is absorbed from the rat stomach.* J Agric Food Chem, 2002. **50**(3): p. 618-21.

304. Deschner, E.E., et al., *QUERCETIN AND RUTIN AS INHIBITORS OF AZOXYMETHANOL-INDUCED COLONIC NEOPLASIA.* Carcinogenesis, 1991. **12**(7): p. 1193-1196.

305. Mahmoud, N.N., et al., *Plant phenolics decrease intestinal tumors in an animal model of familial adenomatous polyposis.* Carcinogenesis, 2000. **21**(5): p. 921-927.

306. Yang, K., et al., *Chemoprevention studies of the flavonoids quercetin and rutin in normal and azoxymethane-treated mouse colon.* Carcinogenesis, 2000. **21**(9): p. 1655-1660.

307. Araujo, J.R., P. Goncalves, and F. Martel, *Chemopreventive effect of dietary polyphenols in colorectal cancer cell lines.* Nutr Res, 2011. **31**(2): p. 77-87.

308. Cheng, G.W.W. and C.H. Crisosto, *Iron-polyphenol complex formation and skin discoloration in peaches and nectarines.* Journal of the American Society for Horticultural Science, 1997. **122**(1): p. 95-99.

309. Galvano, F., et al., *Cyanidins: metabolism and biological properties.* J Nutr Biochem, 2004. **15**(1): p. 2-11.

310. Tsuda, T., F. Horio, and T. Osawa, *Absorption and metabolism of cyanidin 3-O-beta-D-glucoside in rats.* FEBS Lett, 1999. **449**(2-3): p. 179-82.

311. Miyazawa, T., et al., *Direct intestinal absorption of red fruit anthocyanins, cyanidin-3-glucoside and cyanidin-3,5-diglucoside, into rats and humans.* J Agric Food Chem, 1999. **47**(3): p. 1083-91.

312. Matsumoto, H., et al., *Orally administered delphinidin 3-rutinoside and cyanidin 3-rutinoside are directly absorbed in rats and humans and appear in the blood as the intact forms.* J Agric Food Chem, 2001. **49**(3): p. 1546-51.

313. Cai, H., et al., *Determination of anthocyanins in the urine of patients with colorectal liver metastases after administration of bilberry extract.* Biomed Chromatogr, 2011. **25**(6): p. 660-3.

314. Talavera, S., et al., *Anthocyanins are efficiently absorbed from the small intestine in rats.* J Nutr, 2004. **134**(9): p. 2275-9.

315. Matuschek, M.C., et al., *The jejunum is the main site of absorption for anthocyanins in mice.* J Nutr Biochem, 2006. **17**(1): p. 31-6.

316. Fang, J., *Bioavailability of anthocyanins.* Drug Metabolism Reviews, 2014. **46**(4): p. 508-520.

317. Kahle, K., et al., *Studies on apple and blueberry fruit constituents: do the polyphenols reach the colon after ingestion?* Mol Nutr Food Res, 2006. **50**(4-5): p. 418-23.

318. Czank, C., et al., *Human metabolism and elimination of the anthocyanin, cyanidin-3-glucoside: a (13)C-tracer study.* Am J Clin Nutr, 2013. **97**(5): p. 995-1003.

319. de Ferrars, R.M., et al., *The pharmacokinetics of anthocyanins and their metabolites in humans.* Br J Pharmacol, 2014. **171**(13): p. 3268-82.

320. Aura, A.M., et al., *In vitro metabolism of anthocyanins by human gut microflora.* Eur J Nutr, 2005. **44**(3): p. 133-42.

321. Hanske, L., et al., *Contribution of gut bacteria to the metabolism of cyanidin 3-glucoside in human microbiota-associated rats.* Br J Nutr, 2013. **109**(8): p. 1433-41.

322. Chen, P.-N., et al., *Mulberry anthocyanins, cyanidin 3-rutinoside and cyanidin 3-glucoside, exhibited an inhibitory effect on the migration and invasion of a human lung cancer cell line.* Cancer Letters, 2006. **235**(2): p. 248-259.

323. Sun, C., et al., *Purification and anti-tumour activity of cyanidin-3-O-glucoside from Chinese bayberry fruit.* Food Chemistry, 2012. **131**(4): p. 1287-1294.

324. Olsson, M.E., et al., *Inhibition of cancer cell proliferation in vitro by fruit and berry extracts and correlations with antioxidant levels.* J Agric Food Chem, 2004. **52**(24): p. 7264-71.

325. Wu, Q.K., et al., *Berry phenolic extracts modulate the expression of p21(WAF1) and Bax but not Bcl-2 in HT-29 colon cancer cells.* J Agric Food Chem, 2007. **55**(4): p. 1156-63.

326. McDougall, G.J., et al., *Berry extracts exert different antiproliferative effects against cervical and colon cancer cells grown in vitro.* J Agric Food Chem, 2008. **56**(9): p. 3016-23.

327. Gopalan, A., et al., *The health benefits of blackcurrants.* Food & Function, 2012. **3**(8): p. 795-809.

328. Hart, J.J., et al., *Identification of Black Bean (Phaseolus vulgaris L.) Polyphenols That Inhibit and Promote Iron Uptake by Caco-2 Cells.* Journal of Agricultural and Food Chemistry, 2015. **63**(25): p. 5950-5956.

329. Perron, N.R. and J.L. Brumaghim, *A review of the antioxidant mechanisms of polyphenol compounds related to iron binding.* Cell Biochem Biophys, 2009. **53**(2): p. 75-100.

330. Song, Q., et al., *Enhanced uptake and transport of (+)-catechin and (-)-epigallocatechin gallate in niosomal formulation by human intestinal Caco-2 cells.* Int J Nanomedicine, 2014. **9**: p. 2157-65.

331. Baba, S., et al., *In Vivo Comparison of the Bioavailability of (+)-Catechin, (−)-Epicatechin and Their Mixture in Orally Administered Rats.* The Journal of Nutrition, 2001. **131**(11): p. 2885-2891.

332. Vaidyanathan, J.B. and T. Walle, *Transport and metabolism of the tea flavonoid (-)-epicatechin by the human intestinal cell line Caco-2.* Pharmaceutical Research, 2001. **18**(10): p. 1420-1425.

333. Donovan, J.L., et al., *(+)-Catechin is more bioavailable than (-)-catechin: relevance to the bioavailability of catechin from cocoa.* Free Radic Res, 2006. **40**(10): p. 1029-34.

334. Borges, G., et al., *Bioavailability of dietary (poly)phenols: a study with ileostomists to discriminate between absorption in small and large intestine.* Food & Function, 2013. **4**(5): p. 754-762.

335. Yang, C.S., et al., *Blood and urine levels of tea catechins after ingestion of different amounts of green tea by human volunteers.* Cancer Epidemiol Biomarkers Prev, 1998. **7**(4): p. 351-4.

336. Warden, B.A., et al., *Catechins are bioavailable in men and women drinking black tea throughout the day.* J Nutr, 2001. **131**(6): p. 1731-7.

337. Du, G.J., et al., *Epigallocatechin Gallate (EGCG) Is the Most Effective Cancer Chemopreventive Polyphenol in Green Tea.* Nutrients, 2012. **4**(11): p. 1679-1691.

338. Agullo, G., et al., *Comparative effects of flavonoids on the growth, viability and metabolism of a colonic adenocarcinoma cell line (HT29 cells).* Cancer Letters, 1996. **105**(1): p. 61-70.

339. Simons, C.C.J.M., et al., *Dietary flavonol, flavone and catechin intake and risk of colorectal cancer in the Netherlands Cohort Study.* International Journal of Cancer, 2009. **125**(12): p. 2945-2952.

340. Theodoratou, E., et al., *Dietary flavonoids and the risk of colorectal cancer.* Cancer Epidemiol Biomarkers Prev, 2007. **16**(4): p. 684-93.

341. Toyokuni, S., *Iron-induced carcinogenesis: the role of redox regulation.* Free Radic Biol Med, 1996. **20**(4): p. 553-66.

Chapter 2

Alginate iron binding:

a chemical characterisation.

2.1   Introduction and aims

Sodium alginate was chosen as a potential iron binding compound since there is evidence to imply that it has the desired characteristics required for a 'luminal iron chelator', namely non-absorbability,[1-3] iron binding [4, 5] and safe for human consumption.   The chemical interaction of alginate with iron has not been fully characterised.[5-7] The majority of reports of an alginate-iron interaction are around the formation of iron-oxide nanoparticles, where the alginate is employed as a scaffold.[8-14]   Whether this nanoparticle formation within the environments of the gastro-intestinal tract occurs is unknown, however in the chemical synthesis of such nanoparticles, harsh basic pH conditions are utilised to drive formation.[13] One report estimates the iron(III) alginate binding constant of K = 5.04 x 10^4 M^{-1}.[5]   With regards to other metal ions, it is known that calcium readily coordinates with alginate with a strong affinity to form gels.[15-20]   It is also known that the affinity and strength of interaction of alginates with calcium is dependent upon alginate chemical composition; a factor with respect to iron binding that is unknown.[7, 20]

In consideration of this, the binding of iron to alginate needs be assessed at a molecular level in order to understand the nature of their complexation and most pertinently to establish if sodium alginate is a suitable candidate as an iron chelator with respect to its iron binding ability. A series of alginates will be characterised, such that any differences in iron binding can be rationalised by the differences in their chemical composition similarly to the interaction of calcium with alginate. Likewise, the effect of competing metal cations also needs to be assessed since other metals are also found in the colon. Thus, the aims of this chapter are:

1. To determine the iron binding potential of a series of alginates with a range of chemical compositions.

2. Understand the effect of competing metal ions such as calcium on iron binding.

3. To investigate and propose a mechanism of the alginate-iron interaction using solution and surface modalities.

4. Chemically characterise the alginate series to determine molecular weights and G:M compositions.

2.2   Results and Discussion

2.2.1   Iron binding of alginate using dialysis techniques

Dialysis techniques were employed to screen the alginate series for their iron binding potential. Alginate was confined within a dialysis membrane and incubated in a solution of aqueous ferrous sulphate that was in excess of the alginate molarity. Since ferrous sulphate was used as the iron source, it could be suggested that some iron oxo-hydroxide would be

present due to ferrous irons hydrolytic nature in aqueous solutions. The dialysis bag was subsequently washed to remove freely-dialysable (non-bound) iron from the alginate, to allow assessment of the total iron bound to alginate (method 2.5.1). The concentration of iron that was used was similar to that reported in the colon (0.2 mM).[21] Analysis of iron concentrations revealed that all alginates bind iron and at equal amounts under the dialysis conditions (figure 2.1).
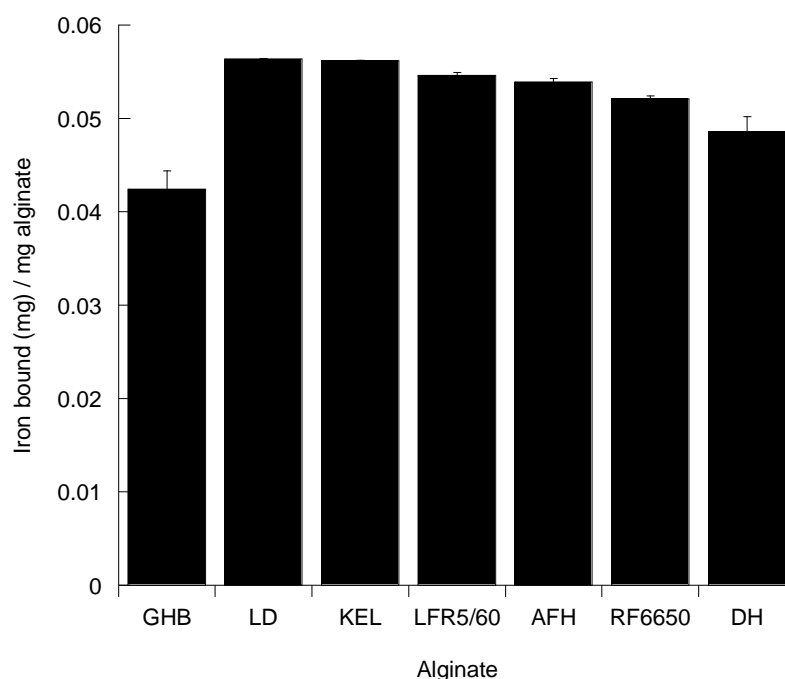
Figure 2.1: Iron concentration (mg/mg alginate) of dialysed alginate incubated in FeSO$_4$·7H$_2$O (0.2 mM) and washed to remove non-alginate-bound iron. Error bars denote ± SEM, n = 3.

The alginate series tested all bind iron, with 1 g of alginate calculated to bind between 0.42 and 0.56 g of iron(II) with a mean iron binding potential of 0.52 g of iron (II) per gram of alginate. The reported molecular weight of alginate LFR5/60 is ca. 35,000 Da.[22] The monomer unit size of the guluronic or mannuronic acid monomers (C$_6$H$_{10}$O$_7$) is 194 Da, which calculates to 180 monomer units per alginic acid polymer. As hypothesised earlier

from the coordination studies of different transition metals, the carboxylate residue of the uronic acid unit is the host for an iron ion and can accommodate one ferrous or ferric ion. This estimation can be used to calculate a total *theoretical* iron binding potential of 0.28 g of iron(II) per gram of LFR5/60. This indicates from the results of the dialysis experiments that more iron is binding than a typical 1:1 monomer unit:carboxylate interaction since almost double the amount of iron was chelated. An estimation for the other alginates used in this experiment could not be calculated as their molecular weights are unknown.

As reviewed, the use of alginates and their interaction with calcium is well established and the strength of binding is known to be strong. It is important to consider competition from other metal cations, especially in the context of sodium alginate being used as a medicine to chelate iron within the gastro-intestinal tract as other metal cations (such as calcium) will be present within this environment. With this, the extent of this competition was determined by titrating increasing amounts of calcium chloride into the iron solution that the alginates are incubated (figure 2.2).
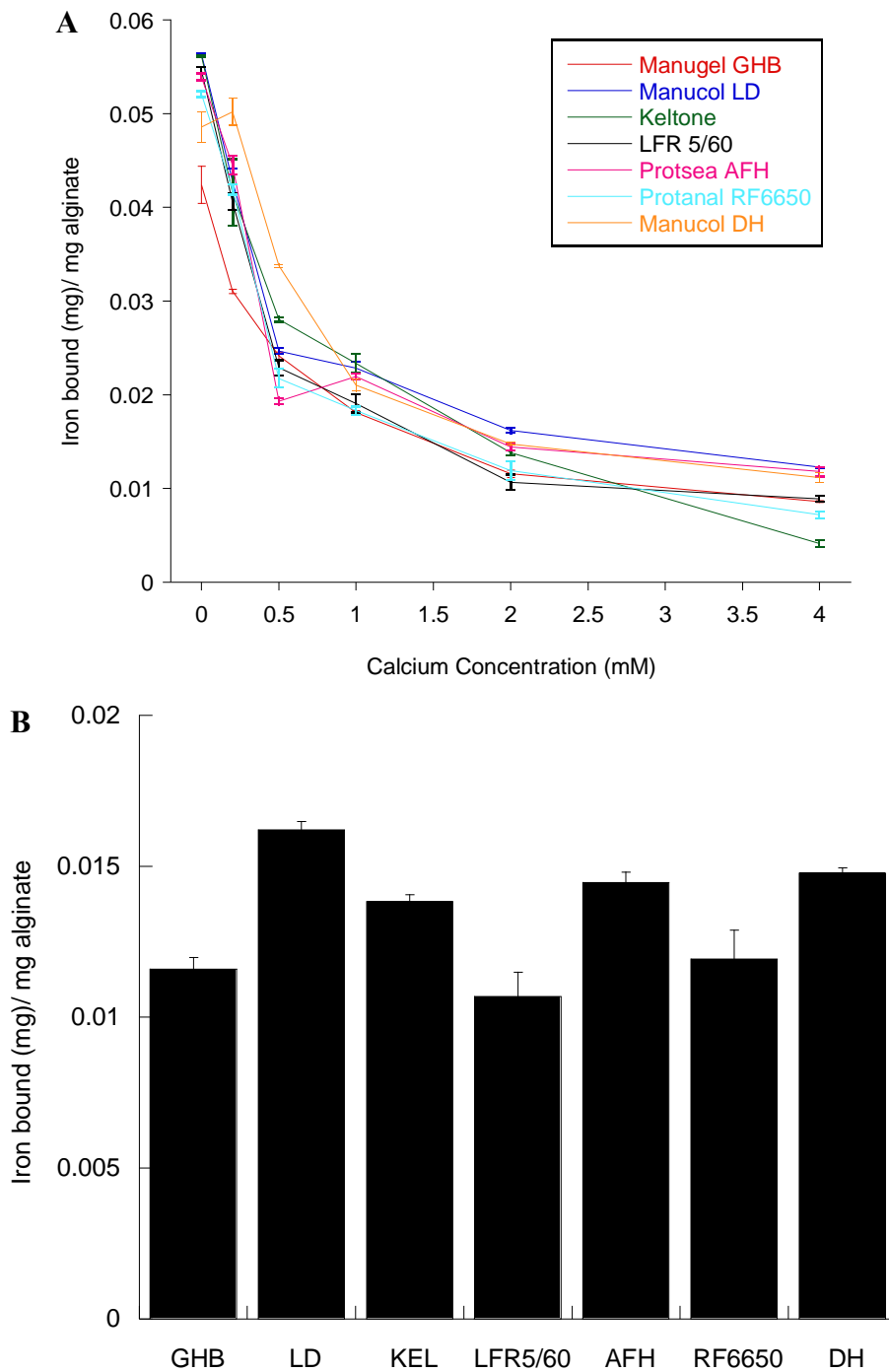
Figure 2.2: (A) Iron concentration of dialysed alginate incubated in $FeSO_4 \cdot 7H_2O$ (0.2 mM) with $CaCl_2 \cdot 2H_2O$ titrated in at concentrations of 0-4 mM. (B) Specific iron binding potentials of the alginate series at 2 mM $CaCl_2 \cdot 2H_2O$. Error bars denote ± SEM, n = 3.

Iron displacement due to calcium binding to alginate is evident (figure 2.2). This is expected based on the affinity series described earlier (cf. $Ba^{2+} > Sr^{2+} > Ca^{2+} \gg Mg^{2+} > Be^{2+}$). The

titration of calcium demonstrates that as little as 1 mM calcium chloride is able to displace 50% of the iron that is bound to alginate. At the 2 mM calcium concentration (the concentration calculated to be present within the colon),[23] the proportion of displacement continues yet differences become apparent between the alginates. Manucol LD retains 53% more iron than alginate LFR5/60; Protsea AFH and Manucol DH also retain significant iron-binding at this concentration of calcium. Iron binding by the alginates at physiologically relevant concentrations of calcium can be stratified as such; LD>DH≈AFH>KEL>RF5560≈GHB>LFR5/60.

The rate of loss of iron from the alginate by both diffusion and also by calcium displacement can be measured using an amended technique of the alginate dialysis method, whereby alginate samples are taken periodically and iron is measured at specific time points. This allows the measurement of iron loss over a timed period and the rate of loss can be calculated with the loss of iron related to the effect of calcium competition only (figure 2.3).
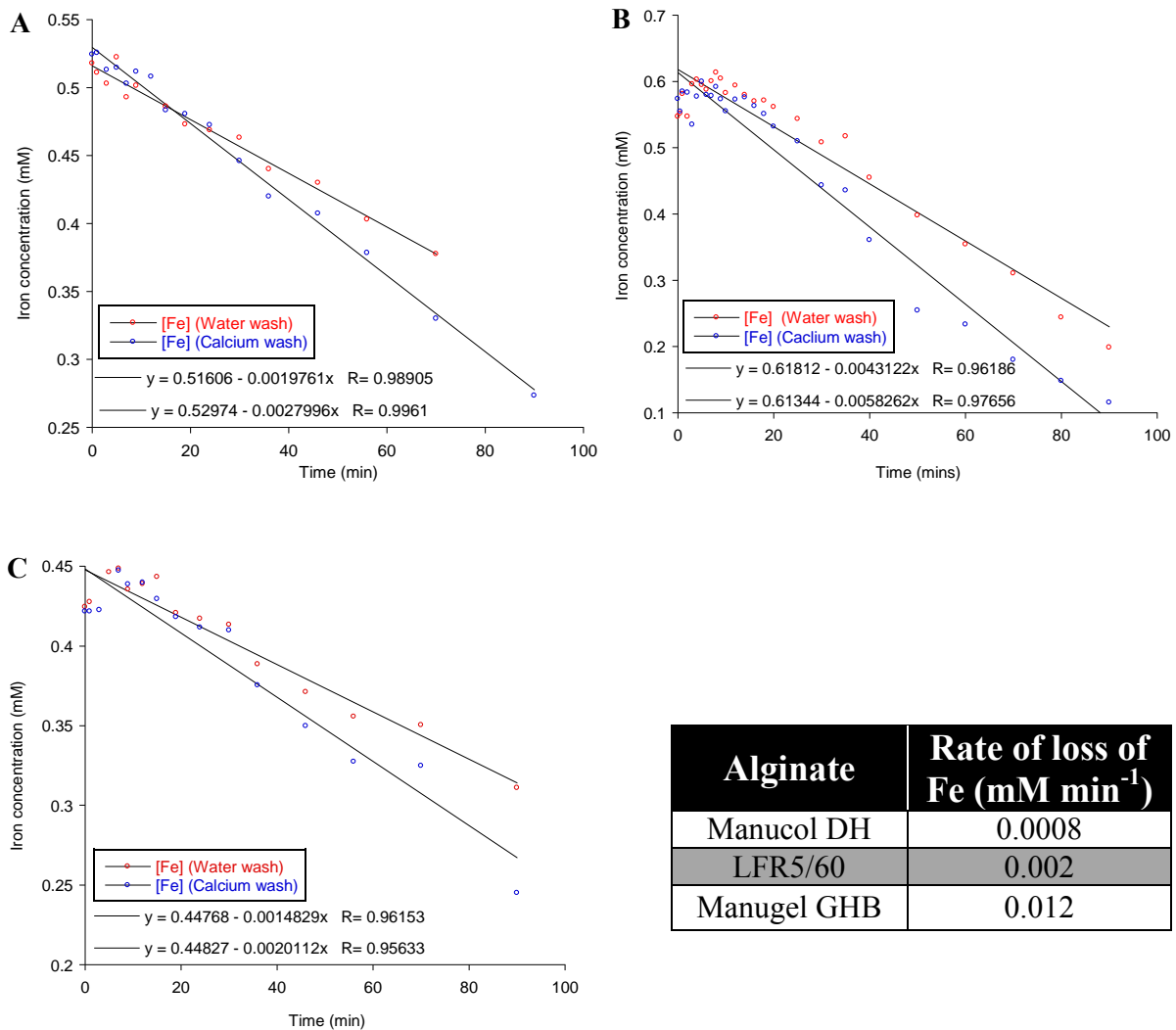
Figure 2.3: Loss of iron from alginate (incubated originally in $FeSO_4 \cdot 7H_2O$ (0.2 mM)) due to diffusion (subsequent incubation in water) and displacement by calcium (subsequent incubation in $CaCl_2 \cdot 2H_2O$ (0.2 mM)) for (A) Manucol DH, (B) LFR5/60 and (C) Manugel GHB.

As evident by the rate of loss of iron for Manucol DH, LFR5/60 and Manugel GHB (0.0008, 0.002 and 0.012 mM min^{-1} respectively) there are large differences between the alginates. These results corroborate the initial displacement experiment, whereby the alginates that were most affected by calcium addition are those with the higher rates of iron loss.

These dialysis experiments indicate that all the alginates do indeed bind iron. It becomes evident that these similarities are no longer apparent when the alginates are subject to competition by calcium. Manucol LD, Manucol DH and Protsea AFH retain higher proportions of iron binding under calcium-competitive conditions. It could be hypothesised that these differences can be rationalised based on the chemical composition differences of the alginate series. Calcium is known to bind to alginate arranged in the supramolecular 'egg-box' structure (as discussed in section 1.4.5), whereby calcium ions have a higher affinity towards the G-units than the M-units along the alginate backbone. It could be the case that these three alginates that retain higher iron binding under calcium-competitive conditions have the lower proportion G-units of the alginate series, attenuating their affinity towards calcium.

2.2.2 Calcium-alginate Isothermal Titration Microcalorimetry

Since it has been demonstrated that calcium impacts on the iron chelation properties of alginate, the affinity of calcium towards alginate was examined using Isothermal Titration Microcalorimetry (ITC). ITC is a sensitive technique which measures the energetics of a chemical reaction or molecular interactions. Aliquots of Ca(II) were titrated into stirred alginate solutions at a constant temperature of 37 °C and the heats of each titration were measured, integrated and plotted onto thermograms (method 2.5.3) (figure 2.4).[20]
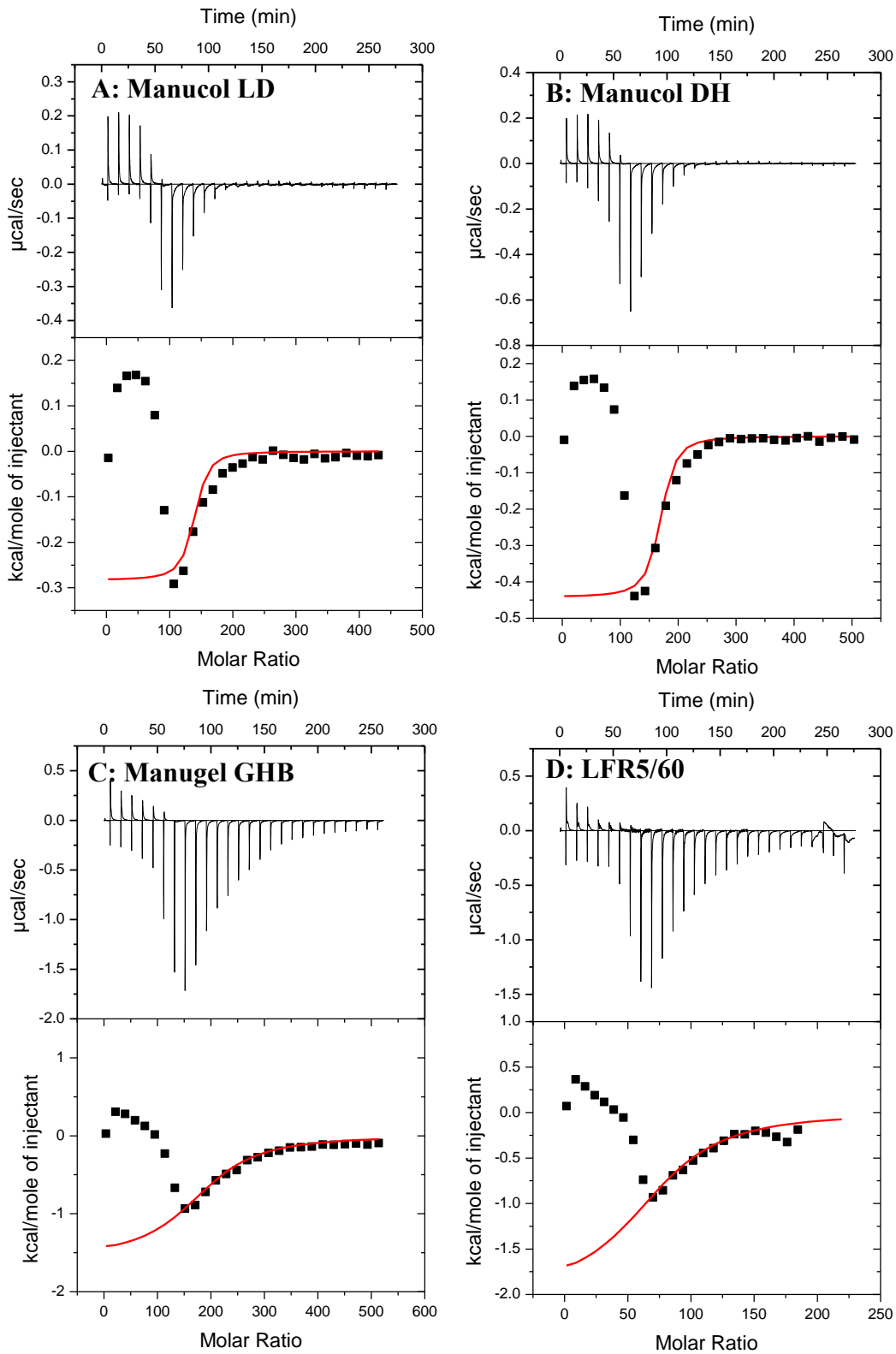
Figure 2.4: ITC thermograms recorded for injecting 10 μL aliquots of CaCl$_2$·2H$_2$O (7.5 mM) into (a) Manucol LD, (b) Manucol DH, (c) Manugel GHB and (d) LFR5/60 (0.052%) at 37 °C in acetate buffer (20 mM, pH 5). Alginate solutions were dialysed against acetate buffer prior to titration to eradicate heat changes due to pH changes and ionic-strength miss-matches between the titrant and titrand. Corresponding isotherms are displayed below the thermograms and binding curves were plotted using a model of independent binding sites.

Values obtained for the number of binding sites (N), enthalpy of binding (H), the binding constant (K) and the entropy of interaction (S) were calculated (table 2.1).

Table 2.1: Binding parameters obtained from alginate-calcium ITC.

Alginate	N	K (M^{-1})	ΔH (cal mol^{-1})	ΔS (cal mol^{-1} K^{-1})
Manucol LD	133 ± 4.6	$3.26 \times 10^5 \pm 2.42 \times 10^5$	-283	24.5
Manucol DH	163 ± 3.7	$3.26 \times 10^5 \pm 1.67 \times 10^5$	-441.8 ± 32.98	23.8
Manugel GHB	187 ± 9.34	$1.91 \times 10^4 \pm 2.68 \times 10^3$	-1557 ± 145.1	14.6
LFR5/60	75.8 ± 12.9	$1.09 \times 10^4 \pm 3.04 \times 10^3$	-1978 ± 568	12.1

The binding isotherms were obtained by integrating the injection peaks of calcium titration into alginate and subtracting the corresponding heats of dilution of Ca(II) titration into acetate buffer (control titration). The ITC thermograms show a two-step binding motif, whereby the second step was fitted to a 'one set of sites' binding model (equation 2.5). This second event corresponds to the binding of calcium to G-units on the alginate and egg-box formation.[20]

$$Q = \frac{nM_t \Delta H V_o}{2}\left[1 + \frac{X_t}{nM_t} + \frac{1}{nKM_t} - \sqrt{\left(1 + \frac{X_t}{nM_t} + \frac{1}{nKM_t}\right)^2 - \frac{4X_t}{nM_t}}\right]$$

Figure 2.5: One set of sites model for fitting the binding isotherms. This model assumes that a ligand can bind one or multiple binding sites of another molecule with identical affinity and identical binding mechanisms where Q = heat content of the solution, n = number of binding sites, M_t = total concentration of macromolecule in V_o, V_o = active cell volume, H = enthalpy, X_t = total ligand concentration and K = the binding constant.

The number of binding sites (N) increases as such; LFR5/60 < Manucol LD < Manucol DH < Manugel GHB. Interestingly, the binding enthalpy for each alginate towards calcium follows the same trend identified for the binding affinity in the dialysis experiments, whereby LFR5/60 has the highest enthalpy for calcium binding (-1978 cal mol^{-1}) and the lowest iron retention in competitive dialysis experiments. On the other hand, Manucol LD, which has the lowest enthalpy of interaction (-283 cal mol^{-1}) retains the highest iron binding when calcium is present in the equilibrium dialysis experiments.   This again may reflect the G:M composition of the alginates, where those with higher G-compositions are likely to have higher binding enthalpies for calcium. The calcium binding constants (K) were all within one order of magnitude for each alginate. Similar to the experiment detailed earlier, a difference would not be expected since the model is fitted to the binding of calcium to specifically G-units only, which between the alginates are the same. However, these experiments alongside the results generated from the dialysis experiments displays the need to determine the chemical composition of the series of alginates.

2.2.3   Guluronic acid and mannuronic acid composition determination

The possible range of G:M compositions of different alginates is extensive. Not only can alginates have varying compositions in terms of G:M ratios, they can also vary in terms of their sequence structure too. For example, a 50:50 G:M alginate may have sequence structure GGGMMM (block-wise arrangement) or GMGMGM (alternating arrangement) as two extreme examples (figure 2.6). Determination of the G:M compositions of alginates was examined by i) circular dichroism spectroscopy, which reveals the relative G-unit content

between alginates and ii) Nuclear Magnetic Resonance (NMR) spectroscopy, which reveals

the absolute G:M composition.

G   G   G   M   M   M

G   M   G   M   G   M
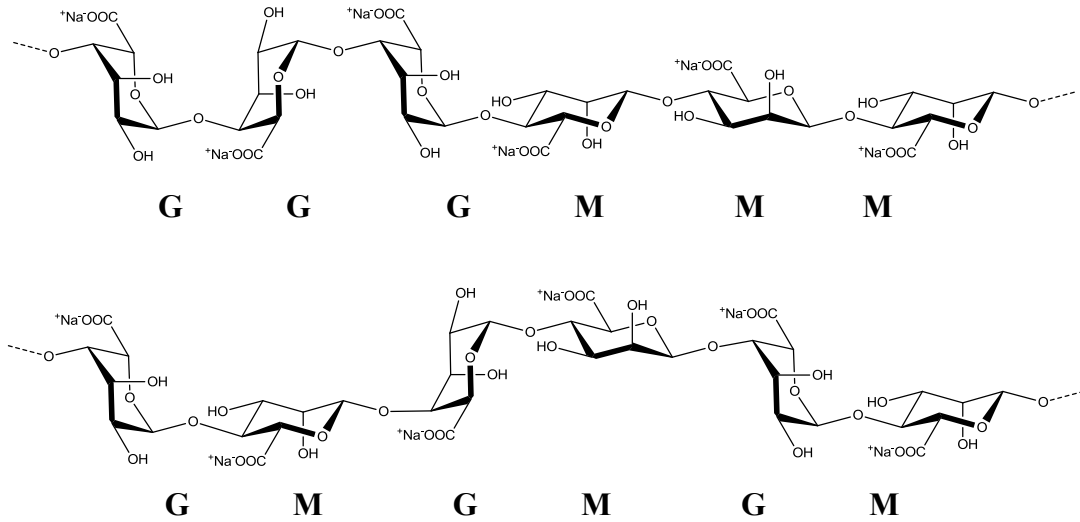
Figure 2.6: Chemical compositions of a 50:50 G:M alginate demonstrating extremes in possible sequence, featuring a blocked arrangement (top) and alternating arrangement (bottom).

2.2.3.1 Determination of composition by circular dichroism spectroscopy

The negative circular dichroism exhibited at ca. 210 nm gives a relative estimation of the G-unit composition of the alginate (figure 2.7).[15]
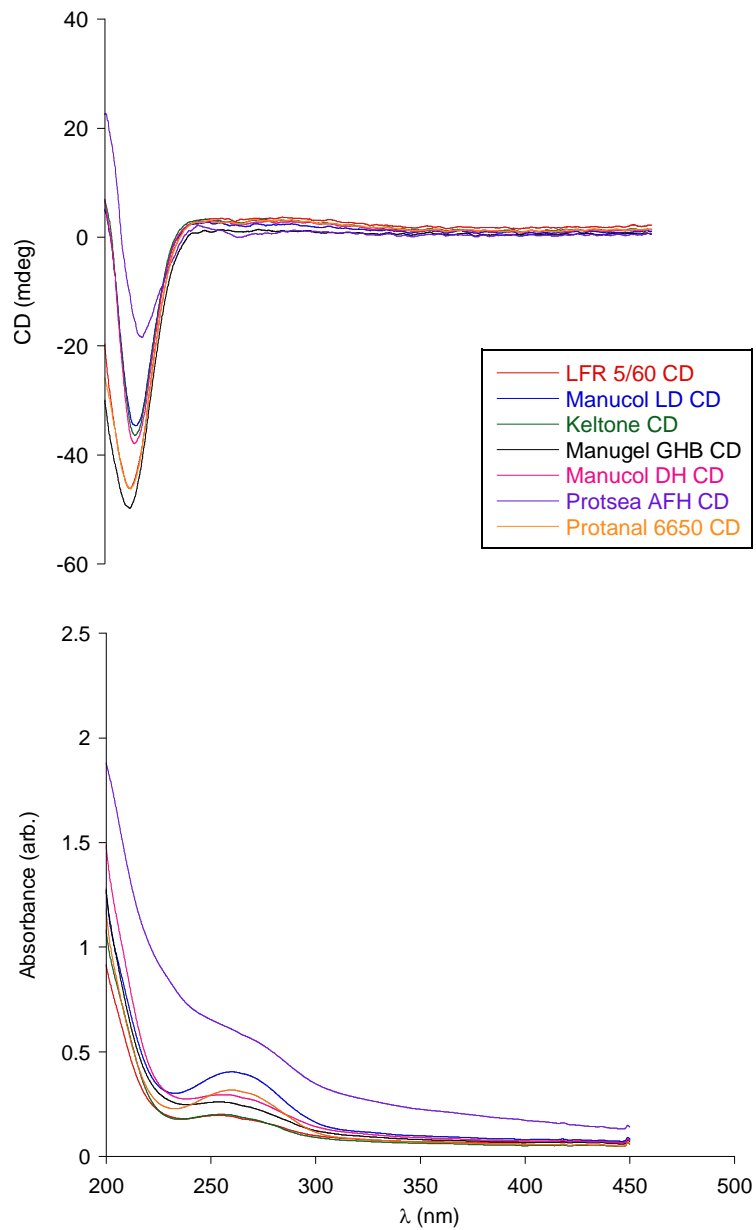
Alginate	CD (mdeg) at 210 nm
Manugel GHB	-49.3
Protanal 6650	-45.4
LFR5/60	-45.3
Manucol DH	-31.7
Keltone	-29.7
Manucol LD	-28.6
Protsea AFH	-7.4

Figure 2.7: CD of alginate series (0.1% w/v) in DI H_2O and corresponding UV-Vis spectra.

It is evident from the CD spectra that there is a wide range of alginate G-unit compositions throughout the alginate series, with some alginates containing 42% more G-unit monomers than the higher M containing alginates. M-unit composition is immeasurable from CD spectroscopy. M-units have a CD absorption at lower wavelength to G-units (ca. 200 nm), but the high absorptivity of G-units masks any apparent M-unit profile. Protsea AFH has a different profile to the other alginates within the series, with a marked attenuation of CD signal at 210 nm. Protsea AFH is the only coloured alginate throughout the series, which may rationalise this anomalous recording.

2.2.3.2 Determination of composition by nuclear magnetic resonance spectroscopy

Despite CD spectroscopy being a convenient method for assessing relative G-content, NMR spectroscopy is an alternative method that can be used to determine absolute G and M alginate composition. The integrals of resonances acquired by the spectrometer correlate to environment-specific protons on the alginate polysaccharide thus allowing absolute G:M ratios to be calculated. The line-width of resonances (and thus overall peak height) obtained from NMR is inversely related to the tumbling time (τ) of the molecule. Large polymers that are viscous in solution will have a low tumbling rate and thus high τ, and so signal-to-noise ratios for alginate resonances within the ^{1}H NMR will be low. Heating the sample alleviates this as alginates acquire more kinetic energy, become less viscous and have a decreased tumbling time. This increases the signal-to-noise ratio observed and as such all NMR spectra were acquired at 90 °C (figure 2.8).
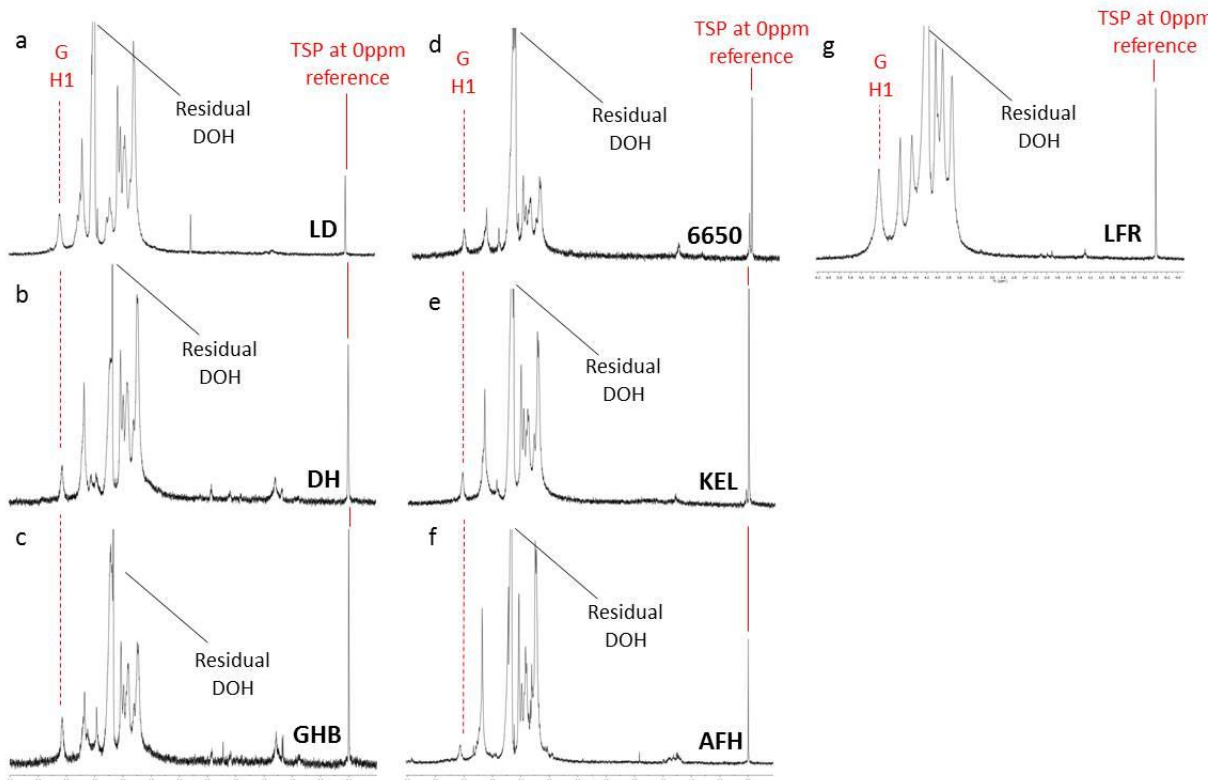
Figure 2.8: Comparison of ^{1}H NMR spectra for the alginate series, (a) Manucol LD, (b) Manucol DH, (c) Manugel GHB, (d) Protanal RF6650, (e) Keltone, (f) Protsea AFH and (g) LFR5/60 at 90 °C in D$_2$O.

Spectra resonances are broad for alginates due to their inherent hydroxyl content. At 90 °C the residual DOH resonance does not interfere with the assignment peaks, allowing integration of the G(H1) and M(H1) protons (method 2.5.5) (figure 2.10).
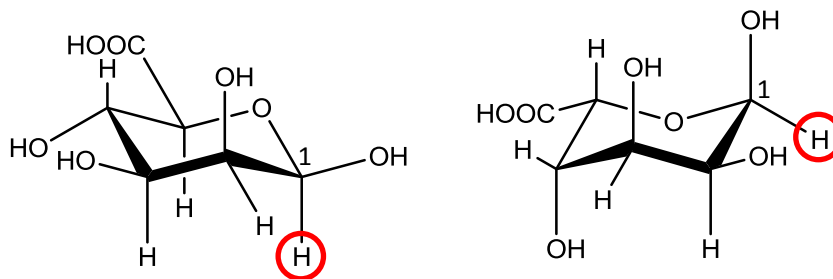
Figure 2.9: Chemical compostions of G and M-units, depicting the H1α and H1β anomeric protons respectivly.

Determination of integrals under the resonances at specific ppm values is proportional to the number of hydrogens in the environment which that resonance represents. Since the signals for the G(H1) and M(H1) anomeric protons at 5.6 ppm and 4.8 ppm respectively are well resolved, the G:M ratio of each alginate can be determined. Different analyses for the determination of uronic acid composition have been reported whereby integration at the following ppm values calculates the ratio of G:M:

A) $G(\mathbf{1H}):M(\mathbf{1H}) = \int_{5.1-6.0 \text{ ppm}} : \int_{4.68-4.64 \text{ ppm}}$ [24]

B) $G(\mathbf{1H}):M(\mathbf{1H}) = \int_{5.1-5.0 \text{ ppm}} : \int_{4.72-4.68 \text{ ppm}}$ [25]

C) $G(\mathbf{1H}):M(\mathbf{1H}) = \int_{5.1-6.0 \text{ ppm}} : \int_{4.6-4.67 \text{ ppm}}$ [26]

Integration of the peaks at these signals and setting $\int_{G(H1)} = 1$ reveals the absolute G:M ratio of the alginate (Table 2.2).

Table 2.2: Integration of 1H NMR analysis of each alginate in the series according to different protocols described above (A, B and C).[24, 26, 27]

Alginate	Protocol	$\int_M$	%G	%M	$\bar{\chi}$ (%G)
Protsea AFH	A	1.82	35	65	29
	B	2.17	31	69	
	C	3.74	21	79	
Manucol LD	A	1.45	40	60	38
	B	1.38	42	58	
	C	2.1	33	67	
Manucol DH	A	1.16	53	47	40
	B	1.22	55	45	
	C	2.28	70	30	
Keltone	A	0.83	55	45	46
	B	1.04	49	51	
	C	1.85	35	65	
Manugel GHB	A	0.77	56	44	53
	B	0.59	63	37	
	C	1.37	41	59	
Protanal RF6650	A	0.47	68	32	60
	B	0.60	62	38	
	C	1.08	48	52	
LFR5/60	A	0.41	71	29	62
	B	0.58	63	36	
	C	0.96	51	49	

Analysis revealed a range of G:M compositions; with the lower %G alginates Protsea AFH and Manucol LD containing 29 and 38% G-units respectively to the highest, LFR5/60, which has 62 % G content. The results obtained from CD spectroscopy mirror the results here verifying the alginate compositions (figure 2.7).

It is evident by comparing the results from the dialysis and calcium ITC experiments with the composition results found here that alginates with higher G-unit content have a stronger affinity for calcium than those with more M-unit composition. It is thus implicit that an alginate with limited G-unit content is likely to be of most benefit for iron chelation studies.

2.2.4 Determination of alginate molecular weight by analytical ultracentrifugation

To fully characterise the alginates, their molecular weights were also determined. Analytical ultracentrifugation (AUC) relies on sedimentation forces to enable the calculation of molecular weight. The method is applicable to small compounds that are hundreds of daltons in weight to larger polymeric compounds and thus is ideally suited to alginate biopolymers where conventional mass spectrometery techniques fail.[28] Alginates were all characterised by sedimentation velocity experiments by analytical ultracentrifugation to establish their molecular integrity using a least squares method.[29] A sedimentation velocity experiment involves high speed centrifugation to sediment the solute (in this case alginate) towards the bottom of the cell sample chamber (method 2.5.6). The rate of movement of the solute can be measured and the rate of movement is proportional to the molecular mass of the alginate (figure 2.10).
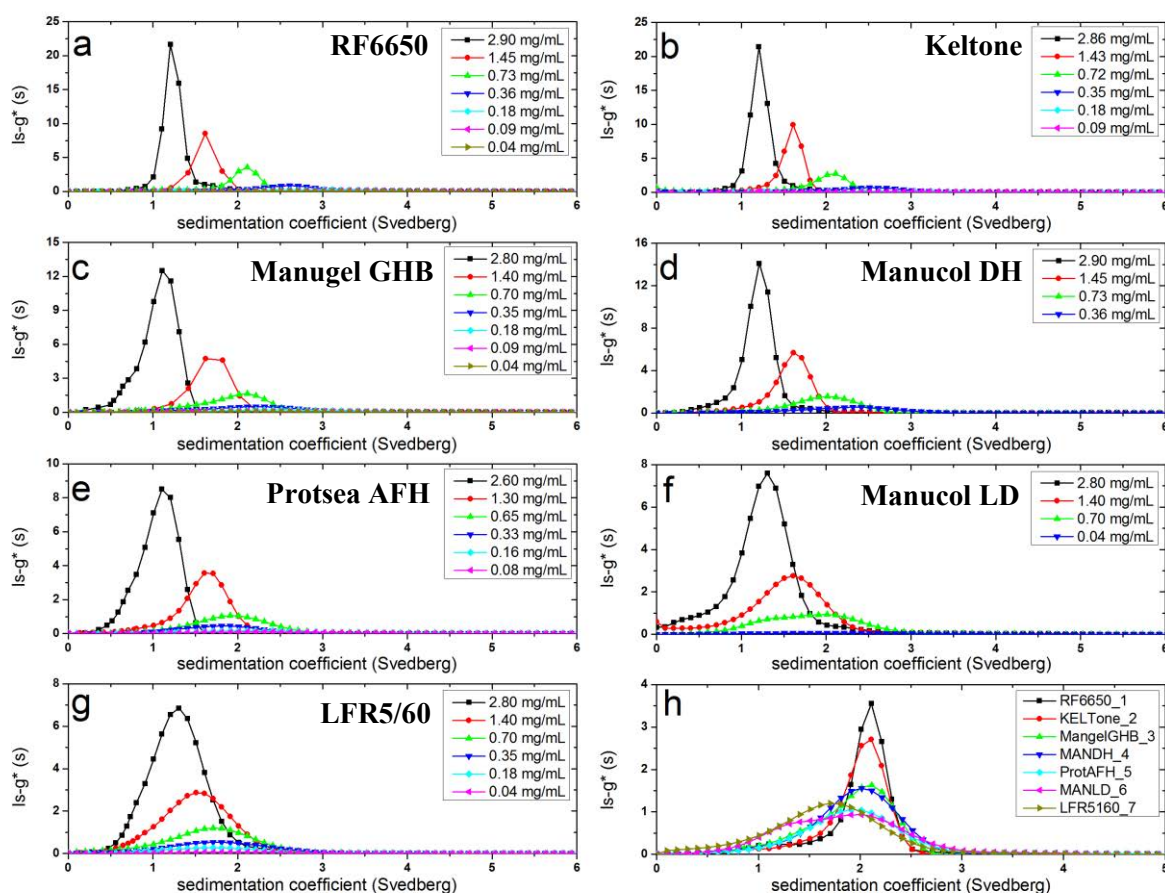
Figure 2.10: Sedimentation coefficient distribution profiles obtained from sedimentation velocity experiments for (a) Protanal RF6650 (b) Keltone (c) Manugel GHB (d) Manucol DH (e) Protsea AFH (f) Manucol LD (g) LFR5/60 and (h) all alginate samples at one concentration (0.7 mg mL^{-1}). S is Svedberg and 1 S = 10^{-13} sec.

The alginate that exhibited the lowest sedimentation coefficient (2.0 ± 0.1 S) was LFR5/60 whereas Protanal RF6650 had the highest value (3.1 ± 0.2 S) indicating the lowest and highest molecular weight of the series. All the alginates demonstrated unimodal distributions indicating homogeneity throughout the series, with no alginates having compositions of variable molecular weight entities.

The weight average molecular weight of the alginate series was estimated from the sedimentation equilibrium using a SEDFIT-MSTAR software. Due to the effect of non-

ideality arising from co-exclusion and polyelectrolyte effects (which normally are non-significant under conditions of high dilution), each alginate was run at different concentrations (0.2 -5.0 mg mL^{-1}) such that weight average molecular weight values can be obtained (figure 2.11).
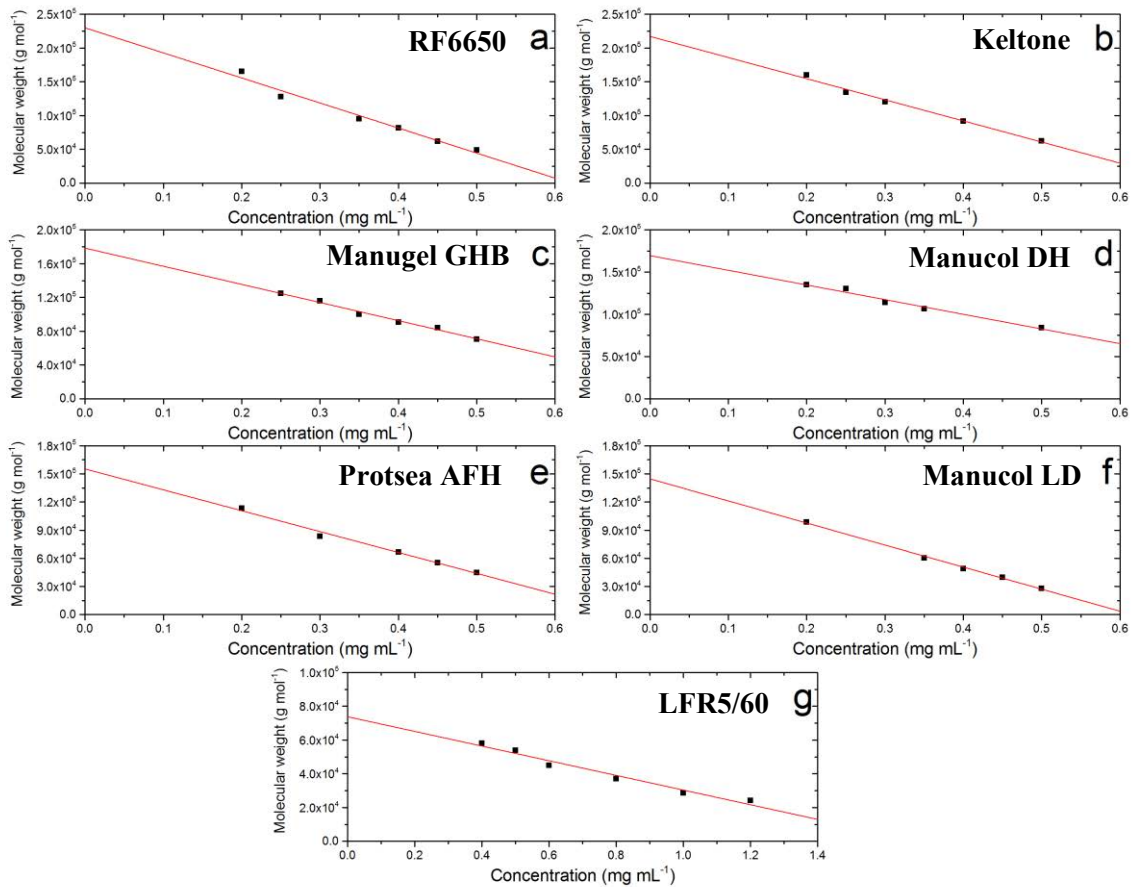
Figure 2.11: Plots of the apparent weight average molecular weight (M$_{w, app}$) against concentration c (mg mL^{-1}): the conventional plot (M$_{w, app}$ vs c), for (a) Protanal RF6650 (b) Keltone (c) Manugel GHB (d) Manucol DH (e) Protsea AFH (f) Manucol LD and (g) LFR5/60.

Alginate molecular weights corroborate the relationship of increasing sedimentation coefficient, validating the molecular weight values obtained (table 2.3).

Table 2.3: Average molecular weight values of alginates obtained by analytical ultracentrifugation.

Alginate	Sedimentation rate (S)	Molecular Weight (kDa)
Protanal RF6650	3.1±0.2	230±10
Keltone	2.9±0.2	220±15
Manugel GHB	2.6±0.1	180±18
Manucol DH	2.5±0.1	170±6
Protsea AFH	2.3±0.2	155±5
Manucol LD	2.2±0.1	145±5
LFR5/60	2.0±0.1	74±3

Interestingly, these results also verify the N values (binding site number) obtained from the ITC experiments, where longer polymeric alginates were identified with more calcium binding sites. However, it is important to note that N values will also depend on the G:M ratio of the alginate.

2.2.5   Alginate iron binding profiles using UV-Vis spectroscopy

With the series of alginates fully characterised, chemical iron binding analysis could be performed. UV-Visible spectroscopy allows changes in absorbance or wavelength shifts to be monitored with the continual introduction of iron; the spectral change observed corresponds to a binding event. Provided an excess of guest (iron) is titrated into the host (alginate) and saturation of binding is reached, binding constants can be calculated by fitting the data to relevant binding equations. Alginates with their viscous and gelling nature are not ideal candidates for spectroscopic titrations since any gelling of the alginate would result in light scattering and absorption values would not represent a binding interaction. Thus the smallest

molecular weight alginate LFR5/60, with its low viscosity, was selected for UV-Visible titrations (method 2.5.7). Titration of an aqueous solution of Fe(III) to an aqueous solution of sodium alginate LFR5/60 revealed the growth of a band at 270 nm (figure 2.12). Since Fe(III) was used in this experiment in its aqueous form, it is likely that iron oxo-hydroxides were the species titrated into the alginate for spectrophotometric analysis.
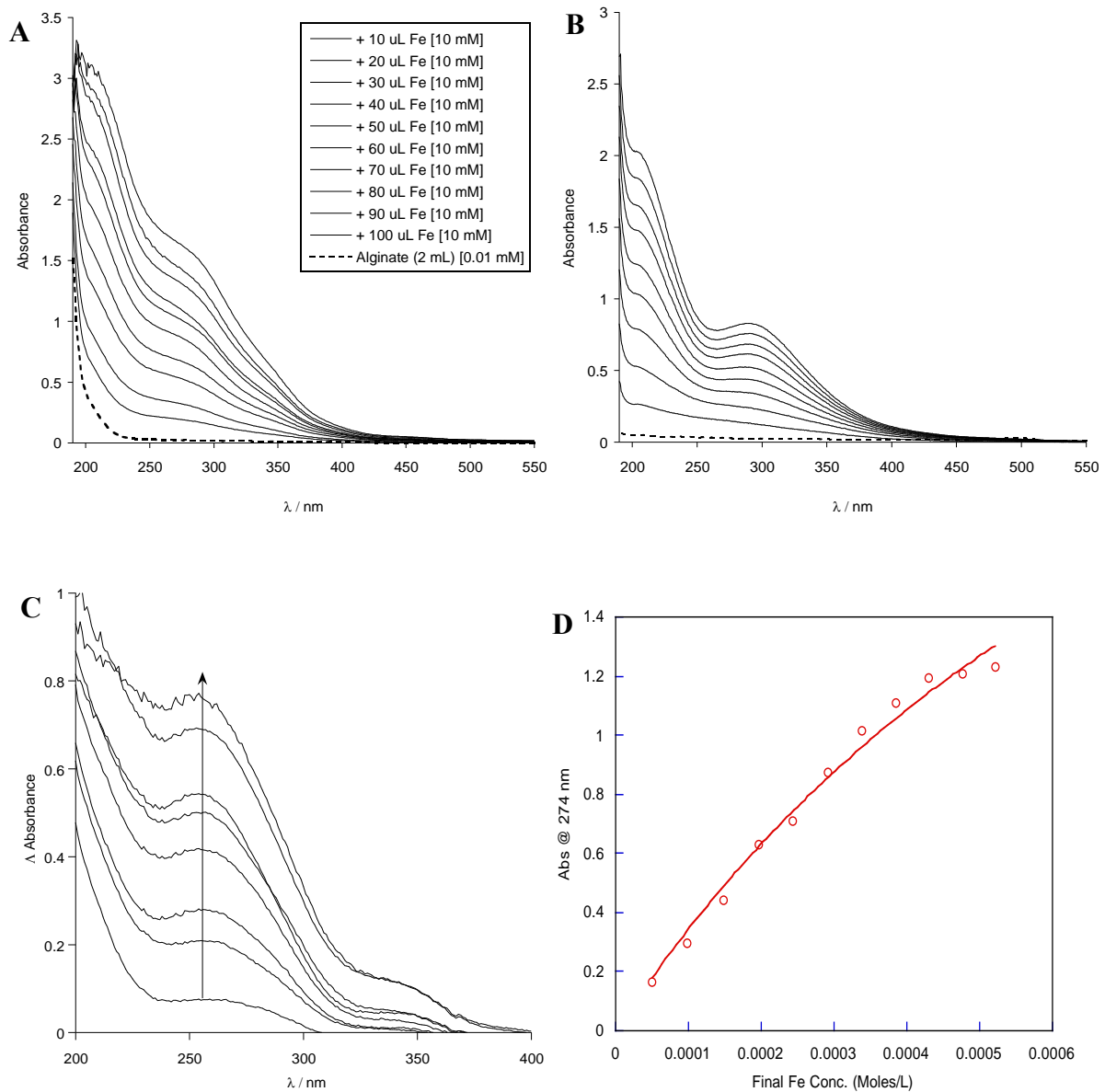
Figure 2.12: (A) UV-Visible titration spectra of FeCl$_3$·6H$_2$O (10 mM) titrated into LFR5/60 (0.1 % w/v). (B) UV-Visible normalisation spectra of FeCl$_3$·6H$_2$O (10 mM) titrated into an equal volume water control. (C) Difference spectra (iron-alginate titration normalised by the equimolar iron-water titration) indicating the profile changes upon addition of iron. (D) Absorption at 273nm plotted against iron concentration to obtain a binding curve and fitted to a 1:1 binding equation.

The titration of iron(III) (iron oxo-hydroxides) into alginate revealed a distinctive profile change with a band growth at 280 nm with sequential additions of iron. Iron oxo-hydroxide itself however, has an inherent absorption profile which needed to be accounted for and as

such, an equimolar control titration was recorded and subtracted from the alginate titration. This so called 'difference spectra' would only show absorption changes if an interaction was incident, which did indeed reveal growth of a band at λ_{max} = 273 nm. This indicates an interaction between iron and alginate under the conditions of the titration. The λ_{max} values can be plotted against the final iron molarity to acquire a binding plot, to which a binding curve based on a model of 1:1 binding can be fitted (figure 2.14). The binding constant was calculated to be K = 1 x 10^3 ± 280 M^{-1}. This value is comparable to that found previously (5.04 x $10^4 M^{-1}$) by Sreeram *et al*,.[5]

$$\Delta I = \frac{\Delta \delta max}{2\,[G]o} \cdot \frac{1}{2}\left[\left([H] + [G] + \frac{1}{Ka}\right) + \frac{1}{2}\sqrt{([H] + [G] + \frac{1}{Ka})^2 - 4\,[H][G]}\right]$$

Figure 2.13: Equation used for the least squares quadratic curve to fit the binding data, whereby ligand concentration ([H]), the maximal response (ΔI_{max}) and iron concentration ([G]) were initially set and iterations were made to acquire the best fit.

The peak at 280 nm on the UV-Vis spectra has previously been reported as identification of an iron-oxide species, attributed to a ligand-to-metal charge transfer electronic transition originating from the OH$^-$ ligands to the Fe ion.[30] This suggests that an iron-oxide form of iron may be present upon binding to alginate under these conditions.

2.2.6 Alginate iron binding using Isothermal Titration Microcalorimetry

Similarly to estimating calcium-alginate interactions using isothermal titration microcalorimetry (ITC), iron titrations were performed to examine the overall strength of the interaction of iron with alginate LFR5/60. This alginate was selected due to its lower gelling

propensity.   An adapted protocol that determined metal binding constants of other
biopolymers in aqueous conditions was used, whereby aliquots of aqueous iron(III) chloride
were titrated to a solution of LFR5/60 and a drop in the integrated heats of each addition is
observed (method 2.5.3) (figure 2.14).
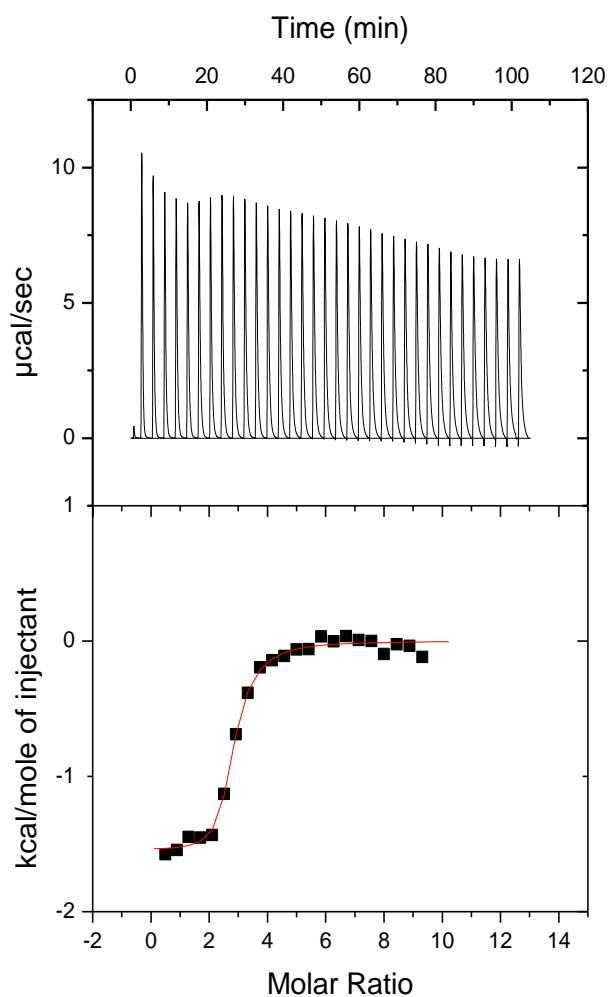
Figure 2.14: Isothermal titration microcalorimetry thermogram of 8 μL injectants of
FeCl$_3$·H$_2$O (5 mM) into LFR5/60 (0.04 mM) at 37 ^{O}C with a binding curve plotted once the
heats have been integrated.

Saturation of iron binding by alginate occurred at a molar ratio of iron:alginate of 3:1, with a
5 times excess of iron used to ensure saturation of all the binding sites on the alginate. Data

analysis revealed two binding events between alginate and iron with the estimated binding constants calculated as $K_1 = 1 \times 10^6$ and $K_2 = 3 \times 10^4$ M^{-1} respectively. Entropy is positive in both cases (18.4 and 23.2 cal mol^{-1} K^{-1}), which is due to the increased ordering of the alginate when iron complexes. This suggests that not all of iron's hydration sphere is displaced upon coordination. Enthalpy values were found to be exothermic for both binding events (-704 x 10^4 and -1548 cal mol^{-1}) as expected for these conditions.[12, 14]

It is interesting to note that K_2 (N=3) is 100 times stronger than K_1 (N=1). This may elucidate a binding mechanism whereby there is an initial binding of iron ions followed by alginate reorganisation to accommodate further iron ions to bind. Structural reorganisation of alginate polymers during metal binding is commonplace and was discussed earlier for that of calcium, and this may rationalise the high entropy values obtained in these titrations.

2.2.7 Iron-alginate binding by circular dichroism spectroscopy

Since CD spectroscopy proved useful in the determination of alginate G:M composition and it has been demonstrated how CD spectroscopy allowed the conformational changes to be probed during calcium titrations and the formation of the egg-box model of binding, it would be beneficial to undertake similar experiments with iron. Alginate-iron complexes were isolated using similar equilibrium dialysis experiments as in section 2.3.1. The CD spectrum of the isolated LFR5/60-Fe bound complexes shows the appearance of a peak at $\lambda = 280$ nm, at the same wavelength to that found in the UV-Vis experiments (figure 2.15).
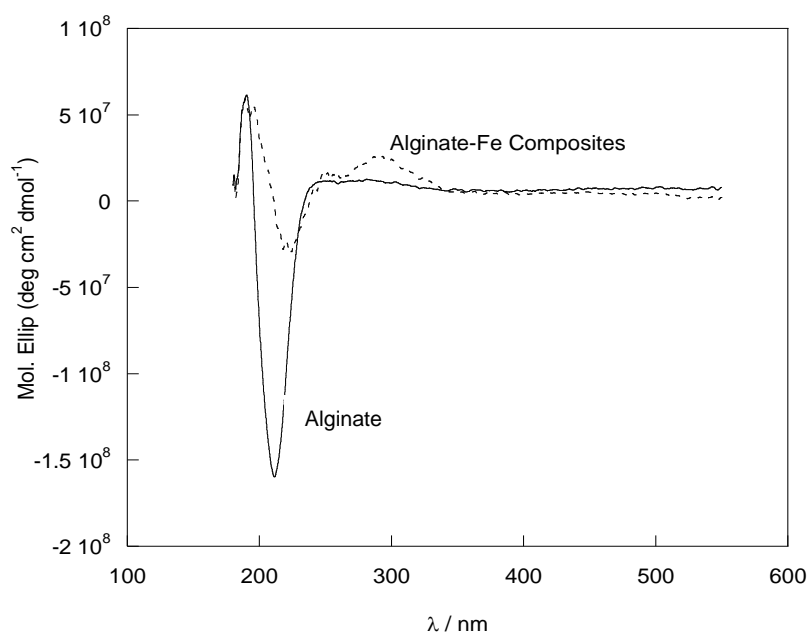
Figure 2.15: CD spectra of alginate-iron composites isolated via equilibrium dialysis.

The peak in the CD, as verified by the UV-Vis spectra, is attributed to iron-hydroxide (Fe-OH) presence.[30]   As discussed, a CD signal is only observed by chiral compounds, of which iron is not. However, once a non-chiral iron becomes complexed to a chiral host it can exhibit an induced CD signal, which is observed here. This induced signal observed is indicative of iron oxo-hydroxide binding and confirms that the changes observed in the UV-Vis spectrum are attributed to the alginate binding to Fe-OH species in solution.

2.2.8   Conformational changes of alginate upon iron complexation

The polymeric nature of alginates enables an elaborate range of confirmations and structures to be adopted upon complexation to a metal ion. Previous studies discussed earlier have

demonstrated that alginate can template the formation nanoparticles, yet in these experiments iron-centred nanoparticles are fabricated using chemically controlled conditions.[13] Here, utilisation of the dialysis technique ensures simple mixing of the alginate with iron making the interaction much more physiologically relevant. The solution studies undertaken thus far have provided insights into the mechanism of iron binding. More iron ions bind to alginate than a typical 1:1 carboxylate unit:iron interaction. Circular dichroism spectra revealed alginate structural reorganisation upon iron binding, and analysis alongside UV-Vis spectroscopy indicates the presence of an iron-hydroxide species. Isothermal titration microcalorimetry demonstrated that two distinct binding events occur upon iron complexation.

2.2.8.1 Alginate-iron structural morphology analysis by scanning transmission electron microscopy

Alginate iron complexes, as prepared by the equilibrium dialysis technique were used in the scanning transmission electron microscopy (STEM) studies; these complexes were prepared similarly to those used in the CD spectroscopy experiments for direct comparison. LFR5/60-iron complexes (50 µL) were drop cast onto the copper TEM grid and the excess collected underneath and dried to completion before visualisation (method 2.5.8). The alginate-iron complexes were initially imaged at low magnification, which revealed a long range extended gel-like network suspended over the holey-carbon film (present on the grid) (figure 2.16 A). Within this gel-like network, brighter features could be observed that were much denser in composition. Further magnification into these denser regions revealed the presence of spherical nano-particulate composites with a broad size distribution and a mean diameter of

1.78 ± 0.70 nm (figure 2.16 C and D). The range of structures observed and broad size distribution can be attributed to the method of formation (simple mixing), which is uncontrolled allowing a plethora of composites to be formed naturally.
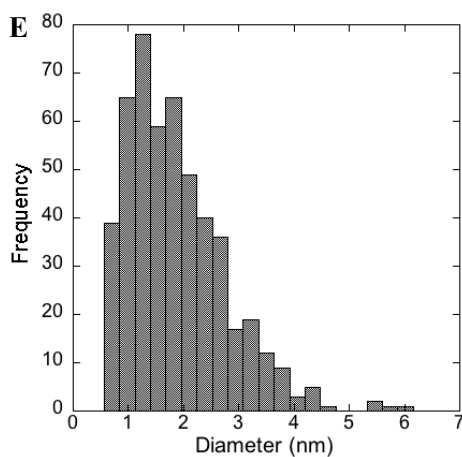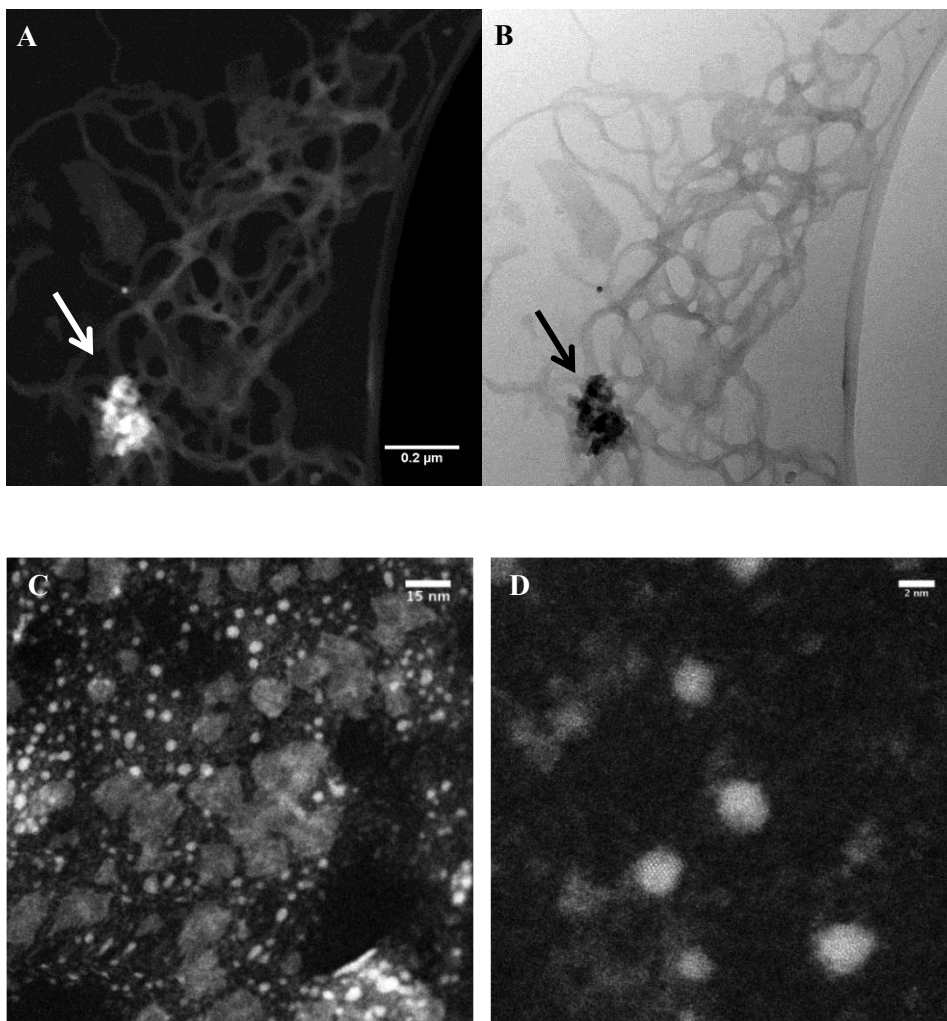
Figure 2.16: (A) low magnification, high-angle annular dark-field (HAADF) image of gel-like alginate network with dense particulate sites and (B) bright-field (BF) image of gel-like alginate network with dense particulate sites. (C) Higher magnification of the dense sites revealing nanoparticulate matter. (D) Higher magnification of the nanoparticles. (E) Distribution chart of nanoparticle diameters.

It can be hypothesised that iron is binding to alginate within the binding sites along the alginate backbone, which is forming the long-stranded gel-like network that was visualised within the STEM. Then within the gel structures, denser regions are present. It could be inferred that in these regions, alginate is initiating iron nucleation sites supporting nanoparticle formation (figure 2.17 D). Dialysis studies detailed earlier, demonstrated that more iron was bound than the calculated 1:1 alginate:iron interaction supports these results. With respect to the ITC results, the two binding events may relate to the initial iron binding along the alginate backbone and the collapse of the alginate to form iron nanoparticles at a critical point of iron complexation. Control experiments were performed where iron only was examined, which revealed no nano-particulate matter; this indicates that it is likely that 'free' iron (as opposed to particulate iron) is binding to alginate initially, and then templated into nanoparticles.

2.2.8.2 Nanoparticle composition analysis by STEM and EDX

Circular dichroism and UV-Visible spectroscopy both indicated the presence of iron in its hydroxide form bound to alginate. Ultra high resolution STEM enabled the visualisation of the nanoparticles present at the highest magnification which revealed lattice structures within the core of individual nanoparticles (figure 2.17).
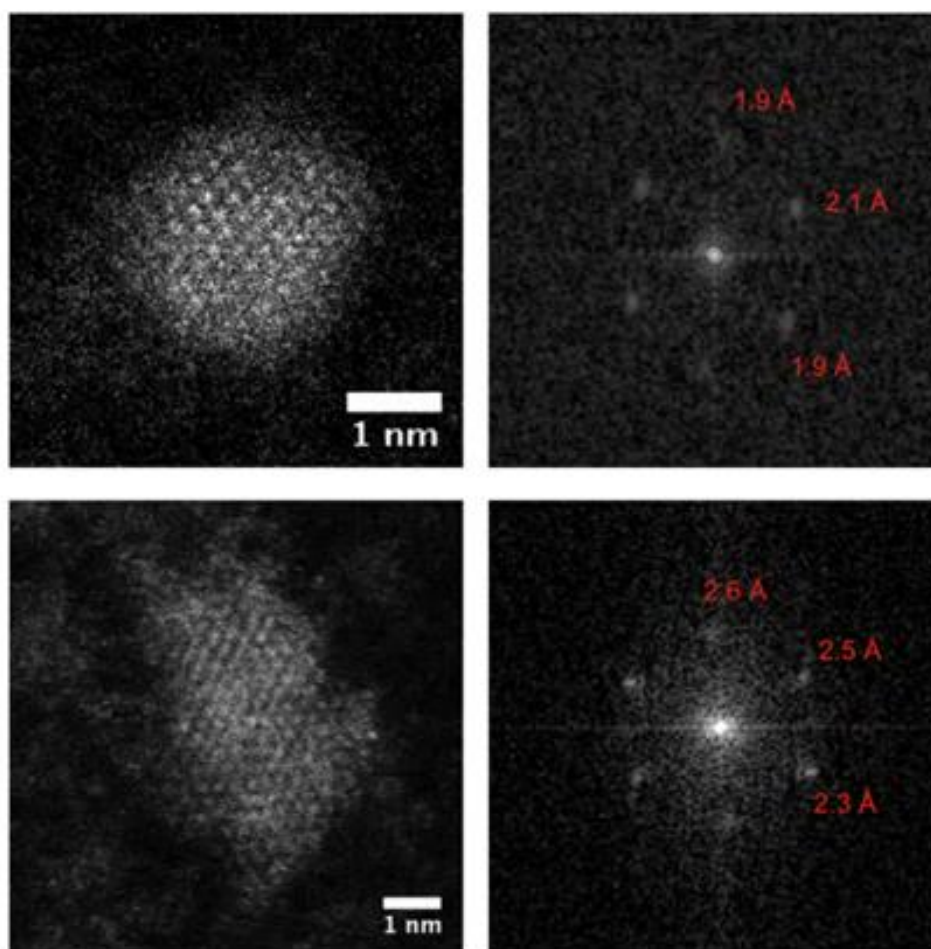
Figure 2.17: Fourier transform analysis of high-angle annular dark-field HAADF-STEM images of single nanoparticles with lattice structures present.

The arrangement of atoms within the lattice structure could be further analysed by Fast Fourier transform and it was found that the lattice arrangements matched those of Fe_2O_3 (hematite), with atomic spacing calculated to be between the range 1.47 to 2.97 Å.[8] Hematite, which is an iron oxide mineral, rationalises the presence of iron oxo-hydroxide species initially binding to alginate and depicts the binding mechanism as a whole. Iron initially binds to alginate in its hydroxide form. At a critical iron concentration and at specific points along the alginate backbone, nucleation sites are formed where by alginate collapses upon the condensation of iron-hydroxide to form iron-oxide rich nanoparticles (figure 2.18).

It is important to note that electron beam energy can affect samples under investigation during examination in an electron microscope. Electron beam damage can result in structural and/or chemical particle-phase conversion. This could indeed result in a phase conversion from, for example, a ferrihydrite particle to a haematite arrangement found here. The electron dose received at the highest magnification was 9.8×10^6 electron nm^{-2}, which is within the range for this phase transition to occur.[32]
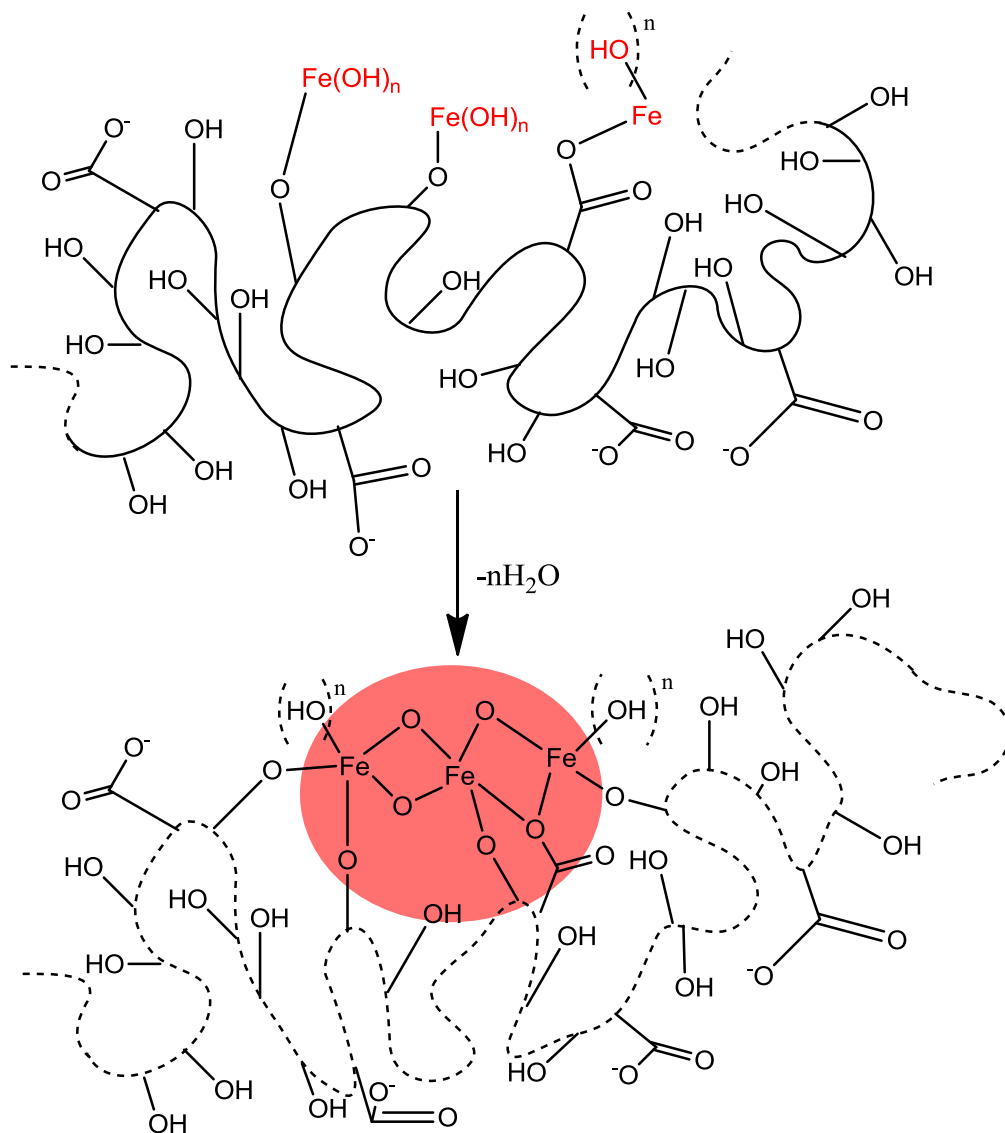
Figure 2.18: Schematic of the possible condensation mechanism of alginate iron-oxide nanoparticle formation.

To confirm the elemental species present within the dense particulate areas found within the extended gel-like network, Energy-Dispersive X-ray spectroscopy (EDX) was carried out on the alginate-iron dialysis extracts (figure 2.19)
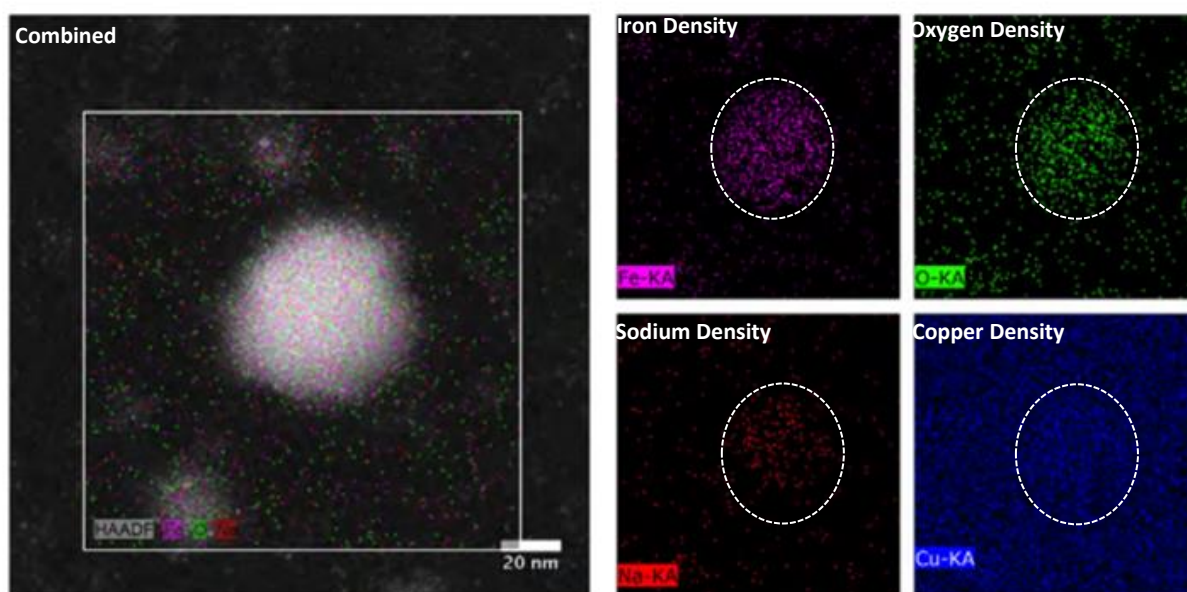
Figure 2.19: EDX mapping of iron-alginate dialysis composites with iron, oxygen, sodium and copper signals obtained and highlighted.

EDX demonstrates that both iron and oxygen is localised in the same region of the alginate-iron complex, further verifying iron-oxide presence within the nanoparticles. Sodium is also somewhat localised, arising from the inherent sodium alginate and copper was the control signal obtained from the copper grid used.

2.3 Conclusions and summary

All the alginates in the series tested chelated iron. This is unsurprising since alginates are poly-anionic and are electrostatically attracted to cationic metal ions. It can be concluded from these experiments that the affinity and capacity to bind iron is similar for all the alginates tested, despite there being a plethora of alginate compositions in terms of G:M ratio and molecular weight. Alginate stratification is however quantifiable with respect to their iron binding under calcium competitive conditions. Alginates with higher M-unit content were shown to withhold their iron affinity compared to alginates with greater G-unit composition. This result was verified when calcium binding constants were obtained which demonstrated that alginates with higher G:M ratios have stronger binding enthalpies towards calcium chelation. There was no correlation found between molecular weight and iron affinity. It could be argued that larger molecular weight alginates with greater chain lengths will have more conformational strain associated with molecular structure changes to accommodate metal binding than smaller chain length analogues. However, these experiments have generated no evidence to suggest this. Lastly with respect to interactions at a molecular level, it can be confirmed that iron and calcium do indeed share the same binding site, however this does not mean that they bind to alginate in the same mode (i.e. the 'egg-box' model).

Iron binding parameters were derived from spectroscopic and calorimetric experiments, calculating iron binding constants for sodium alginate LFR5/60 as $K = 1 \times 10^3$ and $K_1 = 1 \times 10^6$ and $K_2 = 3 \times 10^4$ M^{-1} respectively. These values are relatively low for a host-guest interaction (cf. $K > 10^{30}$ for some bacterial siderophores).[33] However, the interpretation of the data and analysis of results relies upon a 1:1 host:guest interaction approximation since an

equation describing nanoparticle formation would be complex. As well as this, it is important to consider alginates not as discrete chemical units with discrete binding sites, but to view them more as proteins where their secondary structure forms metal binding sites; more simply, the interaction of iron with a carboxylate moiety may be strong but this is immeasurable in the face of the whole alginate polymer collectively binding iron.

Of most interest is the observation that alginates form nanoparticles under the simple mixing conditions employed. The use of alginates to fabricate nanoparticles under chemically forcing conditions is commonplace, yet there is no evidence of nanoparticle formation by simple mixing of the reactants. The solution and surface techniques utilised allows a mechanism of nanoparticle formation to be proposed whereby alginate initially binds to iron either as an aqueous hydroxide or binds to alginate as iron where it is converted to an iron oxo-hydroxide. Subsequently, at a critical concentration of iron loading the alginate collapses and forms a nucleation site where iron hydroxide condensation can take place to form iron-oxide centred nanoparticles; the whole process templated by alginate (figure 2.20). This mode of nanoparticle formation provides evidence for the combination of the 'site binding mode' and 'colloidal mode' proposed earlier.[12]
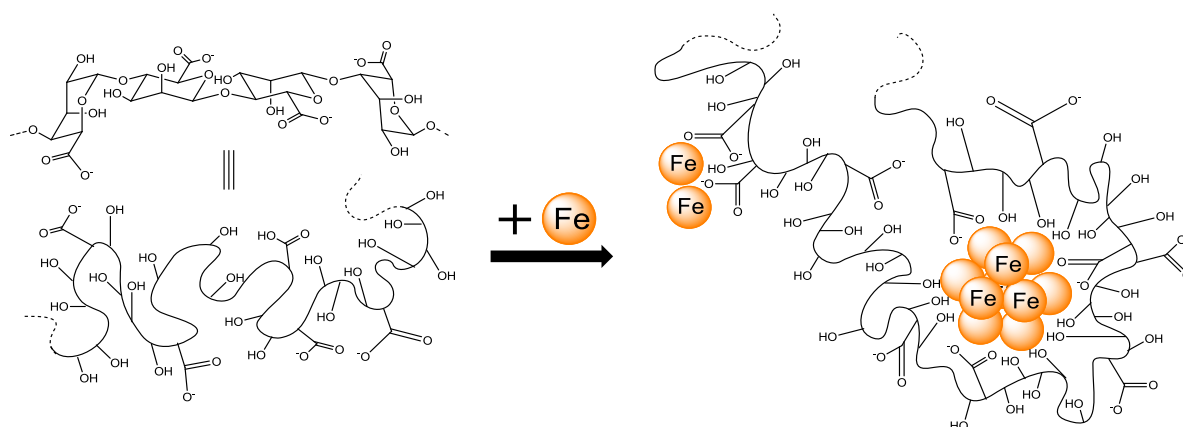
Figure 2.20: Schematic representation of iron binding to alginate and nanoparticle fabrication.

The original hypothesis of this study detailed the characteristics required of a luminal iron chelation, which are; i) must bind iron, ii) be non-absorbable and non-fermentable, iii) be specific towards iron with a high affinity and iv) must be natural and safe for human consumption, two of these characteristics have been assessed here. All alginates examined bind iron and characterisation analyses have shown that a good range of alginate chemical composition has been utilised in this screen. The binding of iron chemically is not strong, yet the chelation of iron by alginates form nanoparticles which may have important physiological consequences. The cellular processing of nanoparticles depends on many factors including nanoparticle size, composition and coating and thus these structural changes may change the bioavailability and could in fact make them bioavailable; this will need to be assessed.[34] How the iron chelated to alginate is transformed to an iron oxide may have a fundamental importance in quenching the toxic effects of iron and since ferritin stores iron in this form it can be viewed as being physiologically inert.[35]

With respect to binding specificity it can be concluded that an alginate with a low G-unit composition would be the ideal candidate for iron binding (for example Manucol LD or Protsea AFH). The contribution of G-unit calcium binding would render a high G:M ratio alginate incompetent as a luminal iron chelator since it would have a greater affinity towards calcium ions and any iron chelation would be displaced by calcium.

It is important to take into account that these chemical stratification studies, regardless of the physiological conditions employed, may not be paralleled *in vitro* and *in vivo*. As such, these stratification experiments must be carried out *in vitro* and *in vivo*, yet data produced thus far indicates that Manucol LD may be the best candidate for iron chelation.

2.4   Acknowledgments

2.5   Experimental methods

2.5.1   Equilibrium dialysis experiments

Sodium alginates, Manucol LD (LD), Manucol DH (DH), Manugel GHB (GHB), LFR5/60, Protsea AFH (AFH), Protanal RF6650 (RF6650) and Keltone (KEL) (0.1% w/v) in DI H_2O, (10 mL) were concealed within a dialysis membrane (MWCO= 12, 400, 33 mm flat width)

using dialysis clips and immersed in aqueous $FeSO_4 \cdot 7H_2O$ (0.2 mM) in DI H_2O (750 mL) with or without $CaCl_2 \cdot 2H_2O$ (ranging concentrations 0-4 mM) in DI H_2O (750 mL) for 210 min and washed in deionised water for a subsequent 30 min. All experiments were performed in triplicate with n=3 per experiment. Iron content was assessed using the ferrozine assay.

For the kinetic studies where alginate samples were taken over a time course, access to the dialysis bag was opened after incubation in an $FeSO_4 \cdot 7H_2O$ solution (1 mM) in DI H_2O (750 mL) for 210 mins and clamped to allow open-ended immersion into either $CaCl_2 \cdot 2H_2O$ (2 mM) in DI H_2O (750 mL) or DI H_2O only (750 mL) and 200 μL samples taken at set time intervals over 90 min. Iron content was assessed using the ferrozine assay.

For production of samples for CD and STEM, LFR5/60-Iron was prepared as above with incubation in $FeCl_3 \cdot 7H_2O$ (10 mM) in DI H_2O (750 mL) for 120 min and washed in DI H_2O for a subsequent 120 min.

2.5.2   Ferrozine assay for the determination of iron concentration

A ferrozine stock solution was prepared consisting of sodium ascorbate (0.23 M, 0.91 g) 3-(2-Pyridyl)-5,6-diphenyl-1,2,4-triazine-p,p′-disulfonic acid monosodium salt hydrate 'ferrozine' (10 mM, 0.089 g) and sodium acetate (2.0 M, 13.77 g) in DI H_2O (122 mL). Each alginate-iron sample (200 μL) was mixed with the Ferrozine stock (600 μL) and plated in triplicate into a 96 well plate. The absorbance was read at $\lambda = 450$ nm. Iron concentrations were determined by producing a calibration curve by dissolving iron at specific concentrations (0-1 mM) into aqueous HCl (0.1% v/v) and used in the same way as alginate samples.

2.5.3   Isothermal Titration Microcalorimetry

For the assessment of calcium-alginate binding, alginates were dissolved (0.052 % w/v) in acetate buffer (20 mM, pH 5) and hydrated overnight to ensure complete dissolution. These alginate solutions were then dialysed against acetate buffer (1000 mL, pH 5) for 24 hours, with the dialyses buffer used to prepare the calcium solutions so that there were no pH differences or ionic strength mismatches; before use, all solutions were degassed at 35 °C. Aliquots of $CaCl_2 \cdot 2H_2O$ (10 μL, 7.5 mM) were titrated into a solution of alginate or acetate buffer at 37 °C with a cell chamber volume of 1360 μL. A total of 28 injections were performed, with an interval of 1000 s between each titration; the initial titration was set to 2 μL and was discarded for the data analysis; this is common practice in ITC experiments. The stirring speed was set at 286 rpm with an initial 60 s delay and a reference power set to 10 μcal s^{-1}. Measurements were performed on a VPITC MicroCalorimeter and data were analysed using MicroCal LLC ITC/Origin software package.

For the assessment of iron-alginate binding an aqueous solution of $FeCl_3 \cdot 6H_2O$ (5 mM) in DI H_2O was titrated in increments of 8 μL aliquots into an aqueous solution of LFR6/50 (0.07 mM) in DI H_2O; all solutions were degassed at 35 °C before use. The cell temperature was set to 37 °C, a stirring speed of 286 rpm and a 10 μcal s^{-1} reference power with the initial injection being small (2 μL) and discarded in the data analysis. A delay of 350 sec between each injection was set to allow the energy difference to reach back to baseline. To account for the high energy changes associated with iron titration into water (the control titration), these heat integrations were subtracted from that of the alginate-iron titration and the subsequent heats of interaction were fitted using a model of two binding sites.

2.5.4   Circular dichroism spectroscopy

For the determination of G:M composition, aqueous alginate solutions (0.1 % w/v) in DI H_2O (10 mL) were prepared and hydrated overnight to ensure complete dissolution. CD measurements were recorded on a Jasco J-810 CD spectropolarimeter (4 accumulations, 1 s response) using a 1 cm path length, blackened quartz cell. Spectra were recorded at an internal temperature of 20 °C.

2.5.5 Nuclear Magnetic Resonance Spectroscopy

1H NMR spectra were recorded on a Bruker AVIII400 spectrometer at 90 °C. Spectra were obtained using a pulse repetition time of 5/6 s and a 30 ° pulse angle with a partial presaturation of the HOD signal.   Alginate solutions (10 mg in 1 mL deuterium oxide (^2H_2O)) were prepared under nitrogen. Nitrogen was subsequently bubbled through the sample for 30 min upon complete dissolution. Chemical shifts were calculated with respect to 3-(trimethylsiyl)-propionic-2,2,3,3-d_4 acid sodium salt at the internal standard. Offline NMR analysis was performed on MestReNova LITE software.

2.5.6   Analytical Ultracentrifugation

Sedimentation velocity and sedimentation equilibrium in (AUC) were performed in a Beckman Optima XL-I analytical ultracentrifuge equipped with Rayleigh Interference Optics and a 30 mW laser wavelength λ = 675 nm. 12 mm optical path length double sector (solution/reference solvent) cells were used in an 8-hole rotor run at speeds between 40,000-45,000 rev min^{-1}, at a temperature of 20 °C. Scans were taken every 1 min and capture by a CCD camera. Sedimentation coefficients and sedimentation coefficient distributions were then evaluated using the SEDFIT algorithm of P. Schuck. Sedimentation coefficients, s (in Svedberg units S, where 1 S = 10^{-13} s) measured in the buffer were corrected to standard

conditions of the density and viscosity of water at 20 °C using a standard formula, to give $s_{20,w}$ values (where the *20,w* means corrected to the density and viscosity of water at 20 °C).

In order to correct for solution non-ideality $s^0_{20,w}$ values are measured at a series of concentrations and extrapolated to zero concentration to give $s_{20,w}$ using the "Gralen" formula:

$$1/_{s20,w} = (1/s^0_{20,w}).(1 + k_sc)$$

Where k_s is the concentration dependence coefficient.

2.5.7 UV-Vis Spectroscopy

Absorption spectra were recorded on a Varian Cary50 or Varian Cary5000 spectrometers with 300 nm min^{-1} increment rates using 1 cm path length quartz cuvettes. Increments of varying volumes of $FeCl_3 \cdot 6H_2O$ (10 mM) were titrated into a stirred solution of LFR5/60 (0.1% w/v) in DI H_2O, allowed to equilibrate for several seconds and then scanned. Measurements were taken up to a point of saturation. To correct for the absorption of aqueous-iron species at the wavelengths of interest difference absorbance spectra were obtained by correction of the alginate titration with the equimolar iron-water control titration.

2.5.8 Scanning Transmission Electron Microscopy

LFR5/60-iron samples used for STEM/EDX were made using the equilibrium dialysis technique as described earlier. Due to the viscous nature of the sample, TEM grids were loaded with 50uL of sample and excess sample was drawn from underneath, effectively pulling the sample through the gird. This produced a thin sample coverage over the grid with many sampling areas.

Electron microscopy images were taken using a 200kV FEG Jeol 2100F scanning transmission electron microscope fitted with a CEOS aberration corrector. Images were simultaneously acquired in high angular annular dark field (HAADF) and bright field (BF) mode using the Gatan DigitalMicrograph software package.

2.6   References

1.   Jonathan, M.C., et al., *Separation and Identification of Individual Alginate Oligosaccharides in the Feces of Alginate-Fed Pigs.* Journal of Agricultural and Food Chemistry, 2013. **61**(3): p. 553-560.

2.   Sandberg, A.S., et al., *ALGINATE, SMALL-BOWEL STEROL EXCRETION, AND ABSORPTION OF NUTRIENTS IN ILEOSTOMY SUBJECTS.* American Journal of Clinical Nutrition, 1994. **60**(5): p. 751-756.

3.   Wölbling, R.H., G. Becker, and W. Forth, *Inhibition of the Intestinal Absorption of Iron by Sodium Alginate and Guar Gum in Rats.* Digestion, 1980. **20**(6): p. 403-409.

4.   Berner, L.A. and L.F. Hood, *Iron Binding by Sodium Alginate.* Journal of Food Science, 1983. **48**(3): p. 755-758.

5.   Sreeram, K.J., H. Yamini Shrivastava, and B.U. Nair, *Studies on the nature of interaction of iron(III) with alginates.* Biochimica et Biophysica Acta (BBA) - General Subjects, 2004. **1670**(2): p. 121-125.

6.   Wang, Z.-Y., et al., *Sol–gel transition of alginate solution by the addition of various divalent cations: 13C-nmr spectroscopic study.* Biopolymers, 1993. **33**(4): p. 703-711.

7.   Haug, A., *The Affinity of Some Divalent Metals for Different Types of Alginates.* Acta Chemica Scandinavica 1947 - 1999, 1961. **15**: p. 1794-1795.

8.   Kroll, E., F.M. Winnik, and R.F. Ziolo, *In situ preparation of nanocrystalline gamma-Fe2O3 in iron(II) cross-linked alginate gels.* Chemistry of Materials, 1996. **8**(8): p. 1594-&.

9.   Llanes, F., D.H. Ryan, and R.H. Marchessault, *Magnetic nanostructured composites using alginates of different M/G ratios as polymeric matrix.* International Journal of Biological Macromolecules, 2000. **27**(1): p. 35-40.

10.   Shen, F., et al., *Properties of a novel magnetized alginate for magnetic resonance imaging.* Biotechnology and Bioengineering, 2003. **83**(3): p. 282-292.

11.   Ma, H.L., et al., *Preparation and characterization of superparamagnetic iron oxide nanoparticles stabilized by alginate.* International Journal of Pharmaceutics, 2007. **333**(1-2): p. 177-186.

12.   Jones, F., H. Cölfen, and M. Antonietti, *Iron oxyhydroxide colloids stabilized with polysaccharides.* Colloid and Polymer Science, 2000. **278**(6): p. 491-501.

13.   Gupta, A.K. and M. Gupta, *Synthesis and surface engineering of iron oxide nanoparticles for biomedical applications.* Biomaterials, 2005. **26**(18): p. 3995-4021.

14.   Jones, F., H. Cölfen, and M. Antonietti, *Interaction of κ-Carrageenan with Nickel, Cobalt, and Iron Hydroxides.* Biomacromolecules, 2000. **1**(4): p. 556-563.

15.   Morris, E.R., D.A. Rees, and D. Thom, *CHARACTERIZATION OF ALGINATE COMPOSITION AND BLOCK-STRUCTURE BY CIRCULAR-DICHROISM.* Carbohydrate Research, 1980. **81**(2): p. 305-314.

16. Morris, E.R., D.A. Rees, and D. Thom, *CHARACTERIZATION OF POLYSACCHARIDE STRUCTURE AND INTERACTIONS BY CIRCULAR-DICHROISM - ORDER-DISORDER TRANSITION IN CALCIUM ALGINATE SYSTEM.* Journal of the Chemical Society-Chemical Communications, 1973(7): p. 245-246.

17. Thom, D., et al., *CHARACTERIZATION OF CATION BINDING AND GELATION OF POLYURONATES BY CIRCULAR-DICHROISM.* Carbohydrate Research, 1982. **100**(MAR): p. 29-42.

18. Seely, G.R. and R.L. Hart, *The Binding of Alkaline Earth Metal Ions to Alginate.* Macromolecules, 1974. **7**(5): p. 706-710.

19. Smidsrød, O. and A. Haug, *The Effect of Divalent Metals on the Properties of Alginate Solutions. I. Calcium Ions.* Acta Chemica Scandinavica 1947 - 1999, 1965. **19**: p. 143-152.

20. Fang, Y., et al., *Multiple Steps and Critical Behaviors of the Binding of Calcium to Alginate.* The Journal of Physical Chemistry B, 2007. **111**(10): p. 2456-2462.

21. Nelson, R.L., *Dietary iron and colorectal cancer risk.* Free Radical Biology and Medicine, 1992. **12**(2): p. 161-168.

22. Houghton, D., et al., *Biological activity of alginate and its effect on pancreatic lipase inhibition as a potential treatment for obesity.* Food Hydrocolloids, 2015. **49**(0): p. 18-24.

23. A, A., *Biologische Daten für den Kinderarzt: Grundzüge einer Biologie des Kindesalters.* Archives of Disease in Childhood, 1956. **31**(159): p. 426-426.

24. Davis, T.A., et al., *H-1-NMR study of Na alginates extracted from Sargassum spp. in relation to metal biosorption.* Applied Biochemistry and Biotechnology, 2003. **110**(2): p. 75-90.

25. Holtan, S., et al., *Characterization of the hydrolysis mechanism of polyalternating alginate in weak acid and assignment of the resulting MG-oligosaccharides by NMR spectroscopy and ESI-mass spectrometry.* Biomacromolecules, 2006. **7**(7): p. 2108-2121.

26. Associates, P.N. *Algiante NMR analysis*. 2015 [cited 2015.

27. ASTM, I. *ASTM F2259-10. Standard test method for determining the chemical composition and sequence in alginate by proton nuclear magnetic resonance (1H NMR) spectroscopy.* 2010 [cited 2015; Available from: http://www.astm.org/Standards/F2259.htm.

28. Ralston, G., *Introduction to Analytical Ultracentrifugation.* Beckman: Dept of Biochemistry, University of Sydney.

29. Schuck, P., et al., *SEDFIT-MSTAR: molecular weight and molecular weight distribution analysis of polymers by sedimentation equilibrium in the ultracentrifuge.* Analyst, 2014. **139**(1): p. 79-92.

30. Stefánsson, A., *Iron(III) Hydrolysis and Solubility at 25 °C.* Environmental Science & Technology, 2007. **41**(17): p. 6117-6123.

31. Karlsen, V., E.B. Heggset, and M. Sorlie, *The use of isothermal titration calorimetry to determine the thermodynamics of metal ion binding to low-cost sorbents.* Thermochimica Acta, 2010. **501**(1-2): p. 119-121.

32. Pan, Y., et al., *Electron beam damage studies of synthetic 6-line ferrihydrite and ferritin molecule cores within a human liver biopsy.* Micron, 2006. **37**(5): p. 403-11.

33. Neilands, J.B., *Siderophores: Structure and Function of Microbial Iron Transport Compounds.* Journal of Biological Chemistry, 1995. **270**(45): p. 26723-26726.

34. Jiang, W., et al., *Nanoparticle-mediated cellular response is size-dependent.* Nature Nanotechnology, 2008. **3**(3): p. 145-150.

35. Pan, Y.-H., et al., *3D morphology of the human hepatic ferritin mineral core: New evidence for a subunit structure revealed by single particle analysis of HAADF-STEM images.* Journal of Structural Biology, 2009. **166**(1): p. 22-31.

Chapter 3

Alginate iron chelation *in vitro* and *in vivo*.

3.1   Introduction and aims

Confirmation of the iron binding abilities of alginate warrants further study into their iron chelation ability in a cellular and physiological setting. There is inconsistency within the literature reporting the effect of alginate on iron metabolism, suggesting both enhancement and reduction of iron uptake both *in vitro* and *in vivo*.[1-4] With such little and inconsistent evidence surrounding alginate modulation of iron homeostasis, further investigation is required.

Chemical data presented in chapter 2 suggests iron binding potential, which is dependent upon alginate composition. However, whether these differences have any effect ultimately on cellular iron metabolism is not known. Furthermore, the cellular localisation of alginate *in vitro* needs to be verified; therapeutic iron chelation will be useless if alginates are absorbable at a cellular level. The aims of this study are thus:

1. Determination of the absorbability of alginate in cell culture conditions.

2. Determination of the effect of alginate on cellular iron metabolism in cell culture conditions.
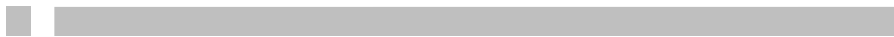
3.2 Results and discussion

3.2.1 Assessment of alginate bioavailability

An important property of alginate that must be confirmed to ensure specific luminal iron chelation is that of non-absorbability. Alginate must not be able to permeate the cell membrane as intracellular iron chelation or systemic iron chelation is not desired.

3.2.1.1 Alginate FITC conjugation

As a method to localise alginate *in cellulo* and to assess the absorbability of alginate, the fluorophore fluoresceinamine (FITC-NH$_2$) was chemically conjugated to alginate. The reactivity of the carboxylates present on the alginate were utilised for a well-established protein coupling reaction (method 3.5.7) (figure 3.1).
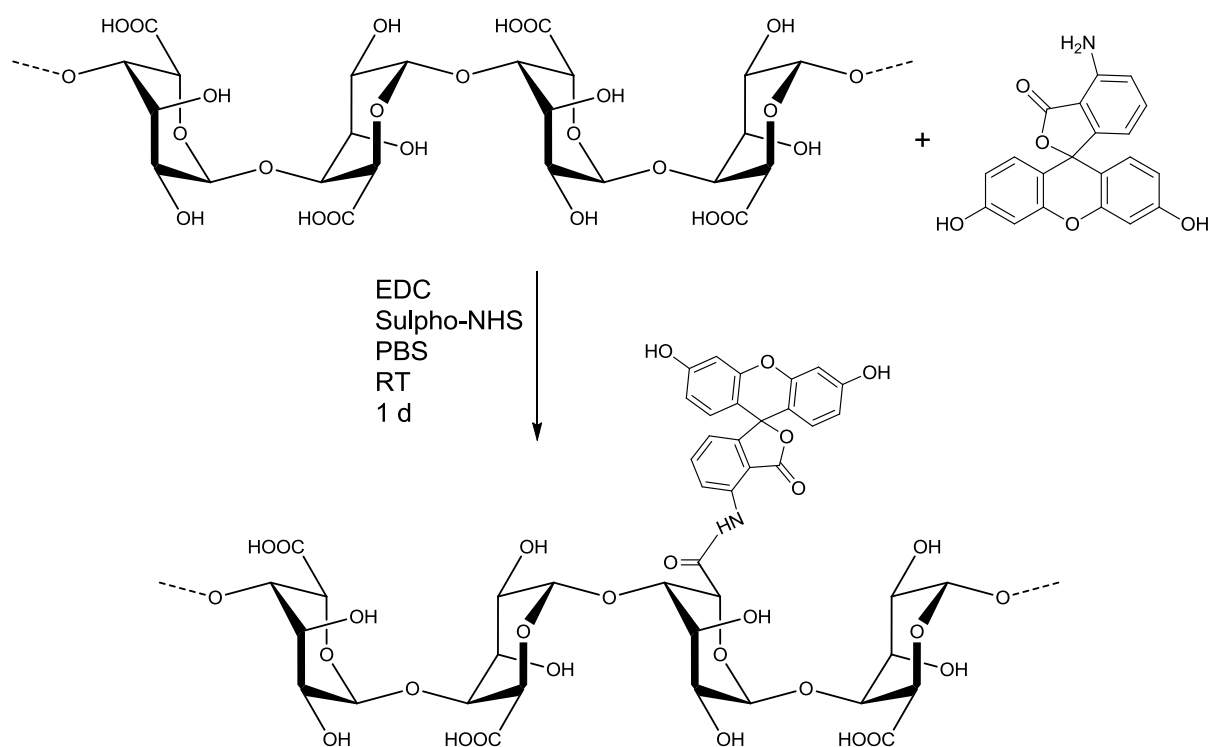
Figure 3.1: Reaction scheme of FITC-NH$_2$ conjugation to alginate under peptide coupling conditions.

Alginate is water soluble and as such is an ideal candidate for these coupling conditions. Sodium alginate LFR5/60 was stirred at room temperature in solution with 1-ethyl-3-(3-dimethylaminopropyl)carbodiimide (EDC) and n-hydroxysulfosuccinimide sodium salt (Sulpho-NHS) for 24 hours to produce a bright orange coloured solution. This crude mixture was dialysed extensively to ensure complete removal of any unreacted materials. The loss of fluorescence within the dialysate was monitored using UV-Vis spectroscopy, with complete loss of free fluorophore evident after dialysis against 35 L of water over a period of 12 days. Photophysical studies on the starting alginate reactant and conjugated alginate (**FITC-LFR5/60**) revealed emission and absorption profile changes upon reaction, indicative of conjugation and chemical change (figure 3.2). **FITC-LFR5/60** has a $\lambda_{max} = 490$ nm whereas

the non-conjugated FITC has a $\lambda_{max} = 450$ nm; changes in the luminescence spectra are also evident. Sodium alginate LFR5/60 was now fluorescent.
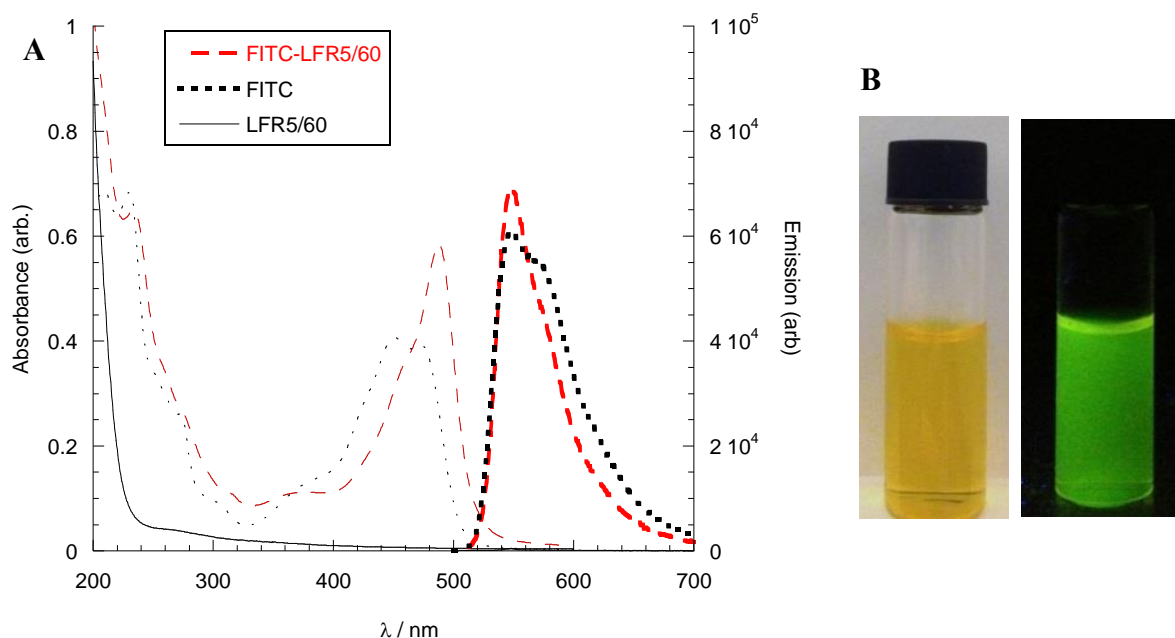
Figure 3.2: (A) Luminescence and UV-Vis spectra of the fluorescent alginate, **FITC-LFR5/60** product and starting reactants, LFR5/60 and FITC where $\lambda_{ex} = 440$ nm and a 455 nm filter is used. Spectra recorded with FITC concentration normalised samples (0.86 μM) (B) Image of **FITC-LFR5/60** in normal light and under $\lambda = 365$ nm UV light.

Percentage modification was calculated to assess the amount of fluorophore attachment; this was to ensure the extent of conjugation was kept minimal such that alginate chemical structure changes were not significant. A molar modification of 6% was estimated using a combination of the phenol-sulphuric acid assay and absorption intensities to assess alginate and FITC concentrations respectively.[5] This would suggest a sufficient fluorescence attachment with approximately 10 of the calculated 180 uronic acid residues modified with a peptide linkage, which should induce little disruption to the natural alginate form.

3.2.1.2 Monitoring of fluorescent alginate FITC-LFR5/60 *in vitro*

Fluorescence microscopy was employed to determine cellular localisation of **FITC-LFR5/60.** RKO colon carcinoma cells were co-cultured with **FITC-LFR5/60** for 24 hours on microscope slides and thereafter the condition media was removed and cells thoroughly washed prior to fixation with formaldehyde (method 3.5.8). One experimental group were subject to a cellular permeabilisation step using saponin prior to culture with **FITC-LFR5/60**; this would act as the positive control effectively allowing fluorescent alginate to enter the cell. Cells were co-stained with Hoechst and DeepRed cellular stains to define the nucleus and membrane respectively (figure 3.3).
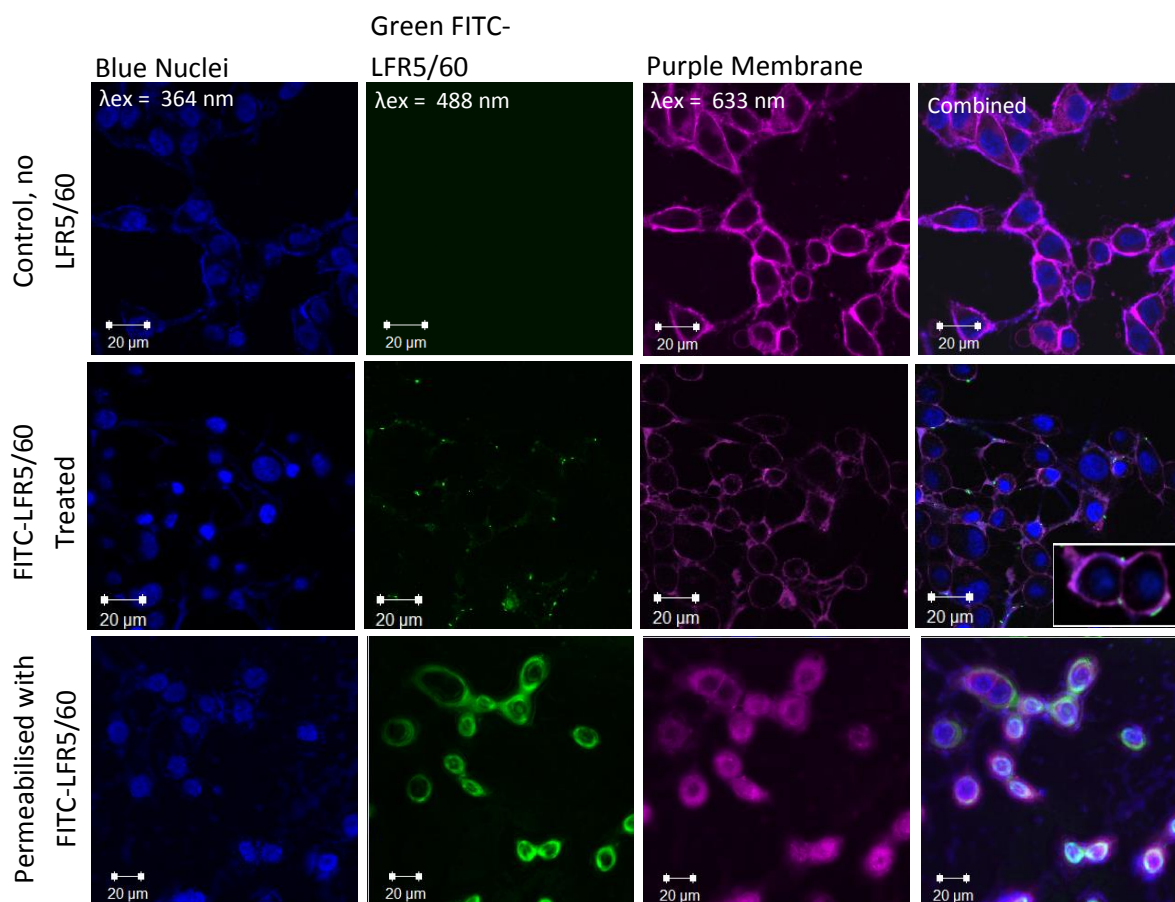
Figure 3.3: Confocal image selection with images taken from three fluorescent channels; blue, green, and far red at λ = 364, 488 and 633 nm respectively. Top row is control where no alginate was cultured with cells, middle row is **FITC-LFR5/60** + iron treated cells, and the bottom row is **FITC-LFR5/60** treated with cell-membrane permeabilisation.

Confocal image analysis revealed that no **FITC-LFR5/60** was present inside of the cell confirming the non-bioavailability of sodium alginate under these physiological conditions. However, negligible **FITC-LFR5/60** could be localised at the cell periphery; this finding authenticates the application of alginates in mucoadhesive preparations. When cells were membrane-permeabilised and co-cultured with **FITC-LFR5/60**, green fluorescence was evident throughout the cell, indicating the limited bioavailability of alginate in non-permeabilised cells. This result defines alginate as a non-absorbable bio-polymer and that if iron chelation does indeed take place *in vitro*, it would render alginate as a luminal iron

chelator. However, it has been demonstrated that alginate can be degraded by specific colonic bacteria.[6, 7] As such, these experiments do not preclude that alginate fermentation by the colonic microbiome does not take place, but does indicate that alginate would not be absorbable in its intact form.

3.2.2 Manucol LD binds iron *in vitro*

It has been confirmed that all alginates chemically bind iron and that under conditions of cationic competition, some alginates retain higher iron binding affinities than others. It is important to consider that in the following *in vitro* experiments cell culture conditions were employed whereby conditioned media contains inorganic salts (such as calcium (0.2 g L^{-1}, 1.4 mM) and magnesium) and is buffered at pH 7.3. This may have an influence on the alginate activity in this setting and results may not parallel those found chemically despite physiological conditions employed at every possibility.

3.2.2.1 Total cellular iron concentration by ferrozine assessment

The simplest method of determining cellular iron content is to exploit the ferrozine ligand that allows the colourimetric visualisation of iron; the use of this spectrophotometric reagent is validated and widely used (method 3.5.9).[8] RKO cells were challenged with a ferrous iron-enriched media (100 μM FeSO$_4$·7H$_2$O + 500 μM sodium ascorbate) with or without sodium alginate Manucol LD, Manucol DH, Manugel GHB, LFR5/60, Keltone, Protanal RF6650 and Protsea AFH (LD, DH, GHB, LFR5/60, KEL, RF6650 and AFH respectively, 0.3% (w/v))

and after 24 hour incubation period, the cells were washed and lysed for ferrozine assessment (figure 3.4).
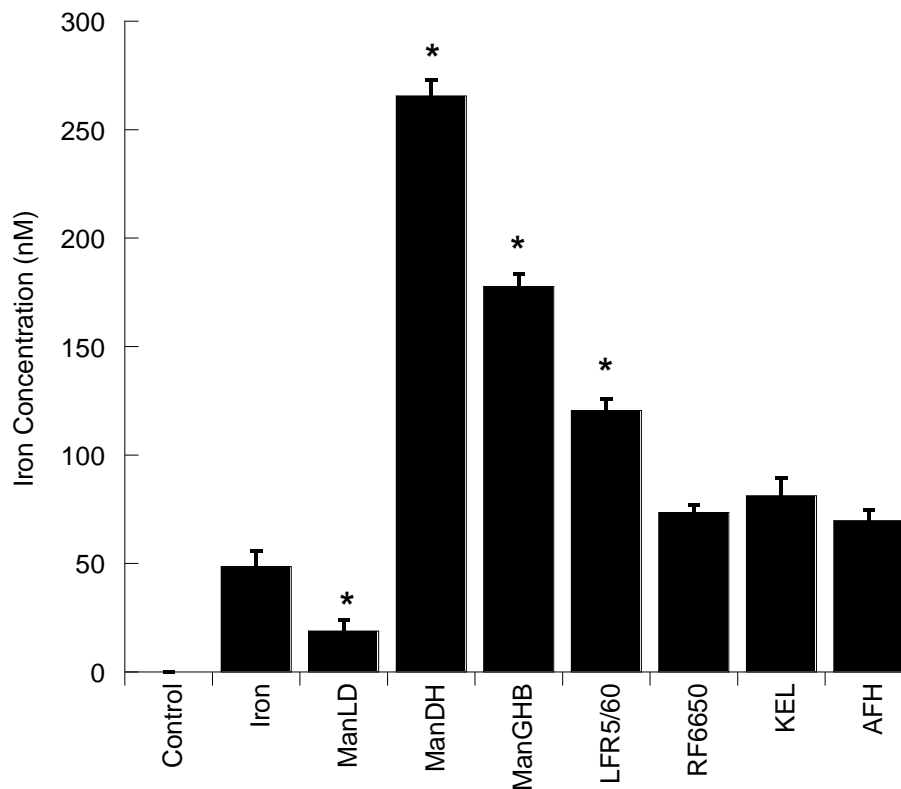
Figure 3.4: Total iron concentrations as assessed by the ferrozine assay in RKO cells cultured with or without the alginate series for 24 hours. Error bars denote ± SEM, n = 3. * denotes statistical significance, $p < 0.05$ versus iron only control.

RKO cells treated with iron resulted in cellular iron loading to contain a concentration of ca. 50 nM total cellular iron; the basal levels of iron within the control group were not measureable by this assay. It was found that Manucol LD significantly decreased cellular iron loading by 62% ($p < 0.05$), indicating iron chelation under these conditions. Interestingly, no other alginates demonstrated this behaviour with either no-change or an increase in total cellular iron levels observed.

In comparison to the chemical analysis of iron binding it was demonstrated that Manucol LD was least effected by calcium in competition studies and here this alginate is the only one from the series examined to attenuate cellular import of iron. It was concluded that an alginate with an analogous chemical composition to that of Manucol LD would be the best choice for a luminal iron chelator and results here support this conclusion. Increases in total iron concentrations by alginates are assessed further in section 3.2.5, however, this increase in total *cellular* iron may not be a true increase in *intracellular* iron. It may be argued that alginates that have chelated iron are incorporated onto the cell membrane due to their polymeric and mucoadhesive nature, as evident from the confocal microscopy; simplistically, the alginates are 'sticking' to the cell membrane. Hence this assay is measuring total cellular iron (including intracellular iron and any iron associated with the cell), producing a misleading apparent increase in measured iron concentration. A better and more validated experiment would only measure intracellular iron or biomarkers thereof such as the estimation of ferritin expression.

3.2.2.2 Iron chelation analysis by ferritin expression

RKO cells were challenged with an iron-enriched media (100 μM $FeSO_4·7H_2O$ + 500 μM sodium ascorbate) with or without sodium alginate (ManLD, ManDH, ManGHB, LFR5/60, KEL, RF6650 and AFH 0.3% (w/v)) and after 24 hour incubation period, the cells were washed and lysed for protein extraction. Western blotting revealed that ferritin expression in RKO cells treated with iron was higher than that of control media as expected, since expression would be augmented to store the increased intracellular iron. If iron chelation was taking place by the alginates then this increased ferritin signal would be dampened, since the

availability of iron would be lower due to chelation occurring in the extra-cellular media (figure 3.5).
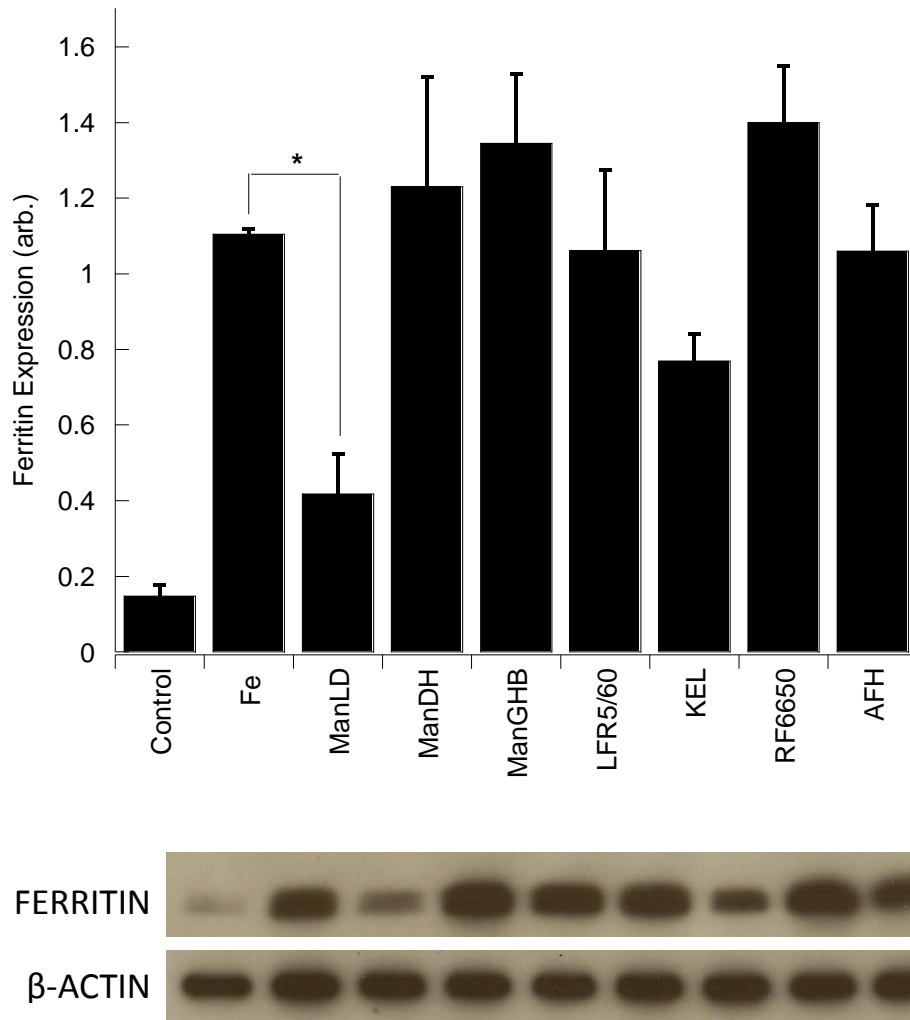
Figure 3.5: Ferritin expression in RKO cells incubated with iron challenged with or without the alginate series. Data points represent mean fold change in protein expression, normalised to β-actin, relative to control. Error bars denote ± SEM, * denotes statistical significance, $p < 0.03$, $n = 3$.

Alginate Manucol LD statistically decreased the iron-mediated induction of ferritin expression by 60% ($p < 0.05$) compared to the iron only control. The other alginates in the series tested had no statistical effect on ferritin expression. This suggests that iron is being chelated by Manucol LD within the media hindering its intracellular uptake. This result

corroborates that of the ferrozine assessment, where Manucol LD was highlighted as the only iron chelating alginate. The trends here were verified and validated using a ferritin ELISA (figure 3.6).
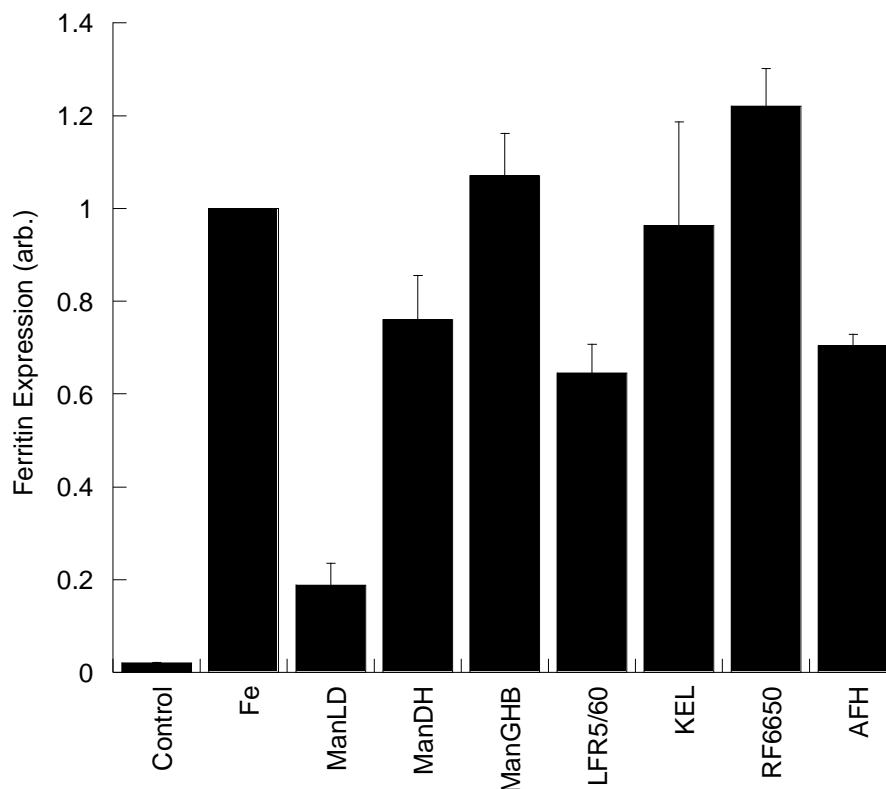
Figure 3.6: Ferritin expression in RKO cells incubated with iron challenged with or without the alginate series as examined by ferritin ELISA. Data points represent mean fold change in protein expression, error bars denote $\pm$ SEM, n = 2.

In light of the dialysis experiments performed in section 2.2.1, the effect of Manucol LD on ferritin expression is unsurprising since this alginate retained the highest iron binding affinity within the competition experiments (which should be compared here since there will be significant competition from other metal ions present within the media). With this comparison, it may be the case that the other alginates within the series may bind iron at lower concentrations of iron present within the stimulation media. That is, if their binding

capacity has not been saturated from calcium coordination. As such RKO cells were again challenged with an iron enriched media, but at lower iron concentrations (10 fold and 100 fold lower) than previous (100 μM, 10 μM and 1μM $FeSO_4 \cdot 7H_2O$ + 500 μM, 50 μM and 5 μM sodium ascorbate) in the absence or presence of sodium alginate (LD, DH, GHB, LFR5/60, KEL, RF6650 and AFH 0.3% (w/v)) and after 24 hour incubation period, the cells were washed and lysed for protein extraction (figure 3.7).
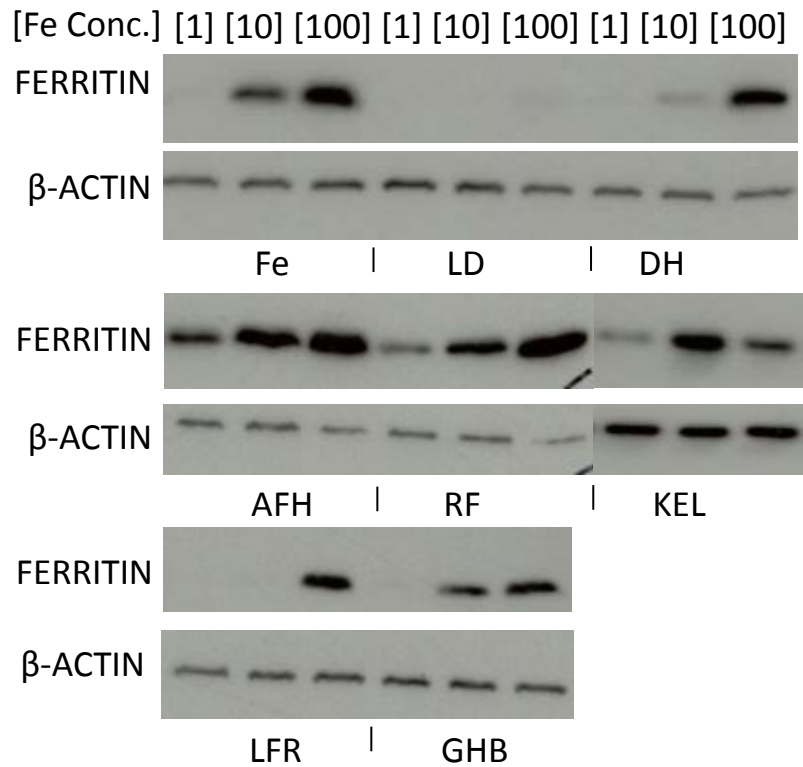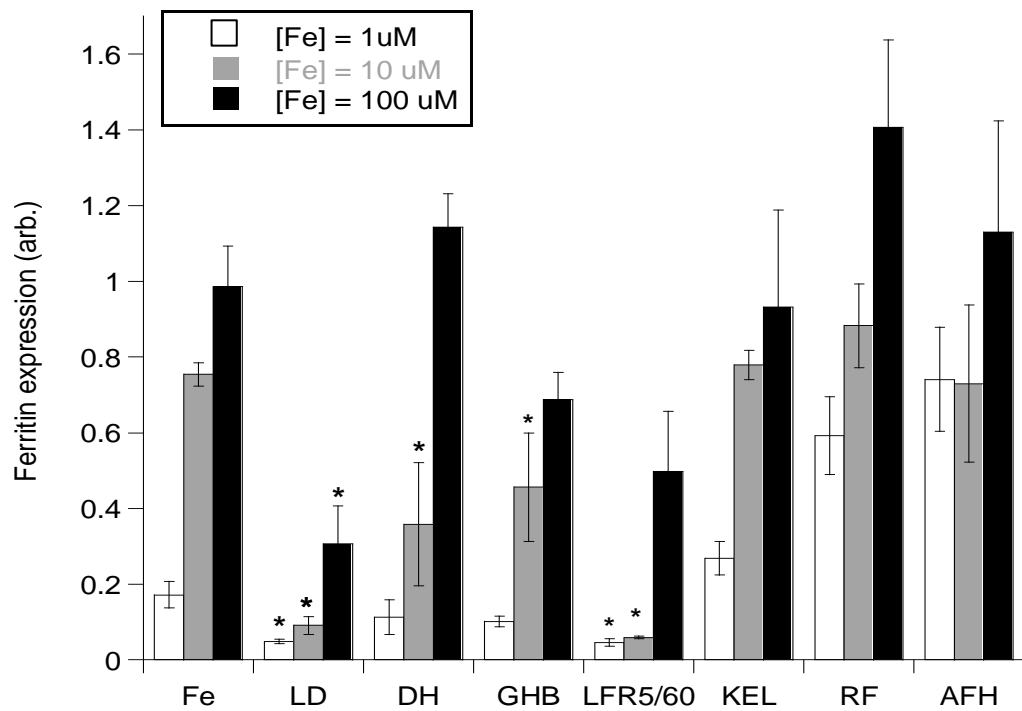
Figure 3.7: Ferritin expression in RKO cells incubated with iron (at concentrations of 100, 10 and 1 μM) challenged with or without the alginate series. Data points represent mean fold change in protein expression, normalised to β-actin, relative to control. Error bars denote ± SEM, * denotes statistical significance, p < 0.05, n = 3.

As evident by the reduction in ferritin expression, other alginates apart from Manucol LD now exhibit *in vitro* iron chelation potential at these lower concentrations of iron, however it is important to note that Manucol LD is the only alginate in the series to significantly reduce ferritin expression at the 1, 10 and 100 µM iron concentrations by 70, 88 and 68 % ($p < 0.05$) respectively. Manucol DH, Manugel GHB and LFR5/60 all show significant ferritin expression reductions at the 10 µM iron incubation concentrations attenuating expression by 58, 47 and 92 % ($p < 0.05$) respectively. This demonstrates the enhanced iron binding affinity observed by Manucol LD in comparison to the other alginates in the series.

3.2.2.3 Iron chelation analysis by TfR1 expression

To verify the chelation effect of Manucol LD *in vitro*, Transferrin Receptor 1 (TfR1) expression was assessed using western blotting (figure 3.8). TfR1 is an alternative biomarker for intracellular iron concentrations whereby in events of low intracellular iron TfR1 expression is upregulated to sequester transferrin-bound circulating iron. Similarly to the protocol for ferritin expression, RKO cells were challenged with an iron-enriched media (100 µM $FeSO_4 \cdot 7H_2O$ + 500 µM sodium ascorbate) with or without sodium alginate (Manucol LD 0.3% (w/v)) and after 24 hour incubation period the cells were washed and lysed for protein extraction.
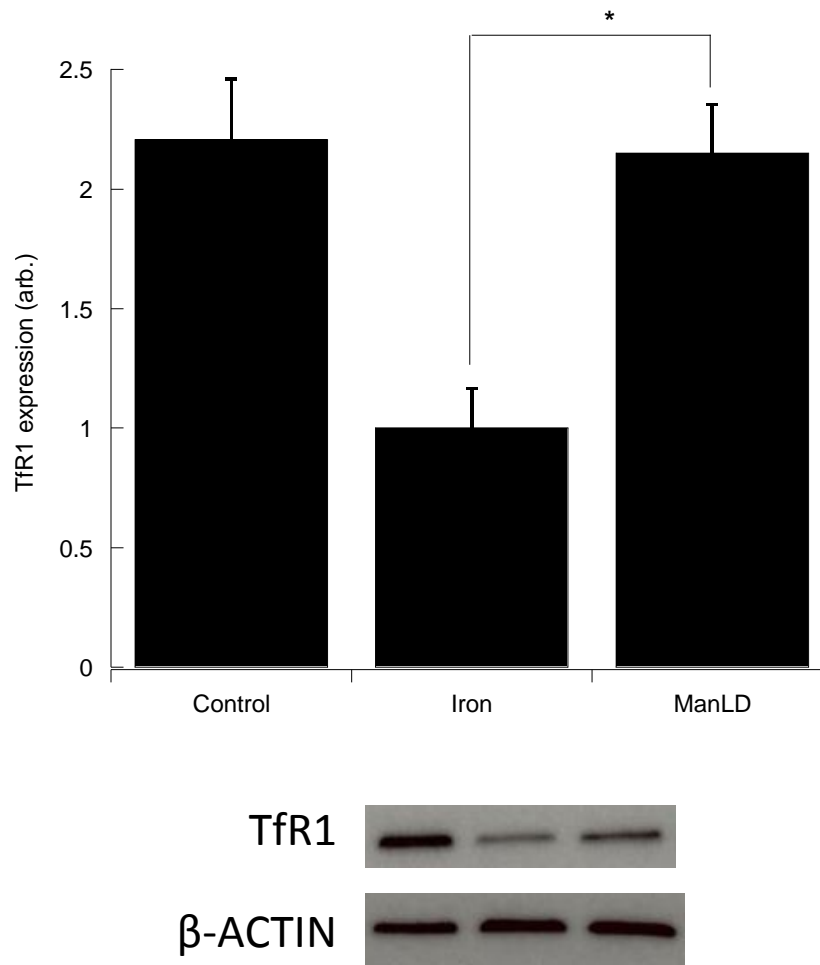
Figure 3.8: Transferrin expression in RKO cells incubated with iron challenged with or without Manucol LD (0.3% (w/v)). Data points represent mean fold change in protein expression, normalised to β-actin, relative to control. Error bars denote ± SEM, * denotes statistical significance, $p < 0.05$, $n = 3$.

Analysis of the western blots revealed that Manucol LD statistically increased TfR1 expression by ca. 50% ($p < 0.05$) compared to iron alone, indicating that this alginate is binding the supplemented iron present in the media hindering its intracellular uptake.

3.2.3 Caco-2 monolayers as an intestinal model for iron absorption

Caco-2 cells and their use in monolayer *in vitro* assays are used extensively in the pharmaceutical industry in bioavailability and uptake studies.[9] The human colon carcinoma cell line (Caco-2) spontaneously differentiate and polarise under standard culture conditions *in vitro*, complete with microvilli, expression of brush border associated enzymes and the presence of tight junctions.[10] This unique property can be used to model the human intestine epithelium when used in combination with bicameral chamber transwell polycarbonate membrane culture dishes (figure 3.9).
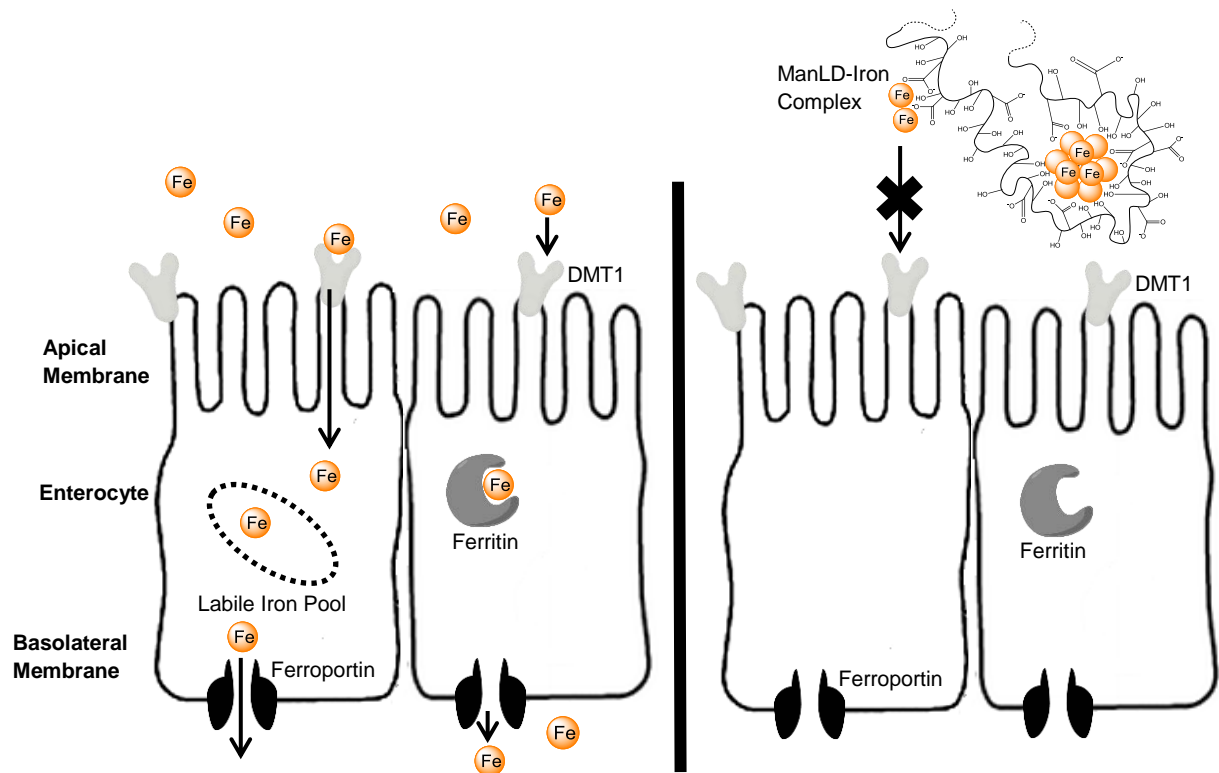
Figure 3.9: Diagrammatic representation of caco-2 monolayers within the bicameral chamber co-cultured with iron challenged with or without alginate.

This method allows the assessment of the transit of iron across the cell monolayer. Iron concentrations can be measured over time in the apical chamber (which represents the

intestinal lumen), the cell monolayer (which represents the intestinal epithelium) and the basal chamber (which indicates movement into the blood).

3.2.3.1 Manucol LD decreases intracellular iron in caco-2 epithelium monolayers

Caco-2 cells, that were grown for 20 days post confluency to allow formation of intestinal-modelled epithelium, were challenged with an iron-enriched, radioactive spiked (^{59}Fe, 10 000 CPM) media (100 μM FeSO$_4$·7H$_2$O + 500 μM sodium ascorbate) with or without sodium alginate (Manucol LD 0.3% (w/v)) and after 24 hour incubation period, the cells were washed and lysed for scintillation counting (method 3.5.13) (figure 3.10).
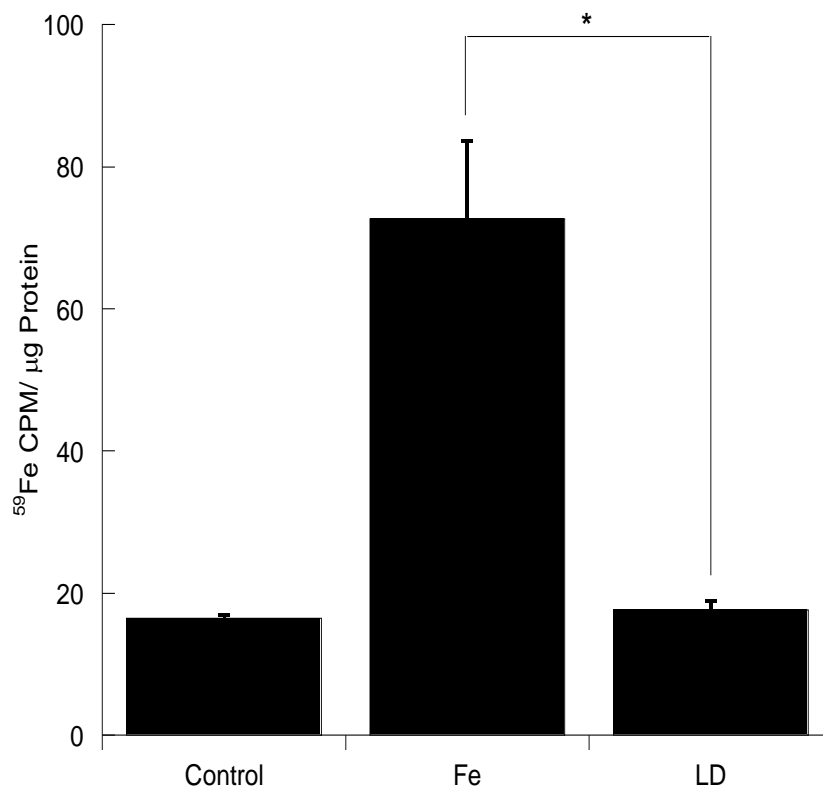
Figure 3.10: Iron concentration within the caco-2 cells of the monolayer when incubated with iron and challenged with or without Manucol LD (0.3% (w/v)). Error bars denote ± SEM, * denotes statistical significance, P < 0.05, n = 3.

Manucol LD significantly decreased intracellular iron concentrations by 70% (p < 0.05) within the Caco-2 monolayer indicating that Manucol LD is chelating iron in the

physiological conditions of this intestinal model. This extent of iron modulation was similarly found in the results obtained from the ferritin expression, TfR1 expression and ferrozine experiments in RKO cells treated with Manucol LD.

The iron concentrations within the apical compartment of the Caco-2 model could be measured over the period of the incubation by taking aliquots of the media from these upper compartments at specific time points. The concentration of iron would be proportional to the amount of unabsorbed iron (figure 3.11).
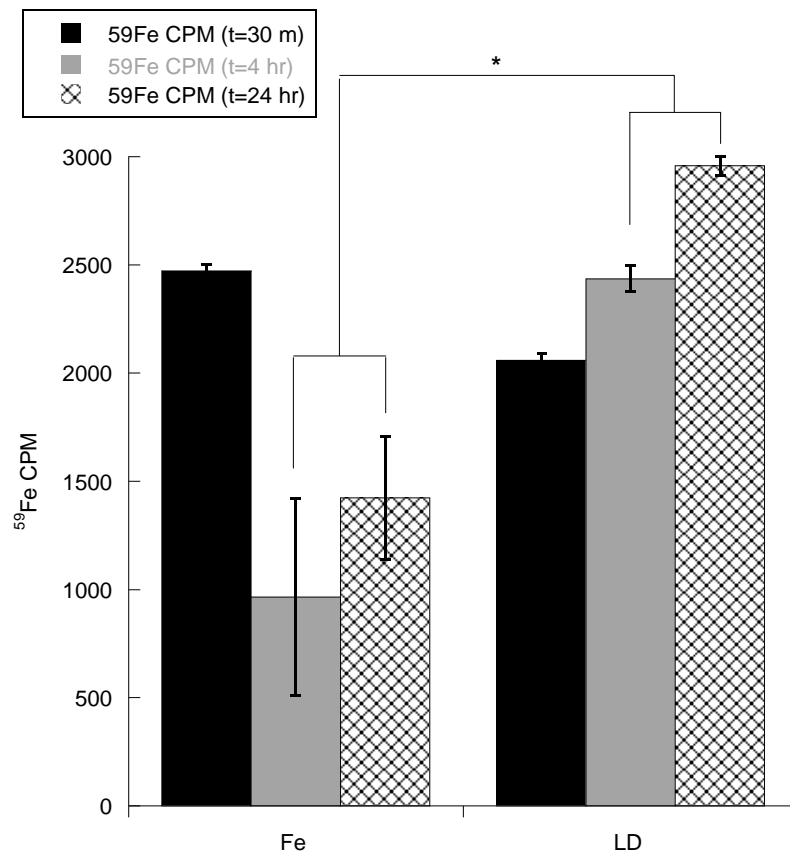
Figure 3.11: Iron concentrations at 30 min, 4 hours and 24 hours of the apical compartment of the caco-2 monolayer for cells treated with iron, challenged with or without Manucol LD (0.3% (w/v)). Error bars denote ± SEM, * denotes statistical significance, $p < 0.05$, $n = 3$. Note: apparent increase in the Manucol LD apical compartment is due to volume changes between the apical and basolateral and a concentration of the alginate-iron complexes within this upper apical chamber.

Co-incubation with Manucol LD at both 4 and 24 hours inhibited cellular uptake by the Caco-2 cells by 60% ($p < 0.05$) compared to the iron alone control. These results validate the observation that Manucol LD is binding iron in the cellular media thus preventing its cellular internalisation.
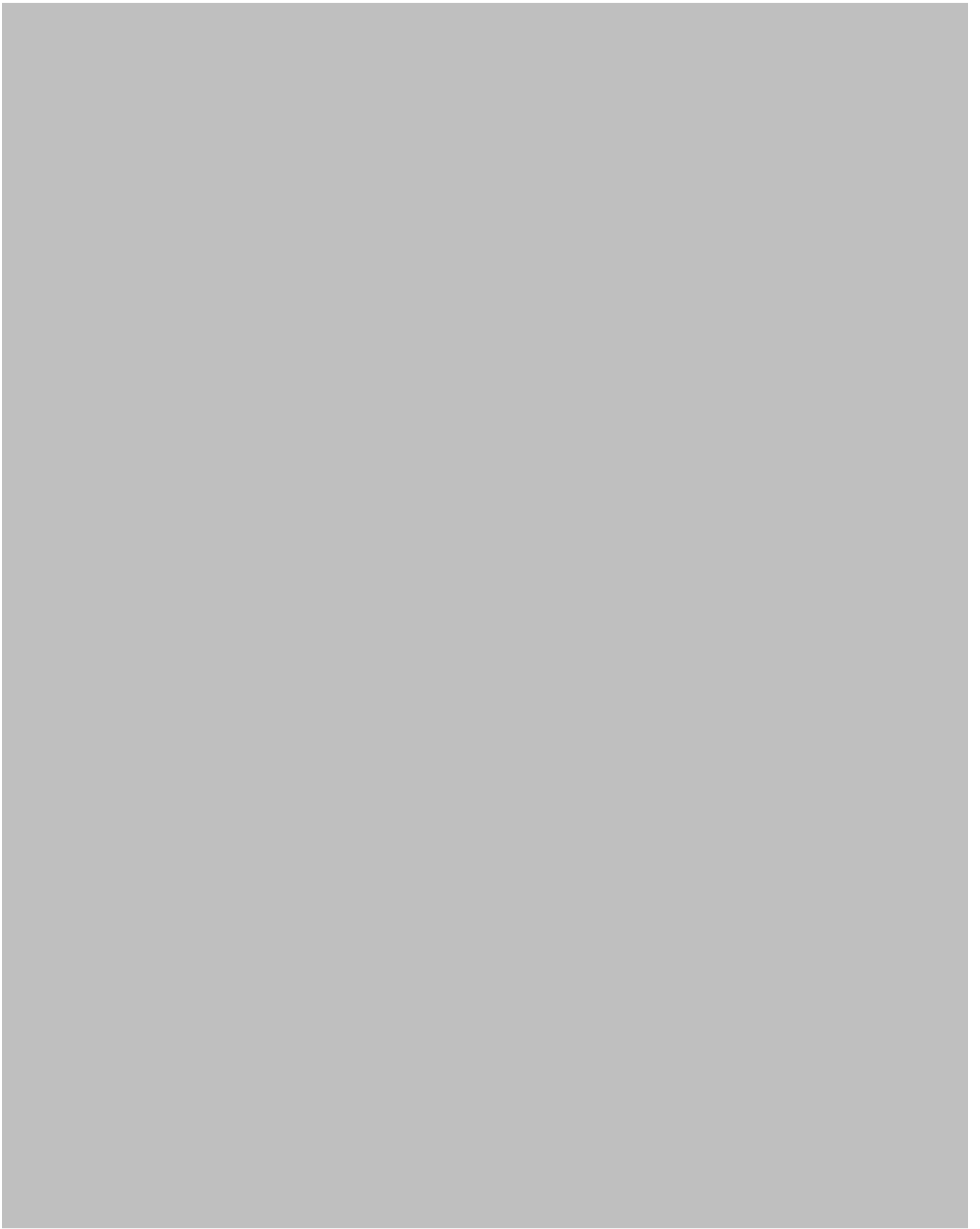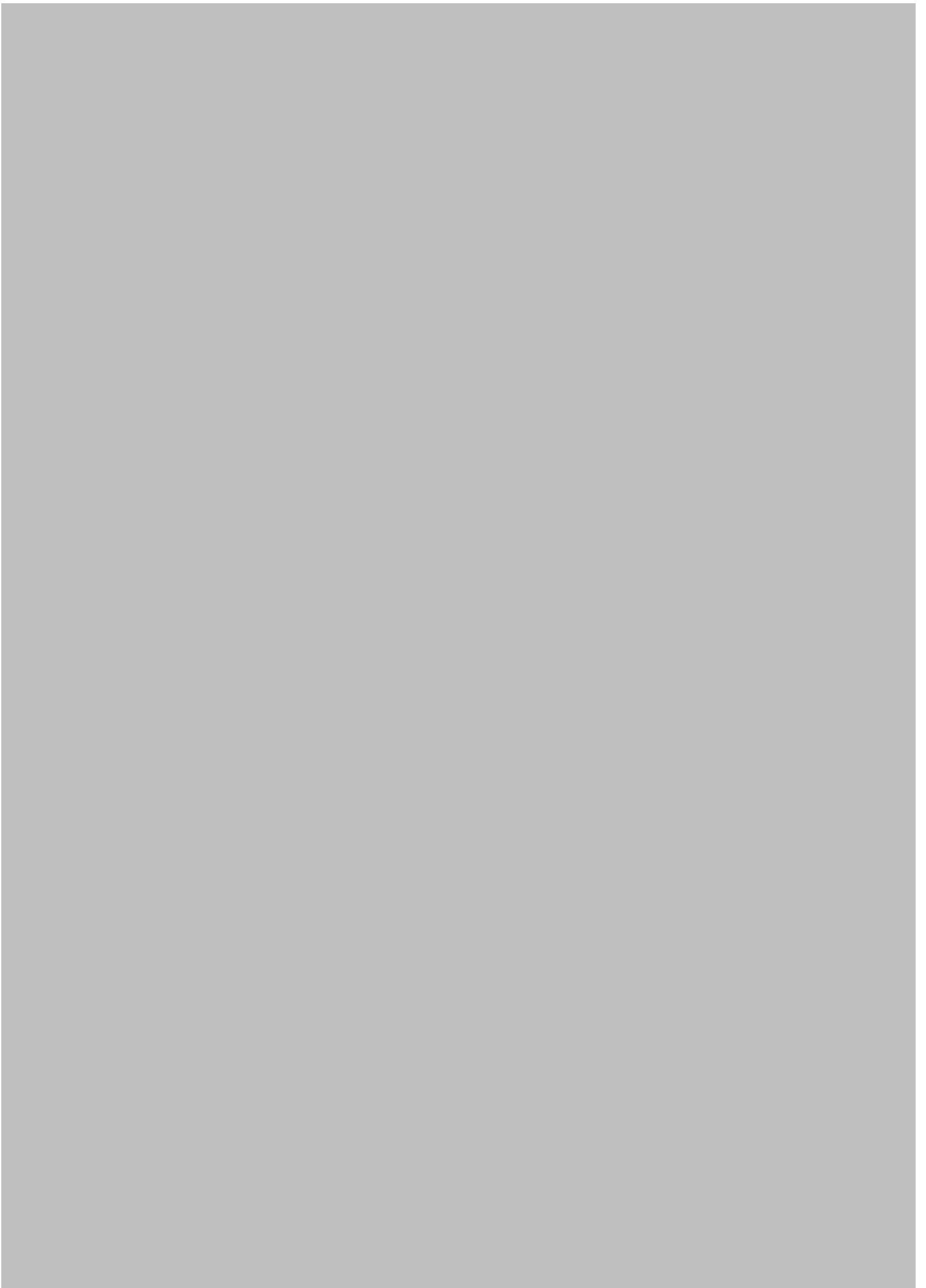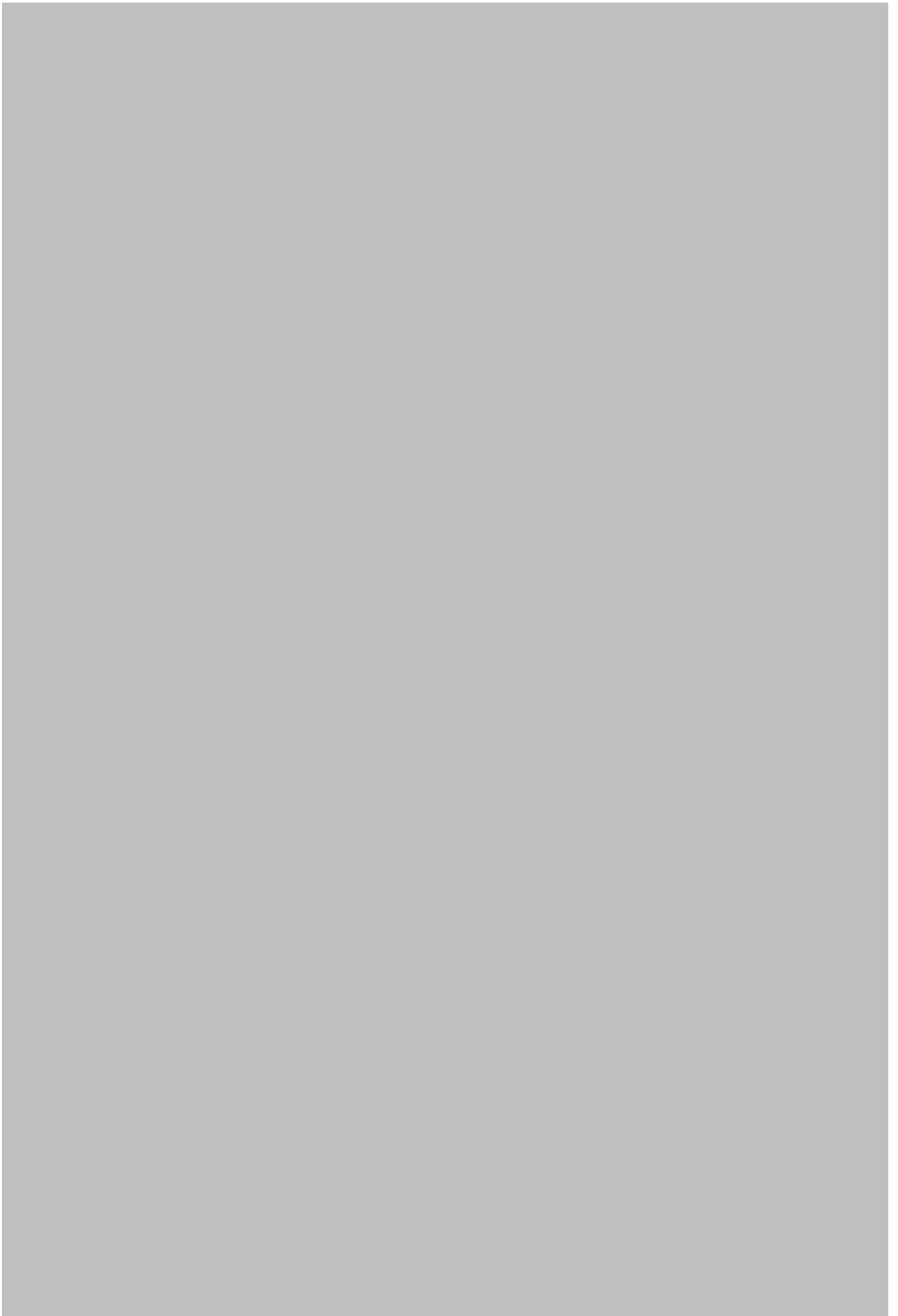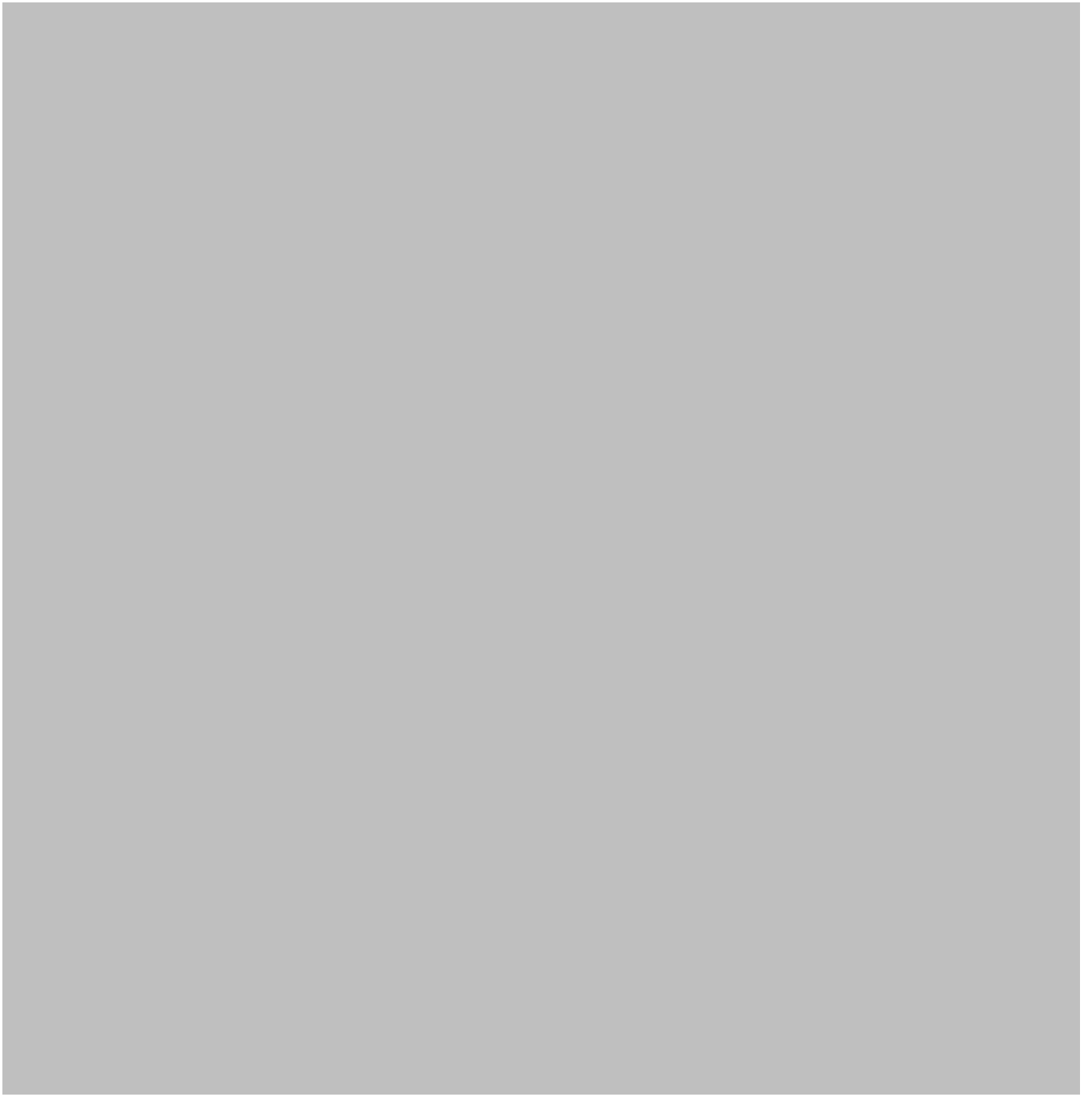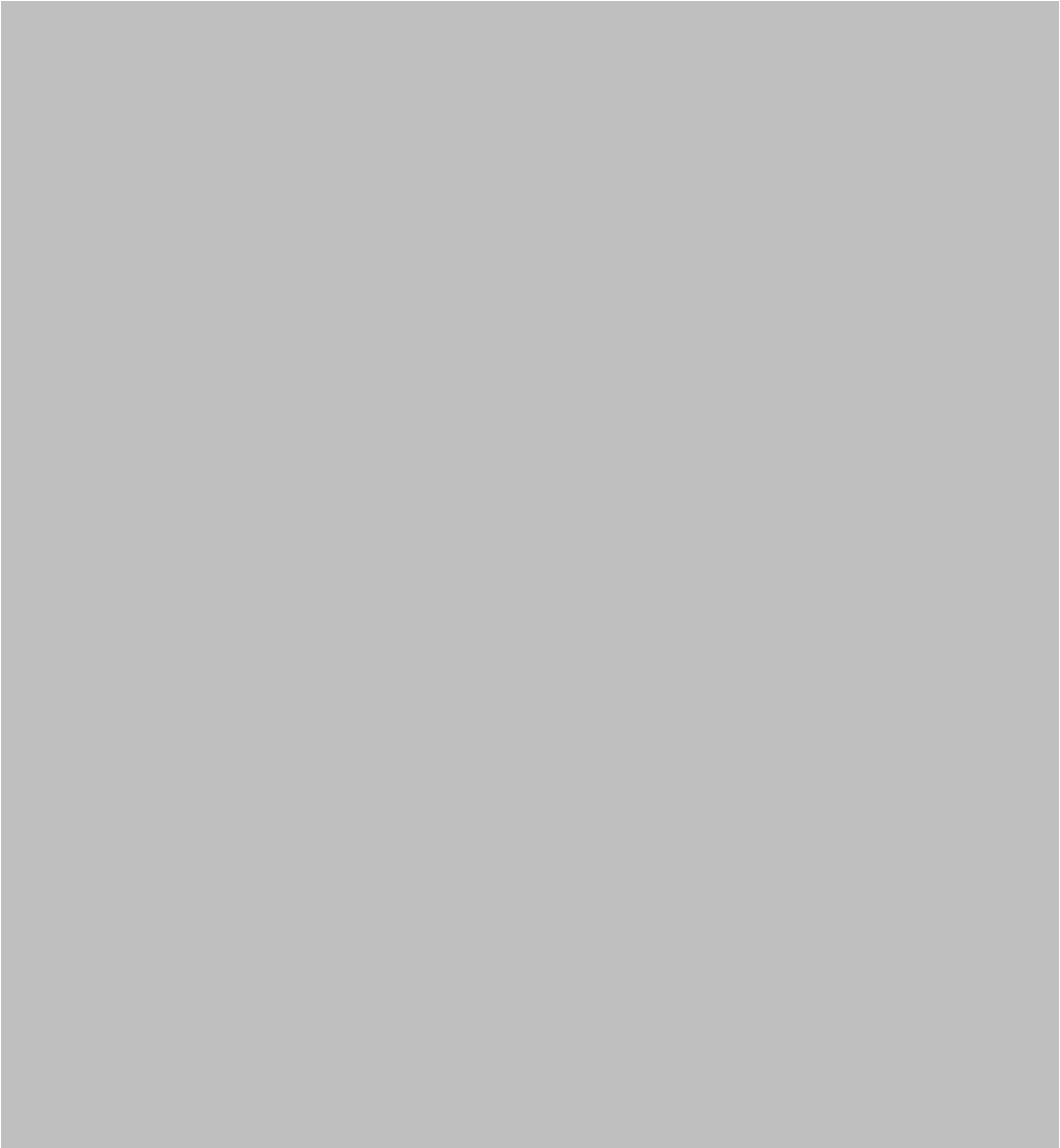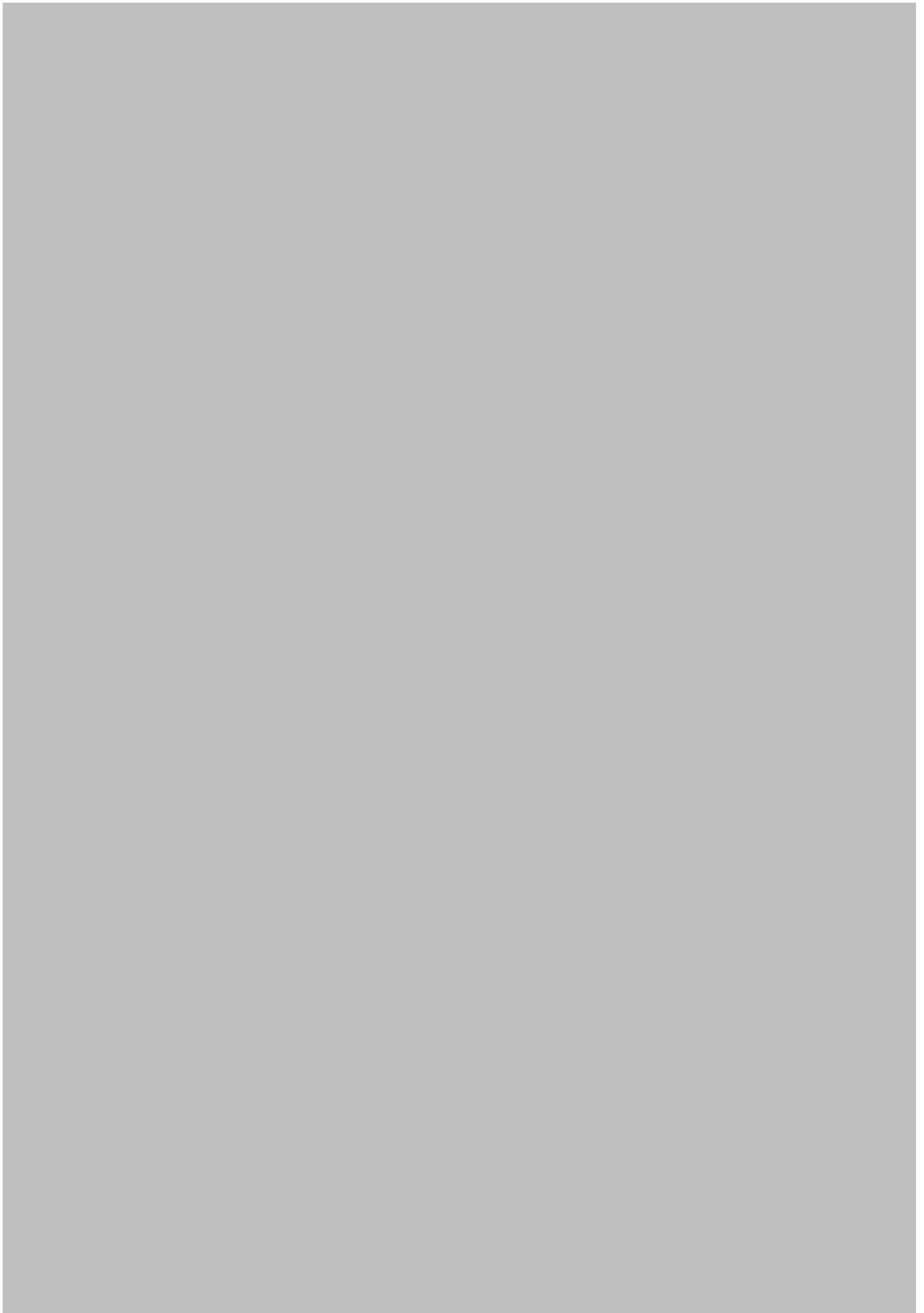
3.2.5 Alginates increase intracellular iron concentrations

With a goal of iron chelation, a focus on alginates decreasing cellular iron concentrations has been highlighted thus far; however it is apparent that throughout the experiments performed, some alginates have actually increased intracellular iron concentrations. This is unsurprising, since it has been discussed how alginates are forming nanoparticles under these conditions and iron-nanoparticle formation has been described as therapeutic intervention for iron deficiency anaemia.[11-16]. Throughout the experiments undertaken, different alginates have been increasing cellular iron concentration or increasing ferritin expression (Table 3.1).

Table 3.1: Table of experiments and relative increases in intracellular iron or protein expression normalised to iron only controls. Ferrozine refers to experiments in section 3.2.2.1, Ferritin expression, ELISA and 1 mm ferritin refers to experiments in section 3.2.2.2.

Experiment \ Alginate	LD	DH	GHB	LFR	KEL	RF	AFH
FERROZINE	0	5.5	3.7	2.5	2	1.5	1.5
FERRITIN EXPRESSION	0	1.1	1.2	0	0	1.3	0
ELISA	0	0	1.1	0	0	1.2	0
1 MM FERRITIN	0	0	0	0	1.6	3.4	4.3

Alginates such as Manucol DH and Protanal RF6650 both show the most evidence of enhancing intracellular iron concentrations. Interestingly, this enhancement effect is most pronounced for all the alginates, apart from Manucol LD, in the ferrozine experiments. This observation was rationalised earlier, whereby actual iron concentrations are measured and not *intracellular* iron specifically. There are several possibilities as to why increased *intracellular* iron concentrations are observed. Firstly, iron-loaded alginate gel networks as identified by STEM could be incorporating into the cell membrane at the cell surface, pseudo-loading the cell with iron causing this apparent increase in cellular iron concentration. This rationality seems plausible based on the evidence provided by confocal microscopy which demonstrated that some alginate-iron composites could be localised to the cell periphery. Secondly, as discussed the alginate-iron nanoparticles are being endocytosed into the cell, yet these iron-rich nanoparticles may not be sensed by the regular mechanisms akin to when iron normally is imported. And lastly, it has previously been reported that metal-Tf conjugated nanoparticles

could become internalised via transferrin mediated uptake.[17]   This is unsurprising since transferrin acquires iron and stores it in an iron-oxide form; the same composition of the alginate iron-oxide nanoparticles determined by STEM (section 2.2.8).

3.2.5.1 Examination of alginate mucoadhesive properties

Alginate iron-composites which are loosely associated with the cell membrane may explain the high iron concentrations overserved by the ferrozine assay when RKO cells were challenged with iron and alginate.   Coupled to the finding that negligible alginate was localised to the cell membrane by confocal microscopy, it is highly plausible that these apparent elevated total cellular iron concentrations were indeed a consequence of so-called alginate 'sticking'.

In order to assess this, different cell culture techniques were utilised. Firstly, RKO cells were challenged with iron and Manucol DH (the alginate to have the most increase total cellular iron) as previously in the ferrozine assay, yet instead of two cell washes performed before lysis, cells were increasingly washed and cells lysed after each wash procedure. These washes would remove any alginate-iron composites that were loosely associated with the cell membrane (figure 3.21).
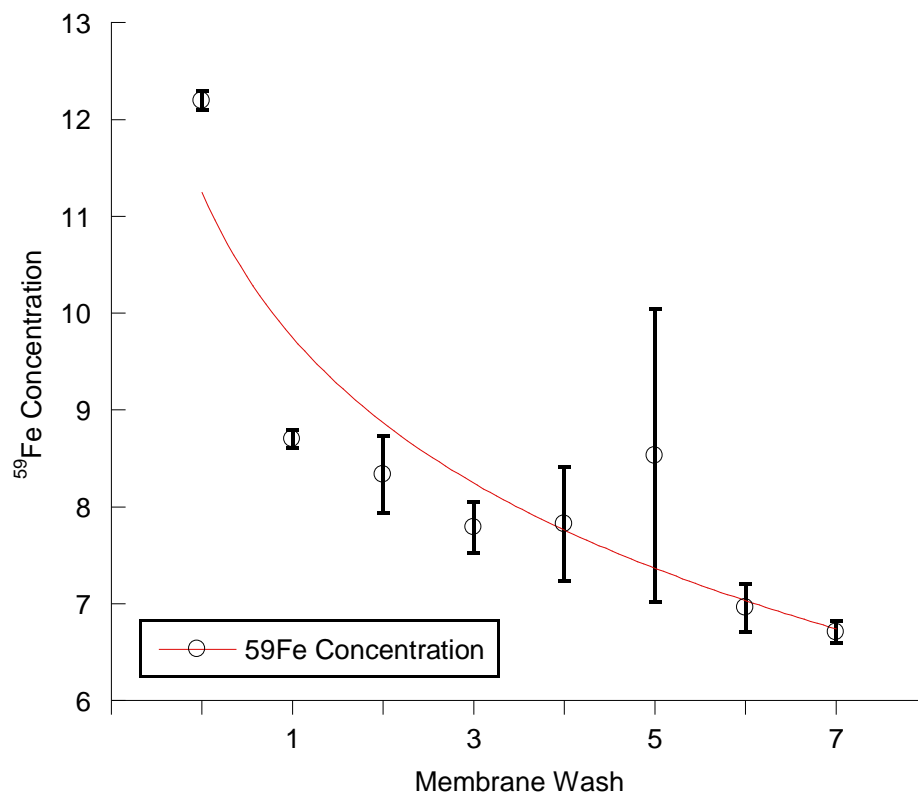
Figure 3.21: ^{59}Fe CPM iron concentration in RKO cells treated with iron and Manucol DH and increasingly washed.

It is apparent that iron-associated to alginate is 'sticking' loosely to the cell membrane, since there is a ca. 25% decrease in iron concentration between wash number 2 and 7. To confirm this, an *ex vitro* chelation step was employed, whereby alginate would have the opportunity to chelate iron present in the media without direct contact with the cells. To perform this, analogous culturing conditions were employed, yet the addition of Manucol DH was confined behind a dialysis membrane and incubated for 24 hours before removal of the alginate and co-incubation with cells (method 3.5.18). This protocol would allow Manucol DH to bind iron and then subsequently it could be removed from the culturing medium, such that if any iron was chelated by the alginate, iron concentrations would be lower and ferritin expression would not be induced compared to the iron only control (figure 3.22).
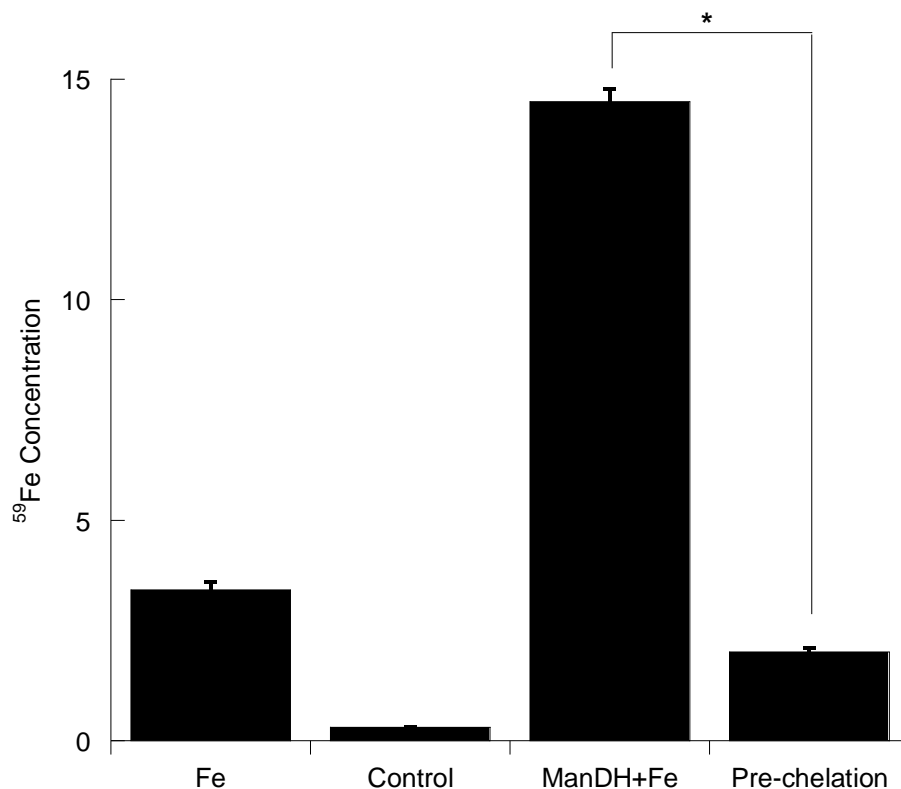
Figure 3.22: Intracellular iron concentration in RKO cells incubated with iron (100 μM) challenged with or without Manucol DH, or conditioned media ('pre-chelated' with Manucol DH).

It is evident that Manucol DH is indeed decreasing intracellular iron uptake when pre-chelation is allowed to take place and subsequent cellular contact is restricted. This result further demonstrates the mucoadhesive effect of specific alginates, increasing the peripheral iron concentration around the cell which may be why increased intracellular iron concentrations are observed.

3.2.5.2 Electron microscopy of endocytosed nanoparticles

Transmission electron microscopy would provide the best confirmation of endocytic nanoparticles or association of iron-loaded alginate with the cell membrane. With this, RKO

cells were treated as previously described (method 3.5.5), washed and subsequently fixed before being embedded into resin and ultrathin sections (50 nm). Staining with uranyl acetate to improve cellular contrast was utilised (figure 3.23 (1)), however since iron has a low atomic number and thus z-contrast, the uranyl cell staining may mask any iron contrast and as such this staining was employed only in some instances (method 3.5.17) (figure 3.23 (2)).
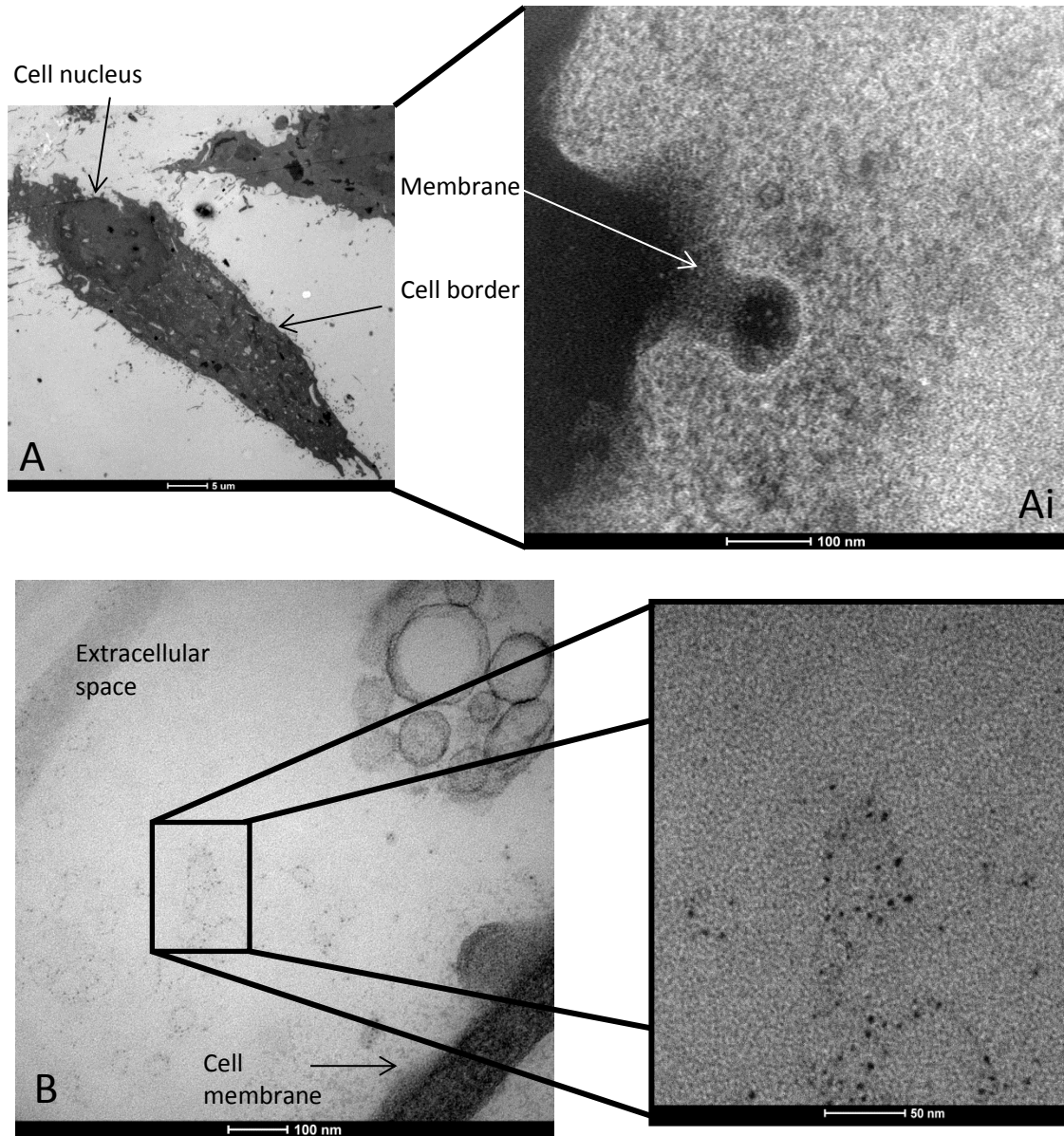
Figure 3.23 (1): Transmission electron micrographs (70 – 90 nm slice width) of RKO cells co-cultured with Manucol DH (0.3 % w/v) and iron (100 μM + 500 μM sodium ascorbate). (A) Stained cell, (Ai) Magnification at cell membrane to an endocytic process. (B) Extracellular space with alginate-type strands and dense contrasting regions with higher magnification (Bi).
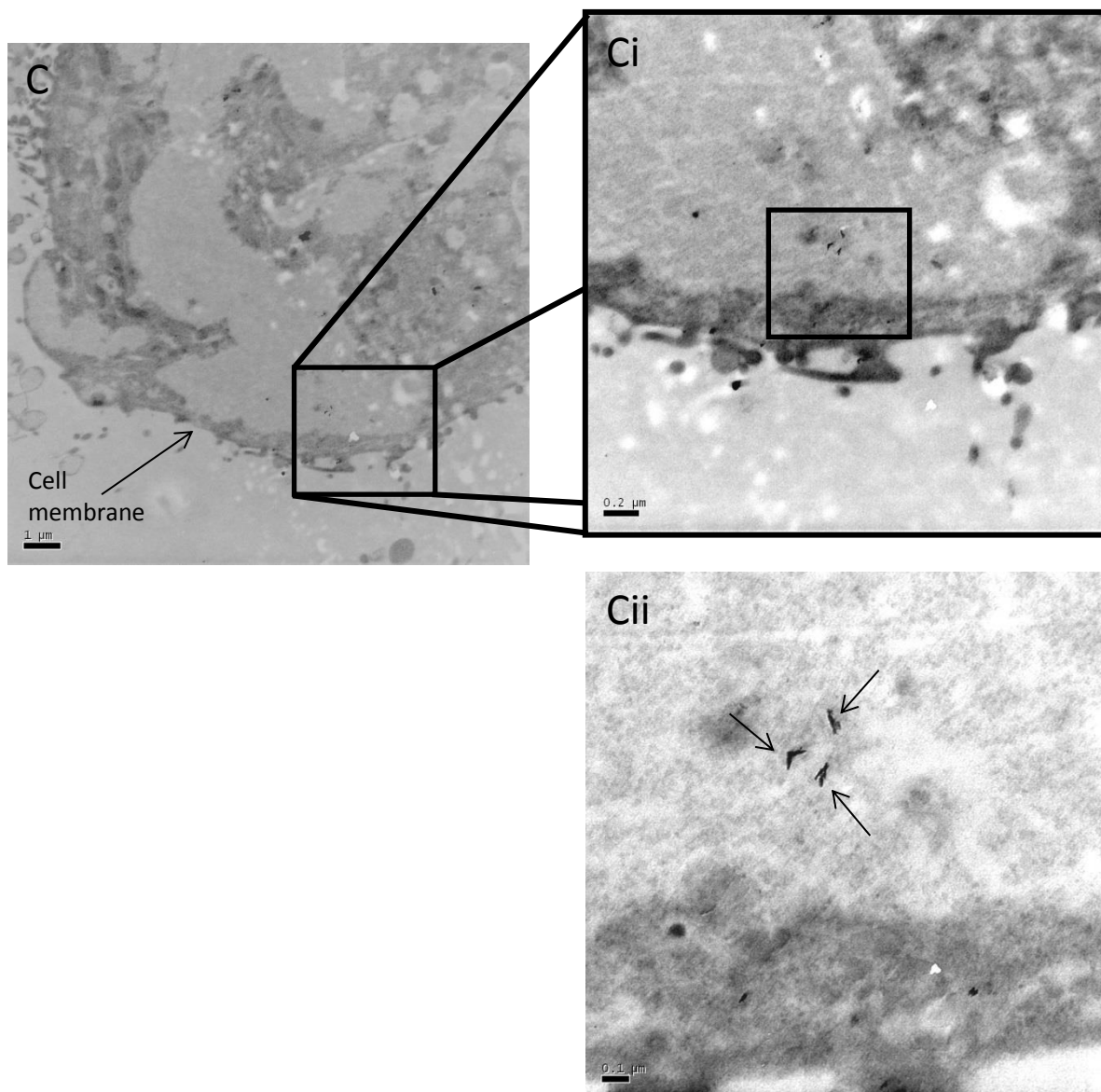
Figure 3.23 (2): Transmission electron micrographs (70 – 90 nm slice width) of RKO cells co-cultured with Manucol DH (0.3 % w/v) and iron (100 μM + 500 μM sodium ascorbate). (C) Unstained cell, (Ci) Magnification at cell membrane to bright contrasting entities at further magnification (Cii).

Cellular staining with uranyl acetate rendered the contrast of the cell too dark to visualise small iron nanoparticles, however this allowed for clear vesicle formation at the initial processes of endocytosis (figure 3.23 A and Ai). Within the extracellular space, near the cell membrane, a strand-like network could be visualised which resembled that found in the

STEM in section 2.2.8.1 (3.23 B). Examination of these strands revealed the presence of small dense areas scattered amongst the chains, that were ca. 5 nm in diameter, a similar size to the nanoparticles found within the dense condensation areas reported earlier (3.23 Bi). This corroborates the previous chemical results that alginates are indeed nucleating nanoparticles, even here in the physiological conditions employed for cell culture. Noteworthy is the localisation of these nanoparticle-enriched strands near the cell membrane. This is in agreement with the confocal microscopy reported earlier (figure 3.3) and could suggest the incorporation of the iron-loaded alginate polymer onto the cell membrane periphery. The clarity of the images improves when cellular staining is not employed, and much darker, highly contrasting particles can be visualised (3.23 C and Ci). The size of these particles are ca. 100 nm in length, much bigger than the nanoparticles found previously; these cannot be confirmed as iron nanoparticles, yet there is a trend to higher localisation concentrations around the cell periphery. The endocytic uptake of iron nanoparticles by intestinal cells has been reported previously.[18]

3.3   Conclusions and summary

The work presented in this chapter has confirmed the use of sodium alginate, specifically Manucol LD as a potential luminal iron chelator. Conjugation of a fluorescent probe to sodium alginate allowed direct visualisation and localisation in cell culture which interestingly established two properties of alginate. Firstly, and most pertinent to this study since iron chelation is required within the lumen of the colon, is the non-absorbable nature of alginate; this corroborates the positive findings of its non-bioavailability previously reported.[1, 2, 19, 20] Secondly, despite lack of evidence for intracellular alginate negligible alginate could be localised to the cell periphery at the membrane; this result confirms the mucoadhesive nature of alginate. Interestingly, transmission electron microscopy identified the presence of iron-loaded alginate strands containing nanoparticulate matter analogous to that identified in scanning transmission electron microscopy previously. This was situated at the cell periphery further confirming these localisation results. The possibility of endocytic uptake of iron nanoparticles has been confirmed previously,[18] and microscopy studies here have eluded to this possibility in the case of alginate-coated iron-oxide nanoparticles.

In vitro Manucol LD decreased ferritin expression by 60%, decreased total cellular iron by 62%, restored TfR1 expression to control and decreased absorption of iron into Caco2 cells by 70%; this was the only alginate to have consistent iron chelation properties. These data reflect the iron binding abilities of alginates *in vitro* previously reported, yet Manucol LD was not utilised in these experiments.[1-4]
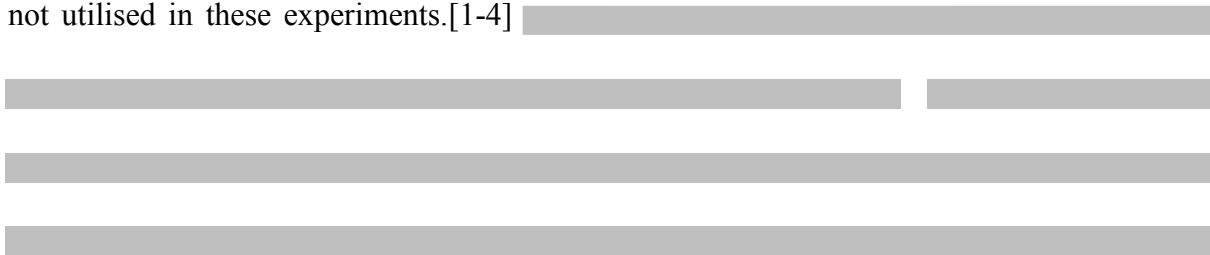
excretion; the exact property desired.

since sodium ascorbate was employed alongside ferrous sulphate for all experiments, it can be inferred that the 'free' ferrous ion would be present within solution, making this species of iron available for chelation by alginate.

Cellular uptake of alginate-coated iron-oxide nanoparticles and the apparent 'sticking' of Manucol DH to the cell membrane may explain the iron-chelation experiments where some alginates notably increased total cellular iron. It could be inferred that some alginates, such as Manucol DH, have greater adhesive properties than others. In fact, this adhesive nature was the cause of the apparent increase in total cellular iron correlating to a greater 'sticking' to the cell membrane. These mucoadhesive properties have been analysed for different alginates and indeed the affinity of 'sticking' is reliant upon alginate composition.[24, 25] It could be inferred that this is the reason for some reports of alginates enhancing iron absorption *in vitro*.[3] These sticking effects were confirmed by a series of experiments, which identified that when you indeed measure the iron chelation ability of alginates *in vitro* and not their adhesive properties they had similar iron binding affinity. Manucol DH has similar iron binding activity as Manucol LD in pre-chelation experiments, however the mucosal adhesive properties of Manucol DH would make it a poor medicinal chelator since this alginate would produce a high local concentrations of iron close to the intestinal mucosa and may allow participation of free-radical reactive oxygen species. With respect to nanoparticulate endocytosis of alginate-coated iron-oxide nanoparticles, it could be the case that only specific alginates form specific nanoparticle characteristics which enable them to be endocytosed.

Manucol LD appears to be an ideal candidate for luminal iron chelation. As such, the results presented thus far have identified a medicinal candidate that meet the criteria originally set out, namely; i) must bind iron, ii) be non-absorbable and non-fermentable, iii) be specific towards iron with a high affinity and iv) must be natural and safe. The next sensible step would undoubtedly be tests in man.

However, the physicochemical properties that underpin the unique nature of Manucol LD are unknown. Alginate G:M composition and molecular weight have been determined, and exclusivity is apparent throughout the series. However, the chemical familiarity between Manucol LD and Manucol DH is appreciable, yet these two alginates demonstrate significant activity differences with respect to iron chelation. This difference could be rationalised on G:M sequence structure along the alginate backbone, with Manucol LD possessing the sequence for a perfect iron binding pocket.

3.4 Acknowledgments

3.5 Experimental methods

3.5.1 Cell culture

Cell lines were cultured in an incubator at 37 °C with a 5% CO_2 atmosphere and 95% relative humidity. RKO cells were grown in Dulbecco's Modified Eagles Medium (DMEM) supplemented with Foetal Calf Serum (10% (v/v)) and penicillin (100 U ml $^{-1}$) and streptomycin (0.1 mg mL^{-1}). Caco2 cells were grown in similar conditions except the medium was supplemented with non-essential amino acids (1% (v/v)). Cell culture experiments were performed in a laminar flow tissue culture cabinet using aseptic technique. Mycoplasma testing was performed to ensure cells remained un-infected and cells were discarded after extensive passage.

All cells lines utilised were adherent cells and as such they were passaged at approximately 90% confluence. For RKO and Caco2 cells, this was performed by aspirating the cell culture medium, washing with sterile phosphate buffered saline (10 mM, pH 7.4) and incubating with trypsin EDTA (5 mL, 0.05% w/v) for ca. 5 min until cells had detached. Trypsin was deactivated by the addition of growth medium (5 mL), cells were disaggregated by tituration

and the subsequent suspension was centrifuged for 5 min at 1500 rpm. The cell pellet was then resuspended in growth medium and reseeded into new growth flasks.

3.5.2 Cell plating

For experimentation, cells were obtained in suspension as per above. From this cell resuspension, cells were seeded into either 6 well, 12 well or 96 well plates at a standard concentration of 1×10^5 cells mL^{-1} (2 mL, 1 mL or 100 μL for each well type respectively). Cell density was calculated using a haemocytometer by counting a representative sample of the cells within the window of view. Cells were plated in their respective growth medium and incubated for 24 hours before experimentation.

3.5.3 Iron cell co-incubation experiments

In cell experiments where iron co-incubation was required, a standard protocol was employed. An iron stock was created by dissolving $FeSO_4 \cdot 7H_2O$ (108.9 mg, 10 mM) and sodium ascorbate (396 mg, 500 mM) into DI H_2O (40 mL), with the resultant solution dark purple in colour. The iron stock was then filtered through a 0.2 μm syringe filter so that it was suitable for use *in vitro*. This stock was then diluted into growth medium at a standard concentration to create an iron-stimulated medium that contained 100 μM Fe(II) and 500 μM sodium ascorbate, equating to a 1:100 dilution. This was a standard protocol employed whenever cells were cultured with iron unless stated otherwise.

3.5.4 ^{59}Fe experimentation

Experiments involving the use of radioactive iron were typically set up as previously discussed, with iron and alginate containing culturing mediums produced following the described methods. To create ^{59}Fe iron mediums, the stock of iron ($FeSO_4 \cdot 7H_2O$ (108.9 mg,

10 mM) and sodium ascorbate (396 mg, 500 mM)) into DI H_2O (40 mL) was spiked with $^{59}FeCl_3$ to reach ca. 10,000 counts per minute (CPM) per well. This was then used as previously, with a 1:100 dilution into growth medium. Cell incubation was performed as described to the specific experiment. Upon cell lysis, conditioned media was removed and cells were washed twice with Versene (1 mL, 0.2 g L^{-1} EDTA in PBS) with the remaining volume of the cell void using a 1 mL pipette. Cells were then lysed in HEPES-saline lysis buffer (150 μL, 10 mM, pH 7.4, NaCl 0.9% (w/v)). To count for radiation content, a specific amount of the sample under investigation (usually ca. 100 μL) was transferred into a scintillation tube and scintillation fluid (1 mL) was added. Radiation CPM counts were normalised to protein concentration as determined in the BCA protein assay.

3.5.5 Alginate co-incubation experiments

In cells experiments where alginate co-incubation was required, a standard protocol was employed. Alginate stocks were created whereby alginate (0.6 g) was vigorously mixed in a tissue culture hood in sterile filtered DI H_2O (30 mL) that was heated to 37 °C. The solution was vigorously shaken for a further 5 min and then incubated at 37 °C until full dissolution was achieved. To create alginate stimulation media, alginate stock (1.5 mL) was mixed with growth medium with or without iron stimulation (8.5 mL) to create a resultant 0.3 % alginate medium. It is important to note that some alginates, due to their viscous nature were transferred whilst warm and sufficient time was given for all alginate solutions to move out of necessary transfer pipettes. This was a standard protocol employed whenever cells were cultured with iron unless stated otherwise.

3.5.6 Western blotting

Cells were plated in 6 well plates according to the protocol above; cells were plated in triplicate for all conditioned cultures used. Cells were incubated in iron and or alginate containing growth mediums for time points according to the experimental conditions. After this time, conditioning media was aspirated and cells were washed x2 in PBS (2 mL) and the remaining volume of the well void. Subsequently, cells were lysed in RIPA lysis solution (1% 4-Nonylphenyl poly(ethylene glycol) (w/v), 0.5% sodium deoxycholate (w/v), 0.1% sodium dodecyl sulphate (w/v), between 150 – 200 μL depending on cell confluency) on ice. Cell lysates were sonicated for 5 min and protein concentrations determined using the Pierce BCA protein assay (detailed below). Cell lysates were prepared for blotting by adding calculated amounts to 5x Laemmli loading buffer (Tris pH 6.7 0.0625 M, glycerol 10% (v/v), sodium dodecyl sulphate 2% (w/v), 2-Mercaptoethanol 1% (v/v) and bromophenol blue 0.001% (w/v)) and heated at 100 $^{\circ}$C for 5 minutes. The concentration of protein added was calculated such that 20 μg of protein would be added to each well in the gel.

Sodium dodecyl sulphate- polyacrylamide gels for electrophoresis were prepared utilising two gel phases (stacking and a resolving phases) in order to achieve optimum resolution of proteins. The resolving gel was made by mixing deionised H_2O (1.9 mL), Tris buffer (10 mL, pH 8.8, sodium dodecyl sulphate 0.2% (w/v)), acrylamide/ bisacrylamide (8.1 mL, 30%/8%), ammonium persulphate (0.03 g) and tetramethylethylenediamine (80 μL). This was mixed rapidly and poured into the glass cast, covered with a small amount of 2-propanol (500 μL) and left aside to set. The stacking gel was placed on top and made by mixing deionised H_2O (3.7 mL), Tris buffer (10 mL, pH 6.8, sodium dodecyl sulphate 0.2% (w/v)), acrylamide/bisacrylamide (1.3 mL, 30%/8%), ammonium persulphate (0.03 g) and tetramethylethylenediamine (80 μL). In both instances, the reagent amounts were sufficient

to cast two gels which were 12.5 % in total acrylamide content; 12.5 % gels were utilised to probe ferritin expression. If TfR1 was under investigation, 10% gels would be used, and as such the resolving gel would consist of deionised H_2O (3.5 mL), Tris buffer (10 mL, pH 8.8, sodium dodecyl sulphate 0.2% (w/v)), acrylamide/bisacrylamide (6.5 mL, 30%/8%), ammonium persulphate (0.03 g) and tetramethylethylenediamine (80 µL). .

Laemmli buffer protein samples were pipetted into their appropriate wells, and gels were run initially through the stacking gel for 15 min at 90 V and then increased to 180 V through the resolving gel in an electrophoresis running buffer made with Tris (25 mM, pH 8.3), glycine (0.192 M) and sodium dodecyl sulphate (0.01% (w/v)).

Protein resolved gels were then transferred onto Hybond PVDF membranes which were prepared by pre-soaking in methanol for one minute, and then washed in transfer buffer which was made using Tris (48 mM), glycine (39 mM), sodium dodecyl sulphate (0.0375% (w/v)) and methanol (20% (v/v)). Transfer was undergone in the same buffer, in a cooled transfer tank, for 90 min at 90 V. Following transfer, the membranes were blocked for one hour in Tris-buffered saline tween made from Tris (150 mM, pH 8.0), sodium chloride (150 mM) and Tween-20 (0.05% (v/v)) supplemented with dried milk powder (5% (w/v)). The membrane was then incubated in the primary antibody (Ferritin light-chain, 1:5000 dilution, Abcam (AB69090) or β-actin, 1:5,000 dilution, Abcam, (AB8226) TfR1, 1:1000, Invitrogen (H68.4)) overnight at 4 ^{0}C with constant agitation. Membranes were subsequently washed repeatedly with TBST (20 mL) each with a wash period of 10 minutes. The membrane was then incubated with the appropriate secondary peroxidase conjugated antibody (1:10,000 dilution, Jackson Laboratories) for 45 min again in TBST supplemented with dried milk powder (5 %(w/v)). A final wash procedure was performed using TBST (20 mL) for five repetitions.

The membranes were exposed to an ECL detection reagent (5 mL, GE Healthcare) for five minutes, gently rubbing the reagent over the sealed membranes prior to development. Developed westerns were analysed using ImageJ image processing software.

3.5.7 Synthesis of fluorescently conjugated alginate

Sodium alginate LFR5/60 (0.32 g, 9.0 μM) was dissolved in a solution of phosphate buffered saline at pH 7.4 (50 mL). 1-ethyl-3-(3-dimethylaminopropyl)carbodiimide) (0.018 g, 92 μM) and n-Hydroxysulfosuccinimide sodium salt (0.02 g, 92 μM) was added to the alginate solution and stirred for two hours. Once mixed, fluoresceinamine (0.0319 g, 92 μM) was added to form a bright yellow solution. The reaction was left to stir in darkness for 24 hours; the resultant solution was opaque orange in colour. Free, unreacted fluorophore was removed by dialysis; one wash in deionised H_2O (3.5 L) at 4 ^{0}C for 24 hours, three washes in NaCl (3.5 L, 1 M) for 24 hours each, then a subsequent six washes in deionised H_2O (3.5 L) for 24 hours each. The loss of free fluorophore was monitored by UV-Vis absorption of the dialysate. Once purified, the pH of the solution was adjusted to 7.4 and stored in the dark at 4 ^{0}C until required.

3.5.8 Confocal microscopy

Slides for confocal microscopy were prepared by growing RKO cells on 22 mm cover slips placed in individual wells of a six well cell culture plate. Cells were seeded in six well plates according to the method described above. Once established, the growth medium was removed and fluorescent-alginate loaded medium (0.04% fluorescent alginate, 100 μM $FeSO_4 \cdot 7H_2O$ and 10 μM sodium ascorbate) was added and incubated for 24 hours. After this period a nuclear stain, Hoechst 33450 (NucBlue Live Cell Stain, Life technologies) was added and a cell plasma membrane stain (CellMask Deep Red plasma, Life technologies) at 1 drop/1

mL media and 3 μg/ mL media concentrations respectively. The medium was removed and the cells were washed three times with 2 mL phosphate buffered saline. Fixation was undergone using a 4% paraformaldehyde solution (pH 7.4) at room temperature for eight minutes. The paraformaldehyde was removed and slides washed with 2 mL PBS and then placed, cell side down, onto a small amount of SureFade (Life technologies) on a microscope cover slide and sealed using nail varnish.

3.5.9 Cellular iron content by the ferrozine assay

Cells were plated in 6 well plates according to the protocol above; cells were plated in triplicate for all conditioned cultures used. Cells were incubated in iron and/or alginate containing growth mediums for time points according to the experimental conditions using the methods described above. After this time, conditioning media was aspirated and cells were washed X2 in PBS (2 mL) and the remaining volume of the well void. Cells were lysed in HEPES-saline lysis buffer (150 μL, 10 mM, pH 7.4, NaCl 0.9% (w/v)). A ferrozine stock solution was prepared by mixing sodium acetate (17 mM, 13.8 g), L-sodium ascorbate (4.6 mM, 0.91 g) and 3-(2-Pyridyl)-5,6-diphenyl-1,2,4-triazine-p,p′-disulfonic acid monosodium salt hydrate (0.18 mM, 0.09 g) into DI H_2O (122 mL). The cell lysate was thoroughly mixed and 90 μL was aspirated and mixed with of a trichloroacetic solution (200 μL , 20% (w/v)), which was then heated at 100 ^{0}C for 10 min and then centrifuged at 12000 RPM for five minutes to pellet the protein precipitate. The supernatant was aspirated and 200 μL was added to 600 μL ferrozine stock solution and mixed thoroughly and absorbance read on a plate reader at λ=550 nm. All results were standardised to protein content using a protein assay kit (Peirce BCA protein assay).

3.5.10 BCA protein assay

Cell lysates (10 µL) were added in triplicate to a 96 well plate as were set protein calibration solutions (2, 1, 0.5 and 0.25 µg µL^{-1}), to which a working solution consisting of reagent A and reagent (A:B mixed in a 50:1 ratio) was added (200 µL). Following an incubation period of 30 min at 37 °C, absorbance was read on a plate reader at λ=550 nm.

3.5.11 Ferritin ELISA

The Spectro Ferritin MT kit was utilised as an additional means of quantifying intracellular ferritin expression to western blotting. Cells were lysed in RIPA lysis solution (1% 4-Nonylphenyl poly(ethylene glycol) (w/v), 0.5% sodium deoxycholate (w/v), 0.1% sodium dodecyl sulphate (w/v), between 150 – 200 µL depending on cell confluency). Cell lysates were sonicated for 5 min at and protein concentrations determined. According to the manufacturers protocol, cell lysates (10 µL) were added to individual wells with a standard set of ferritin calibration solutions (10 µL, 6, 20, 60, 200, 600 and 2000 ng mL^{-1}. To this, unconjugated antihuman ferritin (200 µL) was added before incubating for 2 hours with agitation. Wells were subsequently washed with DI H$_2$O before the addition of 200 µL substrate solution and a further incubation for 30 min. After this, potassium ferricyanide (100 µL, 0.24 % (w/v)) was added to develop the colour with absorption read at λ=490 nm and λ=595 nm. Absorption values at λ=595 nm were subtracted from values obtained at λ=490 nm, and all values obtained for ferritin concentration were normalised to protein concentration.

3.5.12 Luminescence spectroscopy

UV-Vis absorption spectroscopy measurements were performed on a Varian Cary 5000 spectrometer at a 300 nm min^{-1} acquisition rate. Samples were prepared in 1 cm quartz

cuvettes. Luminescence measurements were executed on an Edinburgh Instruments FLS920 spectrometer, with a 450 W xenon arc lamp illumination source. Samples were prepared in quartz cuvettes with entirely transparent faces and appropriate long-pass filters to eliminate second-order photon scattering.

3.5.13 Caco-2 monolayer

Caco-2 cells were routinely cultured according to the protocol above. Prior to experimentation, Caco-2 cells were seeded (2 mL) into pre-treated and dried collagen-coated (200 μL, 10% (v/v) in 0.5%(v/v) acetic acid) 6-well transwell inserts at a concentration of 4 x 10 cells mL^{-1}. Cells were grown for 14 days post confluency, with a media change every other day in both the apical and basolateral chambers.[10]

24 hours prior to challenge with iron and alginate, cell medium was changed to FCS-free MEM (containing epidermal growth factor, 20 μg L^{-1}, triiodothyronine, 0.05 μM, piperazine-N,N'-bis[2-ethanesulfonic acid] 10 mM, hydrocortisone, 11 μM, sodium selenite, 0.02 μM and insulin 0.87 μM.[26] After incubation, cells were stimulated with iron as per the protocol above, however the iron-containing medium was spiked with ^{59}FeCl$_3$ to reach ca. 10,000 counts per minute (CPM) per well. Alginate containing media was prepared as per the protocol above. To the apical layer, FCS-free MEM with iron with or without alginate (2 mL) was added and to the basolateral membrane FCS-free MEM (containing apotransferrin 50 μg mL $^{-1}$, 2 mL) was added. At 30 min, 1, 2, 4 and 24 hour time points samples (200 μL) were removed from the apical and basolateral membranes. After the 24 hour time point the medium was removed and the cells were washed three times with 2 ml Versene (0.2g L^{-1} EDTA in phosphate buffered saline), and lysed in RIPA lysis solution (1% 4-Nonylphenyl

poly(ethylene glycol) (w/v), 0.5% sodium deoxycholate (w/v), 0.1% sodium dodecyl sulphate (w/v), 500 µL).

Samples collected were assessed for iron concentration using scintillation counting. To do this, a set amount of sample (usually 100 µL) was added to scintillation tubes and scintillation fluid added (1 mL) and read on a β-counter.

3.5.17 Transmission electron microscopy

Cell sections for TEM analysis were generated as follows. RKO cells were grown in 6 well plates and treated with iron or alginate according to the protocols above. After incubation, cells were washed with PBS (x3 2 mL) and subsequently incubated with glutaraldehyde in sodium cacodylate buffer (2.5 % (w/v) 500 µL) and stored at room temperature until processed further. Sampling and sectioning of the cells onto TEM grids, mounting and staining was undertaken by University of Birmingham Electron Microscopy services and the technical team of Dr. Paul Verkade (University of Bristol).

3.5.18 *Ex vitro* iron chelation

To prepared so-called 'pre-chelation' conditioned medium, alginates (9 mL, 2% (w/v), in DI H_2O) were confined within a dialysis membrane and immersed in iron containing media (51 mL, 100 µM Fe(II) and 500 µM sodium ascorbate); equilibrium dialysis was performed for 24 hours at 37 °C with intermittent agitation. The resultant supernatant was aspirated and used immediately as conditioned media in subsequent experiments alongside normal 'non pre-chelated' condition mediums.

3.6 References

1. Wölbling, R.H., G. Becker, and W. Forth, *Inhibition of the Intestinal Absorption of Iron by Sodium Alginate and Guar Gum in Rats.* Digestion, 1980. **20**(6): p. 403-409.
2. Sandberg, A.S., et al., *ALGINATE, SMALL-BOWEL STEROL EXCRETION, AND ABSORPTION OF NUTRIENTS IN ILEOSTOMY SUBJECTS.* American Journal of Clinical Nutrition, 1994. **60**(5): p. 751-756.
3. Wawer, A.A., et al., *Evidence for an Enhancing Effect of Alginate on Iron Availability in Caco-2 Cells.* Journal of Agricultural and Food Chemistry, 2012. **60**(45): p. 11318-11322.
4. Wawer, A.A., et al., *Alginate inhibits iron absorption from ferrous gluconate in a randomized controlled trial and reduces iron uptake into caco-2 cells.* PloS one, 2014. **9**(11): p. e112144-e112144.
5. DuBois, M., et al., *Colorimetric Method for Determination of Sugars and Related Substances.* Analytical Chemistry, 1956. **28**(3): p. 350-356.
6. Michel, C., et al., *In vitro fermentation by human faecal bacteria of total and purified dietary fibres from brown seaweeds.* British Journal of Nutrition, 1996. **75**(2): p. 263-280.
7. Salyers, A.A., J.K. Palmer, and T.D. Wilkins, *Degradation of polysaccharides by intestinal bacterial enzymes.* Am J Clin Nutr, 1978. **31**(10 Suppl): p. S128-s130.
8. Riemer, J., et al., *Colorimetric ferrozine-based assay for the quantitation of iron in cultured cells.* Analytical Biochemistry, 2004. **331**(2): p. 370-375.
9. Artursson, P., *Epithelial transport of drugs in cell culture. I: A model for studying the passive diffusion of drugs over intestinal absorbtive (Caco-2) cells.* Journal of Pharmaceutical Sciences, 1990. **79**(6): p. 476-482.
10. Hu, M., et al., *Use of Caco-2 Cell Monolayers to Study Drug Absorption and Metabolism*, in *Optimization in Drug Discovery*, Z. Yan and G. Caldwell, Editors. 2004, Humana Press. p. 19-35.
11. Devi, P.R. and E. Hemananthan, *Synthesis, Characterization and in vitro Evaluation of Ferrous Phosphate Nanoparticles Loaded Iron for Bioavailability Studies.* Asian Journal of Chemistry, 2013. **25**(10): p. 5437-5440.
12. Kim, D.Y., et al., *Bioavailability of Iron-nanoparticles with Ascorbic Acid in Anemic Mice.* Journal of Biomedical Research, 2012. **13**(1): p. 53-63.
13. Powell, J.J., et al., *A nano-disperse ferritin-core mimetic that efficiently corrects anemia without luminal iron redox activity.* Nanomedicine-Nanotechnology Biology and Medicine, 2014. **10**(7): p. 1529-1538.
14. Pereira, D.I.A., et al., *Nanoparticulate iron(III) oxo-hydroxide delivers safe iron that is well absorbed and utilised in humans.* Nanomedicine-Nanotechnology Biology and Medicine, 2014. **10**(8): p. 1877-1886.
15. Latunde-Dada, G.O., et al., *A Nanoparticulate Ferritin-Core Mimetic Is Well Taken Up by HuTu 80 Duodenal Cells and Its Absorption in Mice Is Regulated by Body Iron.* Journal of Nutrition, 2014. **144**(12): p. 1896-1902.
16. Rohner, F., et al., *Synthesis, characterization, and bioavailability in rats of ferric phosphate nanoparticles.* Journal of Nutrition, 2007. **137**(3): p. 614-619.
17. Harush-Frenkel, O., et al., *Targeting of nanoparticles to the clathrin-mediated endocytic pathway.* Biochemical and Biophysical Research Communications, 2007. **353**(1): p. 26-32.
18. Pereira, D.I.A., et al., *Caco-2 Cell Acquisition of Dietary Iron(III) Invokes a Nanoparticulate Endocytic Pathway.* PLoS ONE, 2013. **8**(11): p. e81250.
19. Jonathan, M.C., et al., *Separation and Identification of Individual Alginate Oligosaccharides in the Feces of Alginate-Fed Pigs.* Journal of Agricultural and Food Chemistry, 2013. **61**(3): p. 553-560.
20. Jonathan, M., et al., *In vivo degradation of alginate in the presence and in the absence of resistant starch.* Food Chemistry, 2015. **172**(0): p. 117-120.

21. Berner, L.A. and L.F. Hood, *Iron Binding by Sodium Alginate.* Journal of Food Science, 1983. **48**(3): p. 755-758.

22. Fernandez, R. and S.F. Phillips, *Components of fiber bind iron in vitro.* The American Journal of Clinical Nutrition, 1982. **35**(1): p. 100-6.

23. Radulescu, S., et al., *Luminal Iron Levels Govern Intestinal Tumorigenesis after Apc Loss In Vivo.* Cell Reports, 2012. **2**(2): p. 270-282.

24. Boddupalli, B.M., et al., *Mucoadhesive drug delivery system: An overview.* Journal of Advanced Pharmaceutical Technology & Research, 2010. **1**(4): p. 381-387.

25. Tønnesen, H.H. and J. Karlsen, *Alginate in Drug Delivery Systems.* Drug Development and Industrial Pharmacy, 2002. **28**(6): p. 621-630.

26. Thompson, B., et al., *Development of a modified Caco-2 cell model system for studying iron availability in eggs.* J Agric Food Chem, 2010. **58**(6): p. 3833-9.

27. Drabkin, D.L. and J.H. Austin, *SPECTROPHOTOMETRIC STUDIES: I. SPECTROPHOTOMETRIC CONSTANTS FOR COMMON HEMOGLOBIN DERIVATIVES IN HUMAN, DOG, AND RABBIT BLOOD.* Journal of Biological Chemistry, 1932. **98**(2): p. 719-733.

Chapter 4

Alginate chemical modification: an understanding of iron chelation bioactivity.

4.1   Introduction and aims

The current understanding of alginate chemical composition has been determined by analytical ultra-centrifugation (AUC) and nuclear magnetic resonance spectroscopy (NMR) to reveal the inherent molecular weight and specific G:M compositions respectively (table 4.1).

Table 4.1: Molecular weight and G:M composition of the alginate series tested (see sections 2.2.3 and 2.2.4 for further details).

Alginate	Molecular Weight (kDa)	G:M composition
Protanal RF6650	230 ± 10	60:40
Keltone	220 ± 15	46:54
Manugel GHB	180 ± 18	53:47
Manucol DH	170 ± 6	40:60
Protsea AFH	155 ± 5	29:71
Manucol LD	145 ± 5	38:62
LFR5/60	74 ± 3	62:38

It is clear that, despite a range of alginates tested, the range of distribution of molecular weights and G:M compositions is limited (figure 4.1).
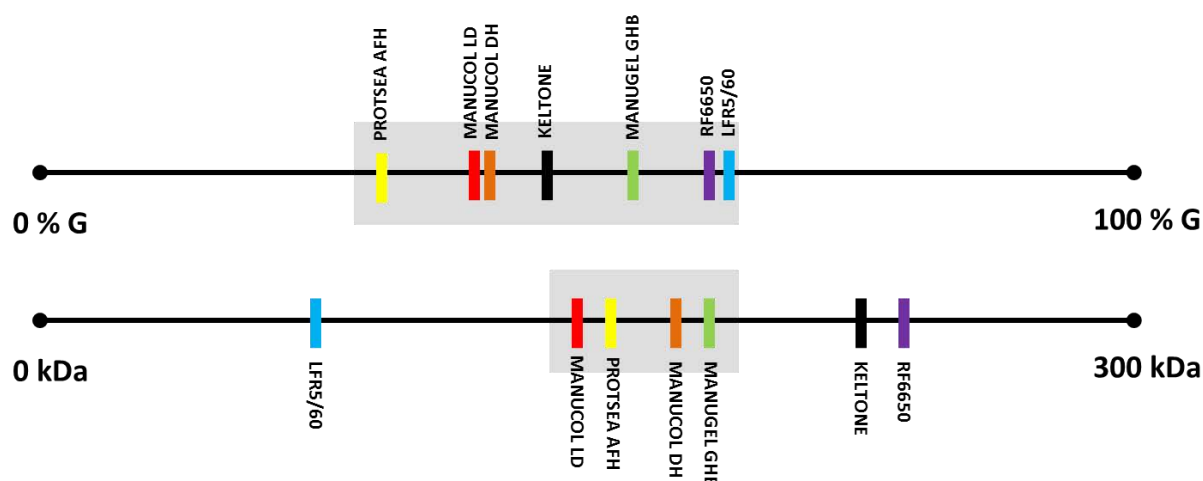
Figure 4.1: Schematic representation of the range of distributions of molecular weight and G:M compositions of the alginate series. Grey shaded areas represent where the majority of MW and G:M compositions are represented along the scale.

On reflection of these chemical characteristics and the observed iron chelation properties, it is apparent that defining chemical iron binding by simple molecular weight and G:M composition differences to allow stratification is not possible; a more complex structure-activity relationship is dictating bioactivity. A purely chemical understanding of how molecular weight and thus polymer length affects iron chelation would be rationalised on the grounds of sterics and entropy. Specifically, the larger the alginate the more ordered the system becomes to coordinate iron; a disfavourable action in entropy energetics. Likewise, the bigger the alginate the more likely the polymer is going to sterically encounter itself when coordinating to iron; again unfavourable in terms of electrostatics. On these grounds it could be concluded that as alginate molecular weight increases iron chelation ability decreases; this has indeed been reported (as discussed in section 1.4).[1] A more 'bio-chemical' view of the interaction would disregard the thermodynamics of coordination and focus on how the alginate tertiary and secondary structure form a binding pocket within the 'protein-like'

complex; indeed the formation of secondary and tertiary structures is highly reliant on the sequence of the protein under investigation, or the alginate in this case. In view of this, depolymerisation of Manucol LD to smaller molecular weight components would demonstrate if polymer chain length dictates iron-chelation ability. Accessing alginates with different MG sequences to Manucol LD (with the same molecular weight) would demonstrate whether purely the specific molecular weight of Manucol LD holds iron chelation activity or if M:G composition also influences iron binding.

Following on from this, it is unapparent why Manucol LD has the desired bioactivity when chemically it is not grossly dissimilar to Manucol DH. Of note, Manucol DH and Manucol LD are extracted from the same raw material (albeit different 'fractions' from the same seaweed). To assess why this is the case, further experimentation into structure-activity relationships will need to be pursued alongside a thorough chemical characterisation of the alginates. This would reveal any specific chemical differences between these two apparently similar alginates. Thus the aims of this study are:

1. Examine the effect of molecular weight modified Manucol LD and Manucol DH on iron-mediated ferritin expression.

2. Determine the effect of G-enrichment (epimerisation) of Manucol LD on iron-mediated ferritin expression.

3. Determine the specific GM sequence of Manucol LD and Manucol DH using high resolution NMR.

Not only will these details provide an understanding of the chemical 'make-up' that endows Manucol LD with its bio-activity, but they will also infer the chemical requirements of

alginates to be 'super iron-binders' and thus provide the blue-prints for next generation alginate chelators.

4.2   Results and discussion

4.2.1   Alginate molecular weight effects on iron chelation

Manucol DH is similar to Manucol LD in terms of M:G ratios (cf. 60:40 vs. 62:38) yet is a larger polymer (cf. 180 vs 145 kDa). Degradation of Manucol DH would provide an alginate with a similar molecular weight to Manucol LD and the same G:M ratio. Heat degradation of alginates provides an easy route to creating shorter polymer length products allowing some control over size prediction by analysing molecular weight changes using viscosity.

Molecular weight is related to viscosity through two empirically determined constants, α (which depends on the polymer-solvent pair and temperature) and K (which describe the size, shape and rigidity of polymers) (figure 4.2).

$$[\boldsymbol{\eta}] = \boldsymbol{KMw^{\alpha}}$$

Figure 4.2: Mathematical relationship between intrinsic viscosity ($[\eta]$) and molecular weight (Mw) which are dependent on the constants K and α.

The intrinsic viscosity $[\eta]$, can be obtained from a series of viscosity parameters, namely the reduced (η_{red}), specific (η_{sp}) and inherent (η_{inh}) viscosities which, when extrapolated to infinite dilution using the Huggins and Kraemer approaches, the intrinsic viscosity is taken as the mean of intercepts from equations (IV) and (V) (figure 4.5).

4.2.1.1 D-glucuronic acid effects on ferritin expression

Prior to any controlled degradation of Manucol DH or Manucol LD, a control experiment was performed to determine the effects of degradation of alginate to its infinite point. Such an experiment would certify if the templating and coordinating effect imposed by the <u>polymeric</u> nature of the alginate is responsible for its iron chelation ability. The monomeric acid building blocks, namely D-glucuronic acid (DGA), was utilised for iron chelation studies. As such, RKO cells were co-cultured with iron ($FeSO_4 \cdot 7H_2O$, 100 µM) with or without DGA (0.1, 0.3 % (w/v)) and analysed for iron concentration using both ferritin expression (as a surrogate biomarker for intracellular iron concentrations) and the ferrozine reporter to reveal direct intracellular iron concentrations (method 4.5.1) (figure 4.3).
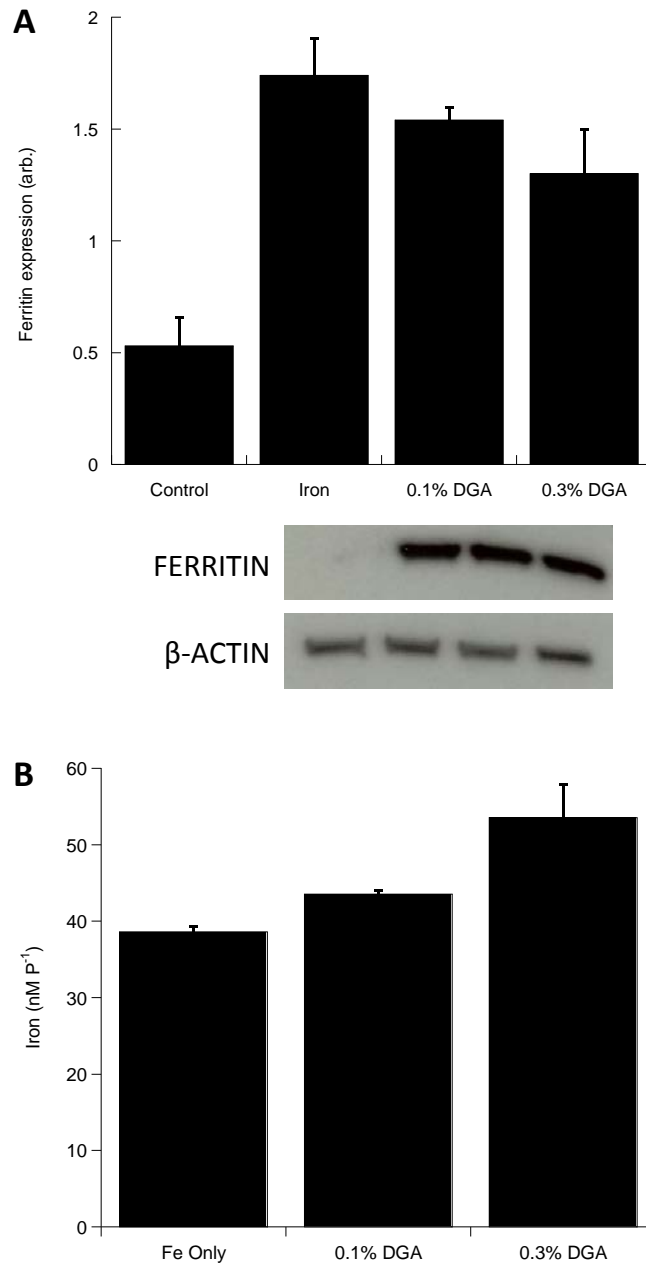
Figure 4.3: (A) Ferritin expression in RKO cells incubated with iron challenged with or without DGA (0.1, 0.3 % (w/v)). Data points represent mean fold change in protein expression, normalised to β-actin, relative to control. Error bars denote ± SEM. (B) Ferrozine reporter assay demonstrating intracellular iron concentrations of RKO cells challenged with or without DGA (0.1, 0.3 % (w/v)). Error bars denote ± SEM.

There was no significant ferritin repression or decrease in intracellular iron concentrations when cells were cultured with iron with DGA. This result demonstrates that the carboxylic

acid iron binding unit from alginate alone is not sufficient to chelate iron and display bioactivity. This was also verified by utilising radioactive iron-59, whereby the same culturing conditions were employed but spiking with ^{59}Fe allowed for a sensitive detection of any intracellular iron concentration differences (figure 4.4).
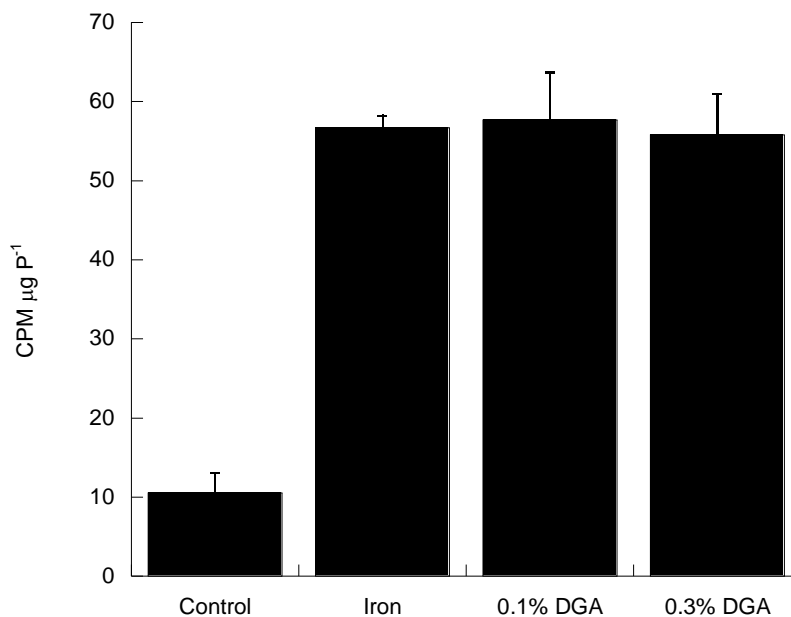
Figure 4.4: Iron concentrations of RKO cells when incubated with iron and challenged with or without DGA (0.1, 0.3 % (w/v)). Error bars denote ± SEM.

As expected, no differences in intracellular iron concentrations were observed. These results considered together are unsurprising since it has been demonstrated that alginates are templating nanoparticle formation and this modulation is likely to control the observed physiological effects.

4.2.1.2 Heat degradation of Manucol DH and Manucol LD

A method of characterising alginate degradation products (ADPs) and to determine their molecular weights would be to use viscosity measurements. Since physical molecular weight measurements of the alginate series are available, calibration of these molecular weights against their viscosity would allow facile characterisation of ADPs. Viscosity is related to molecular weight through various proportionality constants. The relative viscosity (η_r) describes the ratio of viscosities sample:solvent. From this, the specific (η_{sp}) the reduced (η_{red}) and the inherent (η_{inh}) viscosities can be obtained (figure 4.5).

$$\text{I} \qquad \eta_{sp} = \frac{\eta - \eta_o}{\eta_o} = \eta_r - 1$$

$$\text{II} \qquad \eta_{red} = (\eta_r - 1)/c$$

$$\text{III} \qquad \eta_{inh} = ln\,\eta_r\,/c$$

$$\text{IV} \qquad \frac{\eta_{sp}}{c} = [\eta](1 + K_H\,[\eta]\,c)$$

$$\text{V} \qquad \frac{ln\,\eta_r}{c} = [\eta](1 - K_K\,[\eta]\,c)$$

$$\text{VI} \qquad [\eta] = \lim_{c \to 0} \frac{\eta_{sp}}{c} = \lim_{c \to 0} \frac{\eta_r - 1}{c}$$

Figure 4.5: Mathematical relationships between the specific viscosity (I), reduced viscosity (II) and inherent viscosity (III) and the Huggins and Kraemer approximations (IV and V). Extrapolation to zero-concentration allows the intrinsic viscosity to be approximated (VI).

As the concentration dependence of the reduced viscosity and the inherent viscosity approaches zero, intrinsic viscosity can be obtained. This is formally known as the Huggins and Kraemer approximations.

Another approximation of the intrinsic viscosity can be used, namely the Solomon & Ciuta approximation (figure 4.6).[2]

$$[\eta] \sim \left(\frac{1}{c}\right)\sqrt{2\eta_{sp} - \ln(\eta_{rel})}$$

Figure 4.6: The Solomon & Ciuta approximation of intrinsic viscosity.

With this, the intrinsic viscosities for lower molecular weight alginates (Manugel GHB,

Manucol DH, Manucol LD and LFR5/60) were obtained (figure 4.7)
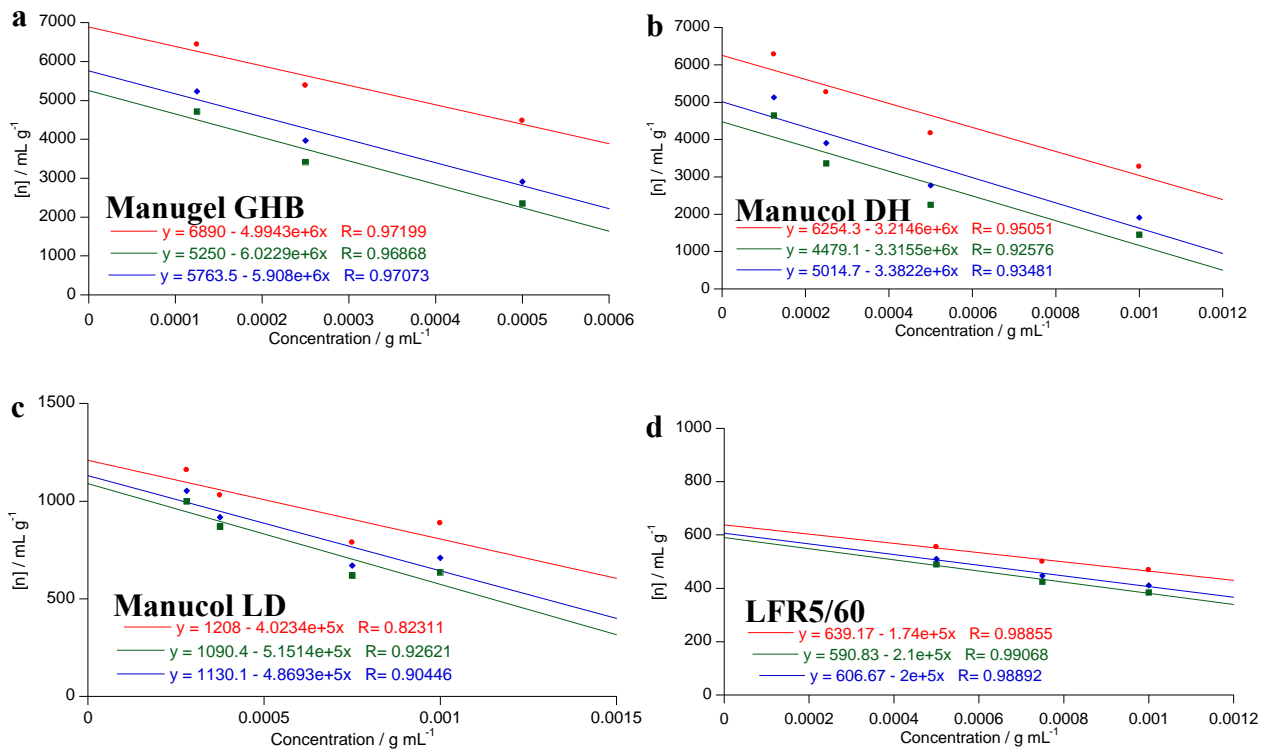
Figure 4.7: Intrinsic viscosity plot for (a) Manugel GHB, (b) Manucol DH, (c) Manucol LD and (d) LFR5/60 in DI H_2O at different concentrations, using Huggins (red), Kraemer (green) and Solomon-Ciuta (blue) extrapolations.

The calculated mean $[\eta]$ values were plotted against the molecular weight values obtained

earlier (section 4.1) to generate a calibration reference (figure 4.8).
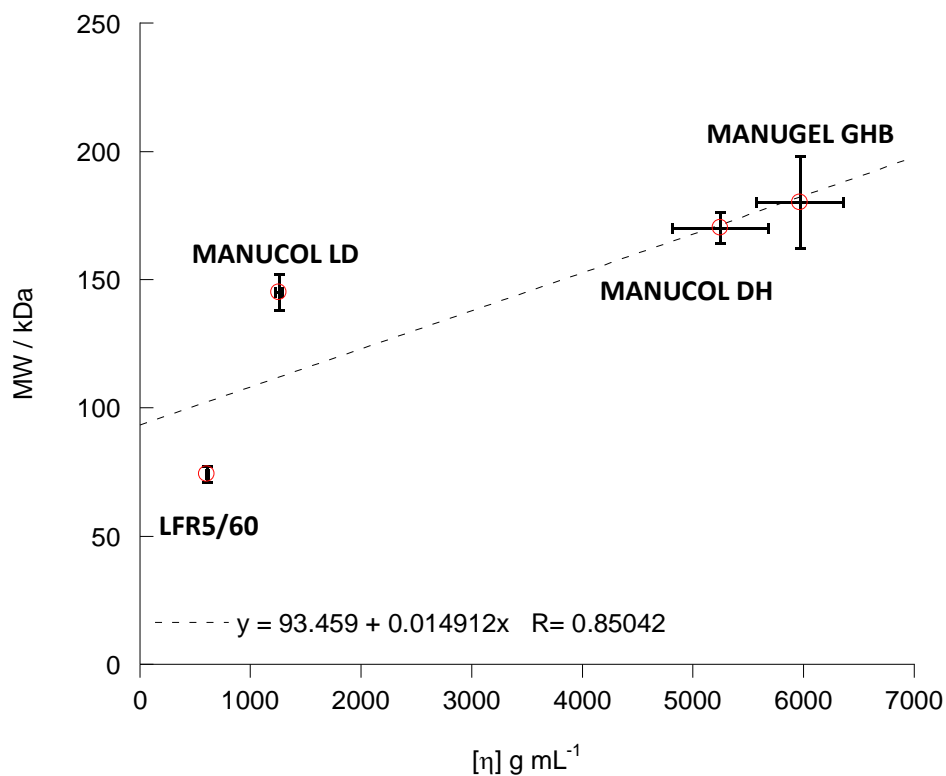
Figure 4.8: Plot of apparent molecular weight as obtained by AUC against intrinsic viscosity. Error bars represent ± SEM on each axis.

It is evident that as molecular weight decreases, intrinsic viscosity decreases which is predictable since the smaller the compounds, the faster the flow rate. The calibration line MW = 0.015 x [η] + 93.5 can be used to determine the molecular weights of the ADPs obtained through heating.

4.2.2   Heat degradation of Manucol DH

Manucol DH was subject to hydrolysis by heating. Manucol DH was heated at 100 ^{0}C for 5, 12, 20, 30, 60, 90, 120 and 180 mins which degraded the alginate to shorter molecular weight components with a progressive decrease in relative viscosities (method 4.5.2) (figure 4.10 A).

The subsequent ADPs were subjected to the Huggins and Kraemer approximations to determine the dependence on intrinsic viscosity decrease with heating time (figure 4.9).
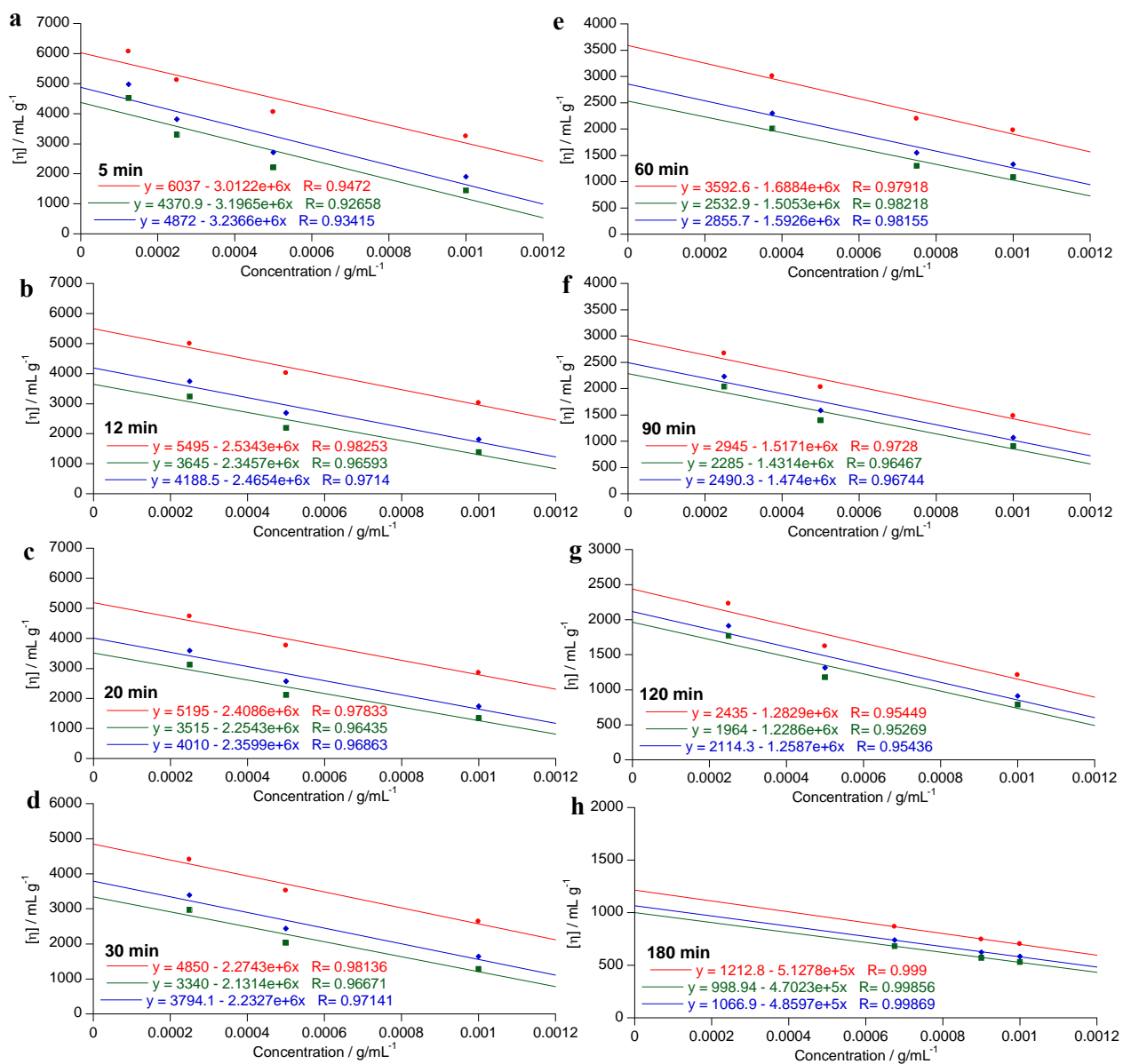
Figure 4.9: Intrinsic viscosity plot for (a) 5 min, (b) 12 min, (c) 20 min, (d) 30 min, (e) 60 min, (f) 90 min, (g) 120 min and (h) 180 min heating times at a temperature of 100 °C in DI H_2O at different concentrations using Huggins (red), Kraemer (green) and Solomon-Ciuta (blue) extrapolations.

The relative viscosity decreases as expected with longer heating times, and the mean values

for intrinsic viscosity obtained can be calibrated against heating time (figure 4.10 B).
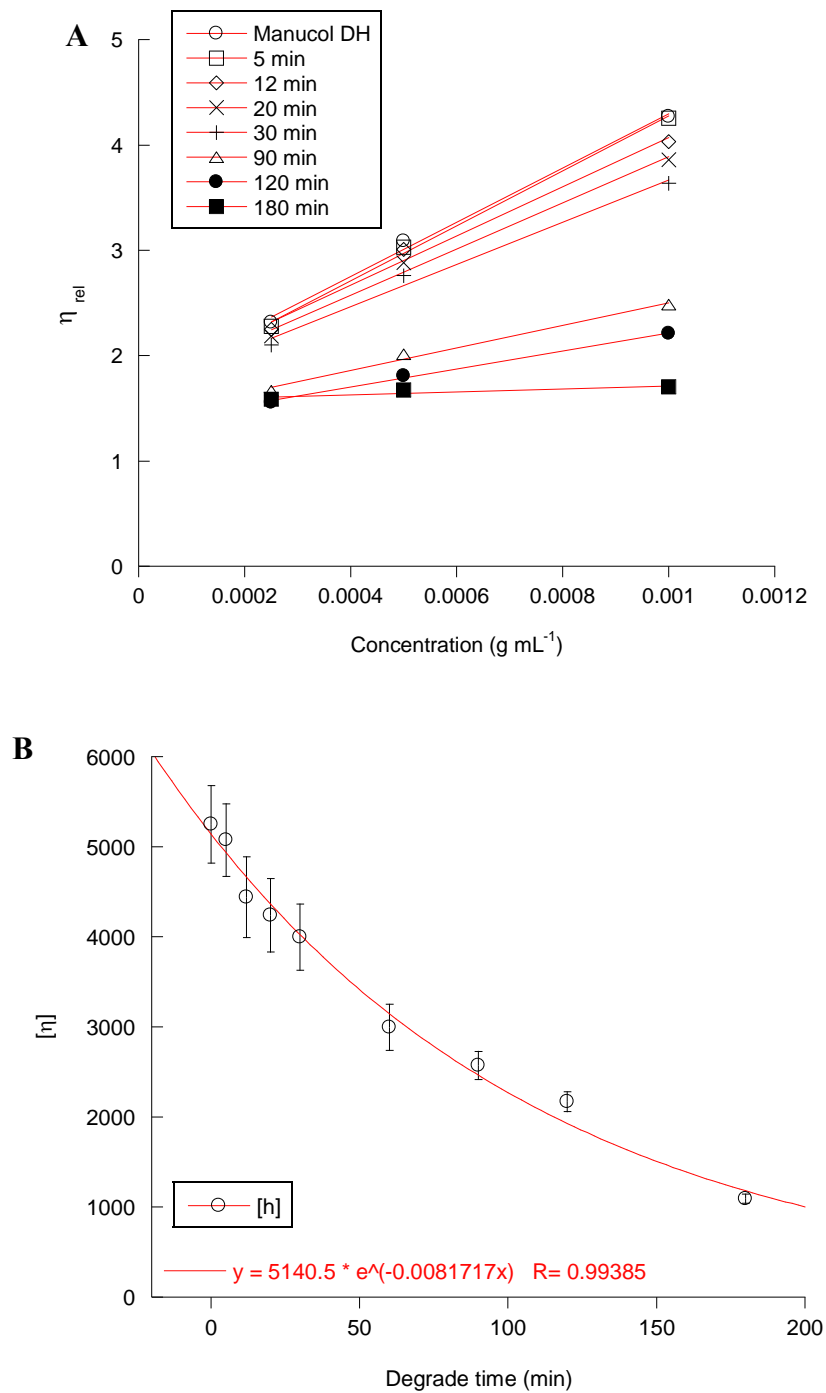
Figure 4.10: (A) Manucol DH ADP decreases with heating time at 100 °C. (B) Plot of intrinsic viscosity against heating time. Error bars denote ± SEM. Red lines represent lines of best fit.

These experiments allow the calculation of the heating time of Manucol DH that would yield a Manucol DH ADP that was similar in molecular weight to Manucol LD. According to the calibration of intrinsic viscosity change against degrade heating time, heating Manucol DH for 172 min would provide an intrinsic viscosity value of 1200 mL g^{-1}, which would give a molecular weight similar to that of Manucol LD at 145 kDa.

To examine the molecular weight distribution spread across the Manucol DH ADPs, size exclusion chromatography using Sephadex G25 was employed (method 4.5.3). Monitoring of the reduced ends of alginate hydrolysis that absorb at $\lambda = 232$ nm would provide some insight into the distribution of ADP products generated through heating. Specifically, whether single distinct degradation products are formed, or a spread of molecular weight entities (figure 4.11).
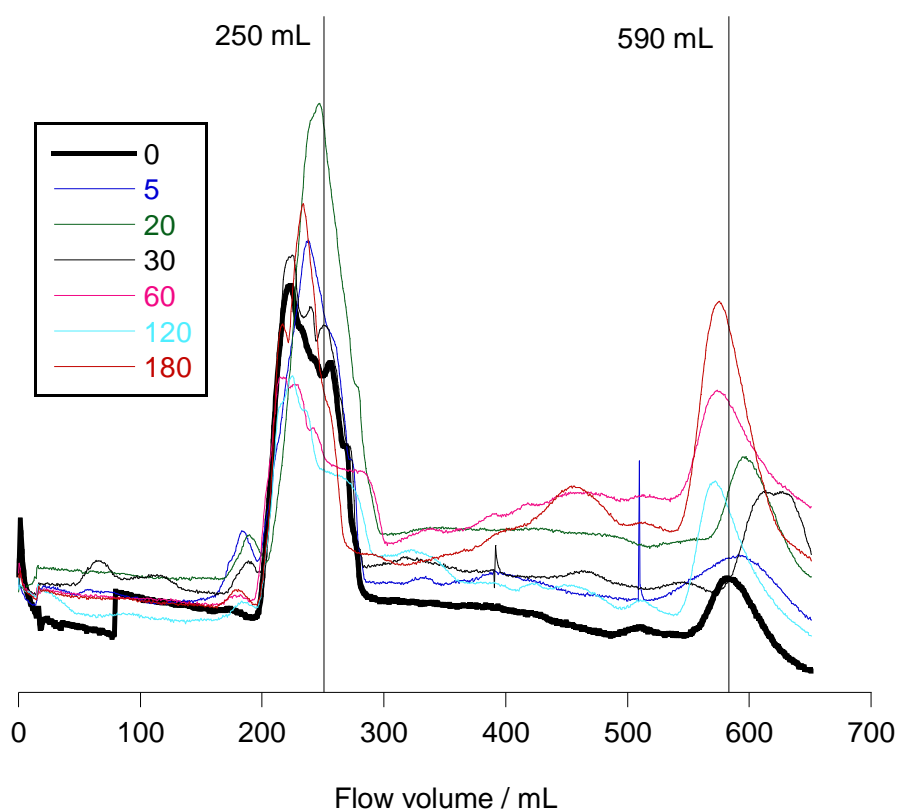
Figure 4.11: Gel chromatography chromatogram of Manucol DH ADPs ran on Sephadex G25 column with an aqueous NaCl (0.2 M) eluent.

It is apparent in comparison to the control that has a high large molecular weight component (at ca. 250 mL) and the smallest small molecular weight component (at ca. 590 mL) that there are no components between these molecular weights. Since a unimodal distribution for Manucol DH was observed in the analytical ultracentrifugation studies, this smaller molecular component can be regarded as insignificant. It can be seen that heating Manucol DH does not only increase the number density of this smaller molecular weight component, but there is also a trend to increase the number and distribution range of degrade products between these two distinctive entities (ca. 300 – 550 mL). There is a distinctive peak (ca. 475 mL) for several degrade mixtures, which is most prominent for the 180 min degrade, a similar heating time which would produce a Manucol LD-like ADPs.

4.2.2.1 *In vitro* iron chelation by heat degraded Manucol DH

Manucol DH (2% (w/v)) was heated at 100 ^{0}C for 20, 40, 60, 80, 160, 180 and 250 mins with estimated intrinsic viscosity values of 4365, 3707, 3148, 2673, 1390, 1181, 666 mL g^{-1} and, as such, molecular weights could be calculated as 164, 160, 156, 153, 145, 144 and 141 kDa respectively for the ADPs using the calibration equation determined between these two alginates (figure 4.12).

The chart shows a calibration plot of MW / kDa (y-axis, 0 to 250) versus [η] g mL^{-1} (x-axis, 0 to 7000) with two data points and a fitted line: y = 137.11 + 0.0062641x   R= 1
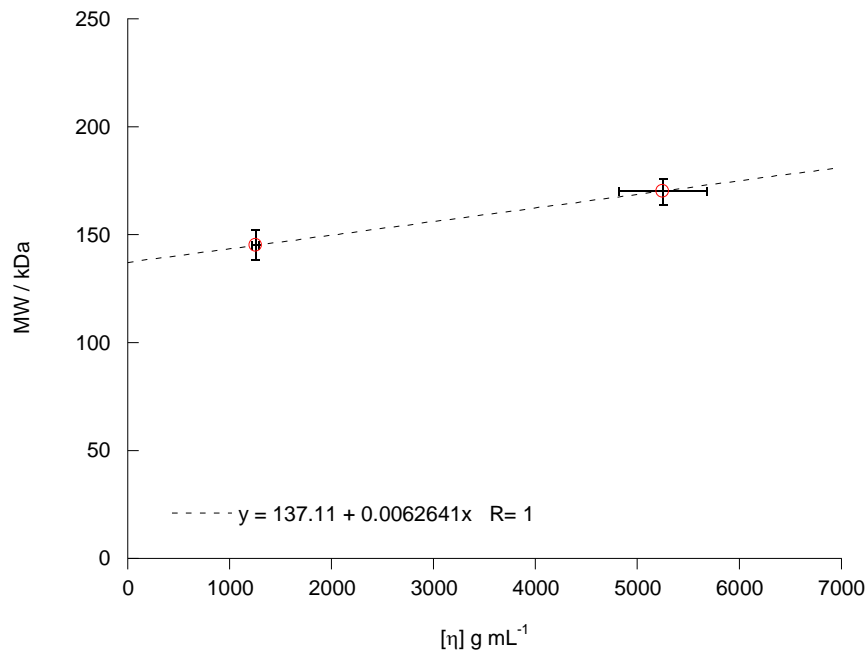
Figure 4.12: Line of calibration between Manucol DH and Manucol LD for the determination of ADP molecular weight. Error bars represent ± SEM.

The resultant ADPs were subsequently utilised in cell culture, whereby RKO cells were challenged with iron, with or without the Manucol DH ADPs (0.3 % (w/v)) for 24 hours before protein extraction and estimation of ferritin expression by western blotting (figure 4.13).
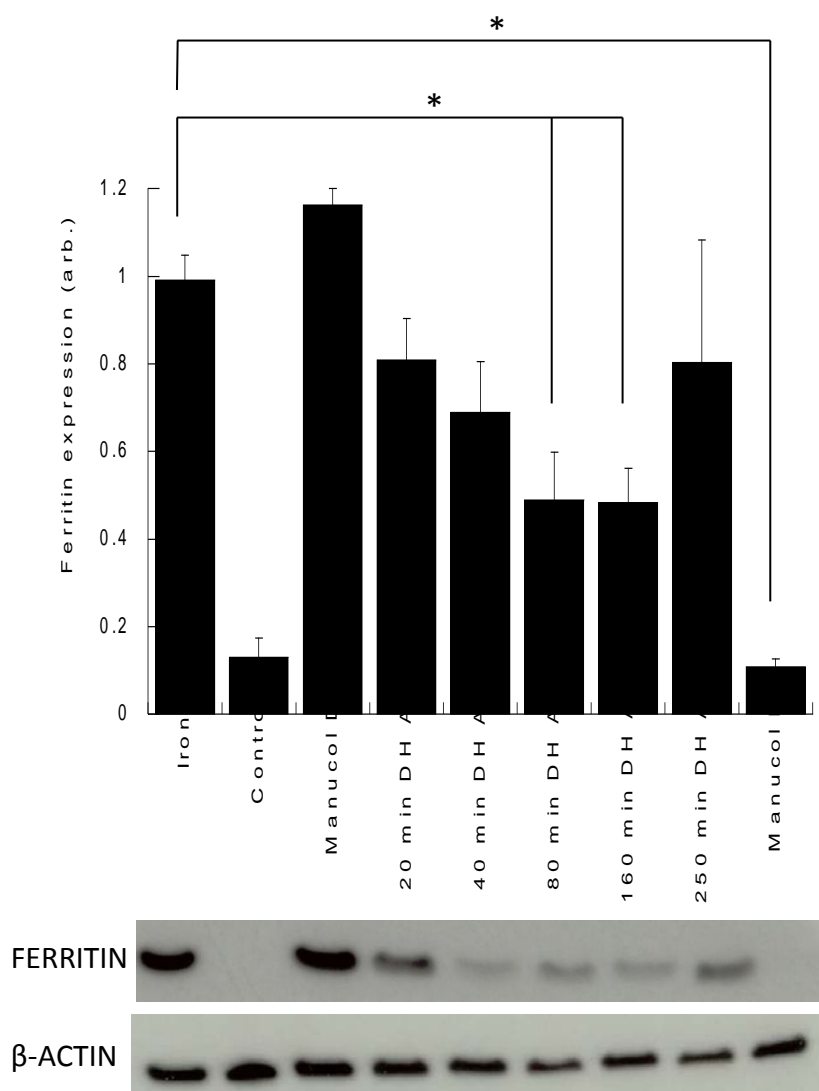
Figure 4.13: Ferritin expression in RKO cells incubated with iron, challenged with or without Manucol DH ADPs (0.3 % (w/v)). Data points represent mean fold change in protein expression, normalised to β-actin, relative to control. Error bars denote ± SEM, * denotes statistical significance, p < 0.05, n = 3.

Co-culturing RKO cells with native Manucol DH does not demonstrate any iron chelation effects as described previously. Heat degradation of Manucol DH for 20 and 40 mins and subsequent co-culture of these ADPs on RKO cells also reveals no iron binding ability. However, heat degradation for 80 and 160 min statistically reduced iron-mediated ferritin expression by ca. 50% (p < 0.05), but not to the extent of Manucol LD. Heating between 80

and 160 min degraded Manucol DH to a molecular weight approximately of Manucol LD and bioactivity (i.e. a diminishment in iron-mediated ferritin expression) was observed. However, further degradation (250 min) resulted in a loss of this bioactivity, yet with huge experimental error. Longer heating times of Manucol DH would not yield shorter ADPs due to the almost linear relationship ($x = $ o) of the line of best fit between [η] and degrade time at these longer time points. To determine whether molecular weight ADPs that are smaller in molecular weight than Manucol LD, Manucol LD itself was used for heat degradation studies.

4.2.3   Heat degradation of Manucol LD

Manucol LD was heated at 100 ^{0}C for 5, 20, 30, 60, 120 and 180 mins which degraded the alginate to shorter molecular weight components with a progressive decrease in relative viscosities (figure 4.15 A). The subsequent ADPs were subject to the Huggins and Kraemer approximations to determine the dependence on intrinsic viscosity decrease with heating time (figure 4.14).
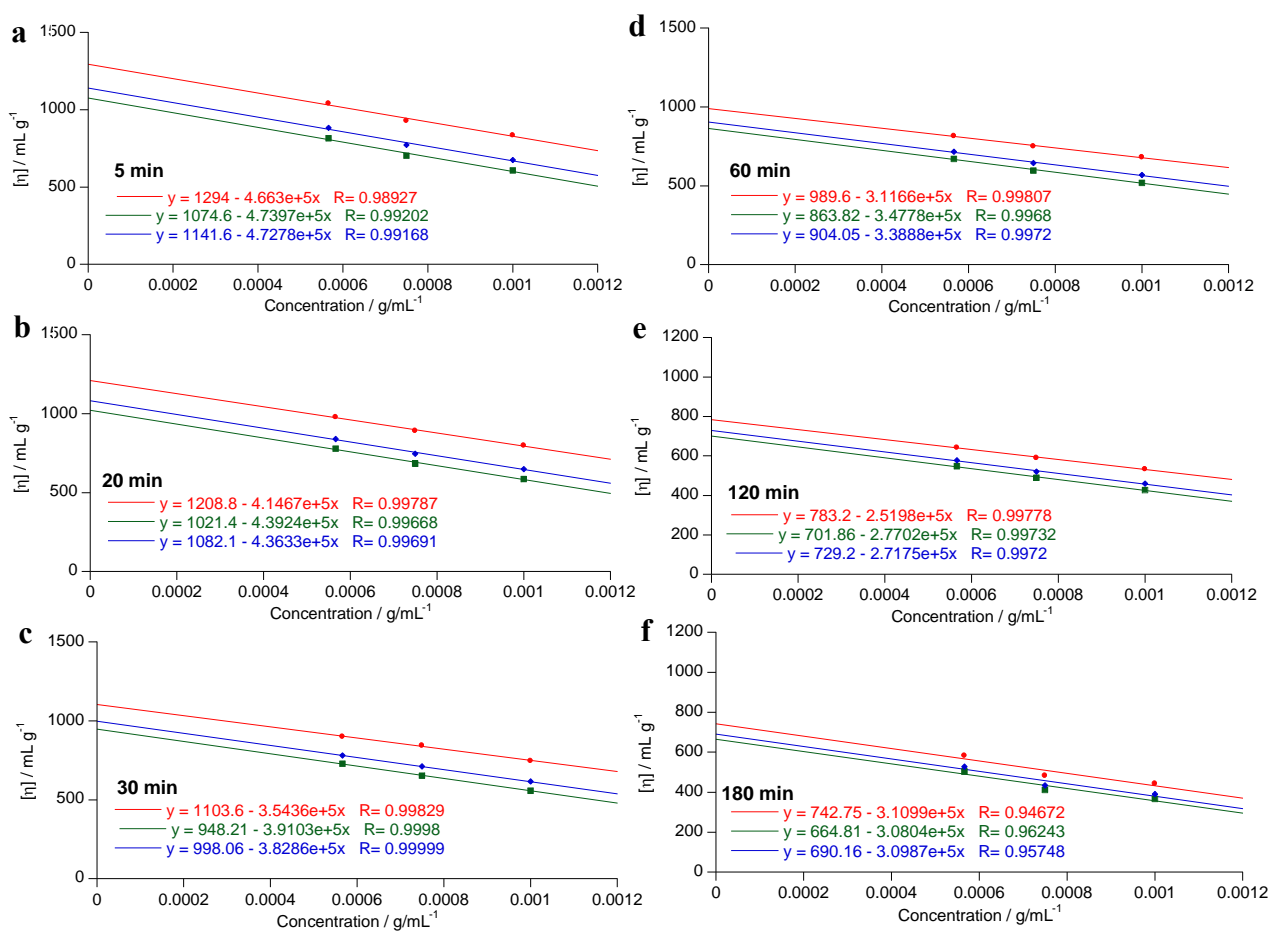
Figure 4.14: Intrinsic viscosity plot for (a) 5 min, (b) 20 min, (c) 30 min, (d) 60 min, (e) 120 min and (f) 180 min heating times at a temperature of 100 °C in DI H_2O, using Huggins (red), Kraemer (green) and Solomon-Ciuta (blue) extrapolations.

As expected, relative viscosity decreases with longer heating times, and the mean values for intrinsic viscosity obtained can be calibrated against heating time (figure 4.15 B).
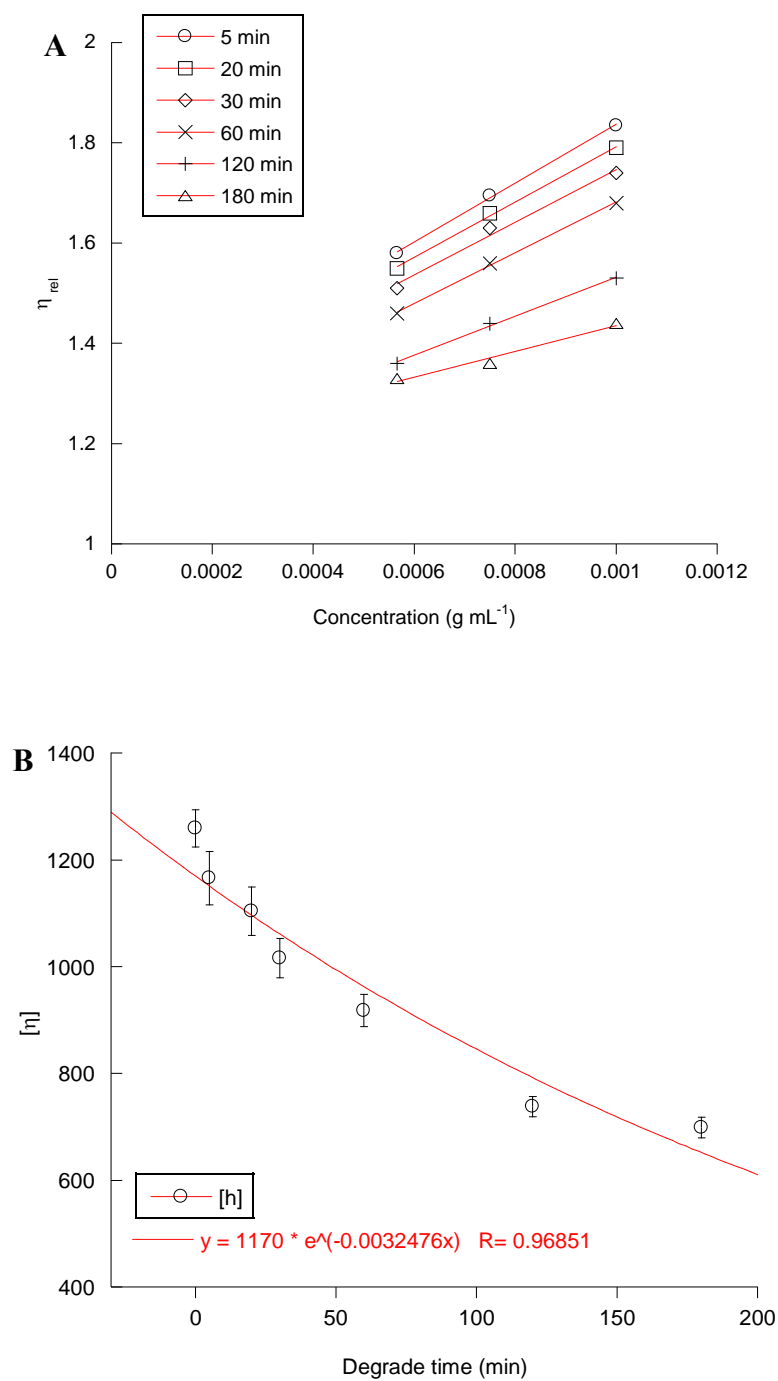
Figure 4.15: (A) Manucol LD ADPs relative viscosity changes with heating time at 100 °C. (B) Plot of intrinsic viscosity against heating time. Error bars denote ± SEM. Red lines represent lines of best fit.

Depolymerisation decreases with time as described previously. Calibration between heating time and change in $[\eta]$ allows approximate molecular weight values for ADPs to be calculated.

4.2.3.1 *In vitro* iron chelation by heat degraded Manucol LD

Manucol LD was heated at 100 ^{0}C for 20, 40, 60, 80, 160, 180, 250 mins with estimated intrinsic viscosity values of 1096, 1027, 962, 902, 695, 652 and 519 mL g^{-1} respectively and as such, molecular weights could be calculated as 109, 108, 107, 106, 103, 102 and 100 kDa respectively for the ADPs.

The resultant ADPs were subsequently utilised in cell culture, whereby RKO cells were challenged with iron, with or without the Manucol LD ADPs (0.3 % (w/v)) for 24 hours before protein extraction and estimation of ferritin expression by western blotting (figure 4.16).
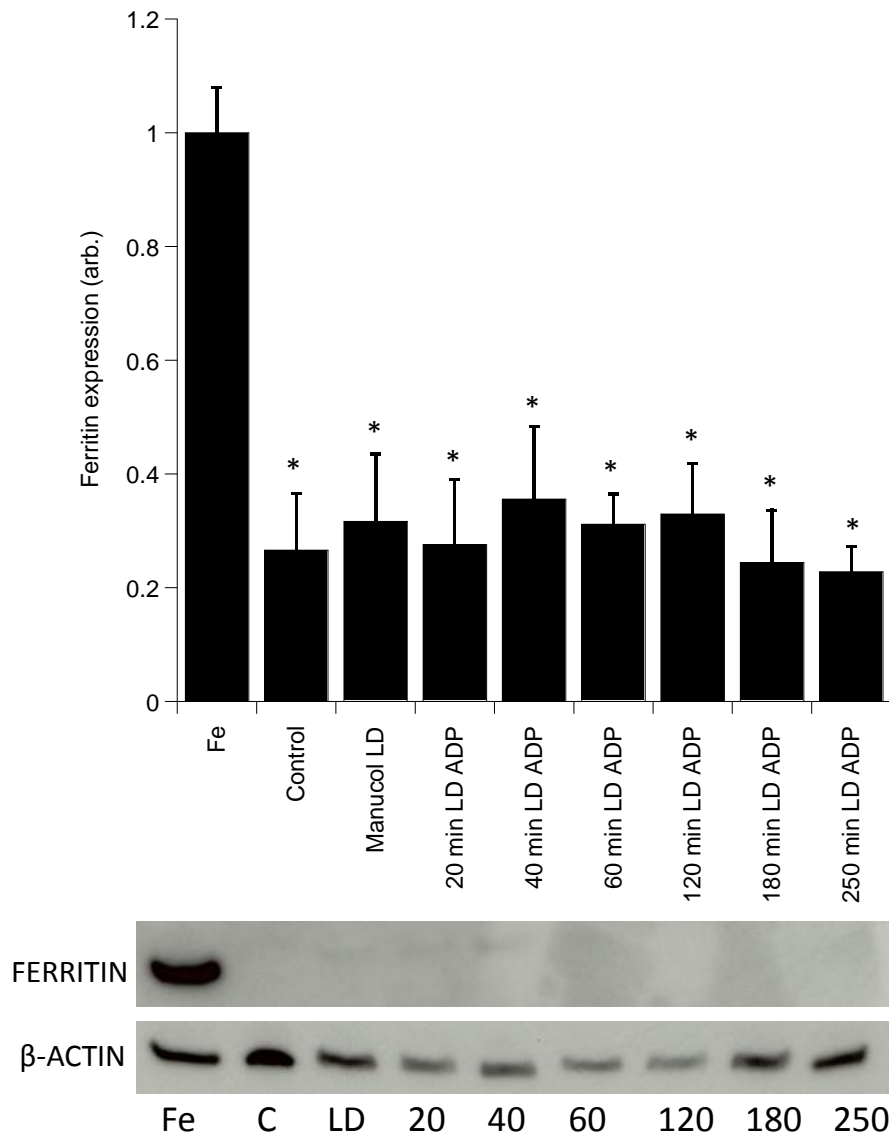
Figure 4.16: Ferritin expression in RKO cells incubated with iron challenged with or without Manucol LD ADPs (represented as heating times in mins). n = 3. * denotes statistical significance, $p < 0.05$.

It is apparent that there were no ferritin expression changes between native Manucol LD incubation and the ADPs. These results would suggest that either the molecular weight dependence on iron binding (at lower molecular weight values of Manucol LD) is not important, or that the molecular weight of these specific ADPs are still within in the range for bioactivity. The molecular weight change from native Manucol LD (cf. 145 kDa) to 109, the

20 min ADP is big, and any differences in iron chelating ability would likely be observed in this hydrolysis process. The subsequent ADP molecular weights (cf. 108-100) have a very little distribution of change in molecular weights and as such, it is unsurprising that no differences in bioactivity are observed. Iron binding activity may not only be dictated by molecular weight but also G:M ratio composition.

4.3.4   Production and validation of epimerase enzyme AlgE1

Ertesvåg *et al.* previously described the cloning, expression and production of eight alginate epimerases from 8 different epimerase genes from *Azotobacter vinelandii*.[3, 4] Specifically, the algE1 gene was cloned into pTrc99A plasmids for the expression of AlgE1 in *E.coli* cells (method 4.5.4). DNA sequencing of the gene insert was conducted to confirm the presence of the algE1 gene inserts within the recombinant plasmids (method 4.5.5). BL21 *E.coli* cultures were transformed with algE1 and subsequently induced to produce the AlgE1 enzyme (method 4.5.6). The expressed and harvested AlgE1 enzyme was purified using ionic-gradient gel-chromatography according to the protocol by Ertesvåg (method 4.5.7) (figure 4.17).[5]
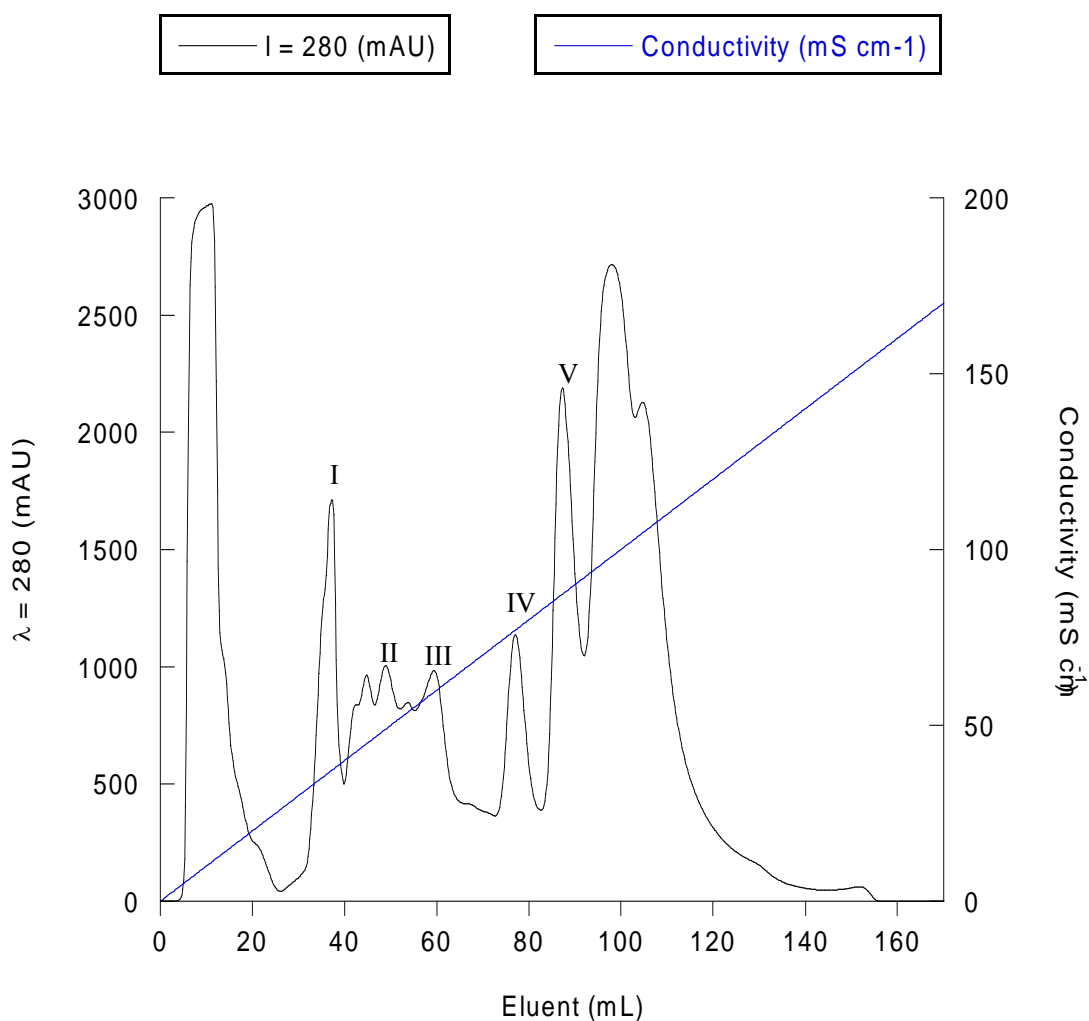
Figure 4.17: Purification chromatogram of AlgE1 epimerase from BL21 *E.coli* expressing bacteria using a gradient NaCl eluent (0-1 M). $\lambda_{abs} = 280$ nm.

A range of well-defined peaks were denoted fractions I – V. Since circular dichroism was previously utilised successfully in the determination of G-content for the alginate series (section 2.2.3.1), it was subsequently employed here to screen purified AlgE1 fractions for epimerisation activity. Manucol LD (0.1% (w/v)) was subject to enzymatic action from fractions I through to V and subsequent Manucol LD G-unit content was examined by CD absorbance at $\lambda = 230$ (method 4.5.8) (figure 4.18).
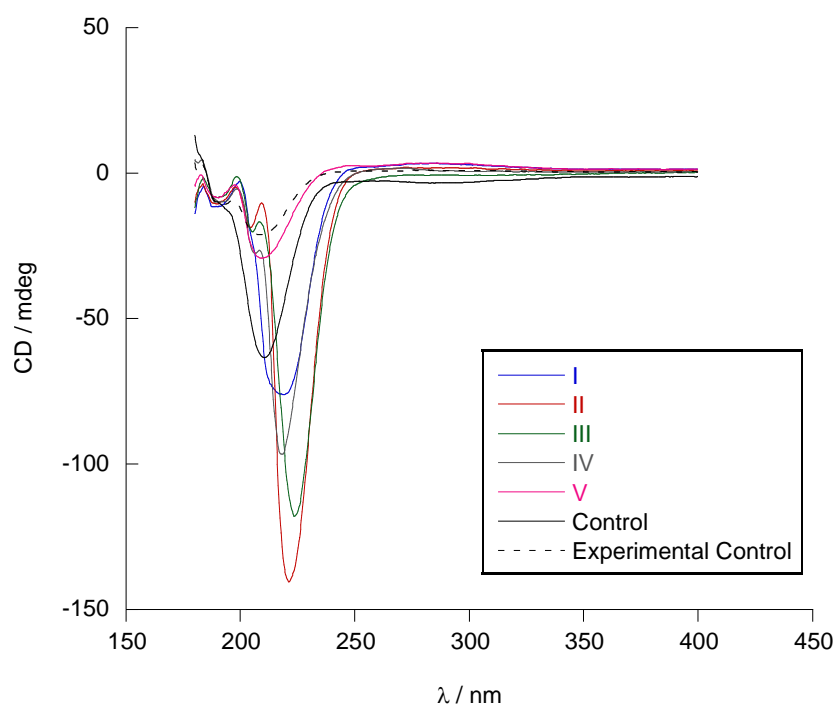
Figure 4.18: CD spectra of Manucol LD and Manucol LD exposed to the epimerase activity of protein fractions collected I to V. An experimental control was run to ensure alginate structure was not influenced by the experimental conditions employed and compared to an alginate-only control.

Epimerase fractions II and III were observed to have the most epimerase activity, with conversions estimated of 90 % and 92 % respectively. These enzymatic fractions were utilised for the epimerisation of Manucol LD in subsequent studies.

4.2.4.1 Epimerisation of Manucol LD

With a view to utilising epimerised Manucol LD (**EpLD**) in subsequent cellular studies, optimisation of the epimerisation protocol was undertaken, and a successful yet somewhat convoluted process of epimerisation was found (method 4.5.9). Briefly, co-culturing alginates with cells requires the use of a high concentration (2% (w/v)) alginate stock,

however it was identified that enzymatic action ceased at these high alginate concentrations. As such, lower concentrations and higher volumes were used with subsequent purification and concentration *in vacuo*. This method yielded a solid **EpLD** which was fortuitous since normalisation on concentration was possible and the extent of modification could be accurately calculated (figure 4.19).
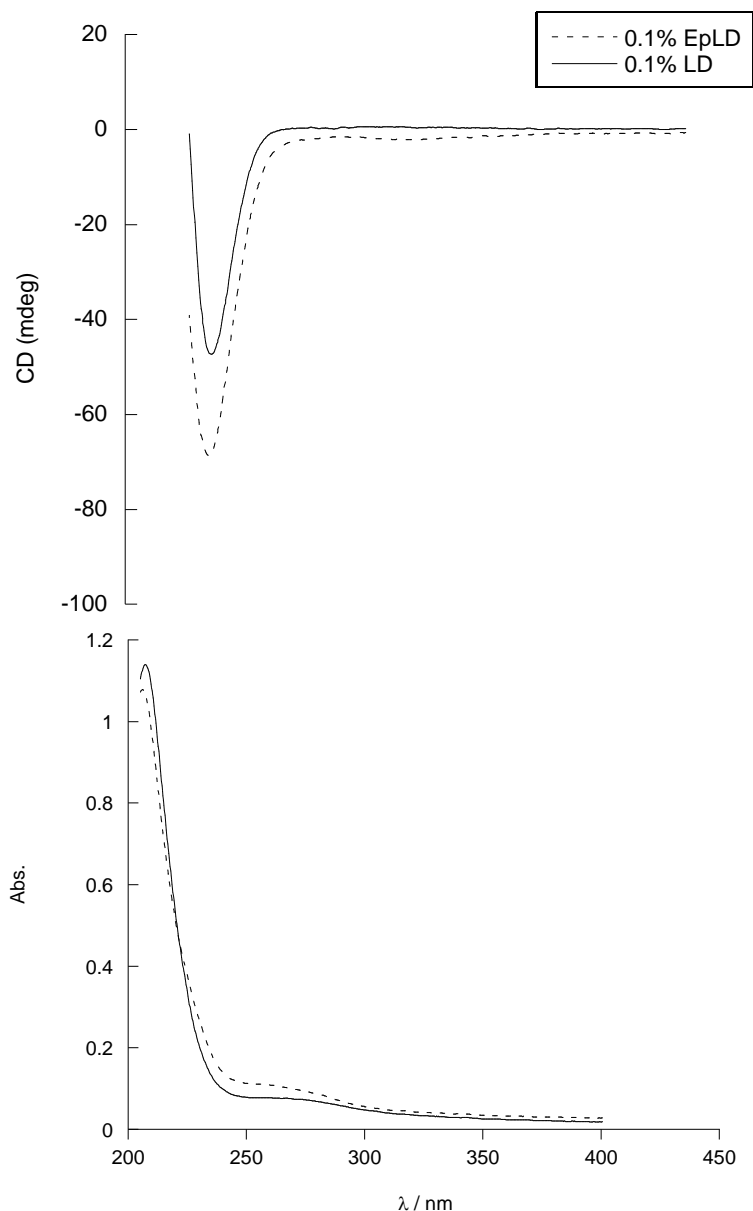
Figure 4.19: Circular dichroism spectra and representative UV-Visible spectra of Manucol LD and **EpLD** (0.1% (w/v)) in DI H_2O.

Treatment of Manucol LD with AlgE1 resulted in a 60 % conversion of the mannuronate units to guluronate units on **EpLD**, resulting in a new M:G ratio of 23:77; the highest G-unit concentration alginate out of the series. There was also very little absorption present at $\lambda =$ 280 nm on the UV-Vis indicating little AlgE1 contaminant.

EpLD was used in cell culture to assess iron chelation ability in comparison to native Manucol LD. With this, RKO cells were challenged with an iron-enriched media (100 μM $FeSO_4 \cdot 7H_2O$ + 500 μM sodium ascorbate) with or without sodium alginates Manucol LD or **EpLD** (0.3 % (w/v)) and after a 24 hour period, the cells were washed and lysed for protein extraction. Western blotting revealed that ferritin expression in RKO cells treated with iron was higher than that of control media only, as expected. Manucol LD diminished ferritin expression by 57 % compared to iron only control (cf. 60 % in previous studies). **EpLD** did not chelate iron *in vitro*, and ferritin expression was equal to levels of the iron only control. This demonstrates the dependence of M:G ratio and/or MG sequence of the alginate in its iron binding capabilities (figure 4.20).
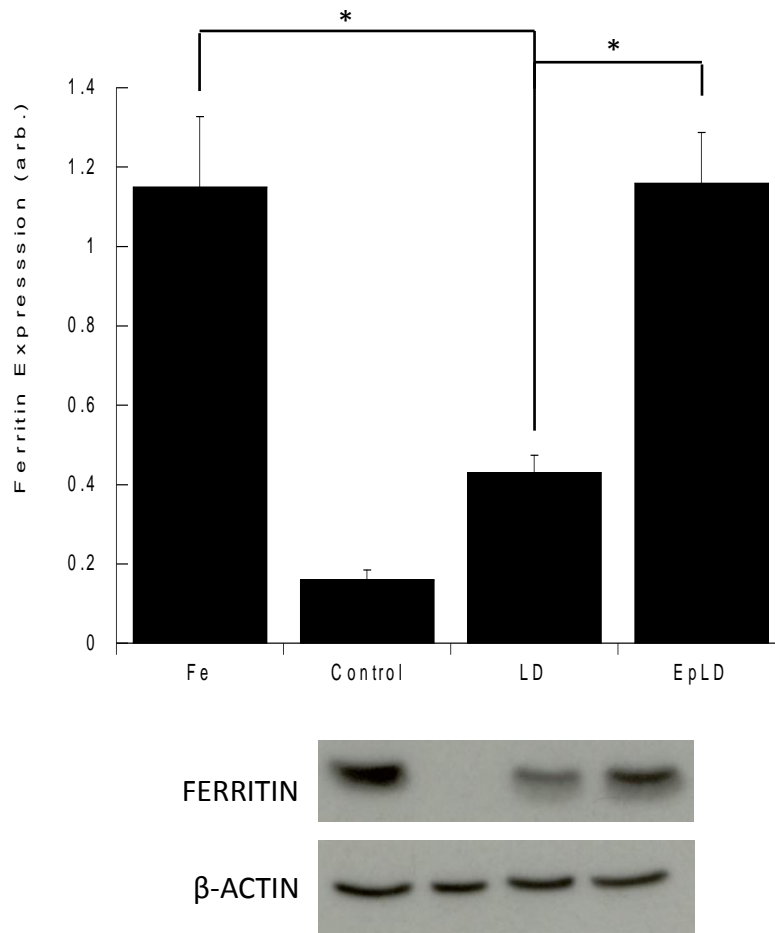
Figure 4.20: Ferritin expression in RKO cells incubated with iron, challenged with or without Manucol LD and **EpLD** (0.3 % (w/v)). Data points represent mean fold change in protein expression, normalised to β-actin, relative to control. Error bars denote ± SEM, * denotes statistical significance, $p < 0.05$, n = 3.

4.2.4.2 High resolution NMR of Manucol DH and Manucol LD

It has been demonstrated that there is a reliance on specific M:G composition for iron binding capability, as verified by epimerising Manucol LD to which a loss in activity is observed. It has also been detailed that there is some trend to increase Manucol DH bioactivity upon lysis. This leads to the understanding that alginate MG sequence has the most influence on iron binding potential, and the gold-standard to test this would be to manipulate Manucol DH in such a way that it had exact sequence homology to Manucol LD; this is indeed an ambitious

task in *de novo* alginate synthesis. Another way to approach this would be to demonstrate that even though Manucol LD and Manucol DH have similar M:G compositions, they have dissimilar sequence homology. Sequencing alginate strands, monomer by monomer, is impossible. However, with the use of high resolution NMR it is possible establish the monad, diad and triad fractions of alginates (method 4.5.10) (figure 4.21). Such data would allude to measureable differences in Manucol LD and Manucol DH MG sequence.
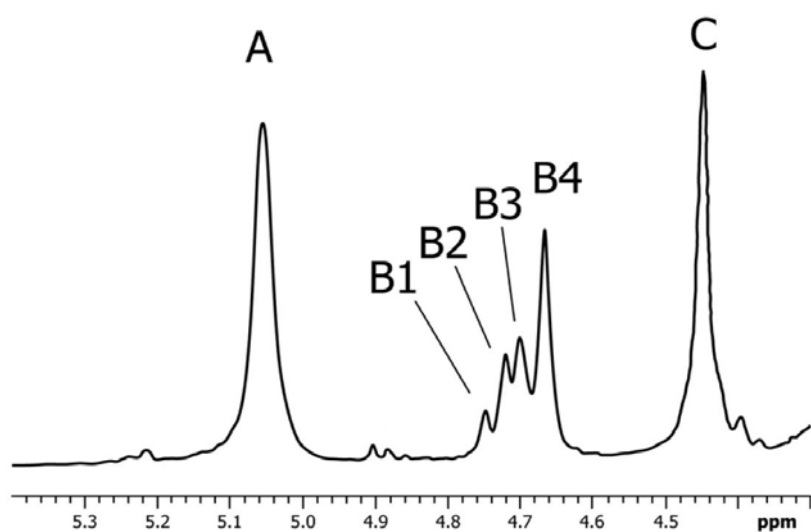
Monad, diad or triad	Relation to frequencies	Fraction of sequence
G	**0.5(A+C+0.5($B1$+$B2$+$B3$))**	$F_G = G/(M+G)$
M	**$B4$+0.5($B1$+$B2$+$B3$)**	$F_M = M/(M+G)$
GG	0.5(A+C−0.5($B1$+$B2$+$B3$))	$F_{GG} = GG/(M+G)$
MG = GM	0.5(B1+B2+B3)	$F_{GM} = F_{MG} = MG/(M+G)$
MM	B4	$F_{MM} = MM/(M+G)$
GGM = MGG	(B1)0.5(B1+B2+B3)/(B1+B2)	$F_{GGM} = F_{MGG} = GGM/(M+G)$
MGM	(B2)0.5(B1 +B2 + B3)/(B1 + B2)	$F_{MGM} = MGM/(M+G)$
GGG	GG – GGM	$F_{GGG} = GGG/(M+G)$

Figure 4.21: Typical NMR spectra of alginate with labelled resonances A, B1, B2, B3, B4 and C denoting specific hydrogen environments for the calculation of alginate monad, diad and triad frequencies.[6]

NMR spectra for Manucol LD and Manucol DH were acquired and analysed using the correlations described and transformed free-induction decays were fitted to lorentzian curves to allow calculation of the specific monads, diads and triads (figure 4.22)

Figure 4.22: Plots of the experimental (red) and simulated (blue) NMR spectra of alginate (A) Manucol DH and (B) Manucol LD for the region of protons 1 and 5 of mannuronic acid and glucuronic acid. The monomer type leading to this chemical shift is underlined whereas the proton position is shown as the index number.
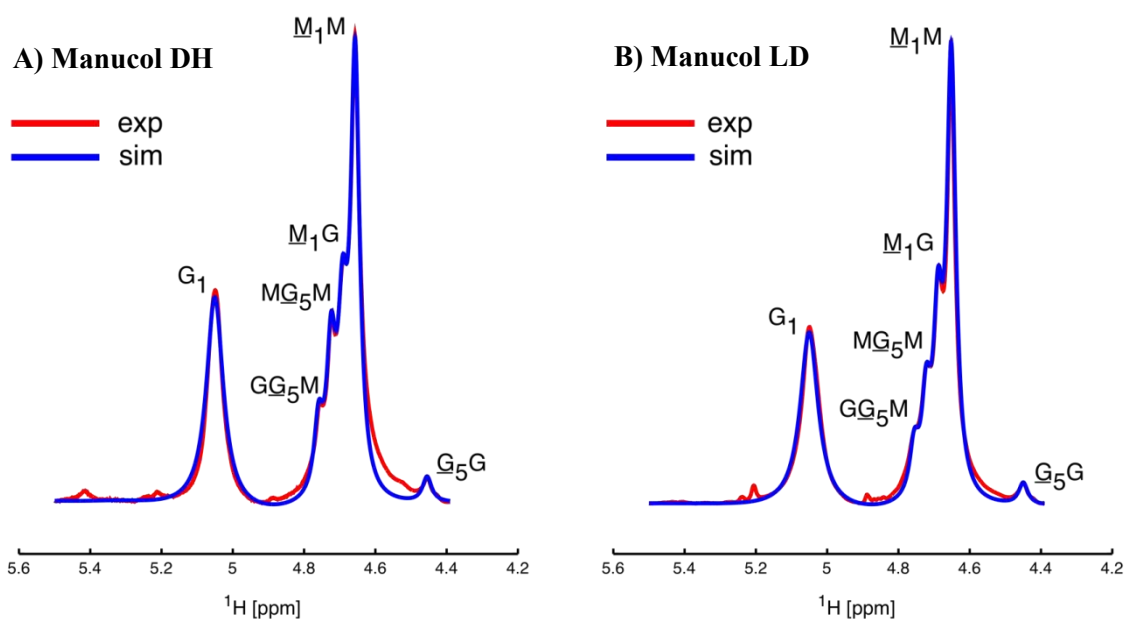
Alginate	F_G	F_M	F_{GG}	F_{MM}	F_{GM}	F_{MG}	F_{GGG}	F_{MGM}	F_{GGM}	F_{MGG}
Manucol LD	31.0	69.0	13.4	51.4	17.6	17.6	7.1	11.4	6.2	6.2
Manucol DH	33.0	67.0	13.3	47.4	19.7	19.7	6.6	13.0	6.7	6.7

Depending on the protons 1 and 5 of each alginate, the chemical shift of these environments is unique. The fitted line width for the signal at 5.05 ppm was 9.0 and 9.6 Hz for Manucol DH and Manucol LD respectively, whereas a value of 4.8 was used for the remainder of the signals. The fitted intensities used to calculate the composition were area under the curve values and therefore independent of line width variations. Simulated lorentzian lines fitted the experimental acquired data well and revealed that the M:G ratio for Manucol LD and

Manucol DH was 69:31 and 67:33 respectively; a subtle difference as previously found. The fraction with the biggest difference was that of the MM content with a ca. 8% more MM diads in Manucol LD compared to Manucol DH.

4.3 Conclusions and summary

Results from this study can be summarised as follows:

i) Heat degradation of Manucol LD to smaller molecular weight products does not alter its iron affinity properties.

ii) Heat degradation of Manucol DH to smaller molecular weight products, similar to that of Manucol LD does impart iron chelation potential.

iii) Epimerisation of Manucol LD to a higher %G alginate abolishes its iron binding abilities.

iv) Manucol LD differs from Manucol DH mostly in compositional differences in the fraction of MM diads.

It seems a plausible rationale that Manucol LD, in resemblance of biological proteins, has a tertiary and secondary structure that forms an iron binding pocket or cavity; this structure is formed by the specific MG sequence of the alginate. This iron binding site acts as the nucleation site for iron deposition and nanoparticle formation as discussed previously. If this were the case, then alteration of the M:G ratio and thus MG sequence on Manucol LD would disrupt the formation of this binding site; this has indeed been demonstrated. It has also been identified that Manucol DH and Manucol LD do indeed have different sequence homologies, which strengthens the case for a strict MG sequence required for iron chelation. Lysis of Manucol LD did not have any effect on its iron binding, which is unsurprising if the theory of

an iron binding pocket is accepted, since lysis would need to take place at critical structural points to disrupt the tertiary structure formation.

The importance of polymer length on iron binding ability has been demonstrated when you consider the results obtained from Manucol DH lysis experiments, since lysis to smaller (Manucol LD sized) products does generate iron chelation activity. This infers that there is some reliance on molecular weight, and as hypothesised, a combination of both is likely to determine iron binding capabilities. Degradation to smaller molecular weight products would be interesting, yet since degradation decreases with time, increasing the heating time would not necessarily decrease molecular weight to any extent; other methods of lysis would need to be utilised (i.e. alginate lyase enzymatic treatment).

In summary, iron chelation by alginates is not dependent on M:G ratio, MG sequence or molecular weight alone, but a combination of all three variables dictates iron binding potential. Manucol LD is unique in its iron binding abilities. To fully understand why this alginate demonstrates such desired activity would require complete alginate GM sequencing, followed by extensive computer-modelled conformation calculations to illustrate the exact solution structure of this alginate. If such studies revealed the presence of a high-affinity iron binding pocket, the sequence structure that imparts the iron binding site could be examined, and if possible, complete sequence-specific alginate synthesis would construct the ideal iron-chelating compound. Simple manipulation techniques here have provided a top-down route to understanding how chemical composition does affect iron binding properties, and until these highly sophisticated techniques become routine procedures Manucol LD remains *the best* alginate iron chelator. Perhaps an alginate molecular weight of 145 kDa and a G:M composition of 38:62 really is the perfect alginate composition for iron binding.

4.4   Acknowledgments

4.5   Experimental

4.5.1   Western blotting and cell work for ferritin expression

For experimental procedure see experimental section 3.5.6.

4.5.2   Heat degradation and viscosity measurements

Since the read-out of alginate degradation fractions requires cellular incubation for ferritin expression, simple heat degradation whereby no additives are required (i.e. enzymes or chemicals) pose the cleanest and easiest route to acquiring alginate degrade products (ADPs).

For the production of Manucol LD and Manucol DH heat degrade products alginates (2×10^{-3} g mL^{-1}) were dissolved into DI H$_2$O (100 mL) with high spin vortex mixing at room temperature and stirred vigorously for 3-5 hours until complete hydration was evident. Alginate aliquots (10 mL) were heated at 100 °C for set time points on a heat block (Techne DRI-BLOCK) and immediately cooled on ice and stored at 4 °C until viscosity measurements were performed.

All viscosity measurements were performed at 25 °C in a constant temperature water bath and alginate concentrations that were used were within the kinematic range of the viscometer

(usually from $0.1 - 1$ mg mL^{-1}). Viscosities were measured on a Cannon-Ubbelohde glass viscometer (Cannon instruments), size 50, with a kinematic viscosity range of $0.8 - 4$ mm^2 s^{-1}. Measurements were made in duplicate for each concentration measured. Alginate samples were equilibrated for 30 min prior to measurement and filtered using a 0.45 μm syringe filter to remove any contaminants.

4.5.3 G25 chromatography

Gel filtration experiments were performed at 20 °C using a Sephadex^{TM} G-25 fine (26/100) column, with a height of 100 cm and a diameter of 26 mm, equalling a column volume of ca. 670 mL, which was attached to an AKTA^{TM} purifier FPLC purification system (GE healthcare). A 5 mL loop was utilised at the injection site, with alginate samples (2 mg mL^{-1}, 5mL) injected prior to filtration. The flow rate was 4 mL min^{-1} with a working pressure of ca. 0.2 MPa. The eluent was aqueous sodium chloride (0.2 M) which was filtered and de-gassed before use. The column was primed with eluent and thoroughly washed between runs. Elution samples were passed through a UV-visible detector set to $\lambda = 280$ and 230 nm.

4.5.4 Plasmid extraction

Agar blocks inoculated with JM 109 containing plasmid pHH1 encoding AlgE1 was donated from Helga Ertesvåg (Norwegian University of Sciences and Technology). Bacterial stocks were produced, which were subsequently plated on an ampicillin-enriched agar plate to obtain single colonies. These were cultured overnight and plasmids were extracted using a QI Aprep Spin Mini Prep kit (Qiagen).

4.5.5 Gene sequencing

Prior to sequencing, DNA concentrations were obtained using a NanoDrop 1000 Spectrophotometer. DNA samples were mixed with forward and reverse primers (Eurofins MWG Operon) before DNA sequencing was conducted by the functional genomics department (University of Birmingham).

Primer name	Base length	Sequence 5' to 3'	GC content (%)
M13_Puc_rev_primer	23	AGCGGATAACAATTTCACACAGG	44
pBAD_rev_primer	18	GATTTAATCTGTATCAGG	33

A restriction digest of the purified plasmid was also performed using the restriction enzyme Nco1 and the resultant digest was separated on a 0.8% agarose DNA gel.
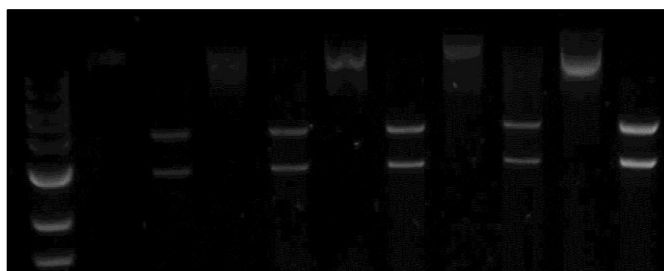
4.5.6 *E.coli* transformation

E.coli bacterial strain BL21 was used for the expression of AlgE1. BL21 were mixed with the plasmid DNA (containing the algE1 gene insert) and transformed by heat shock at 42 °C for 1 min 45 sec. Transformed bacteria were then plated onto ampicillin-enriched agar plates and incubated overnight at 37 °C, thereafter single colonies were selected and subsequently cultured overnight in ampicillin (0.5 µL mL^{-1}) supplemented LB broth to generate starter cultures or glycerol stocks as required.

4.5.7 AlgE1 production and purification

For the production of large amounts of AlgE1, LB broth (x2 1000 mL, 25 g) supplemented with ampicillin (100 µg uL^{-1}) was autoclaved prior to use. A starter culture consisting of LB broth (x2 10 mL) inoculated with the glycerol stock was incubated overnight, which was then transferred into growth LB broth and incubated at 37 °C with slight agitation until an optical density of 0.4 at λ = 600 nm was reached. At this point, the growth cultures were induced with isopropyl β-D-1-thiogalactopyranoside (IPTG) (0.5 mM) and incubated at 25 °C for a further 3 hours. The bacteria were subsequently harvested and pelleted by centrifugation at 6000 RPM at 4 °C (Avanti J-20XP, Beckman Coulter) and the obtained cell pellet was disrupted with continuous aspiration cycles in MC buffer (20 mL) containing protease inhibitors (1 tablet, Roche). MC buffer consisted of MOPS (20 mM, pH 6.9) and CaCl$_2$·2H$_2$O (2.2 mM). At this stage, the cells could be frozen at − 80 °C or purified further. The BL21 cell suspension (20 mL) was disrupted by pressure using an emulsiflex homogeniser (Arestin) at 18,000 PSI at 4 °C. The subsequent cell slurry was centrifuged at 250,000 RPM for 45 mins (Avanti J-20XP, Beckman Coulter) to remove cell debris and the supernatant collected ready for purification.

The supernatant was filtered through a 0.2 µm sized filter, prior to loading onto the column (25 mL). The filtered crude extract was purified on a HiTrap Q Sepharose HP column (Pharmacia) which was pre-equilibrated with MC buffer. Elution of the epimerase was achieved using a continuous NaCl gradient (0.1 − 1.0M) in MC buffer; AlgE1 eluted between 0.3 and 0.6 M NaCl with 4 mL fractions collected throughout the elution.

4.5.8   Assessing for activity of AlgE1

To screen the purified enzyme fractions for epimerisation activity, aqueous Manucol LD (0.1%, (w/v)) in DI H_2O (5 mL) was prepared. Manucol LD solution (2 mL) was mixed with the enzyme fractions (1 mL) and MOPS buffer (80 mM, 1 mL) supplemented with $CaCl_2 \cdot 2H_2O$ (4 mM). The resultant mixture was incubated at 37 °C for 2 hours. To quench the epimerisation, EDTA (50 mM, 500 μL) was added and the subsequent mixtures were transferred to dialysis membranes (MWCO= 12 400, 33 mm flat width). Solutions were dialysed against DI H_2O (1000 mL) for three 24 hour incubation periods at 4 °C. The resultant solutions were used directly in the circular dichroism spectrometer. CD measurements were recorded on a Jasco J-810 CD spectropolarimeter (4 accumulations, 1 s response) using a 1 cm path length, blackened quartz cell. Spectra were recorded at an internal temperature of 20 °C.

4.5.9   Epimerisation of Manucol LD for cell culture use

Aqueous Manucol LD (0.2%, (w/v)) was prepared in DI H_2O (100 mL) to which, MOPS buffer (180 mM, 25 mL) supplemented with $CaCl_2 \cdot 2H_2O$ (40 mM) was added and the enzyme fractions identified with activity (20 mL) was also added. The resultant solution was gently agitated at 37 °C for 24 hours, before enzyme deactivation was initiated with the addition of EDTA (0.5 M). The mixture was cooled to 4 °C and transferred to a dialysis membrane to allow the Ca-EDTA complexes to dialyse out. Dialysis was carried out at 4 °C in 4000 mL DI H_2O for three 24 hour incubations. The subsequent alginate product was aspirated, pH adjusted to pH = 7.4, and concentrated *in vacuo* to an intermediate volume of ca. 50 mL. At this point, precipitation of protein could be seen, and as such, this was centrifuged at 1500

RPM for 10 min to a pellet, and the supernatant dried *in vacuo* to completion. The resultant product was glass-like, clear and solid.

4.5.10 High resolution NMR

Alginate samples Manucol DH and Manucol LD were prepared by dissolving alginates (0.5 g) into D_2O aliquots (1 mL) and stirred vigorously to ensure complete dissolution. The solutions were transferred to NMR tubes, and slightly centrifuged to move the sample to the bottom of the sample tube.

^{1}H NMR spectra were acquired on a Bruker Avance III 600MHz instrument equipped with a 5mm TCI Cryoprobe. The residual solvent resonance was further suppressed using a NOESY presat pulse sequence. A total of 32 transients and 16 steady state scans were acquired with 16384 complex data points. The spectral width was set to 7184 Hz and the sample temperature to 340 K. The free induction decays were multiplied with a 0.3 Hz broadening exponential window function and zero filled to 32768 real data points prior to Fourier transformation. They were then manually phase and baseline corrected, using a spline baseline correction. Signals for the anomeric protons of the different alginate constituents were fitted to lorentzian lines. All data processing and analysis was performed using the matlab based MetaboLab software package.[7]

4.6 References

1.   Sreeram, K.J., H. Yamini Shrivastava, and B.U. Nair, *Studies on the nature of interaction of iron(III) with alginates.* Biochimica et Biophysica Acta (BBA) - General Subjects, 2004. **1670**(2): p. 121-125.

2. Harding, S.E., *The intrinsic viscosity of biological macromolecules. Progress in measurement, interpretation and application to structure in dilute solution.* Prog Biophys Mol Biol, 1997. **68**(2-3): p. 207-62.

3. Svanem, B.I.G., et al., *Cloning and Expression of Three New Azotobacter vinelandii Genes Closely Related to a Previously Described Gene Family Encoding Mannuronan C-5-Epimerases.* Journal of Bacteriology, 1999. **181**(1): p. 68-77.

4. Ertesvag, H., et al., *The Azotobacter vinelandii mannuronan C-5-epimerase AlgE1 consists of two separate catalytic domains.* J Biol Chem, 1998. **273**(47): p. 30927-32.

5. Ertesvåg, H. and G. Skjåk-Bræk, *Modification of Alginate Using Mannuronan C-5-Epimerases*, in *Carbohydrate Biotechnology Protocols*, C. Bucke, Editor. 1999, Humana Press. p. 71-78.

6. ASTM, I. *ASTM F2259-10. Standard test method for determining the chemical composition and sequence in alginate by proton nuclear magnetic resonance (1H NMR) spectroscopy.* 2010 [cited 2015; Available from: http://www.astm.org/Standards/F2259.htm.

7. Ludwig, C. and U.L. Gunther, *MetaboLab--advanced NMR data processing and analysis for metabolomics.* BMC Bioinformatics, 2011. **12**: p. 366.

Chapter 5

Polyphenolic iron complexation: a chemical and cellular study.

5.1   Introduction and aims

Similar to alginates, dietary iron chelators include the vast class of compounds known as polyphenols.   Being small molecular weight compounds, their effect on cellular iron metabolism could be one to enhance iron bioavailability or to decrease cellular iron concentrations (both through possible solubility changes, chelation or direct protein modulation mechanisms).   Such contrasting mechanisms are observed with two dietary iron chelators, tannic acid and ascorbic acid.[1, 2]   The four polyphenol complexes selected for this study (screened using the requirements for iron binding set out by Khokhar *et al.*)[3] were quercetin, rutin, cyanidin-3-O-glucoside and catechin.   The preceding literature review based on these compounds (section 1.5) can be summarised in table 5.1.

Table 5.1: Summary of iron binding properties, bioavailability and anti-neoplastic effects for the polyphenols assessed (summarised from section 1.5).

Polyphenol	Iron binding ability	Bioavailability	Anti-carcinogenic potential
Quercetin	Confirmed. Strong binding ability.	Poor.	Strong murine evidence. Conflicting human results.
Rutin	Confirmed. Strong binding ability.	Low.	Limited evidence but mainly inconclusive.
Cyanidin-3-O-glucoside	No evidence.	Absorbable and highly metabolised, yet presence within large intestine confirmed.	*In vitro* evidence of some effects.
Catechin	Limited evidence.	Very poor.	Limited evidence.

It is apparent that polyphenol bioavailability is a complex field of study, despite this there are reports of the listed polyphenols reaching the large intestine.[4-9] This allows the selected four polyphenol candidates to be assessed for their iron binding potential. Thus, the aims of this chapter are to:

1) Understand the chemical iron-binding nature of the listed polyphenols;

2) Examine how these polyphenol compounds impact on cellular iron metabolism.

3) Rationalise these iron-binding properties and delineate mechanisms that may contribute towards an anti-carcinogenic potential.

5.2   Results and discussion

5.2.1   Assessment of iron binding by isothermal titration microcalorimetry

Isothermal titration microcalorimetry is ideally set up to probe interactions of iron with polyphenols and since physiological conditions can be employed throughout the titration, this

increases the relevancy of results upon translation into an *in vitro* setting. However, the use of these neutral pH environments in the presence of iron require specific titration controls since the titration of acidic aqueous iron solutions titrated into a pH = 7 solution will produce considerable heat changes. With this aliquots of either aqueous iron(III) chloride or iron(II) sulphate were titrated into a stirred solution of polyphenol (0.05 mM) at a temperature of 37 °C in a physiological pH 7.0 buffer with the relevant control titration (iron into buffer only) subtracted from each isotherm (method 5.4.2) (figure 5.1).
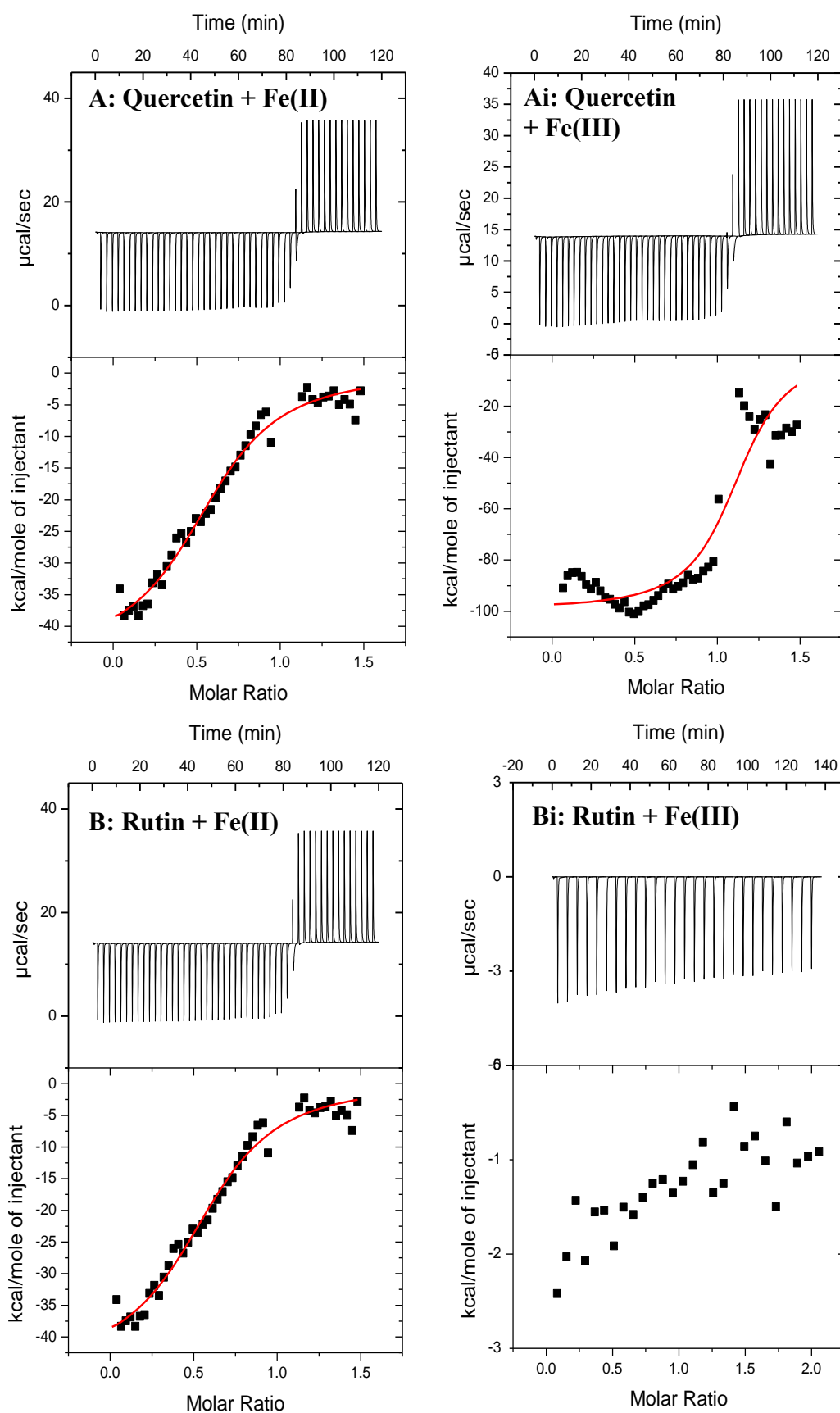
Figure 5.1: (1) Thermograms and corresponding isotherms for iron (II) binding to (A) quercetin and (B) rutin with titrations for iron (III) binding to (Ai) quercetin and (Bi) rutin. Control titrations and recorded heats were subtracted from the respective experiments. The solid lines represent the curve fitting results using the model of best fit.
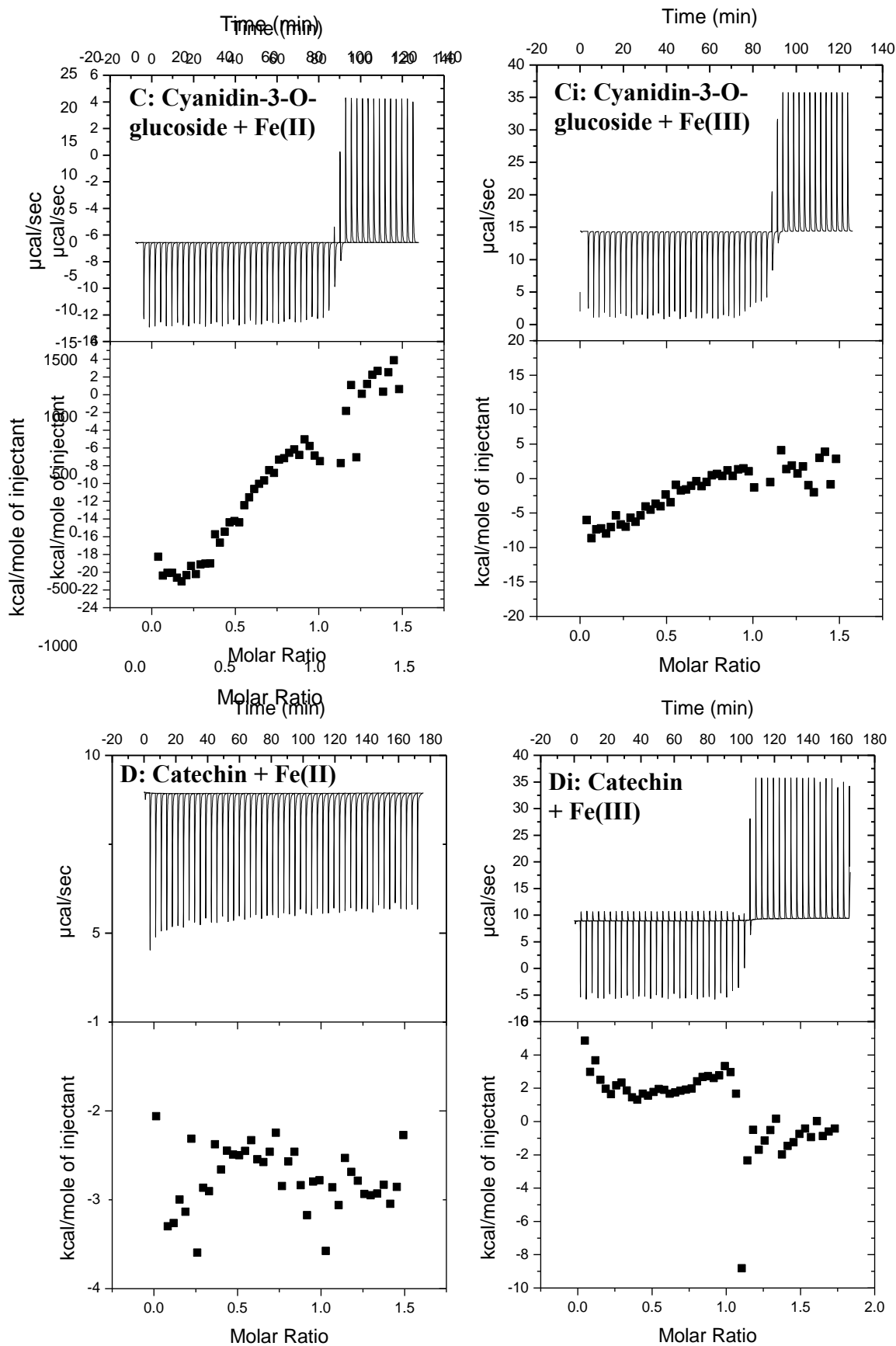
Figure 5.1: (2) Thermograms and corresponding isotherms for iron (II) binding to (C) cyanidin-3-O-glucoside and (D) catechin with titrations for iron (III) binding to (Ci) cyanidin-3-O-glucoside and (Di) catechin. Control titrations and recorded heats were subtracted from the respective experiments. The solid lines represent the curve fitting results using the model of best fit.

228

Isotherms were fitted using models of host-guest interactions that best fitted the data. It is evident that quercetin is binding iron in these environments. For both ferrous and ferric iron the number of binding sites on quercetin was estimated to be N = 0.63 and 1.16 respectively, indicating one preferred iron binding site on quercetin in parallel to that found in previous work.[3, 10] Iron binding constants were K = 8.3 x 10^5 and 3.86 x 10^6 M^{-1} for ferrous and ferric iron binding respectively. The higher affinity of interaction with ferric iron than ferrous can be rationalised based on electrostatics, with a greater charge density on iron (III) enhancing the columbic interaction between the host and guest. These iron binding constants match those previously reported.[11]

For rutin, iron complexation mechanisms were interesting. Iron binding by rutin could only be demonstrated with ferrous iron; no iron binding was evident with ferric iron. This could be attributed to the oxidative nature of rutin in the presence of iron whereby interaction proceeds via a chemical reaction rather than complexation.[12] Isotherms for ferrous iron interactions with rutin were best fitted using a two-site model of binding. This is interesting since in rutin, the glycone of quercetin, the most favourable iron binding site is blocked by the rutinoside due to steric hindrance. In part, iron complexation would occur via the two remaining iron binding sites of which one is strong (K = 3.2 x 10^8 M^{-1}) and one is weaker (K = 2.2 x 10^4 M^{-1}). It can be eluded that the C5 OH – C3 keto would complex iron with the greater affinity compared to the C3'-C4' OH on ring B due to greater electron density at this moiety. This corroborates the structural chemical differences identified earlier.[3] For both cyanidin-3-O-glucoside and catechin, no appreciable iron binding parameters could be obtained. For cyanidin-3-O-glucoside, it was documented that considerable structural rearrangements take place at neutral pH conditions which could yield non-iron chelating products.[13] A slow redox reaction between ferrous iron and catechin has been reported, which could contribute to

the lack of iron binding observed by ITC.[14]   Both catechin and cyanidin-3-O-glucoside do not possess the 5-OH or 3-OH in conjunction with the C4 keto group which was identified as an important iron-binding moiety in flavonoids.[3]

5.2.2   Assessment of iron chelation by ferritin expression

The assessment of cellular biomarkers of intracellular iron concentration would allude to the iron chelation abilities of the selected polyphenols *in vitro*. The assessment of ferritin levels would demonstrate as to whether iron chelation was taking place in the extracellular media to limit iron absorption and hence decrease iron-mediated ferritin expression. To interrogate this, RKO cells were challenged with an iron rich media (100 µM $FeSO_4 \cdot 7H_2O$ + 500 µM sodium ascorbate) with or without the polyphenols (quercetin, rutin, cyanidin-3-O-glucoside and catechin) (method 5.4.3) (figure 5.2).
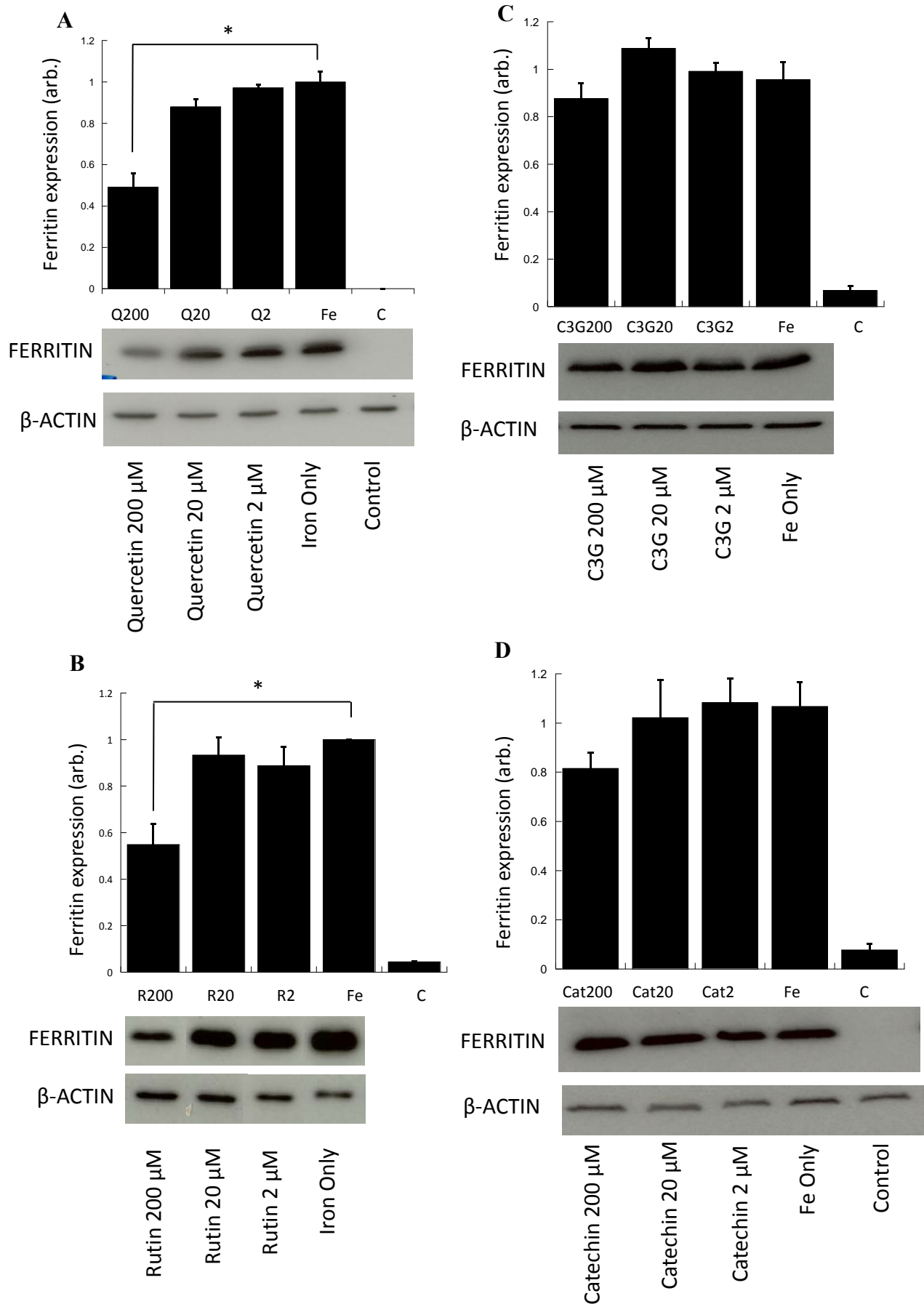
Figure 5.2: Expression values for RKO cells co-cultured with quercetin, rutin, cyanidin-3-O-glucoside and catechin for ferritin (A-D) respectively. Concentrations of polyphenols co-cultured with iron without iron were 200, 20, 2 and 0 μM respectively. Data points represent mean fold change in protein expression normalised to β-actin, relative to control. Error bars donate ± SEM with * indicating statistical significance with p < 0.05 and n = 3.

231

Quercetin statistically decreased ferritin expression at higher concentrations (200 μ M) by 51% (p < 0.05) compared to the iron only control. There was some trend to decrease ferritin expression at the lower incubation concentrations of quercetin yet this was not significant. This data is suggestive of an iron chelation effect of quercetin *in vitro*, which is in agreement with other *in vitro* data detailed previously.[15-17]

The rutinoside of quercetin (rutin) had identical effects to quercetin with respect to iron modulation *in vitro* by decreasing ferritin expression by 54% statistically (p < 0.05) at 200 μM incubation concentrations but having no significant effects at lower concentrations. This data would suggest that despite the glycosylation status of rutin in comparison to quercetin, no iron chelation differences are observed *in vitro*. This identically is also reflected in the ITC experiments where both polyphenols were able to chelate ferrous iron with similar iron binding constants.

Cyanidin-3-O-glucoside and catechin demonstrated no iron chelation abilities *in vitro* as no discernible changes in ferritin expression were found; this corroborates the lack of iron binding affinity identified in the ITC results (figure 5.1 (2)).

5.2.2.1 Assessment of intracellular iron concentrations by ^{59}Fe experiments

Assessment of the surrogate biomarkers for intracellular iron concentration (such as ferritin) provide an understanding of cellular iron concentrations, yet only for iron that is accessible to IRE/IRP binding. Practically, this means that there would be no discrimination between iron chelation taking place extracellularly, whereby subsequent iron-polyphenol complexes remain extracellular or the converse whereby iron chelation is taking place, yet the polyphenol iron complex can shuttle between an intracellular state or extracellular one. Simply it may be the

case that even though a decreased intracellular iron concentration is observed by ferritin, iron concentrations maybe higher if the polyphenol-iron complex cannot be sensed by IRE/IRP2. With respect to the polyphenols examined here this is significant since the absolute bioavailability of the polyphenol or the iron complexes are not fully understood. To examine the effect of this radioactive ^{59}Fe was employed in similar conditions as to the protein expression studies since ^{59}Fe levels will reflect actual intracellular iron concentrations (method 5.4.4) (figure 5.3)
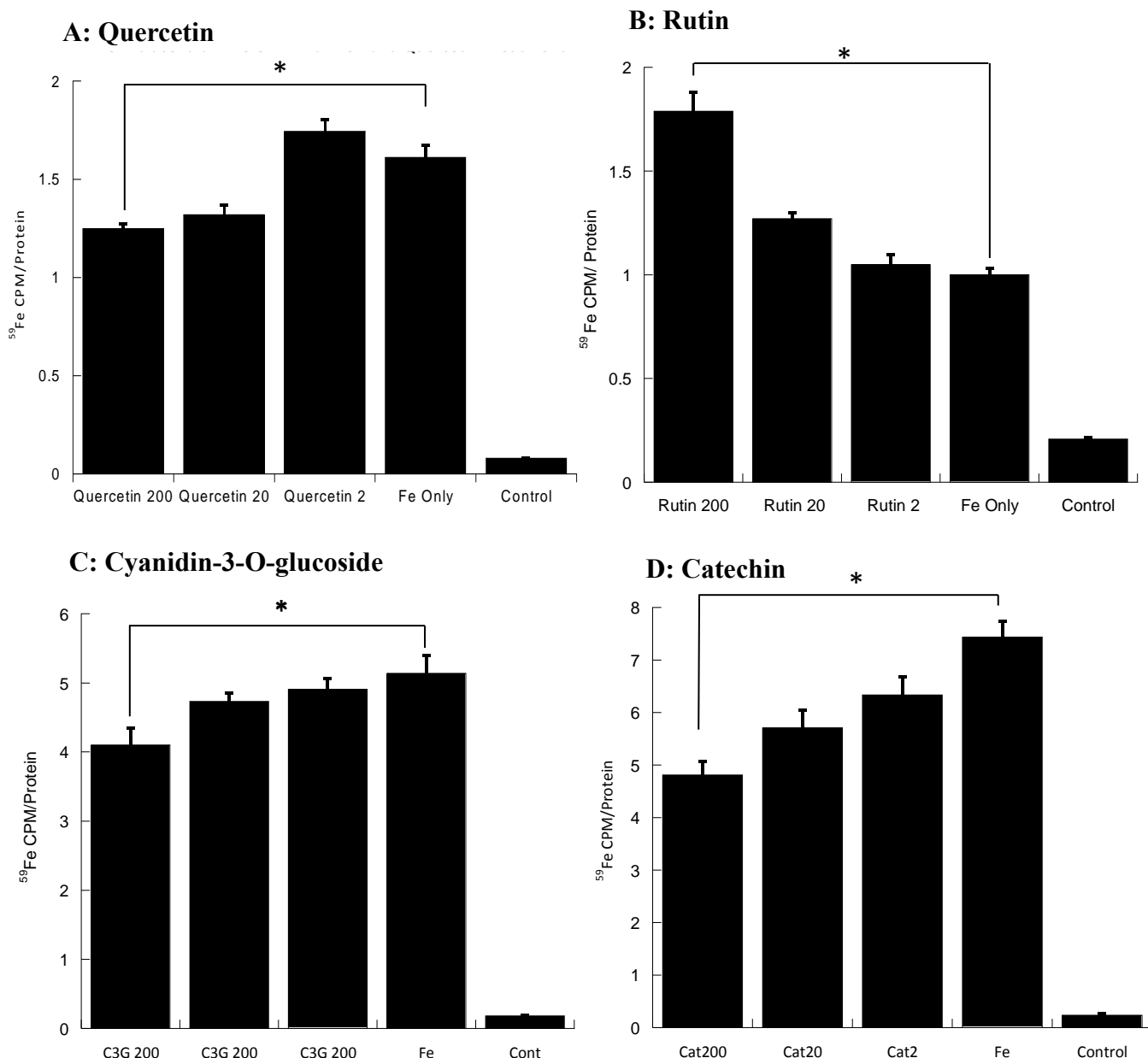
Figure 5.3: Intracellular ^{59}Fe iron concentrations for RKO cells treated with (A) quercetin, (B) rutin, (C) cyanidin-3-O-glucoside and (D) catechin at 200, 20, 2 and 0 μM concentrations. * denotes statistical significance ($p < 0.05$) vs. iron only control. Error bars denote ± SEM, n = 12.

It was found that quercetin statistically decreased intracellular ^{59}Fe by 21% and 18% ($p < 0.05$) at the 200 and 20 μM incubation concentrations respectively. These results verify the ferritin expression findings, suggesting that quercetin is indeed chelating iron extracellularly and the subsequent iron-quercetin complex does not become intracellular. It has been

discussed however that quercetin iron complex can readily efflux the cell and the experiments performed here do not rule out the possibility that quercetin is chelating intracellular iron. In both cases quercetin is chelating iron which is subsequently non-intracellular. Conversely, it is demonstrated that the rutin-iron complex is intracellular since at co-incubation concentrations of 200 and 20 μM an increase in ^{59}Fe of 78% and 27% are found respectively. This infers that despite the fact that rutin is chelating iron, as evidenced by decreased ferritin expression, the chelated iron is non-IRP2 sensed despite accumulating within the cell. The site of iron chelation maybe questioned as the combination of these data suggest it either intracellular or extracellular iron chelation. The rutin-iron complex may also be able to traverse the cell membrane. Considering it has been established that rutin has a low bioavailability, it is possible that the rutin-iron complex is able to traverse the cell membrane or perhaps, the bioavailable-metabolite of rutin is able cell membrane permeable.

Cyanidin-3-O-glucoside, despite showing no bioactivity in the iron chelation and ferritin expression studies, did in-fact induce a 20% decrease (p < 0.05) in intracellular iron concentration only at the 200 μM cyanidin-3-O-glucoside. This may reflect the poor affinity of cyanidin-3-O-glucoside for iron, whereby no diminishment in ferritin expression was found but a small decrease in intracellular iron levels was evident.

Catechin, despite eliciting no iron chelation results previously did decrease intracellular iron concentrations dramatically by 35, 22 and 14% at 200, 20 and 2 μM incubation concentrations statistically compared to control (p < 0.05). This result is confusing since no decrease in ferritin was associated with this response. It has however been documented how catechin is able to induce iron release from ferritin.[18] It could be speculated that catechin is not binding iron initially, allowing ferritin expression. Upon ferritin synthesis and subsequent

iron-storage, catechin is able to sequester this iron removing it from the cell. This is the only

possible rationality for the iron-modulation effects observed.
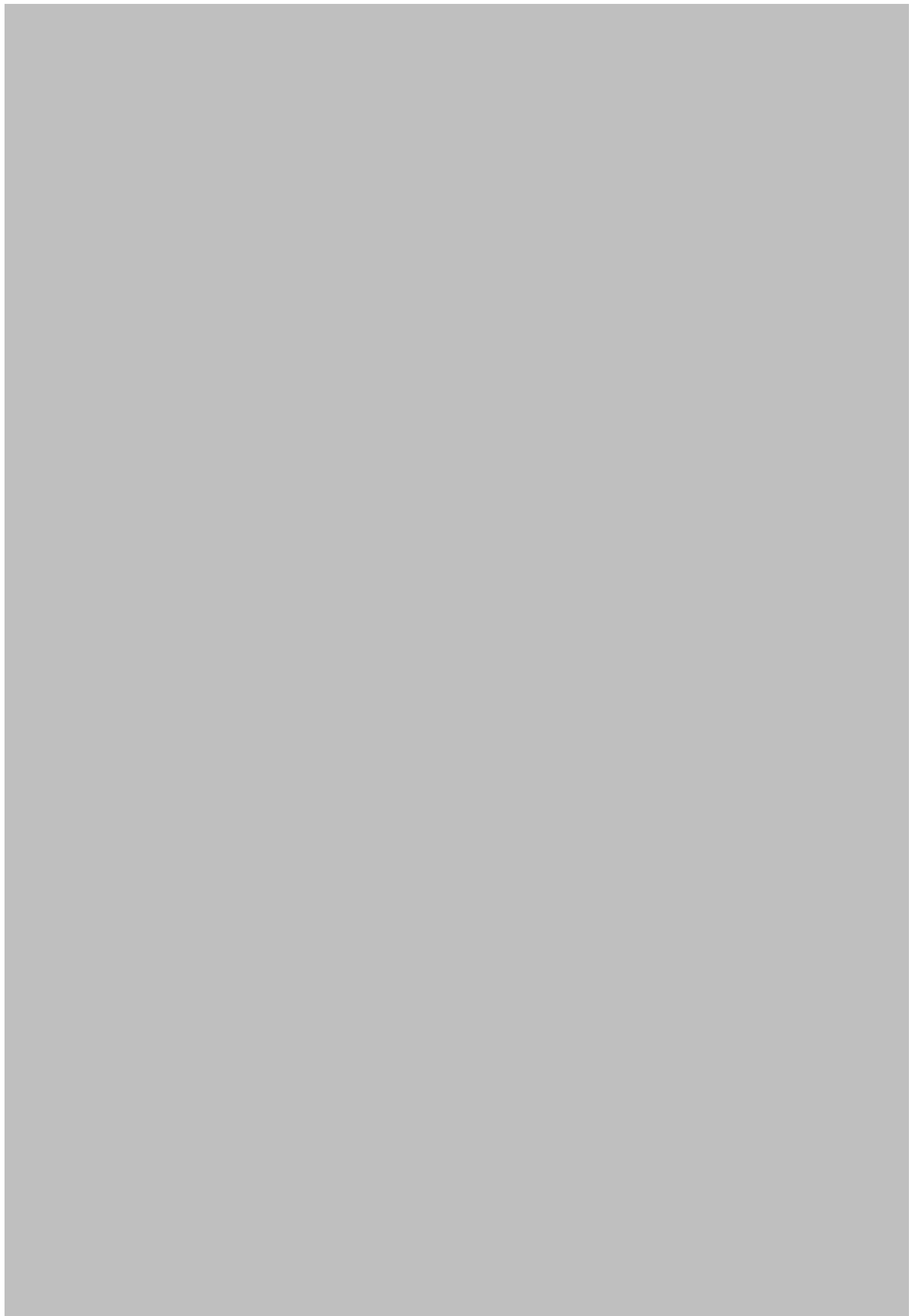
5.2.4 Anti-oxidant action

It is well established that polyphenols have anti-oxidant properties.[19, 20] It was discussed earlier that there are several mechanisms to anti-oxidant action, with one invoking the

chelation of iron to limit its catalytic redox activity in Fenton type reactions.[16, 21] In order to elucidate whether the anti-oxidant effects of these polyphenols is provided through an iron chelation mechanism, a series of experiments were performed to delineate the polyphenol role (method 5.4.6). Firstly, to confirm the anti-oxidant action of these polyphenols in the presence or absence of iron, RKO cells were pre-incubated with an intracellular ROS-activatable fluorescence ligand and subsequently challenged with the polyphenol series with or without iron. After 3, 12 and 24 hours the intracellular ROS content was determined (figure 5.7).
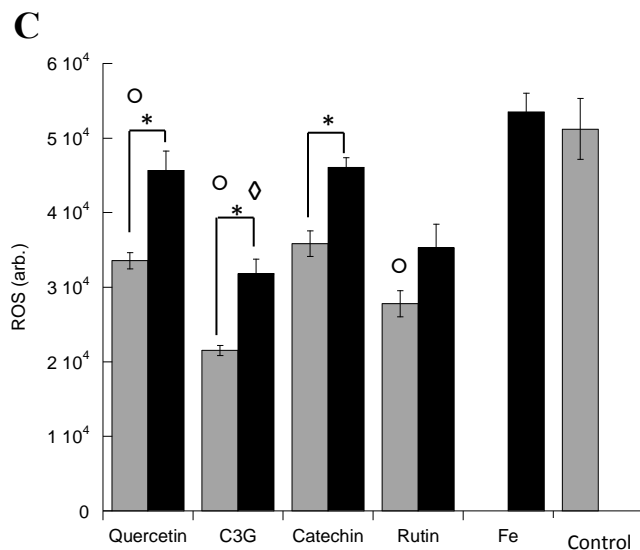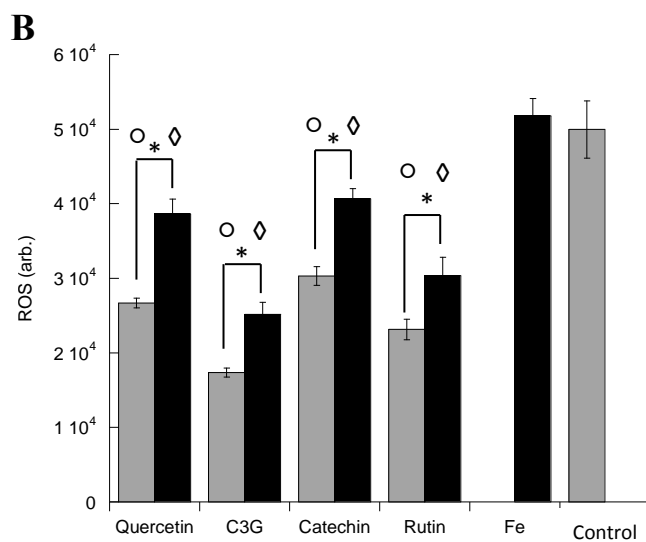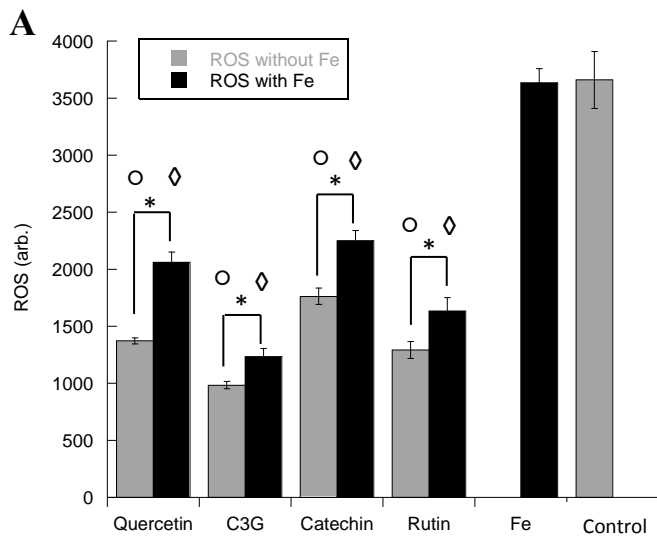
Figure 5.7: Intracellular ROS concentration in RKO cells co-cultured with the polyphenols series, with or without iron for (A) 3 hours, (B) 12 hours and (C) 24 hours. Iron only and media were used as experimental controls. * denotes statistical significance, $p < 0.05$. ○ denotes statistical significance ($p < 0.05$) vs. iron only control. ◊ denotes statistical significance ($P < 0.05$) vs. media only control. Error bars denote ± SEM, n = 12.

The first finding is that iron is not catalysing ROS formation in these cells, since incubation with iron does not induce ROS formation to levels greater than when no iron was present; the basal levels of ROS in RKO cells must be constitutively high.[22, 23] Co-culturing with polyphenol only, without iron, all the polyphenols statistically decreased intracellular ROS formation (except rutin and quercetin at 24 hours). This demonstrates the direct anti-oxidant activity of the polyphenols, which is iron independent. It can be seen that there was elevated ROS levels present when cells were co-cultured with iron as expected. At three hours post incubation, quercetin, cyanidin-3-O-glucoside, catechin and rutin decreased ROS formation by 40, 26, 36 and 26 % respectively. At 24 hours of exposure, quercetin, cyanidin-3-O-glucoside, catechin and rutin diminished ROS production by 26, 32, 22 and 21 % respectively. In this case cyanidin-3-O-glucoside was the polyphenol with the highest anti-oxidant activity, and since this polyphenol demonstrated no iron binding activity, the ROS-quenching ability of this polyphenol is likely to be a direct mechanism. From these experiments it is difficult to demonstrate if any ROS-sequestering activity is associated with iron chelation since all the polyphenols diminish ROS levels directly.

In order to probe the mechanism further, RKO cells were pre-loaded with iron for 12 hours prior to co-culture with the polyphenol compounds. In this experiment, since the cells would have high cellular iron contents prior to exposure to the polyphenol compounds where no iron was present, results would demonstrate the ability of the polyphenol to enter the cell and bind iron, where, if an iron-chelation mediated mechanism of antioxidant activity was occurring, ROS activity would be dampened (figure 5.8).
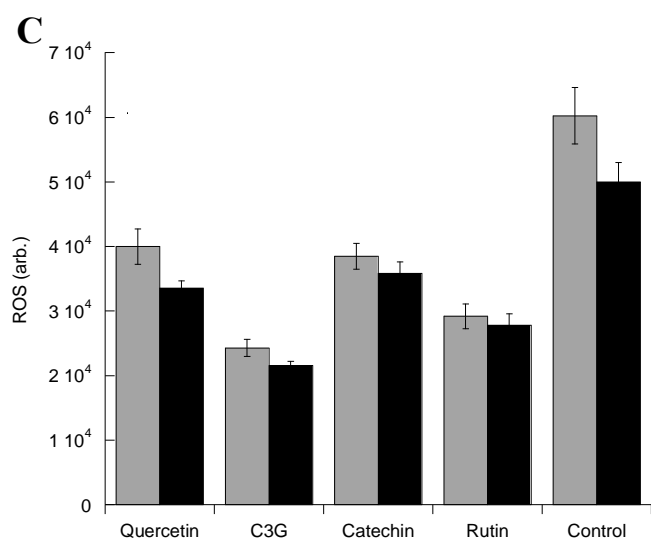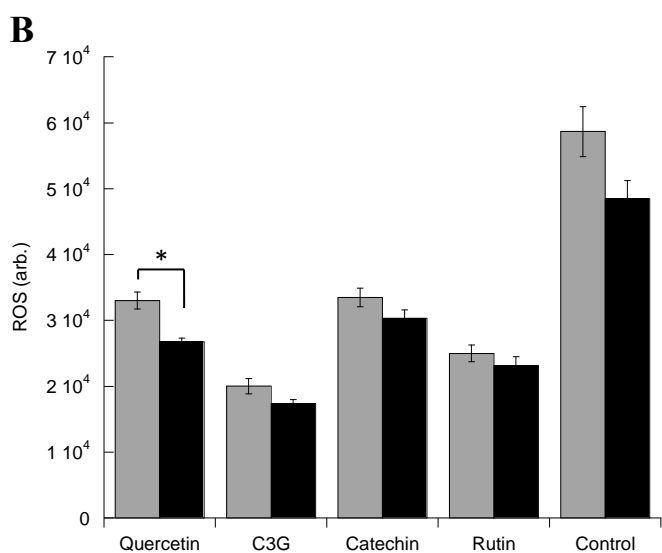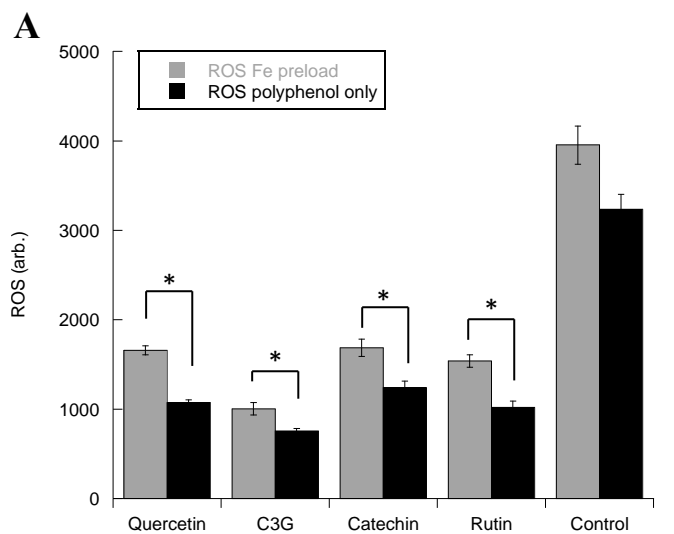
Figure 5.8: Intracellular ROS concentration in RKO cells co-cultured with or without iron for 12 hours prior to culturing with the polyphenols series, without iron for (A) 3 hours, (B) 12 hours and (C) 24 hours. Control incubations include iron co-culture for 12 hours followed by media only, or media only throughout. * denotes statistical significance, $p < 0.05$ vs. no iron pre-load. Error bars denote $\pm$ SEM, n = 12.

Evidently, whether cells were pre-loaded with iron or not, in both cases ROS concentration was significantly lower in all cases to their respective controls ($p < 0.05$). When iron was pre-loaded, in comparison to the non-preload case where polyphenol was added only, at three hours, all the polyphenols demonstrate increased ROS production in the presence of iron compared to polyphenol only; increases of 35, 24, 26 and 19% were calculated for quercetin, cyanidin-3-O-glucoside, catechin and rutin respectively. However, as time progresses and at 24 hours of incubation, no polyphenols demonstrate a statistical increase in ROS production when cells are iron-loaded. This suggests two possibilities; 1) that all the polyphenols over time are able to quench the effects of the high pre-loaded cellular iron generating ROS or, that 2) the ROS-scavenging effects of the polyphenols is saturated and hence both conditions reach equal levels of ROS. If it were indeed hypothesis 1, that all the polyphenols over time are quenching ROS in this time dependent manner, a way to determine if this was through their iron chelation ability would be to repeat the experiment, but incubated iron-preloaded cells with polyphenols already bound to iron. If their ROS quenching ability over time did not occur, then it could be suggested that this is because they alleviate ROS levels through an iron binding mechanism (figure 5.9).
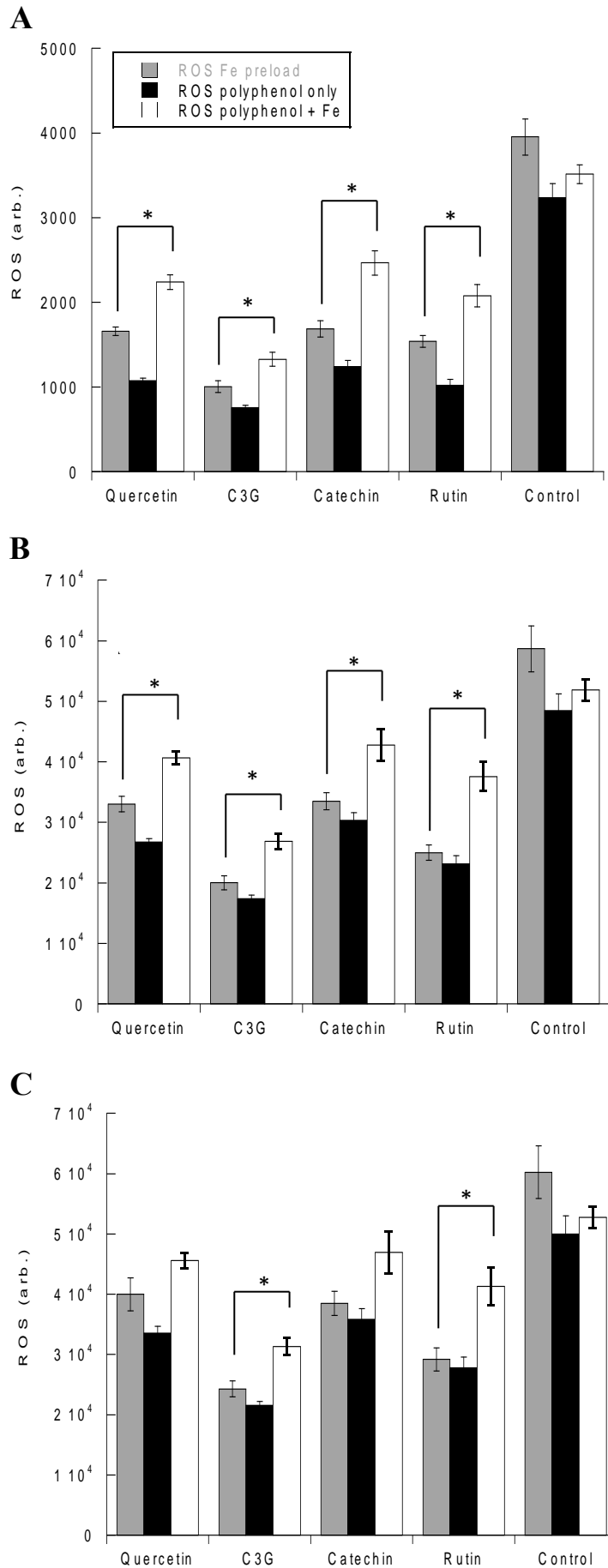
Figure 5.9: Intracellular ROS concentration in RKO cells co-cultured with or without iron for 12 hours prior to culturing with the polyphenol series, with iron (white bars), for (A) 3 hours, (B) 12 hours and (C) 24 hours. Control incubations include iron co-culture for 12 hours followed by media only, or media only throughout, or media with iron. * denotes statistical significance, $p < 0.05$ vs. no iron pre-load. Error bars denote $\pm$ SEM, n = 12.

245

As detailed, when cells are loaded with iron, and then incubated with polyphenol initially, the pre-loaded cells have more ROS associated with them than their non- iron-preloaded counterparts. After time (24 hours) the difference in ROS concentrations is elevated, and ROS levels in both groups are equal and this suggests that over time, the polyphenols may be inhibiting the ROS generation potential of iron. If this was through an iron chelation mechanism, then saturating their iron binding potential would result in no amelioration of these ROS levels between the two groups. Based on this hypothesis, it is found that for quercetin and catechin this seems to be the case. Since cyanidin-3-O-glucoside and rutin have statistically elevated ROS levels at longer time periods, compared to when they are not iron-loaded, this would suggest that they require iron-chelation for their ROS reducing ability. Considering this experiment as a whole, by loading the polyphenols with iron, their ROS diminishing activity decreases, with all increased ROS levels detected at 3 hours of incubation for all the polyphenols, specifically, quercetin, cyanidin-3-O-glucoside and rutin demonstrate a 26, 24, 31 and 39% increase in ROS production. At 24 hours, this representation shifts, and only quercetin and catechin are able to restore ROS levels to their original values; suggestive that at these later time points, antioxidant activity does not involve an iron chelation mechanism.

5.2.5   Iron redox activity

A simple way of quantifying polyphenolic affinity for iron would be to employ a competitive ligand that yields a colourful complex upon coordination with iron; the ferrozine ligand is able of achieving this (method 5.4.7). The significance of this experiment is that ferrozine will only coordinate with ferrous iron. Using ferrous iron as the iron source will detail which

polyphenol compounds chelate iron the best in these competition studies. On the other hand, using ferric iron as the iron source will detect if any polyphenol compounds are having redox activity to oxidise iron to its ferrous form. In this experiment, polyphenol compounds were introduced into pH = 7 buffer solutions with the ferrozine ligand, with either ferric or ferrous iron and incubated over night to mimic the conditions used *in vitro* (figure 5.10).

Using ferrous iron to determine the extent of iron chelation, cyanidin-3-O-glucoside displayed no iron-chelation ability paralleling the findings using ITC. Quercetin, catechin and rutin chelated iron by 14, 18 and 20 % respectively compared to control. When ferric iron was used as the iron source, under these pH = 7 buffered conditions, all polyphenols demonstrated some redox activity, with rutin, catechin, cyanidin-3-O-glucoside and quercetin increasing Fe(II) concentrations by 18, 34, 82 and 82 respectively compared to control.
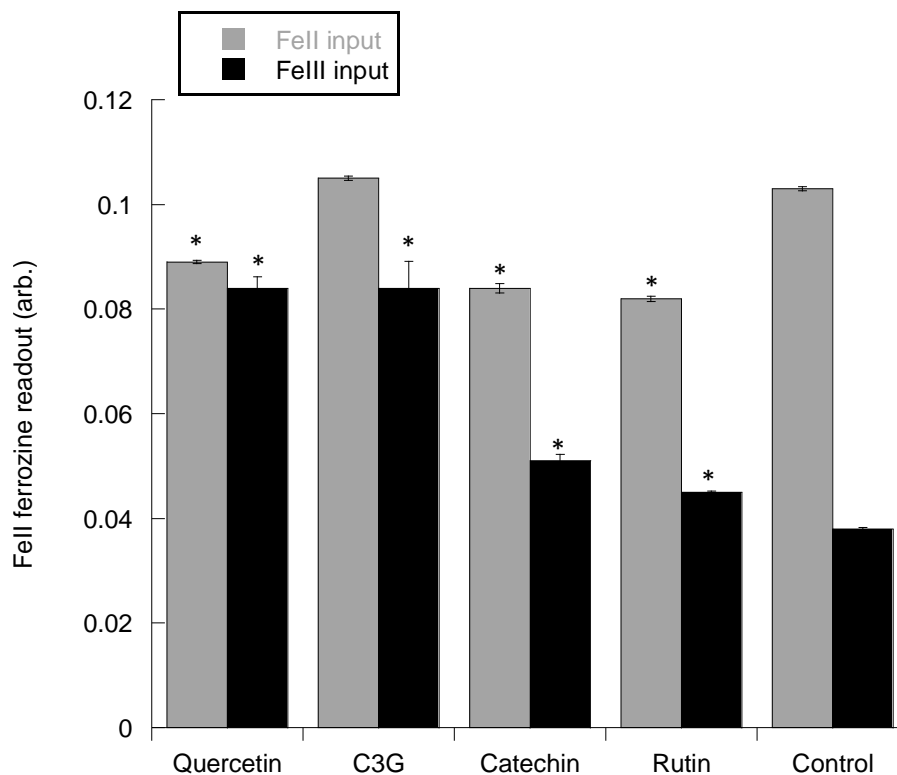
Figure 5.10: Redox potential of iron(II) and iron(III) in the presence of polyphenolic compounds. * denotes statistical significance ($p < 0.05$) with respect to the relevant control. Error bars represent ± SEM, n = 3.

5.3 Conclusions and summary

The results obtained here highlight the complexity of polyphenolic iron chelation both chemically and within the physiological conditions *in vitro* and *in vivo*. Calorimetric experiments identified that under physiological conditions only quercetin and rutin are able to bind iron, with catechin and cyanidin-3-O-glucoside demonstrating no iron-binding activity. With respect to redox activity however, cyanidin-3-O-glucoside and quercetin were able to redox react with ferric iron to form ferrous iron. Catechin, rutin and quercetin all demonstrated iron binding ability in the ferrozine assessment of iron binding. These three polyphenols demonstrated similar activity when intracellular iron was assessed as they invoked intracellular iron concentration changes. Catechin was able to hinder iron absorption,

as well as quercetin, however it was found that rutin increased intracellular iron concentrations.

Rutin was found to increase intracellular iron concentrations, yet diminish ferritin concentrations alluding to iron-chelation with the rutin-iron complex becoming intracellular. As discussed the nature of this is confusing and further work needs to be carried out to verify why this is the case.

Considering all the experiments involving iron modulation it can be concluded that quercetin presents itself as the ideal iron chelator for luminal iron chelation; it bound both Fe(II) and Fe(III) in the ITC experiments; it reduction in iron-mediated ferritin expression and in inhibited intracellular iron concentrations. Iron chelation activity was not demonstrated *in vivo* however, which is disappointing since in vitro studies identified quercetin as an iron chelator. As discussed earlier, polyphenol iron chelation is very much dependent on concentration and environment and this may be the reason why *in vitro* results were not reflected in mice.

The anti-oxidant activities and mechanisms of the polyphenols are complex. If you describe the results obtained here without and prior knowledge of iron binding by the polyphenols used the following conclusions can be made. All polyphenols are able to reduce the ROS generation potential of iron when co-cultured with iron. When you pre-load cells with iron, and then subsequently expose them to the polyphenols, all the polyphenols in the short term demonstrate a diminished effect of antioxidant activity by observed increases in intracellular ROS concentrations. The polyphenol which augmented ROS the most was quercetin at the short term (this maybe because its mechanism is through an iron binding process, which is unable to take place when iron is intracellular). At 24 hours, the antioxidant ability of the

polyphenols was restored back to the non-iron-preloading state. By repeating this experiment but blocking the polyphenol iron binding site by adding iron, in the short term all the polyphenols further lost their ability to reduce ROS. In the long term, both quercetin and catechin were able to restore lower ROS concentrations; this is interesting since these were the two polyphenols that reduced total cellular iron concentrations.

The results presented demonstrate a dominance of a non-iron chelation mechanism of ROS diminishment, since all the polyphenols tested had ROS reducing activity when they were pre-loaded with iron, even polyphenols identified as having no iron binding activity. This mechanism of ROS sequestration is becoming more accepted, with a direct action of polyphenols reducing intracellular ROS levels.[21, 24]

In summary, polyphenols represent a complex and diverse range of naturally occurring compounds. Their digestive bioavailability and degradation by colonic microbiota make them a difficult collection of potential luminal iron-chelators to assess; it has however been established that, despite lack of conclusively there is evidence to suggest presence within the colon.

Iron binding capabilities have been established with quercetin demonstrating high iron binding affinities. These results were parallel *in vitro* yet *in vivo* no iron chelation ability was evident; this reflects the complex nature of the bio-distribution and metabolism of polyphenols *in vivo*.

With regards to the original aim, specifically, 'to develop a colonic iron chelator, that will chelate excess, free iron, present within the colon, rendering it inert' it can be concluded that quercetin may indeed fit this requisite. The iron modulatory effects of quercetin *in vitro* are interesting, and alongside the report of quercetin supplementation attenuating the progression

of cancer in ApcMin/+ mice, warrants further research into the precise mechanism of action.[25] Whether iron is toxic in the colon by generating ROS is unknown, yet the anti-oxidant nature of the polyphenols here have been established in a colorectal cancer cell line. These results are preliminary in understanding the role of these polyphenols in modulating iron homeostasis, yet with the abundance of possible iron-chelating polyphenols much more experimentation is required to fully understand physiological polyphenol iron binding.

5.4   Experimental

5.4.1   Chemicals and reagents

Cyanidin-3-O-gluocoside (MW = 484.3) was purchased from Polyphenols Laboratories AS and met purification specifications.   Rutin trihydrate (MW = 664.6), quercetin (MW = 302.24) and (+)-catechin hydrate was purchased from Sigma Aldrich; specific catechin concentration was determined using UV-Visible spectroscopy and its specific extinction coefficient.   Chemicals were used as purchased with no further purification.   Intracellular ROS ligand was purchased from LifeTechnologies.

5.4.2   Isothermal Titration Microcalorimetry

Assessment of polyphenol-iron binding, quercetin, rutin, and catechin were dissolved in DMSO to produce a 0.05 M stock solution. Cyanidin-3-O-glucoside was reconstituted in DI H_2O to produce a 0.05 M stock solution. Polyphenols were diluted in potassium phosphate buffer (0.1 M, pH = 7, 4.6 g $HNa_2O_4P \cdot 12H_2O$, 1.6 g H_2KO_4P and 2.9 g NaCl) in DI H_2O (1000 mL) to a concentration of 0.05 mM. Iron chloride solution was prepared by dissolving $FeCl_3 \cdot 6H_2O$ (0.5 mM, 0.054 g) in aqueous HCl (0.1 M) and for ferrous sulphate which was

prepared by dissolving $FeSO_4 \cdot 7H_2O$ (0.5 mM, 0.056 g) in aqueous HCl (0.1 M). All solutions were degassed at a temperature of 35 °C for 5 min before use. Aliquots of ferric or ferrous iron (10 μL, 0.5 mM) were automatically titration into a solution of polyphenol at a temperature of 37 °C with a cell chamber volume of 1360 μL. A total of 40 injections were performed, with a time interval of 500 s between each subsequent injection; the initial titration was set to 2 μL and was discarded in the data analysis. The stirring speed was set to 307 rpm with an initial delay of 60 s and a reference power set to 10 μcal s^{-1}. Measurements were performed on a VPITC MicroCalorimeter and were analysed using MicroCal LLC ITC/Origin software package.

Control titrations were recorded whereby the exact parameters as above were employed, yet buffer only was present in the titration chamber; the heats of these titrations were subtracted from the respective experiments. Data fitting was performed using the MicroCal LLC ITC/Origin software package according to the model of best fit for each data set.

5.4.3 Ferritin western blotting

RKO cells were routinely cultured as previously described in section 3.4.

Sterile polyphenol stock solutions were created by dissolving quercetin, rutin and catechin (0.05 M) in NaOH (0.2 M) and vortexing until complete hydration was evident. Cyanidin-3-O-glucoside was also formulated into a stock solution (0.05 M) in DI H_2O. An iron stock solution was creating by dissolving $FeSO_4 \cdot H_2O$ (108.9 mg, 10 mM) and sodium ascorbate (396 mg, 500 mM) in DI H_2O (40 mL); the resultant solution was dark purple in colour. To create polyphenol stimulation media, polyphenol stocks (60, 6 and 0.6 μL) were mixed with growth medium (15 mL) to create resultant 200, 20 and 2 μM polyphenol-containing mediums. To mediums requiring iron, iron stock (150 μL) was added to the relevant

mediums and mixed. For experimentation, cells were seeded into 6 well plates at a standard concentration (1 x 10^5 cells mL^{-1}, 2 mL) and incubated for 24 hours before growth medium was replaced with stimulation media (2 mL). Cells were incubated for 24 hours and subsequently washed x2 in PBS (2 mL) and the volume of the well void. Subsequently, cells were lysed in RIPA lysis solution (1% 4-Nonylphenyl poly(ethylene glycol) (w/v), 0.5% sodium deoxycholate (w/v), 0.1% sodium dodecyl sulphate (w/v), between 150 – 200 µL depending on cell confluency) on ice.

Western blotting procedure was performed as described earlier in section 3.6

5.4.4   Cellular ^{59}Fe uptake studies

Experiments involving the use of radioactive iron were typically set up as previously discussed, with polyphenol and iron containing culture solutions produced following the described methods. To create ^{59}Fe iron mediums, the stock of iron was spiked with ^{59}FeCl$_3$ to reach ca. 10,000 counts per minute (CPM) per well; this was then used as previously described with a 1:100 dilution into the polyphenol-containing growth medium.

Cells were seeded into 12 well plates at a standard concentration (1 x 10^5 cells mL^{-1}, 1 mL) and incubated for 24 hours before growth medium was replaced with stimulation media (1 mL). Cells were incubated for 24 hours and subsequently washed x2 (2mL) in Versene (0.2 g L^{-1} in PBS) and the volume of the well void. Cells were then lysed in HEPES-saline lysis buffer (150 µL, 10 mM, pH 7.4, NaCl 0.9% (w/v)). To count for radiation content, a specific amount of the sample under investigation (usually ca. 100 µL) was transferred into a scintillation tube and scintillation fluid (1 mL) was added. Radiation CPM counts were normalised to protein concentration as determined in the BCA protein assay (as described previously in section 3.6.

5.4.6   Reactive oxygen species assay

Several perturbations of this experiment were carried out:

i)   *Polyphenol incubation with or without iron*

RKO cells were seeded into 96 well plates at a standard concentration (1×10^5 cells mL^{-1}, 100 µL) and incubated for 24 hours before growth medium was

removed. Cells were subsequently washed x3 with PBS (200 μL). The ROS ligand (Cm-H$_2$DCFDA, 50 μg) was dissolved in 100% ethanol and made to a working concentration (5 μM) in PBS) and was pipetted onto the cells (100 μL) and incubated for 1 hour. After this time period, a baseline reading was taken (t=0) at λ = 485/535 nm. The ROS ligand was removed from the cells and again, cells were washed x3 with PBS (200 μL) before the addition of the polyphenol containing media with or without iron (as prepared in the above protocol). Time points were recorded at 3 hours, 12 hours and 24 hours.

ii) *Preload with iron followed by polyphenol incubation*

RKO cells were seeded into 96 well plates at a standard concentration (1 x 10^5 cells mL^{-1}, 100 μL) and incubated for 12 hours before the addition of ferrous sulphate (1 μL, FeSO$_4$·7H$_2$O, 100 μM in DI H$_2$O) and subsequently incubated for a further 12 hours. Iron-rich growth medium was removed and Cells were subsequently washed x3 with PBS (200 μL). The ROS ligand (Cm-H$_2$DCFDA, 50 μg) was dissolved in 100% ethanol and made to a working concentration (5 μM) in PBS) and was pipetted onto the cells (100 μL) and incubated for 1 hour. After this time period, a baseline reading was taken (t=0) at λ = 485/535 nm. The ROS ligand was removed from the cells and again, cells were washed x3 with PBS (200 μL) before the addition of the polyphenol containing media (catechin, rutin, cyanidin-3-O-glucoside and quercetin, 20 μM) **without** iron (as prepared in the above protocol). Time points were recorded at 3 hours, 12 hours and 24 hours.

iii) *Preload with iron following by polyphenol with iron incubation*

The same protocol as outlined in (ii) was undertaken, yet upon incubation in the polyphenol containing media, iron ($FeSO_4 \cdot 7H_2O$, 100 μM) was present.

In each experiment, a control plate containing polyphenol only with no cells was prepared such that the absorption arising from the polyphenols could be subtracted.

5.4.7 Redox activity assay

For the assessment of redox acivty, quercetin, rutin, and catechin were dissolved in DMSO to produce a 1 mM stock solution. Cyanidin-3-O-glucoside was reconstituted in DI H_2O to produce a 1 mM stock solution. Polyphenols were diluted in potassium phosphate buffer (0.1 M, pH = 7, 4.6 g $HNa_2O_4P \cdot 12H_2O$, 1.6 g H_2KO_4P and 2.9 g NaCl) in DI H_2O (1000 mL) to a concentration of 12.5 μM such that the resultant volume was 4 mL. To this, ferrozine solution (5 mM, 200 μL) was added and vigoursly mixed. Ferric iron ($FeCl_3 \cdot 6H_2O$) or ferrous iron ($FeSO_4 \cdot 7H_2O$) was prepared (1 mM in 0.1 M HCl) of which 25 μL was added and the resultant mixture vortexed. Solutions were incubated in the dark for 24 hours at 37 °C. After this period, solutions were well mixed and pipetted in triplicate onto a 96 well plate ready for reading on a plate reader at λ = 550 nm. In order to account for the absorption observed due to the inhert absoabtive nature of the polyphenols, alike concentrations were mixed as above without the additon of the ferrozine ligand. These were similar read and the values subtracted from those obtained from the ferrozine ligand.

5.5   References

1.   Graham, H.N., *Green tea composition, consumption, and polyphenol chemistry.* Preventive medicine, 1992. **21**(3): p. 334-350.
2.   Jin, F., et al., *Effects of ascorbic acid, phytic acid and tannic acid on iron bioavailability from reconstituted ferritin measured by an in vitro digestion-Caco-2 cell model.* Br J Nutr, 2009. **101**(7): p. 972-81.

3. Khokhar, S. and R.K. Owusu Apenten, *Iron binding characteristics of phenolic compounds: some tentative structure–activity relations.* Food Chemistry, 2003. **81**(1): p. 133-140.

4. Williamson, G. and C. Manach, *Bioavailability and bioefficacy of polyphenols in humans. II. Review of 93 intervention studies.* The American Journal of Clinical Nutrition, 2005. **81**(1): p. 243S-255S.

5. Yang, C.S., et al., *Blood and urine levels of tea catechins after ingestion of different amounts of green tea by human volunteers.* Cancer Epidemiol Biomarkers Prev, 1998. **7**(4): p. 351-4.

6. Kahle, K., et al., *Studies on apple and blueberry fruit constituents: do the polyphenols reach the colon after ingestion?* Mol Nutr Food Res, 2006. **50**(4-5): p. 418-23.

7. Czank, C., et al., *Human metabolism and elimination of the anthocyanin, cyanidin-3-glucoside: a (13)C-tracer study.* Am J Clin Nutr, 2013. **97**(5): p. 995-1003.

8. Manach, C., et al., *Bioavailability of rutin and quercetin in rats.* FEBS Letters, 1997. **409**(1): p. 12-16.

9. Manach, C., et al., *Bioavailability and bioefficacy of polyphenols in humans. I. Review of 97 bioavailability studies.* Am J Clin Nutr, 2005. **81**(1 Suppl): p. 230s-242s.

10. Ryan, P. and M.J. Hynes, *The kinetics and mechanisms of the reactions of iron(III) with quercetin and morin.* Journal of Inorganic Biochemistry, 2008. **102**(1): p. 127-136.

11. Guo, M., et al., *Iron-binding properties of plant phenolics and cranberry's bio-effects.* Dalton transactions (Cambridge, England : 2003), 2007(43): p. 4951-4961.

12. Nowak, D., A. Kuźniar, and M. Kopacz, *Solid complexes of iron(II) and iron(III) with rutin.* Structural Chemistry, 2010. **21**(2): p. 323-330.

13. Fang, J., *Bioavailability of anthocyanins.* Drug Metabolism Reviews, 2014. **46**(4): p. 508-520.

14. Elhabiri, M., et al., *Complexation of iron(III) by catecholate-type polyphenols.* Inorganica Chimica Acta, 2007. **360**(1): p. 353-359.

15. Vlachodimitropoulou, E., P.A. Sharp, and R.J. Naftalin, *Quercetin–iron chelates are transported via glucose transporters.* Free Radical Biology and Medicine, 2011. **50**(8): p. 934-944.

16. Lesjak, M., et al., *Quercetin Inhibits Intestinal Iron Absorption and Ferroportin Transporter Expression <italic>In Vivo</italic> and <italic>In Vitro</italic>.* PLoS ONE, 2014. **9**(7): p. e102900.

17. Baccan, M.M., et al., *Quercetin as a shuttle for labile iron.* Journal of Inorganic Biochemistry, 2012. **107**(1): p. 34-39.

18. Hynes, M.J. and M.n. Ó Coinceanainn, *Investigation of the release of iron from ferritin by naturally occurring antioxidants.* Journal of Inorganic Biochemistry, 2002. **90**(1–2): p. 18-21.

19. RiceEvans, C.A., N.J. Miller, and G. Paganga, *Structure-antioxidant activity relationships of flavonoids and phenolic acids.* Free Radical Biology and Medicine, 1996. **20**(7): p. 933-956.

20. RiceEvans, C.A., J. Miller, and G. Paganga, *Antioxidant properties of phenolic compounds.* Trends in Plant Science, 1997. **2**(4): p. 152-159.

21. Perron, N.R. and J.L. Brumaghim, *A review of the antioxidant mechanisms of polyphenol compounds related to iron binding.* Cell Biochem Biophys, 2009. **53**(2): p. 75-100.

22. Szatrowski, T.P. and C.F. Nathan, *Production of large amounts of hydrogen peroxide by human tumor cells.* Cancer Res, 1991. **51**(3): p. 794-8.

23. Storz, P., *Reactive oxygen species in tumor progression.* Front Biosci, 2005. **10**: p. 1881-96.

24. van Acker, S.A., et al., *Influence of iron chelation on the antioxidant activity of flavonoids.* Biochem Pharmacol, 1998. **56**(8): p. 935-43.

25. Velazquez, K.T., et al., *Quercetin Supplementation Attenuates the Progression of Cancer Cachexia in Apc(Min/+) Mice.* Journal of Nutrition, 2014. **144**(6): p. 868-875.

Chapter 6

Conclusions and future work.

There is a clear role for iron in the pathogenesis of intestinal disease, most notably in colorectal cancer and inflammatory bowel disease. Iron, with its ability to catalyse the formation of damaging redox species, alongside its ability to have direct effects on cellular oncogenic processes and also its requirement in proliferating cells justifies iron as a target for therapeutic intervention. However, it is unknown how iron is contributing to an inflammatory and carcinogenic phenotype. In addition, the form of iron present within the large intestine that is driving this process is unknown. Regardless of this, it has been demonstrated that excess iron present within the intestinal lumen is responsible for the development of colorectal cancer, and the development of a luminal iron chelator is sought.

To achieve luminal iron chelation, the therapeutic compound must not demonstrate any cellular absorbability and it must chelate iron to render its toxic nature inert. Of the dietary iron chelators tested herein, Manucol LD has been identified as the ideal therapeutic agent that demonstrates the stated characteristics. The chemical composition that imparts Manucol LD with this bioactivity was probed and it was identified that Manucol LD contains a unique iron

binding structure, formed from a specific sequence arrangement of its chemical monomer units. Iron binding within this cavity results in efficient chelation, where it has been identified that the form of iron within this unit is an iron-oxide nanoparticle. This formatting of iron into nanoparticles endows Manucol LD with its desired physiological properties.

In order to fully validate Manucol LD as a luminal iron chelator the next step would be to test the tolerability and efficacy of this compound in man. Formulation of Manucol LD would need to be carefully investigated as specific luminal iron within the colon needs to be targeted. Alongside *in vivo* studies, it would also be scientifically worthwhile probing the iron-chelation mechanism of Manucol LD further and demonstrating its anti-neoplastic activity was mediated through an iron chelation mechanism. Using the techniques established in this thesis would allow the modification of any alginate and, with subsequent composition analysis, the chemical requirements of an alginate that bestows it with its iron-chelation ability would be identified; such information would allow synthesis of 'next generation' luminal iron chelators that may have an ever great affinity towards iron.

Looking towards the future, the influence of diet on the intestinal microbiome is currently becoming an evermore popular research area, and as such it could be speculated that iron is generating a carcinogenic phenotype through the modulation of intestinal microbiota. If this were the case, then a new area of study understanding the role of iron in manipulating the gut flora enterotype could be established. Alginates such as Manucol LD may have efficacy in this respect, acting as pre-biotic through its iron chelation ability. In light of this, the major form of iron present within the large intestine must be characterised, since this information will be central in understanding how iron may be modulating the gut environment.

In conclusion, alginate Manucol LD has been established as a novel luminal iron chelator. The work presented here demonstrates the rationale in utilising these types of natural biopolymers for the treatment of gastrointestinal disease and the prevention of colorectal cancer.

Appendices:

A1: Materials and suppliers

SIGMA ALDRICH (POOLE, DORSET)	(+)-catechin hydrate 1-ethyl-3-(3dimethylaminopropyl)carbodiimide 2-Mercaptoethanol 2-propanol 3-(2-Pyridyl)-5,6-diphenyl-1,2,4-triazine-p,p'-disulfonic acid monosodium salt 3-(trimethylsilyl)-propionic-2,2,3,3-d4 4-Nonylphenyl poly(ethylene glycol) Acetic acid Acetone Ammonium persulphate Apo-transferrin Bromophenol blue Calcium chloride dehydrate Chloroform Deuterium oxide Dialysis membrane Dimethyl sulfoxide Ferrous sulphate heptahydrate Fluoresceinamine Formaldehyde Glycerol, glycine Hydrochloric acid Hydrocortisone Hydrogen peroxide Isopropanol Isopropyl beta-D-1-thiogalactopyranoside lauryl sulphate LB Broth Methanol MOPS n-Hydroxysulfosuccinimide sodium salt Non-essential amino acid solution Paraformaldehyde Phosphate buffered saline Piperazine-N,N'bis[2-ethanesulfonic acid] Quercetin Rutin trihydrate Sodium acetate Sodium ascorbate Sodium carbonate Sodium chloride Sodium deoxycholate Sodium dodecyl sulphate sodium selenite Tamoxifen tetramethylethylenediamine

	tri-sodium citrate trichloroacetic acid triiodothyronine Tris HCl Trizma base Tween 20
FMC BIOPOLYMER (DENMARK) *A KIND GIFT FROM DR. TROND HELGERUD*	Manucol LD, Manucol DH, Manugel GHB, LFR5/60, Protsea AFH, Protanal RF6650 and Keltone.
INVITROGEN (PAISLEY, RENFREWSHIRE)	Dulbecco's Modified Eagles Medium Foetal calf serum Maxi prep Penstrep Trizol Trypsin EDTA
ROCHE APPLIED SCIENCE (LEWES, EAST SUSSEX)	Proteinase and phosphatase inhibitor cocktail
GENEFLOW (SOUTHAMPTON)	Acrylamide/ bisacrylamide
FISHER SCIENTIFIC (LOUGHBOROUGH, LEICESTERSHIRE)	BCA protein assay
CHANCE PROPPER (SMETHWICK, WEST MIDLANDS)	Glass coverslips
AMSERSHAM PHARMACIA (AMSERSHAM, BUCKINGHAMSHIRE)	ECL reagent Hybond PVDF membranes Hyerfilm x-ray film
JACKSON LABS (BALTIMORE, PA)	Secondary peroxidase linked antibodies Anti-rabbit (1:10,000 dilution) Anti-mouse (1:10,000 dilution)
PERKIN ELMER (COVENTRY, WEST MIDLANDS)	Iron-59 Radionuclide: 1mCi Optiphase HiSafe 3Scintillation fluid
ABCAM (CAMBRIDGE)	β-actin, 1:5,000 dilution AB8226 Ferritin light-chain, 1:5000 dilution AB69090 TfR1, 1:1000, Invitrogen H68.4
LIFE TECHNOLOGIES (PAISLEY)	CellMask Deep Red plasma Hoechst 33450 Intracellular ROS ligand SureFade
ATI ATLAS (CHICHESTER, WEST SUSSEX)	Spectro Ferritin MT Kit
MP BIOMEDICALS (LOUGHBOROUGH	Insulin

LEICESTER)	
VWR INTERNATIONAL MARKETPLACE (LUTTERWORTH, LEICESERSHIRE)	Sephadex^{TM} G-25 HiTrap Q Sepharose HP column (Pharmacia)
NEW ENGLAND BIOLABS (HERTFORDSHIRE)	Human Epidermal Growth Factor (hEGF)
QIAGEN	QI Aprep Spin Mini Prep kit
EUROFINS GENOMICS (EBERSBERG)	Reverse primers
POLYPHENOL LABORATORIES (SANDNES)	Cyanidin-3-O-gluocoside

A2: Full paper publications

Horniblow, R. D., M. Dowle, T. H. Iqbal, G. O. Latunde-Dada, R. E. Palmer, Z. Pikramenou and C. Tselepis (2015). "*Alginate-Iron Speciation and Its Effect on In Vitro Cellular Iron Metabolism*." PLoS One 10(9): e0138240.

Bedford, M. R., S. J. Ford, **R. D. Horniblow**, T. H. Iqbal and C. Tselepis (2013). "*Iron Chelation in the Treatment of Cancer: A New Role for Deferasirox?*" Journal of Clinical Pharmacology 53(9): 885-891

A3: Abstract publications

Horniblow, R., S. Radulescu, M. Schneider, M. Dowle, T. Iqbal, R. Palmer, G. Latunde-Dada, Z. Pikramenou and C. Tselepis (2014). "*Iron chelation by biopolymers for an anti-cancer therapy; binding up the 'ferrotoxicity' in the colon.*" European Journal of Cancer 50: S173-S173.

Horniblow, R., D. Stones, S. Radulescu, O. Sansom, Z. Pikramenou and C. Tselepis (2013). "*BINDING OF LUMINAL IRON USING ALGINATES AS A THERAPY FOR BOWEL CANCER.*" American Journal of Hematology 88(5): E182.

RESEARCH ARTICLE

Alginate-Iron Speciation and Its Effect on *In Vitro* Cellular Iron Metabolism

Richard D. Horniblow[1], Miriam Dowle[2], Tariq H. Iqbal[1], Gladys O. Latunde-Dada[3], Richard E. Palmer[2], Zoe Pikramenou[4☉], Chris Tselepis[1☉]*

1 University of Birmingham, School of Cancer Sciences, College of Medical and Dental Sciences, Vincent Drive, Edgbaston, Birmingham, B15 2TT, United Kingdom, 2 University of Birmingham, School of Physics, College of Engineering and Physical Sciences, Edgbaston, Birmingham, B15 2TT, United Kingdom, 3 Diabetes and Nutritional Sciences, King's College London, Franklin Wilkins Building, 150 Stamford Street, London, SE1 9NH, United Kingdom, 4 University of Birmingham, School of Chemistry, College of Engineering and Physical Sciences, Edgbaston, Birmingham, B15 2TT, United Kingdom

☉ These authors contributed equally to this work.
* c.tselepis@bham.ac.uk

Abstract

Alginates are a class of biopolymers with known iron binding properties which are routinely used in the fabrication of iron-oxide nanoparticles. In addition, alginates have been implicated in influencing human iron absorption. However, the synthesis of iron oxide nanoparticles employs non-physiological pH conditions and whether nanoparticle formation *in vivo* is responsible for influencing cellular iron metabolism is unclear. Thus the aims of this study were to determine how alginate and iron interact at gastric-comparable pH conditions and how this influences iron metabolism. Employing a range of spectroscopic techniques under physiological conditions alginate-iron complexation was confirmed and, in conjunction with aberration corrected scanning transmission electron microscopy, nanoparticles were observed. The results infer a nucleation-type model of iron binding whereby alginate is templating the condensation of iron-hydroxide complexes to form iron oxide centred nanoparticles. The interaction of alginate and iron at a cellular level was found to decrease cellular iron acquisition by 37% (p < 0.05) and in combination with confocal microscopy the alginate inhibits cellular iron transport through extracellular iron chelation with the resulting complexes not internalised. These results infer alginate as being useful in the chelation of excess iron, especially in the context of inflammatory bowel disease and colorectal cancer where excess unabsorbed luminal iron is thought to be a driver of disease.

Introduction

Alginates are a diverse class of biopolymers extracted from brown algae that are composed of 1–4 linked β-D-mannuronic acid (M) and α-L-guluronic acid (G) monomers. The polymers can vary in both chain length and composition which, in conjunction with their ability to interact with divalent metal cations, endows alginates with a wide range of physicochemical properties. Thus unsurprisingly alginates are widely used in the food industry, primarily due to their

gelling capacity, and are also used in a range of medical applications, for example, in wound-healing preparations[1], controlled drug release systems[2,3] and anti-reflux formulations.[4] In addition, alginates are used for the construction of iron-oxide nanoparticles which have a myriad of applications from drug delivery to magnetic resonance imaging.[5]

The use of alginate as a scaffold for nanoparticle formulation is a well-accepted synthetic strategy, however, in these reactions the iron-oxide nanoparticles are fabricated using chemical-forcing conditions whereby highly basic conditions are used to form the iron hydroxide.[5–8] These conditions are considered optimal for the formation of iron oxide nanoparticles, with mean diameters ranging between 9 to 10 nm.[9,10] However, whether these iron oxide nano-particles can form spontaneously in the gastrointestinal tract of man and in particular at low pH conditions of the stomach, (the first reasonable site of interaction between iron and alginate consumed in the diet) is unknown.

Supporting the concept of alginate binding iron, there is an increasing body of evidence emerging that alginates impact on iron metabolism in man.[11,12] A recent human study identified that an alginate supplemented diet resulted in decreased serum iron levels, alluding to the role of alginates chelating iron and thus limiting its absorption in the small bowel.[12] On the contrary, cellular studies have previously shown alginate as having an enhancing effect on intracellular iron concentration as assessed by ferritin expression; a surrogate biomarker for cellular iron levels.[13] However, whether these observed changes in cellular iron metabolism are related to the formation of alginate-iron nanoparticles is unknown. Interestingly, iron-oxide nanoparticles have been studied with respect to their cellular uptake with a potential application in iron fortification to treat anaemia.[14–16] No toxicity was associated with the uptake of these nanoparticles and results indicated that these Fe(III) nanoparticles were directly taken up by enterocytes *in vitro* and markedly increased cellular iron concentrations.

Thus, the existing published literature is inconsistent and it remains unclear how alginates might interact with iron in the context of the gut and whether any resulting complexation may be of use as a platform for iron fortification or chelation.

Therefore, the aims of this study are i) to determine how alginate and iron(III) interact at gastric-comparable pH conditions; ii) to verify the speciation of iron with alginate upon complexation under these conditions and iii) to understand how alginate modulates cellular iron status.

Materials and Methods

Alginate preparation

Sodium alginate LFR5/60 was a kind gift of FMC Biopolymer, Norway. The average molecular weight is 34700 Da and a G/M composition of 65%/35%. Dispersion of alginates into water was achieved through high vortex stirring and solutions left overnight to ensure full hydration.

Isothermal Titration Calorimetry

An adapted protocol was used whereby iron was titrated into LFR5/60 at 37°C.[17] Isothermal Titration Calorimetry (ITC) measurements were performed on a VPITC MicroCalorimeter and data was automatically analysed using MicoCal LLC ITC/Origin software package; the binding isotherm was obtained by integrating injections and fitting them to an appropriate binding model. All alginate solutions were excessively dialysed before use, to eliminate errors caused by pH and ionic strength mismatches, and also degassed before use at 2°C below the titration temperature. Typical experimental parameters included: 37°C cell temperature, 10 µcal s^{-1} reference power, stirring speed at 286 rpm with the initial injection being small (2 µl) and discarded in the data analysis. Titration was performed by injection of 8 µl aliquots

of aqueous iron (III) chloride (5mM) in DI H_2O into a solution of aqueous LFR5/60 (0.07 mM, pH = 5.8) in DI H_2O. A delay of 350 sec between each injection was set to allow the energy difference to return back to baseline. To account for the high energy changes associated with iron titration into water (the control titration), these heat integrations were subtracted from that of the alginate-iron titration and the subsequent heats of interaction were fitted using a model of two binding sites.

Equilibrium dialysis preparation of alginate-iron composites

Alginate solutions (0.1% w/v, 10 ml) were sealed into a dialysis membrane (M_r cut off = 12,400 Da) and incubated in aqueous $FeCl_3 \cdot 6H_2O$ (10 mM, 750 ml) for 120 min and washed in deionised water for a subsequent 120 min. The pH changes of the alginate were tracked over the period of the incubation. The pH of the alginate inside the dialysis bag pre-incubation was 5.8 and the pH of iron solution pre incubation was 1.7, equivalent to gastric acidity.[18] The pH of the alginate after incubation was 1.9 and after the wash period this was 3.7.

UV-visible spectroscopy

Absorption spectra were recorded on a Varian Cary50 spectrometer using a quartz cuvette, path length 1 cm. Increments of varying volumes of aqueous $FeCl_3 \cdot 6H_2O$ (10mM) in DI H_2O were titrated into a stirred solution of aqueous alginate (2 mL, 0.1% w/v) in DI H_2O, allowed to equilibrate for several seconds and then scanned. Measurements were taken up to a point of saturation. To correct for the absorption of aqueous-iron species at the wavelengths of interest difference absorbance spectra were obtained by correction of the alginate titration with the equimolar iron-water control titration.

CD-spectroscopy

CD measurements were recorded on a Jasco J-810 CD spectropolarimeter (4 accumulations with 1 s response) using a 1cm path length, blackened quartz cell. Samples for CD measurements were prepared as described for the dialysis preparations above.

Cell culture

Human RKO colorectal carcinoma cells (obtained from the ACTT CRL-2577) were routinely cultured in Dulbecco's modified eagles medium including 10% v/v foetal calf serum, 100 units/ml penicillin and 0.1 mg/ml streptomycin. Cells were seeded in six well plates at a concentration of $1x10^5$ cells/ml and grown in medium alone for 24 hours. Once established, the growth medium was removed and supplemented medium was added (Iron loaded medium: 100 μM $FeSO_4 \cdot 7H_2O$ and 10 μM sodium ascorbate or alginate loaded medium: LFR5/60 (0.3% (w/v)), 100 μM $FeSO_4 \cdot 7H_2O$ and 10 μM sodium ascorbate)) and incubated for 24 hours. Preparation of these media was performed as follows; aqueous $FeSO_4 \cdot 7H_2O$ (100 μL, 10 mM) containing sodium ascorbate (500 mM) in DI H_2O was added to a sample of aqueous sodium alginate (1.5 mL, 2% w/v) in DI H_2O and mixed. Growth medium was then added (8.4 mL) and all constituents were thoroughly mixed. Where alginate was not supplemented, growth medium (9.9 mL) was added to the iron only. After 24 hours the medium was removed and the cells washed three times with phosphate buffered saline (PBS). Cells were lysed on ice in RIPA buffer (nonyl phenoxypolyethoxylethanol 1% (v/v), sodium deoxycholate 0.5% (w/v) and sodium dodecyl sulphate 0.1% (w/v)) containing protease inhibitors. All samples were then sonicated for 10 sec whilst kept at 4°C. A protein assay kit (Peirce BCA protein assay) was used to determine the protein concentration in each sample.

Western blotting

Western blotting was performed as previously described, with monoclonal antibodies to ferritin (1:5000, Abcam, Rabbit AB69090) and β-actin (1:5000, Abcam, Mouse AB8226).[19] All blots were subject to densitometry analysis using ImageJ analysing software and data normalised to respective β-actin loading controls.

Synthesis of FITC-alginate

Synthesis of FITC-alginate was performed according to the protocol of Strand *et al.* [20] Sodium alginate LFR5/60 (0.32 g, 9.2×10^{-6} moles) was dissolved in a solution of phosphate buffered saline at pH 7.4 (50 ml). 1-ethyl-3-(3-dimethylaminopropyl)carbodiimide) (0.018 g, 9.2×10^{-5} moles) and n-Hydroxysulfosuccinimide sodium salt (0.02 g, 9.2×10^{-5} moles) was added to the alginate solution and stirred for two hours. Once mixed, fluoresceinamine (0.0319 g, 9.2×10^{-5} moles) was added and the reaction left to stir in darkness for 24 hours. Free, unreacted fluorophore was removed by extensive dialysis; one wash in deionised H_2O (3.5 L) at 4°C for 24 hours, three washes in NaCl (3.5 L, 1 M) for 24 hours each, then a subsequent six washes in deionised H_2O (3.5 L) for 24 hours each. Once purified, the pH of the solution was adjusted to 7.4 and stored in the dark at 4°C until required.

Confocal microscopy

Slides for confocal microscopy were prepared by growing RKO cells on sterile 22 mm cover slips placed in individual wells of a six well cell culture plate. Cells were seeded in six well plates at a concentration of 1×10^5 cells/ml and grown in medium alone for 24 hours. Once established, cell permeabilisation was performed using saponin (50 μg/ ml) as previously described. [21] The growth medium was replaced with fluorescent-alginate loaded medium (0.04% fluorescent alginate, 100 μM $FeSO_4 \cdot 7H_2O$ and 10 μM sodium ascorbate) and incubated for 24 hours. Cell nuclei and plasma membranes were subsequently stained with Hoechst 33450 (NucBlue Live Cell Stain, Life technologies) and CellMask Deep Red plasma stain, (Life technologies) respectively and cells fixed with a 4% paraformaldehyde solution (pH 7.4) at room temperature. Once fixed images were captured using a Zeiss LSM510 META confocal system with x63 1.4 oil immersion objective.

Intracellular iron assessment

Cells were seeded in six well plates at a concentration of 1×10^5 cells/ml and grown in medium alone for 24 hours. Once established, the growth medium was removed and supplemented medium was added (Iron loaded medium: 100 μM $FeSO_4 \cdot 7H_2O$ and 500 μM sodium ascorbate, or alginate loaded medium: LFR5/60 (0.3% (w/v)), 100 μM $FeSO_4 \cdot 7H_2O$ and 500 μM sodium ascorbate)) and incubated for 24 hours; in both instances iron stimulations were spiked with $^{59}FeCl_3$ to reach ca. 10,000 counts per minute (CPM) per well. To prepare the radio-active iron medium with alginate, aqueous $FeSO_4 \cdot 7H_2O$ (100 μL, 10 mM) in DI H_2O containing sodium ascorbate (500 mM) in DI H_2O was mixed with $^{59}FeCl_3$ in aqueous HCl (0.1M). This was then added to aqueous sodium alginate (1.5 mL, 2% w/v) in DI H_2O and thoroughly mixed. Growth medium was then added (8.4 mL) and all constituents mixed. In iron-only supplemented media, no sodium alginate was added, only the addition of growth medium (9.9 mL) to the radio-active iron. After this incubation period the medium was removed and cells washed three times with 2 ml Versene (0.2g/L EDTA in phosphate buffered saline), and lysed in 150 μl HEPES-saline lysis buffer (10 mM, pH 7.4, NaCl 0.9% (w/v)). To determine cellular iron content, the lysates were pipetted into scintillation tubes containing scintillation fluid (1 mL,

PerkinElmer OPTIPHASE HISAFE3) and counted on a gamma-counter (Packard 2500 TR liquid scintillation counter).

Scanning Transmission Electron Microscopy/ Energy-dispersive X-ray spectroscopy

Alginate-iron samples used for STEM/EDX were made using the equilibrium dialysis technique as described earlier. Preparation of these samples was performed as follows; aqueous sodium alginate (10 mL, 0.1% w/v, pH 5.8) in DI H_2O was sealed within a dialysis membrane and immersed in a pre-mixed solution of $FeCl_3 \cdot 6H_2O$ (10 mM, 750 ml, pH 1.7) for 120 min. The dialysis bag was removed, and subsequently immersed in pure DI H_2O (750 mL) and incubated for another 120 min. Due to the viscous nature of the sample, copper TEM grids coated with lacey carbon were loaded with 50 µl of sample and excess sample was drawn from underneath, effectively pulling the sample through the grid. This produced a thin sample coverage over the grid with many sampling areas.

Electron microscopy images were taken using a 200kV FEG Jeol 2100F scanning transmission electron microscope fitted with a CEOS aberration corrector. Images were simultaneously acquired in high angular annular dark field (HAADF) and bright field (BF) mode using the Gatan DigitalMicrograph software package.

Results

Studies of iron-alginate complexation

Isothermal titration microcalorimetry (ITC) was performed to examine the strength of interaction between iron and alginate (LFR5/60). Iron(III) chloride was titrated into a solution of LFR5/60 and a drop in the integrated heats of each addition was observed (Fig 1A) Saturation of iron binding by alginate occurred at a molar ratio of iron:alginate of 3:1, with a 5 times excess of iron used to ensure saturation of all the binding sites on the alginate. Data analysis, which was best fit using a two-site binding model, revealed two binding events between alginate and iron with the estimated binding constants calculated as $K_1 = 1X10^6$ and $K_2 = 3X10^4$ M^{-1} respectively. The equation that models this binding can be found in S1 Fig. Entropy was positive in both binding events (18.4 and 23.2 cal mol^{-1} K^{-1}). Enthalpy values were found to be exothermic for both binding events (-704 x 10^4 and -1548 cal mol^{-1}).

The binding of ferric ions to alginate was further verified using UV-Visible and Circular Dichroism (CD) spectroscopy. (Fig 1B and 1C) Titration of an aqueous solution of Fe(III) to an aqueous solution of sodium alginate LFR5/60 revealed the growth of a band at 280 nm (Fig 1C); confirming iron binding to alginate. Profile changes were plotted against molar equivalents of iron and a binding plot for alginate iron binding was obtained (Fig 1B). This data can be fitted to a 1:1 binding equation and an alginate iron binding constant of $K = 1X10^3$ M^{-1} calculated (S2 Fig).

To further support the spectroscopic results demonstrating alginate complexation, CD spectroscopy was also performed since its fundamental application is probing transitions within chiral compounds; alginate is highly chiral due to its polymeric nature and the chiral carbon centres on the individual monomers. Alginate-iron complexes were isolated using equilibrium dialysis. The CD spectrum of the isolated iron-alginate complexes shows the appearance of a peak at 280 nm (Fig 1C), which correlates with the peak identified in the UV-visible spectrum (Fig 1B). This profile is indicative of iron hydroxide (Fe-OH) binding and confirms that the changes observed in the UV-visible spectrum are attributed to the alginate binding to Fe-OH species in solution (Fig 1C).
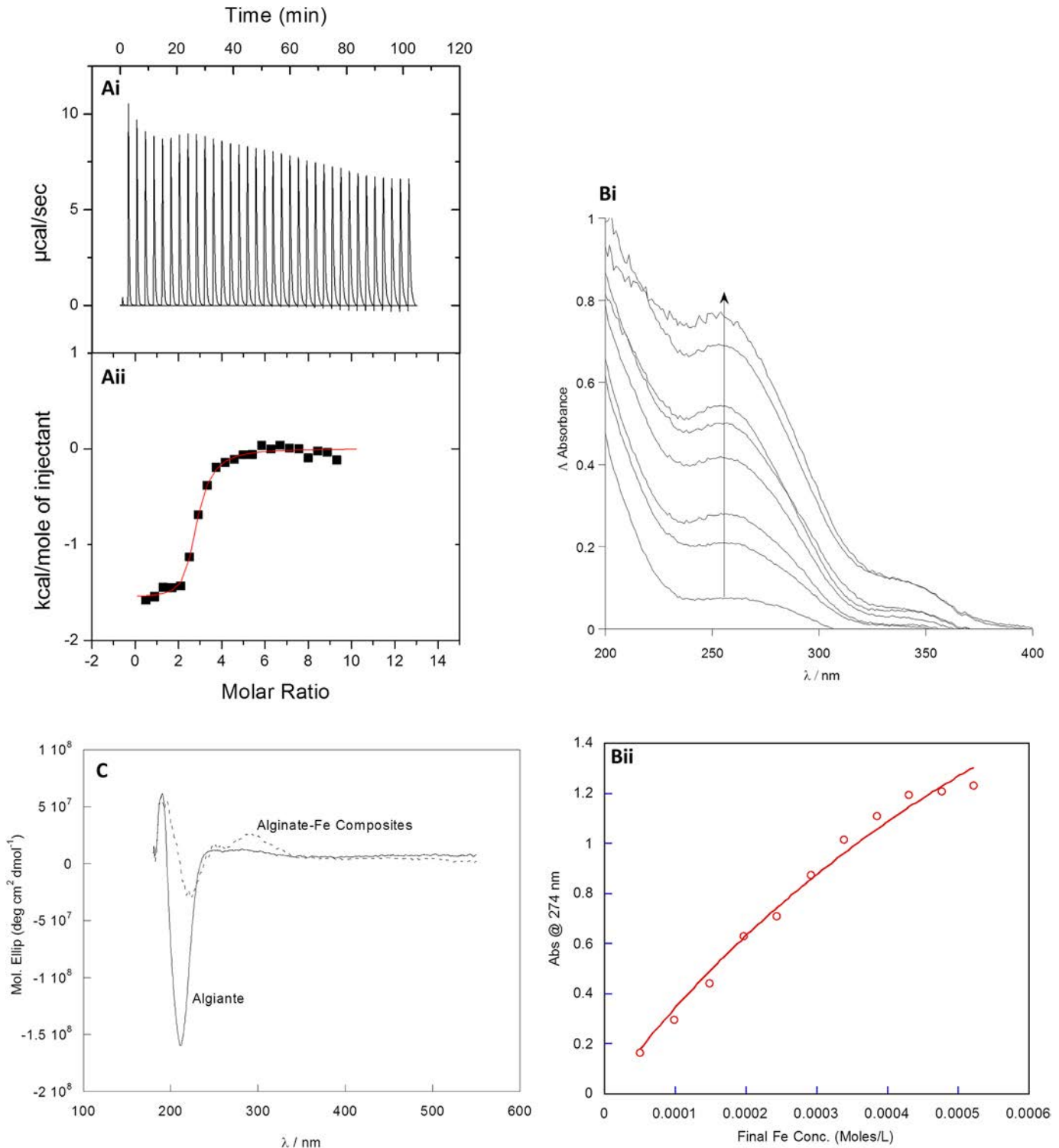
Fig 1. Chemical analysis of iron alginate binding. (Ai) Isothermal titration microcalorimetry thermogram of 8 μl injectants of 5 mM Fe(III) into 0.04 mM alginate at 37°C. (Aii) Corresponding isotherm. (Bi) UV-Visible difference spectra of iron (III) titrated into alginate with a clear absorbance change at ca. 280 nm (Bii) absorbance change at 274nm vs final Fe concentration (M) with binding curve) (C) CD spectra of alginate-iron composites isolated via equilibrium dialysis. An induced CD signal is evident at ca. 280 nm. This correlates to the iron-hydroxide species bonded to the alginate as indicated from the UV-Visible spectra.

Alginates template iron oxide nanoparticle formation under simple mixing conditions

As CD identified the presence of Fe-OH within the alginate-iron composites, these were further characterised using aberration corrected STEM (Fig 2). This is capable of achieving ultra-high resolution with atomic number contrast imaging in the material sciences, but is rarely used to investigate 'biological' samples due to the low atomic number of most bio-materials. [22] However, the iron component of the alginate-iron composites provided distinguishable contrast, thus it was possible to image atomic structure at the highest resolution (Fig 2).

Low magnification HAADF-STEM imaging revealed a gel-like alginate network covered in iron with dense nucleation-sites present (Fig 2A) while energy-dispersive X-ray spectroscopy confirmed that these dense centres indeed contained iron (Fig 2C). Within this gel, small nano-particles with a mean diameter of 1.78 ± 0.70 nm were detected and under higher magnification lattice structures could be visualised within these nanoparticles (Fig 2B). Fast Fourier transform analysis of the lattice arrangements gave diffraction spots (labelled) which were in partial agreement with both Fe_2O_3 hematite, and ferrihydrite, but the small particles yielded insufficient visible bright spots to determine the precise phase of these nanoparticles.[6,23] Samples of aqueous iron chloride alone were imaged and there was no evidence of particulate iron.
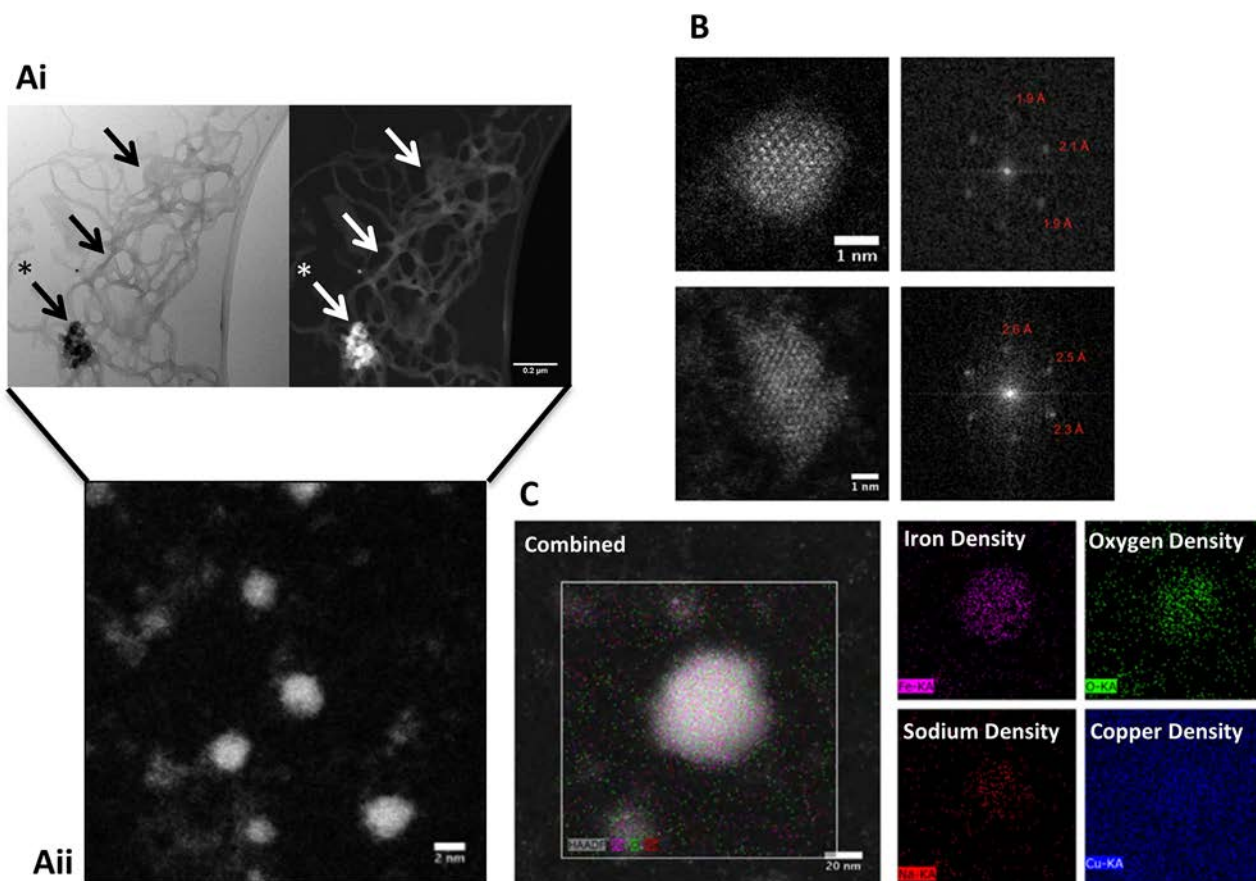

Fig 2. Physical characterisation of alginate iron composites. (Ai) Low magnification STEM images of alginate-iron composites revealed the alginate network 'decorated' in iron (denoted by arrows) with a single highly dense iron nucleation site (denoted with an asterisk). (Aii) A higher magnification image of the nucleation centre revealed nanoparticles of approximately 2–5 nm in diameter. (B) Fast Fourier transform analysis of HAADF-STEM images of two individual nanoparticles. (C) EDX mapping of iron-alginate composites with oxygen, iron and sodium localisation shown in the sample area. The copper from the copper TEM grid functions as a control.

doi:10.1371/journal.pone.0138240.g002
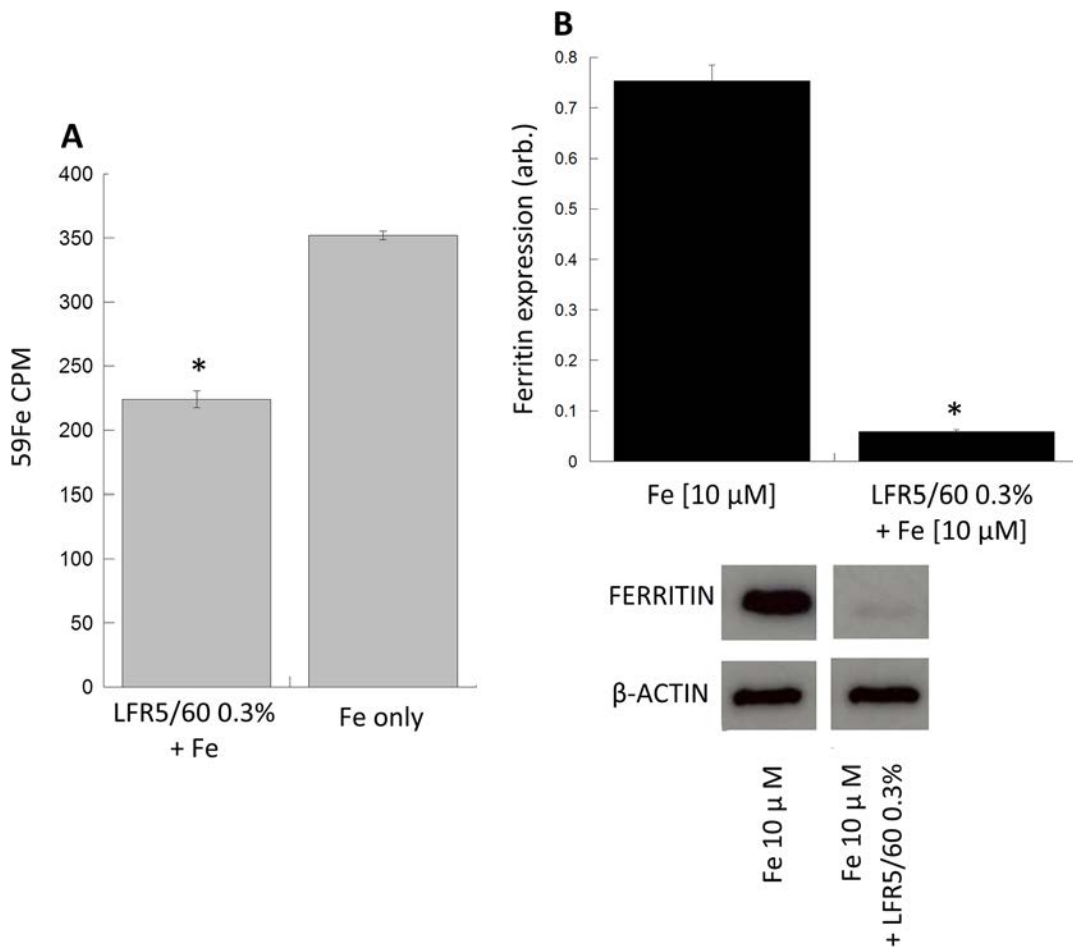
Fig 3. Effects of alginate on cellular iron transport. (A) Intracellular iron concentration decreases when RKO cells were incubated with iron-59 and alginate (0.3% w/v) compared to iron only control (B) Treatment of RKO cells with iron increases ferritin expression whilst co-incubation with alginate (0.3% w/v) significantly suppressed the iron mediated ferritin induction. All experiments were performed in triplicate with error bars representing +/- SEM and * denotes statistical significance at p < 0.05.

doi:10.1371/journal.pone.0138240.g003

The effect of alginate on cellular iron metabolism

To assess the influence of alginate-iron interaction in human intestinal cells, RKO cells were challenged with an iron-enriched media either with, or without alginate LFR5/60. The iron-enriched media was spiked with radio-active iron-59, and after an incubation period of 24 hours the iron-content of the cell was measured ([Fig 3A](#)). Results demonstrated a significant decrease (37%, p < 0.05) in radioactivity in cells co-cultured in the presence of alginate compared to control (no alginate). To support this result ferritin expression, a surrogate marker for cellular iron levels was also determined. Ferritin expression was significantly decreased (17 fold; p < 0.05) when cells were cultured in the presence of iron and alginate compared to iron alone (control) ([Fig 3B](#)).

Alginate iron composites are not cell-permeable

Since alginate depleted intracellular iron, confocal microscopy was performed to assess the localisation of the alginate in these cell culture experiments and specifically to deduce if the alginate is internalised. To assess the bioavailability of alginate LFR5/60 and the composites
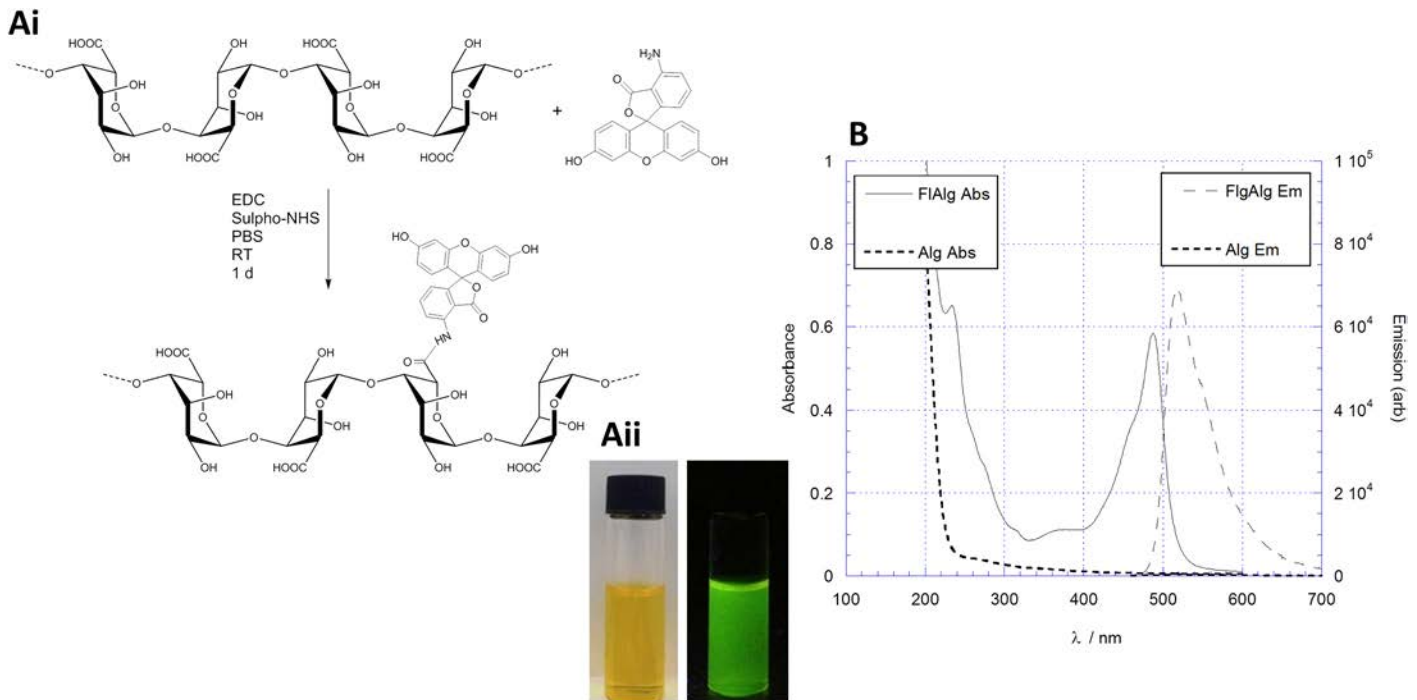
Fig 4. Synthesis of FITC alginate. (Ai) Reaction coupling scheme of FITC onto alginate under peptide coupling conditions. (Aii) Image of fluorescent alginate in normal light (left) and exposed to λ = 365 nm UV light (right). (B) Absorption and emission (red and blue lines respectively) spectra of the fluorescent alginate (FlAlg) product. The native alginate reactant has no absorption or emission profile, however, upon conjugation with FITC a highly absorption and emission peaks are observed.

doi:10.1371/journal.pone.0138240.g004

formed upon interaction with iron a fluorescent analogue was prepared by conjugation with fluoresceinamine (FITC) as schematically illustrated in Fig 4Ai. Absorption and emission spectra were recorded for the fluorescent alginate with absorption and emission maxima ($λ_{max}$) at ca. 490 and 550 nm respectively (Fig 4B).

RKO cells were then cultured in the presence of FITC-alginate with or without a cellular permeabilisation step for 24 hours on microscope slips which were subsequently used for imaging in confocal microscopy. Cells were stained with DeepRed and Hoechst to define the cellular membrane and nucleus respectively (Fig 5).

Confocal image analysis revealed that whilst there was negligible amounts of FITC-alginate bound on the cell periphery (Fig 5B) no FITC-alginate was observed within the cell (Fig 5). As a further control cells were membrane-permeabilised and co-cultured with FITC-alginate, and in this instance, FITC- alginate is able to penetrate the outer cell membrane supporting the limited bioavailability of alginate in non-permeabilised cells.

Discussion

Alginates and their use in nanoparticle formation is well established, however this is the first study to examine the interaction of iron and alginate in gastric-comparable pH conditions. This is particularly warranted since the existing literature is inconsistent in terms of the effect of alginate on cellular iron absorption and ultimate effects on human iron metabolism.[12,13]

Our results unequivocally demonstrate that alginate chelates iron under gastric comparable conditions as evidenced through UV Visible spectroscopy, ITC and CD. We have found by ITC that alginate–iron complexation involves two distinct binding events; an initial iron binding which then facilitates alginate reorganisation to accommodate the final iron binding. This
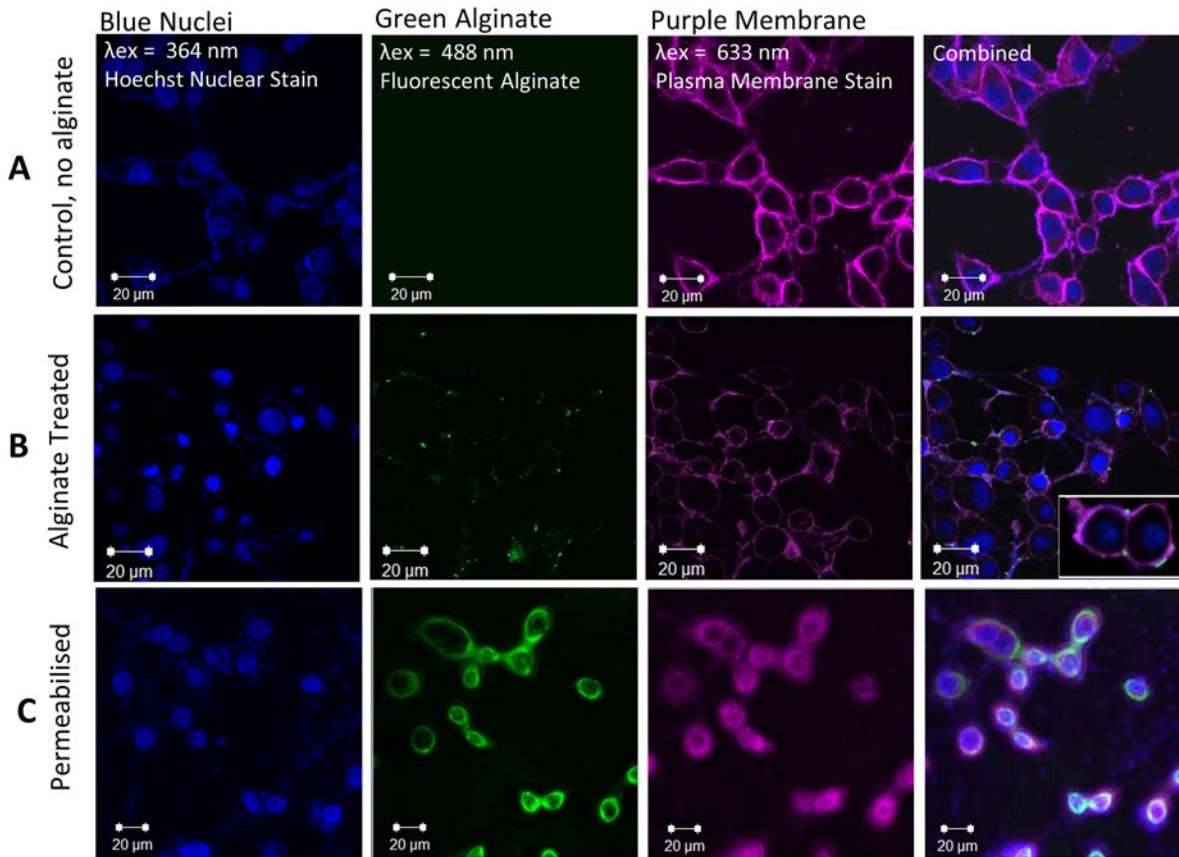
Fig 5. Cellular localisation of alginate with confocal microscopy. Cells were treated with iron alone (control) or iron and FITC alginate with or without cell-membrane permeabilisation. (A) Cells treated with iron alone as expected showed no FITC signal. (B) Cells treated with iron and FITC alginate showed negligible punctate FITC staining on the cell periphery (C) Cells permeabilised with Saponin and then cultured with iron and FITC alginate showed an abundance of intracellular FITC signal which was mostly cytoplasmic in localisation.

is consistent with previous studies which indicate cooperativity of metal binding to alginate. In addition structural reorganisation of alginate polymers during ion binding has been reported previously in the case of calcium. [24,25]

With regards to the species of iron that is complexed to alginate, UV Visible spectroscopy, upon iron titration, revealed a peak at 280 nm which has previously been attributed to the presence of an iron-oxide species. This electronic transition is characteristic to the charge transfer originating from the OH- ligands to the Fe ion.[26] CD Spectroscopy demonstrated that the Fe-OH species were complexed to alginate since an induced CD signal was observed at 280 nm.

To probe the physical structure of the alginate iron composites formed under these physiological conditions HAADF-STEM was utilised. Interestingly, we demonstrate that alginate chelates iron to form a range of composites, from long range gel-like structured strands to smaller nanoparticulate matter. This mix of composites is unsurprising since the way the alginate and iron is brought together is uncontrolled. The combination of solution spectroscopy and high resolution STEM identified the core of the alginate nanoparticles to be iron-oxide in composition. However, it is known that the electron beam energy can affect samples under investigation during examination in an electron microscope and thus it is important to note that there is the possibility of electron beam damage causing structural and/or chemical particle-phase

conversion. This could indeed result in a phase conversion from, for example, a ferrihydrite-particle to a haematite arrangement, which were both found here.[27]

A mechanism of nanoparticle formation can be proposed whereby iron initially binds to alginate forming an iron-hydroxide. Subsequently, at a critical concentration of iron loading, the alginate collapses and forms a nucleation site where iron hydroxide condensation can take place to form iron-oxide centred nanoparticles; the whole process templated by alginate (Fig 6). This mechanism supports the two event binding observed by ITC. Such models have been reported for other biopolymers binding metals including carrageenans. [28]

These findings confirmed the iron-binding ability of alginate, with iron binding constants on par with other biological proteins (e.g. ferritin), [29] and interestingly, ferritin similarly stores iron as its oxide form.[29,30] The formation of these composites may rationalise some of the effects seen in biological systems by others [12]. However, whilst it is clear that the alginate binds iron, what effect this has on cellular and human iron metabolism remains controversial whilst some studies advocating the usefulness of alginate in iron fortification and others iron chelation programmes. [13,31,32]. Our data suggest that alginate has the potential to bind 'free' reactive iron and this leads to the formation of iron-oxide centred nanoparticles. Although whether such 'free' iron exists within the gastrointestinal tract and or what form the residual unabsorbed iron takes still remains to be elucidated; indeed, there is evidence supporting the presence of both the particulate and 'free' forms.[33] Whether alginate is able bind particulate iron, if it exists within the gastrointestinal tract is not known and this clearly warrants further study.

From our own studies it is clear that alginate inhibits cellular iron transport by binding the iron in solution and the resulting complex remaining extracellular. This is evidenced by a suppression in cellular iron transport in the presence of alginate and a lack of any notable alginate present within the cells.[11,34–36] We may hypothesise from these observations that the alginate-iron nanoparticles are unable to be internalised into cells which may be due to a number of factors including nanoparticle size and surface coating.

Thus it can be considered that alginates act as iron chelators and are not bioavailable with respect to cellular uptake. This confirms previous studies, most notably, a recent human study has shown that alginate supplementation inhibits iron absorption in man, [11,36] and this may be attributed to the formation of iron-alginate nanoparticles. Thus in vivo alginate could be considered as an iron chelator and coupled with its inherent non-absorbability would make it
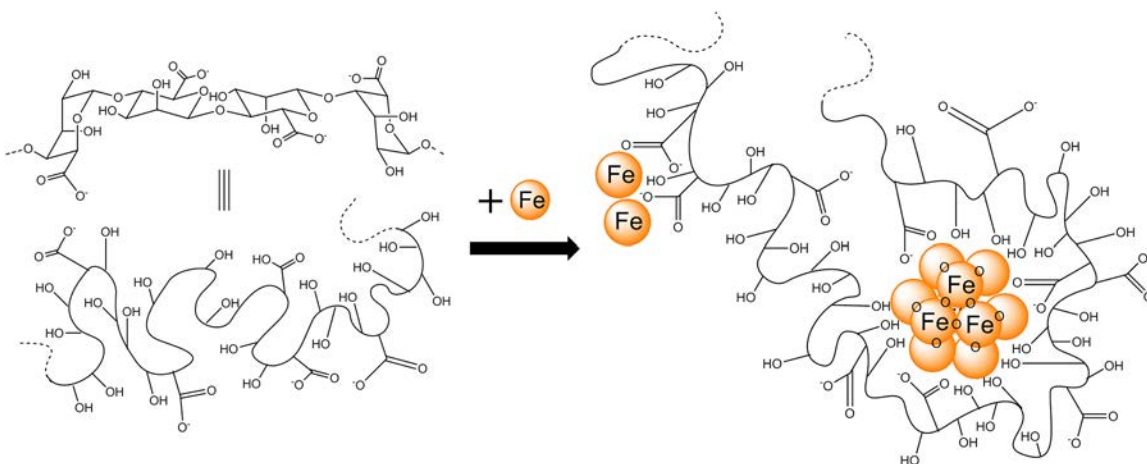

Fig 6. Schematic illustration of the binding arrangement of iron to alginate under simple mixing conditions.

an ideal candidate for use in patients with inflammatory bowel disease and colorectal cancer where excess reactive luminal iron is thought to be involved in the disease process.[37–39] One might predict that alginate supplementation in these groups would enhance their health through iron chelation.

Supporting Information

S1 Fig. ITC model of independent binding sites. Where Q = heat content of the solution, n = number of binding sites, M_t = total concentration of macromolecule in V_o, V_o = active cell volume, H = enthalpy, X_t = total ligand concentration and K = the binding constant. (TIF)

S2 Fig. Equation of the 1:1 binding model. Where [H] = [alginate] and [G] = [Fe]. (TIF)

Acknowledgments

Author Contributions

Conceived and designed the experiments: RH THI REP ZP CT. Performed the experiments: RH MD GOL. Analyzed the data: RH MD GOL ZP. Contributed reagents/materials/analysis tools: REP ZP CT. Wrote the paper: RH REP ZP CT.

References

1. Hoffman AS (2002) Hydrogels for biomedical applications. Advanced Drug Delivery Reviews 54: 3–12. PMID: 11755703

2. George M, Abraham TE (2006) Polyionic hydrocolloids for the intestinal delivery of protein drugs: Alginate and chitosan—a review. Journal of Controlled Release 114: 1–14. PMID: 16828914

3. Hamidi M, Azadi A, Rafiei P (2008) Hydrogel nanoparticles in drug delivery. Advanced Drug Delivery Reviews 60: 1638–1649. doi: 10.1016/j.addr.2008.08.002 PMID: 18840488

4. Hampson FC, Farndale A, Strugala V, Sykes J, Jolliffe IG, et al. (2005) Alginate rafts and their characterisation. International Journal of Pharmaceutics 294: 137–147. PMID: 15814238

5. Ma HL, Qi XT, Maitani Y, Nagai T (2007) Preparation and characterization of superparamagnetic iron oxide nanoparticles stabilized by alginate. International Journal of Pharmaceutics 333: 177–186. PMID: 17074454

6. Kroll E, Winnik FM, Ziolo RF (1996) In situ preparation of nanocrystalline gamma-Fe2O3 in iron(II) cross-linked alginate gels. Chemistry of Materials 8: 1594–&.

7. Llanes F, Ryan DH, Marchessault RH (2000) Magnetic nanostructured composites using alginates of different M/G ratios as polymeric matrix. International Journal of Biological Macromolecules 27: 35–40. PMID: 10704984

8. Shen F, Poncet-Legrand C, Somers S, Slade A, Yip C, et al. (2003) Properties of a novel magnetized alginate for magnetic resonance imaging. Biotechnology and Bioengineering 83: 282–292. PMID: 12783484

9. Maity D, Agrawal DC (2007) Synthesis of iron oxide nanoparticles under oxidizing environment and their stabilization in aqueous and non-aqueous media. Journal of Magnetism and Magnetic Materials 308: 46–55.

10. Laurent S, Forge D, Port M, Roch A, Robic C, et al. (2008) Magnetic iron oxide nanoparticles: Synthesis, stabilization, vectorization, physicochemical characterizations, and biological applications. Chemical Reviews 108: 2064–2110. doi: 10.1021/cr068445e PMID: 18543879

11. Sandberg AS, Andersson H, Bosaeus I, Carlsson NG, Hasselblad K, et al. (1994) ALGINATE, SMALL-BOWEL STEROL EXCRETION, AND ABSORPTION OF NUTRIENTS IN ILEOSTOMY SUBJECTS. American Journal of Clinical Nutrition 60: 751–756. PMID: 7942583

12. Wawer AA, Harvey LJ, Dainty JR, Perez-Moral N, Sharp P, et al. (2014) Alginate inhibits iron absorption from ferrous gluconate in a randomized controlled trial and reduces iron uptake into caco-2 cells. PloS one 9: e112144–e112144. doi: 10.1371/journal.pone.0112144 PMID: 25391138

13. Wawer AA, Sharp PA, Perez-Moral N, Fairweather-Tait SJ (2012) Evidence for an Enhancing Effect of Alginate on Iron Availability in Caco-2 Cells. Journal of Agricultural and Food Chemistry 60: 11318–11322. doi: 10.1021/jf3031309 PMID: 23101614

14. Pereira DIA, Bruggraber SFA, Faria N, Poots LK, Tagmount MA, et al. (2014) Nanoparticulate iron(III) oxo-hydroxide delivers safe iron that is well absorbed and utilised in humans. Nanomedicine-Nanotechnology Biology and Medicine 10: 1877–1886.

15. Powell JJ, Bruggraber SFA, Faria N, Poots LK, Hondow N, et al. (2014) A nano-disperse ferritin-core mimetic that efficiently corrects anemia without luminal iron redox activity. Nanomedicine-Nanotechnology Biology and Medicine 10: 1529–1538.

16. Latunde-Dada GO, Pereira DIA, Tempest B, Ilyas H, Flynn AC, et al. (2014) A Nanoparticulate Ferritin-Core Mimetic Is Well Taken Up by HuTu 80 Duodenal Cells and Its Absorption in Mice Is Regulated by Body Iron. Journal of Nutrition 144: 1896–1902. doi: 10.3945/jn.114.201715 PMID: 25342699

17. Karlsen V, Heggset EB, Sorlie M (2010) The use of isothermal titration calorimetry to determine the thermodynamics of metal ion binding to low-cost sorbents. Thermochimica Acta 501: 119–121.

18. Evans DF, Pye G, Bramley R, Clark AG, Dyson TJ, et al. (1988) Measurement of gastrointestinal pH profiles in normal ambulant human subjects. Gut 29: 1035–1041. PMID: 3410329

19. Brookes MJ, Boult J, Roberts K, Cooper BT, Hotchin NA, et al. (2008) A role for iron in Wnt signalling. Oncogene 27: 966–975. PMID: 17700530

20. Strand BL, Morch YA, Espevik T, Skjak-Braek G (2003) Visualization of alginate-poly-L-lysine-alginate microcapsules by confocal laser scanning microscopy. Biotechnology and Bioengineering 82: 386–394. PMID: 12632394

21. Johnson JA, Gray MO, Karliner JS, Chen CH, MochlyRosen D (1996) An improved permeabilization protocol for the introduction of peptides into cardiac myocytes—Application to protein kinase C research. Circulation Research 79: 1086–1099. PMID: 8943947

22. Sourty E, van Bavel S, Lu K, Guerra R, Bar G, et al. (2009) High-Angle Annular Dark Field Scanning Transmission Electron Microscopy on Carbon-Based Functional Polymer Systems. Microscopy and Microanalysis 15: 251–258. doi: 10.1017/S1431927609090278 PMID: 19460182

23. Kim S-W, Seo H-Y, Lee Y-B, Park YS, Kim K-S (2008) Crystal structure of ferrihydrite nanoparticles synthesized in ferritin. Bull Korean Chem Soc 29: 1969–1972.

24. Wang Z-Y, Zhang Q-Z, Konno M, Saito S (1993) Sol–gel transition of alginate solution by the addition of various divalent cations: 13C-nmr spectroscopic study. Biopolymers 33: 703–711.

25. Fang Y, Al-Assaf S, Phillips GO, Nishinari K, Funami T, et al. (2007) Multiple Steps and Critical Behaviors of the Binding of Calcium to Alginate. The Journal of Physical Chemistry B 111: 2456–2462. PMID: 17305390

26. Sreeram KJ, Yamini Shrivastava H, Nair BU (2004) Studies on the nature of interaction of iron(III) with alginates. Biochimica et Biophysica Acta (BBA)—General Subjects 1670: 121–125.

27. Pan Y, Brown A, Brydson R, Warley A, Li A, et al. (2006) Electron beam damage studies of synthetic 6-line ferrihydrite and ferritin molecule cores within a human liver biopsy. Micron 37: 403–411. PMID: 16466926

28. Jones F, Cölfen H, Antonietti M (2000) Interaction of κ-Carrageenan with Nickel, Cobalt, and Iron Hydroxides. Biomacromolecules 1: 556–563. PMID: 11710181

29. Bou-Abdallah F, Arosio P, Santambrogio P, Yang X, Janus-Chandler C, et al. (2002) Ferrous ion binding to recombinant human H-chain ferritin. An isothermal titration calorimetry study. Biochemistry 41: 11184–11191. PMID: 12220183

30. Pan Y-H, Sader K, Powell JJ, Bleloch A, Gass M, et al. (2009) 3D morphology of the human hepatic ferritin mineral core: New evidence for a subunit structure revealed by single particle analysis of HAADF-STEM images. Journal of Structural Biology 166: 22–31. doi: 10.1016/j.jsb.2008.12.001 PMID: 19116170

31. Berner LA, Hood LF (1983) Iron Binding by Sodium Alginate. Journal of Food Science 48: 755–758.

32. Harmuth-Hoene A-E, Schelenz R (1980) Effect of Dietary Fiber on Mineral Absorption in Growing Rats. The Journal of Nutrition 110: 1774–1784. PMID: 6251185

33. Pereira DIA, Mergler BI, Faria N, Bruggraber SFA, Aslam MF, et al. (2013) Caco-2 Cell Acquisition of Dietary Iron(III) Invokes a Nanoparticulate Endocytic Pathway. PLoS ONE 8: e81250. doi: 10.1371/journal.pone.0081250 PMID: 24278403

34. Thebaudin JY, Lefebvre AC, Harrington M, Bourgeois CM (1997) Dietary fibres: Nutritional and technological interest. Trends in Food Science & Technology 8: 41–48.

35. Trowell H, Southgate DT, Wolever TS, Leeds A, Gassull M, et al. (1976) DIETARY FIBRE REDEFINED. The Lancet 307: 967.

36. Jonathan MC, Bosch G, Schols HA, Gruppen H (2013) Separation and Identification of Individual Alginate Oligosaccharides in the Feces of Alginate-Fed Pigs. Journal of Agricultural and Food Chemistry 61: 553–560. doi: 10.1021/jf304338z PMID: 23249258

37. Radulescu S, Brookes MJ, Salgueiro P, Ridgway RA, McGhee E, et al. (2012) Luminal Iron Levels Govern Intestinal Tumorigenesis after Apc Loss In Vivo. Cell Reports 2: 270–282. doi: 10.1016/j.celrep.2012.07.003 PMID: 22884366

38. Werner T, Wagner SJ, Martinez I, Walter J, Chang J-S, et al. (2011) Depletion of luminal iron alters the gut microbiota and prevents Crohn's disease-like ileitis. Gut 60: 325–333. doi: 10.1136/gut.2010.216929 PMID: 21076126

39. Bedford MR, Ford SJ, Horniblow RD, Iqbal TH, Tselepis C (2013) Iron Chelation in the Treatment of Cancer: A New Role for Deferasirox? Journal of Clinical Pharmacology 53: 885–891. doi: 10.1002/jcph.113 PMID: 23740857